A PREDICTION OF MEANDER MIGRATION BASED ON LARGE-SCALE FLUME TESTS IN CLAY

A Dissertation

by

NAMGYU PARK

Submitted to the Office of Graduate Studies of
Texas A&M University
in partial fulfillment of the requirements for the degree of

DOCTOR OF PHILOSOPHY

December 2007

Major Subject: Civil Engineering

A PREDICTION OF MEANDER MIGRATION BASED ON LARGE-SCALE FLUME TESTS IN CLAY

A Dissertation

by

NAMGYU PARK

Submitted to the Office of Graduate Studies of
Texas A&M University
in partial fulfillment of the requirements for the degree of

DOCTOR OF PHILOSOPHY

Approved by:

Co-Chairs of Committee,	Jean-Louis Briaud
	Kuang-An Chang
Committee Members,	Hamn-Ching Chen
	Christopher C. Mathewson
Head of Department,	David V. Rosowsky

December 2007

Major Subject: Civil Engineering

ABSTRACT

A Prediction of Meander Migration Based on Large-Scale Flume Tests in Clay.

(December 2007)

Namgyu Park, B.S., Sungkyunkwan University, Seoul, Korea;

M.S., University of Michigan, Ann Arbor

Co-Chairs of Advisory Committee: Dr. Jean-Louis Briaud
Dr. Kuang-An Chang

Meander migration is a complex and dynamic process of the lateral movement of a river due to erosion on one bank and deposition on the opposite bank. As a result, the channel migrates in a lateral direction, which might be a major concern for the safety of bridges during their life span of 75 years. Although there are several existing models for predicting meander migration of a river, none of them are based on the physical model tests on a specific type of soil.

A total of eight flume tests are conducted to develop a prediction equation of meander migration in clay. The test results of migration rate follow a hyperbolic function, and spatial distribution of the maximum migration distance is fitted with the Pearson IV function. The proposed equations of the initial migration rate and the maximum migration distance, obtained by a multiple regression technique, are validated with the laboratory data.

A new methodology for risk analysis is developed to process a number of predicted channel locations based on each future hydrograph generated in such a way

that all the hydrographs have the same probability of occurrence. As the output from risk analysis, a CDF map is created for a whole river representing a general trend of migration movement along with the probability associated with new location of the river. In addition, a separate screen is generated with a CDF plot for a given bridge direction so that bridge engineers can read a specific migration distance along the bridge corresponding to the target risk level (e.g. 1 %).

The newly developed components through this research are incorporated with the other components in the MEANDER program which is a stand-alone program and the final outcome of the research team. Verification study of the MEANDER program is conducted with full-scale field data at the Brazos River at SH 105, Texas. The prediction results matched quite well with the measured field data. However, a more extensive verification study for other sites is highly recommended.

DEDICATION

This dissertation is dedicated to my father, my mother, and my wife, Jeonghae Kim. Without their endless support, encouragement, and love, I would never have been able to accomplish this work.

ACKNOWLEDGEMENTS

First, I wish to express my deepest gratitude to Dr. Briaud and Dr. Chang for their exceptional guidance, liberal support, and warm encouragement throughout this study. I want to extend my faithful thanks to Dr. Chen for his kind help and valuable suggestions during this research. I also wish to extend my sincere thanks to Dr. Mathewson for his time and efforts as an advisory committee member.

I would like to thank my colleagues in the same research team, Youngan Chung, Wei Wang, and Po-Hung Yeh, for their strong teamwork and help during various stages of this research. A special thanks also goes to Stephen Mathew James for his great help in preparing the flume tests. I also want to thank Jennifer Nicks and Bradley Smith for their comprehensive proofreading of my dissertation.

In addition, many thanks go to Johnnie Reed for his help in experimental setup in the Hydromechanics Laboratory at Texas A&M University. I wish to express my particular appreciation to Mr. Kayvon Jahedkar of TxDOT in the Bryan district for taking the time to provide me helpful data for the verification study and for helping me to acquire the permission from the property owners.

Finally, I would like to thank all my colleagues at Texas A&M University who have provided tremendous support and encouragement during the most challenging time in my life.

TABLE OF CONTENTS

CHAPTER Page

Page

LIST OF FIGURES

FIGURE Page

FIGURE Page

FIGURE Page

FIGURE Page

FIGURE Page

FIGURE Page

LIST OF TABLES

CHAPTER I

INTRODUCTION AND RESEARCH OBJECTIVES

1.1 INTRODUCTION

Meander migration is a process of the lateral movement of a river due to erosion on one bank and deposition on the opposite bank. It is referred to as a measure of lateral instability of a river, which is a major concern for the safety of bridges. Based on a survey of a number of state highway engineers (Brice and Blodgett 1978), bank erosion associated with meander migration is classified as a major stream-related hazard. Meander migration will most likely undermine bridge piers and abutments during their life span of 75 years, which often results in costly countermeasures or modification of the bridge. Since remedies can cost from $100,000 to $3,000,000 per bridge, the ability to predict river migration will reduce the cost for protecting the susceptible structures against the migration problem (Briaud et al. 2001b). As an example, the SH 105 Bridge over the Brazos River near Navasota, TX (Figure1.1) is going to be replaced by the Texas Department of Transportation (TxDOT) because it has been endangered by excessive bank erosion on the east bound. The new bridge will be located about 228m (760ft) south of the old bridge to avoid the potential problem related to the meander migration during its life span.

This dissertation follows the style of the *Journal of Geotechnical and Geoenvironmental Engineering.*

Figure 1.1 Brazos River at SH 105 (source: Google Earth 2007)

There are several models available for predicting meander migration of a river. The majority of these models are empirical equations (e.g. Keady and Priest 1977; Nanson and Hickin 1983; Hooke 1980; Brice 1982) based on a database of observed data. These empirical studies attempted to correlate the movements of the bank-line or its rate, along with influencing parameters, and then to use regression techniques to acquire a best-fit equation. However, these equations are limited by the extent of the database and the selection of the parameters for a specific site. The primary parameters, such as erodibility of the soil and flow condition needed to erode the soil on the bank,

have not been considered. Recently, several numerical models incorporating the flow field, sediment transport, and bank erosion models (Nagata et al. 2000; Darby et al. 2002) have been proposed to solve the meander migration problem. Although these approaches provide the extensive information on the meander migration processes, their practical use is limited due to extensive calibration work necessary to be a general solution for other sites. Since none of the aforementioned approaches are based on the physical model tests on a specific type of soils, it is valuable to develop a prediction method based on the well-controlled flume tests.

This research is initiated to investigate the meander migration process in clay. This is done by conducting a series of large-scale flume tests and proposing a prediction equation of the meander migration based on the results of those experiments. Additionally, a relatively simple methodology to provide a probabilistic solution for meander migration is also considered a goal of this study. Since the future flow condition, which is a dominant factor for the erosion process, is unknown, it is more reasonable to approach the meander migration problem in a probabilistic manner so that it can provide a certain confidence level achieved with the prediction result.

1.2 RESEARCH OBJECTIVES

The objectives of this research are described as follows:

- Develop a prediction equation of meander migration distance in clay based on large-scale flume tests which will be incorporated into the MEANDER program developed by the research team (Briaud et al. 2007).

- Develop a risk analysis methodology to provide a probabilistic solution for the meander migration problem.
- Develop a computer program (sub-module) to implement the developed risk analysis methodology into the MEANDER Program.
- Verify the prediction of meander migration with the MEANDER program by using the selected full-scale field data from a case history study.

1.3 GENERAL APPROACHES

The general approaches for this research are designed to accomplish the aforementioned research objectives in an efficient way. This includes the following components: large-scale flume tests in clay, application of a hyperbolic model, add-in risk analysis module, implementation of the new components, and verification study.

1.3.1 Maximum Migration Distance Equation for Clay

The prediction equation of maximum migration distance M_{max} for clay is obtained by conducting a series of large-scale flume tests where the laboratory basin is 22.0 m (72.6 feet) long, 10.0 m (33 feet) wide, and 0.9 m (3 feet) deep. The approach varies each primary parameter obtained from dimensional analysis, while keeping the other parameters constant. By doing this, the effect and impact of each individual parameter on meander migration can be examined to provide a basis for parametric study.

During each experiment, both temporal and spatial changes of channel geometry are measured to obtain the migration distances with respect to time and location along the two bank-lines. Then, the collected measurement data is fitted with the proposed

hyperbolic function to acquire the maximum migration distance at each cross-section. Finally, an appropriate function is applied by using a multiple regression technique to fit the spatial distribution of the maximum migration distance.

1.3.2 Hyperbolic Model

Since meander migration is a long-term and incremental process, time is an indispensable component. The hyperbolic model proposed by Briaud et al. (1999, 2001c, 2003) to model the scour process with respect to time has been verified to work reasonably well for various applications such as pier scour, complex pier scour, and contraction scour. The same model is employed for this research because both scour and meander migration are attributed to the same cause: erosion of soil due to the shear force induced by water flow. The hyperbolic model is expressed by the following equations:

$$M(t) = \frac{t}{\frac{1}{\dot{M}_i} + \frac{t}{M_{\max}}} \tag{1.1}$$

or,

$$\frac{t}{M(t)} = \frac{1}{M_{\max}} t + \frac{1}{\dot{M}_i} \tag{1.2}$$

Where,

M (t) = channel migration distance, (cm)
t = time, (hr)
$\dot{M}_i$ = the initial migration rate, (cm/hr)
M_{max} = the maximum migration distance, (cm)

In a hyperbolic model, the channel migration rate has its maximum value at the beginning, which means that the channel quickly erodes within a short period of time. As water continues to erode the channel banks, the migration rate gradually decreases

with a maximum value of the migration distance occurring when the channel reaches its equilibrium state (i.e. $t \rightarrow \infty$).

1.3.3 Risk Analysis Module

A meandering river migrates at a rate controlled by the shear stress at the interface between the water and the channel bank. The hydraulic shear stress imposed by the water is controlled by the velocity of the flow, which is dependent on the hydrograph of the river. Therefore, a meander migration prediction process must take the hydrograph of the river into account. This hydrograph is unknown, however, because it will occur in the future during the design life of the bridge or the highway embankment. Because it is not realistic to make a deterministic prediction of a future hydrograph, it is more desirable to make predictions of many equally possible hydrographs in a probabilistic manner. Based on the method developed by Briaud et al. (2003), Wang (2006) developed a modified methodology to generate a number of future hydrographs for a probabilistic prediction of meander migration. Each hydrograph corresponds to a different predicted position of the meandering channel. The collection of these new locations becomes the input data for the risk analysis for this research.

A new methodology is developed to process the input data in such a way that it produces a probability map showing the predicted channel with its risk level associated with the new location. The primary concern of meander migration is knowing the bank movement at a specific location as well as direction. Thus, a separate output plot is produced, which contains detailed risk information with respect to the predicted migration distance for the selected location and direction.

1.3.4 Implementation into MEANDER Program

The program MEANDER is the final outcome of the research project (Briaud et al. 2007) to develop a new prediction method of meander migration. All the components in the newly developed methodology are implemented into this stand-alone program to provide future users an automated prediction tool. MEANDER is composed of six main components: 1) The prediction equation for the maximum migration distance based on the large-scale flume tests in sand and clay, which is used to calculate the migration distance with respect to time, flow velocity, and channel radius of curvature to width ratio. 2) The prediction equation for the maximum shear stress based on 3-D numerical simulations, which is used to calculate the maximum shear stress at the interface between the water and the channel bank. 3) The implemented hyperbolic model to accumulate the migration distance. 4) The erodibility-curves of soil from Erosion Function Apparatus (EFA) test (Briaud et al. 2003) to calculate the initial migration rate with the assistance of the shear stress equation. 5) The algorithm of the geometry study to fit a number of best-fit circles, representing the meandering bends along the river. 6) The risk analysis module, which is used to evaluate the possibilities of the channel movement.

Among those components listed above, the prediction equation of the maximum migration distance in clay and the risk analysis module are developed by this research, and to be incorporated with the other components in the MEANDER program.

1.3.5 Field Verification Study

As with any new methods developed based on an experimental and numerical study, it is necessary to validate the results with a verification study. This allows the developer to check whether the new method is applicable to field cases. If not, any modification and/or improvement is needed. Generally, the verification can be done through case studies with field data and/or other available data resources.

In this research, one full-scale case study is conducted to evaluate the MEANDER program's prediction of the historical migration movement. The selected site is Brazos River at the SH 105 Bridge. The SH 105 Bridge over the Brazos River is located near Navasota, Texas. There is a meandering bend that approaches from the northeast at several hundred meters upstream of the bridge crossing. The meander map obtained from the 1981 and 1995 aerial photos and the recent Google satellite image indicates that the meandering bend migrated towards the highway (SH105) about 100 m (300 ft) from 1981 to 2006. Moreover, the channel is expected to move continuously in the future. As a result, TxDOT has decided to replace the bridge to avoid potential damage due to excessive bank erosion. The new bridge will be located about 228m (760ft) south of the old bridge. This implies the chosen site might be an ideal case for the verification study.

The prediction results using the MEANDER program during the pre-determined period (i.e. 1981~2006) are compared with the measured data. The results of the verification study are discussed in this dissertation.

CHAPTER II

MEANDER MIGRATION

2.1 FUNDAMENTAL CONCEPT

A natural river runs in a sinuous pattern rather than straight. It is nearly impossible to see the perfectly straight river in nature. The distance of the relatively straight portion of a meandering stream typically does not exceed ten times the river width (Wolman and Leopold 1957). The channel pattern of a river can be classified as straight, sinuous, meandering, or braided based on its sinuosity and other characteristics of the channel (Morisawa 1985), as shown in Figure 2.1(a). The typical characteristic of each pattern are summarized in Table 2.1. A meandering channel has a sinuosity larger than 1.5, and it can be distinguished by a series of alternating meander bends which is the channel reach between two inflection points (Julien 2002). The sinuosity can be defined in various ways, but the most common definition might be a ratio of channel length to meander belt axis length, and these dimensions are defined in Figure 2.1(b). Talweg in Figure 2.1(b) is a line connecting the deepest part of the cross-sections along a river, and it swings from the outer bank to the following outer bank towards the downstream of the river.

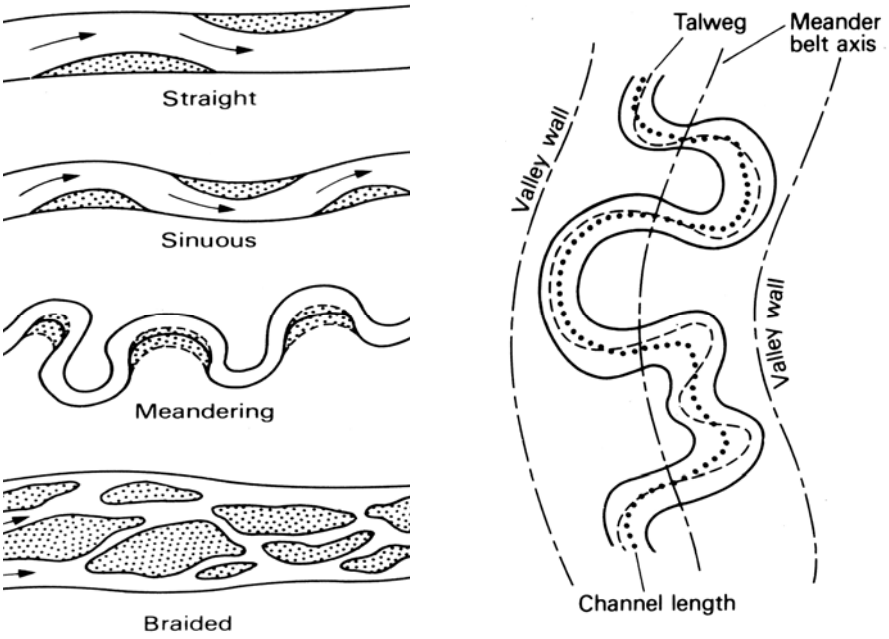

(a) Channel Patterns (b) Sinuosity

Figure 2.1 Channel Patterns and Geometry Parameters (after Morisawa 1985)

Table 2.1 Classification of River Patterns (after Morisawa 1985)

Type	Sinuosity	Load-Type	Erosive Behavior	Depositional Behavior
Straight	< 1.05	Suspension-mixed or bedload	Minor channel widening & incision	Skew shoals
Sinuous	> 1.05 < 1.05	Mixed	Increased channel Widening & incision	Skew shoals
Meandering	> 1.5	Suspension or mixed load	Channel incision, meander widening	Point bar formation
Braided	> 1.3	Bedload	Channel widening	Channel aggradation, mid channel bar formation

Pools, riffles, and asymmetrical cross-sections at bends are the essential components comprising a meandering river as shown in Figure 2.2. The sequence of these three elements is repetitive to form a whole river (Morisawa 1985). As a result of high flow velocity, asymmetrical cross-sections are mostly deeper on the outer (concave) banks in which pools appear. The transverse bed slope in this cross-section is correlated with the channel curvature (Chang, 1984): as a channel curvature increases, a transverse bed slope increases, reaching the maximum value under a maximum channel curvature (or minimum radius of curvature). Riffles are relatively symmetrical in cross-section, and are transition zones between two consecutive meandering bends in mostly opposite directions.

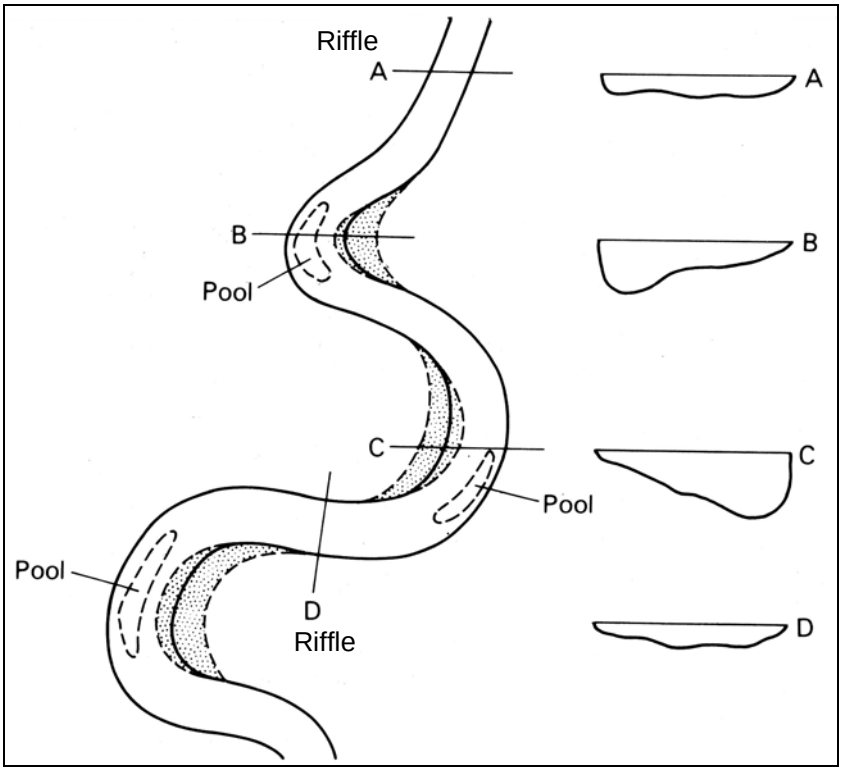

Figure 2.2 Cross-sectional Profiles in a Meandering River (after Morisawa 1985)

According to Morisawa (1985), the mechanism of meander migration is explained as follows: In a real river, streamlines of flow separate at bends or at obstructions (i.e. any irregular boundary), which increases the flow velocity and creates turbulence. As a result, the water is prone to erode the channel bed or bank when the hydraulic shear stress is high. If the bank is eroded and flow is distorted erratically, the meandering pattern will be initiated. Since the flow direction changes due to meandering bends, the centrifugal force results in a superelevated water surface along the outer bank (Leopold and Langbein 1960). This generates a non-uniform velocity and pressure distribution in the cross-section. As a result, downward and transversal flow patterns, as shown in Figure 2.3, are created, which is called helical flow. Chang (1984) explained the helical motion attributed to the difference of centrifugal forces between the top and bottom layer of the flow. The circulatory flow motion (i.e. secondary flow) will erode the outer (concave) bank, and then transport the eroded materials toward the inner (convex) bank. As this process is continued, the channel will shift its location laterally, which is meander migration.

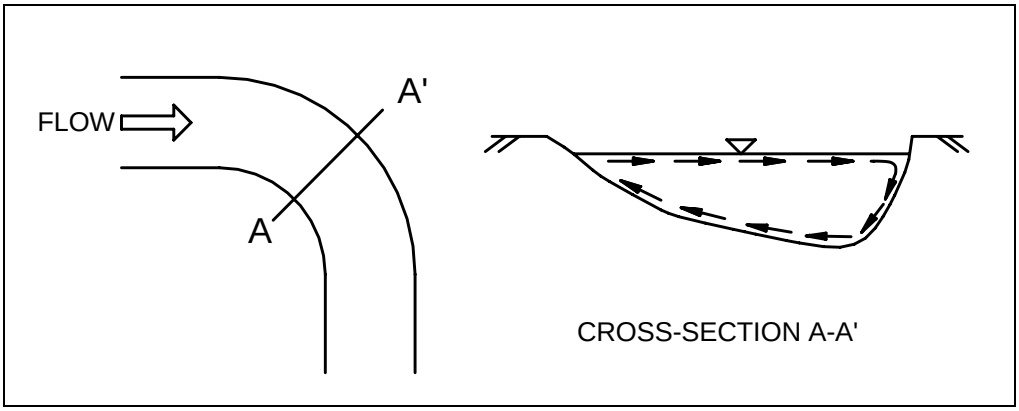

Figure 2.3 Secondary Flow Circulations

The direction of meander migration at a meandering bend depends primarily on the geometric condition of that bend and the previous upstream bend. It is very useful to have an idea for the possible ways in which the meander loop will migrate or create (Brice 1982), especially if there is a bridge crossing the meandering bend. He proposed several possible modes of meander loop development as shown in Figure 2.4. Mode A illustrates the extension type which is a common type of the development of a meander loop of low amplitude. Mode B describes the translation type which mostly occurs only if meander bends are constrained by valley sides on a narrow flood plain. Mode C is the rotation type which is a typical mode for fully developed meanders with fairly unstable banks. A highly meandering stream or a stream with a large meander loop usually follows Mode D. When the meandering bend becomes too big, secondary meanders are created along the existing loop. Mode E is quite similar to Mode D, but cut off is expected in this type. A locally braided sinuous or meandering stream would follow Mode F or Mode G.

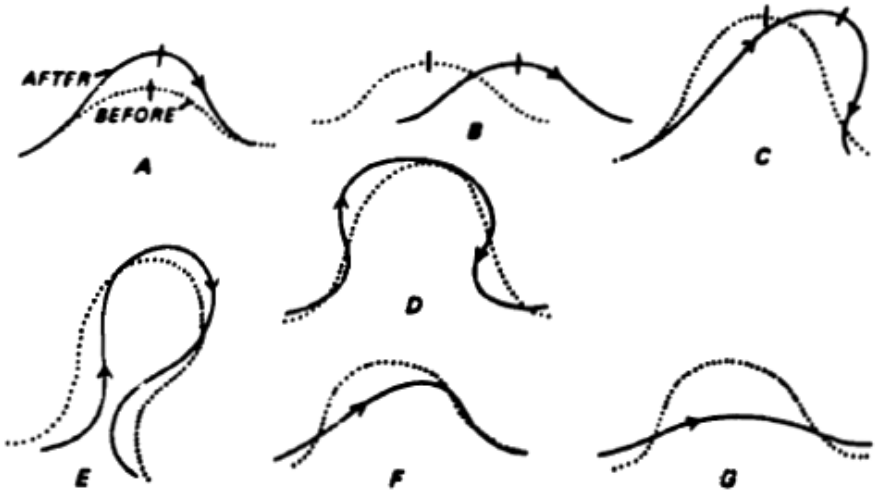

Figure 2.4 Mode of Meander Loop Development (Brice 1977)

2.2 MEANDER PARAMETERS TO DESCRIBE GEOMETRY

A typical river runs in irregular patterns and thus it is quite difficult to describe it in terms of a limited number of parameters. In order to reduce the complexity, each meandering bend can be simplified to an arc. A relatively straight portion of the river which has very low sinuosity or very high radius of curvature can be considered as a straight line. Consequently, a river can be represented numerically by constructing it with a series of arcs and straight lines. The parameters to describe the geometry of a meandering river are shown in Figure 2.5, and the definitions of these parameters are as follows:

A = meander amplitude

M = channel migration distance

R = radius of curvature

W = channel width

ϕ = bend angle

θ = relative angle ($0 \leq \theta \leq \phi$) within each bend

t = time

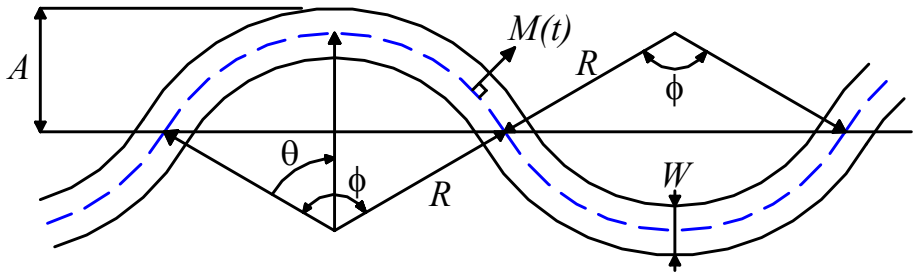

Figure 2.5 Parameters Defining Meander Geometry

2.3 FACTORS AFFECTING MEANDER MIGRATION

Meander migration is a complex and dynamic process at the interface between soil and water. The rate/amount of erosion of a certain type of soil is attributed to not only the soil's erodibility but the shear stress induced by the water. Consequently, the properties of the soil and the conditions of the flow are primary influencing factors for meander migration. Since the flow condition in a river is strongly affected by its geometric condition, the geometry of a river also needs to be taken into account. In other words, the necessary parameters to describe meander migration process are boiled down to three fundamental categories: soil, water, and geometry. In addition to the primary parameters of these categories, other supplementary factors are helpful to better understand the meander migration phenomenon, and those can be found from other literature. For example, Briaud et al. (2001b) identified other influential factors with respect to meander migration, listed as follows:

- stream pattern (straight, meandering, braided);
- free surface slope;
- channel roughness;
- sediment load;
- vegetation;
- debris problem;
- channel relocation;
- human activities on the floodplain of rivers.

CHAPTER III

LITERATURE REVIEW

A review of the extensive literature provides a remarkable insight into previous appreciation of the problem. It often gives great ideas or useful hints for new research concerning the same type of problem. The past research works related to the prediction of meander migration were studied in order to have a better understanding of the existing techniques and an idea of a more reasonable/improved approach to the problem. In addition, available literature for the flume tests related to the meander migration was carefully reviewed to design an appropriate flume test setup for this research. Finally, the existing techniques with regard to risk analysis were investigated for developing a new methodology of risk analysis in the prediction of meander migration. The selected studies in each category are described in the following sections.

3.1 MEANDER MIGRATION PREDICTIONS

There are a number of different models available for the prediction of meander migration, which include empirical equations (Keady and Priest 1977; Nanson and Hickin 1983; Hooke 1980; Brice 1982), time-sequence maps and extrapolations (Lagasse et al. 2003, 2004a, 2004b; Briaud et al. 2001a), and numerical models (Nagata et al. 2000; Darby et al. 2002). Note that time-sequence approach is covered in the risk analysis section (3.3) because this model can provide a certain type of risk level associated with the predicted migration.

3.1.1 Keady and Priest (1977)

Keady and Priest collected the published meander migration data up to 1977 to develop a prediction equation of meander migration. The collected data from eight different river reaches are tabulated in Table. 3.1. They proposed that the rate of downstream meander migration is related to the shear stress on the boundary. They further assumed that the shear stress is related to the free surface slope of the channel, geometric shape of the channel, and acceleration due to gravity. The final form of their model in terms of the above factors is expressed as follows;

$$\frac{V}{\sqrt{gA}} = f(S) \tag{3.1}$$

Where,

V = migration rate, (ft/yr) = dM/dt in Figure 2.3

A = meander amplitude, (ft) in Figure 2.3

g = acceleration of gravity, (ft/sec^2)

s = free surface slope

f = function of s given in Figure 3.1

Braiud et al. (2001a) conducted an evaluation study for the existing techniques including Keady and Priest's equation (Eq. 3.1). Additional data points from this study are added into the original plot as shown in Figure 3.1. The new points are scattered from the proposed trend line in the graph. Comparison between measured and predicted migration rate as shown in Figure 3.2 indicates that their method over-estimates the meander migration rate in the added cases. This implies that the proposed prediction equation is not a general solution for all cases.

Table 3.1 Data Used by Keady and Priest (after Keady and Priest 1977)

Identification	Velocity of Migration (ft/yr)	Meander Amplitude (ft)	Slope
Mississippi R (LA)	60	13,000	0.0000436
Mississippi R (MS)	111	11,000	0.0000588
Mississippi R (TN)	225	13,200	0.0000777
Red R (ARK)	350	2,900	0.000132
Pearl R (LA)	20	1,050	0.000200
Red Deer R (Canada)	20	1,200	0.000275
Tombigdee R (MS)	13	800	0.000421
Buffalo R (MS)	17	1,560	0.000689

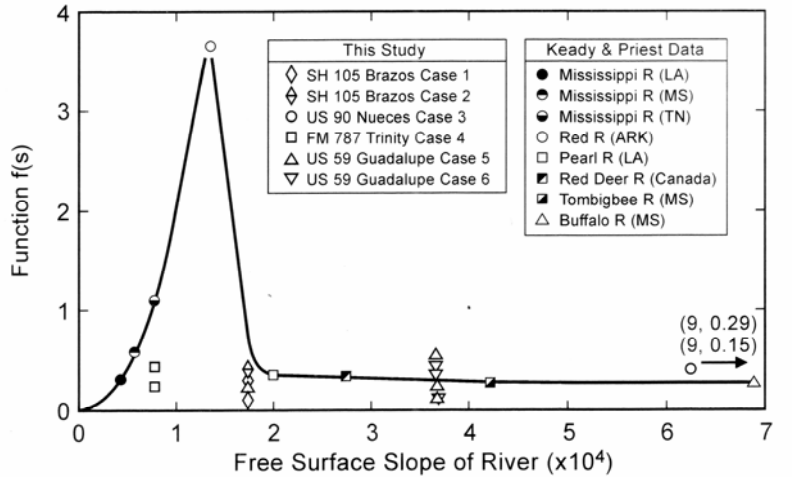

Figure 3.1 Graph for Determining Rate of Meander Migration (Keady and Priest 1977; Briaud et al. 2001a)

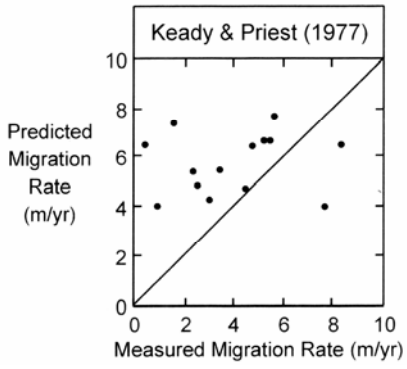

Figure 3.2 Predicted versus Measured Migration Rate using Keady and Priest's Empirical Equation (Briaud et al. 2001a)

3.1.2 Hooke (1980)

Hooke analyzed the meander migration rate on rivers in Devon, England from field measurements taken over 2.5 years. These measured rates were compared with the rates obtained from historical maps for the period from 1840 to 1975. He also compared the measured rates with published rates of bank erosion in the literature, and found that the rate in his study followed the general trend of the worldwide values as shown in Figure 3.3. He expected that there is a reasonable correlation between migration rate and site conditions, which includes catchment area, fine-grained soil content of bank material, presence of gravel layer, width to depth ratio, radius of curvature, slope, and bank height. It turned out that the primary influencing factor is catchment area from multiple regression analysis, and it has an approximately square-root relationship with migration rate. The proposed equation by Hooke is as follows:

$$M(m/yr) = 2.45A(km^2)^{0.45} \tag{3.2}$$

Where,

M = migration rate

A = catchment area

According to the evaluation study for the existing techniques by Briaud et al. (2001a), this equation often produced overly conservative prediction results as shown in Figure 3.4. This might be due to the fact that Hooke's empirical equation does not consider site specific conditions such as soil properties, flow history, and geometry of the river.

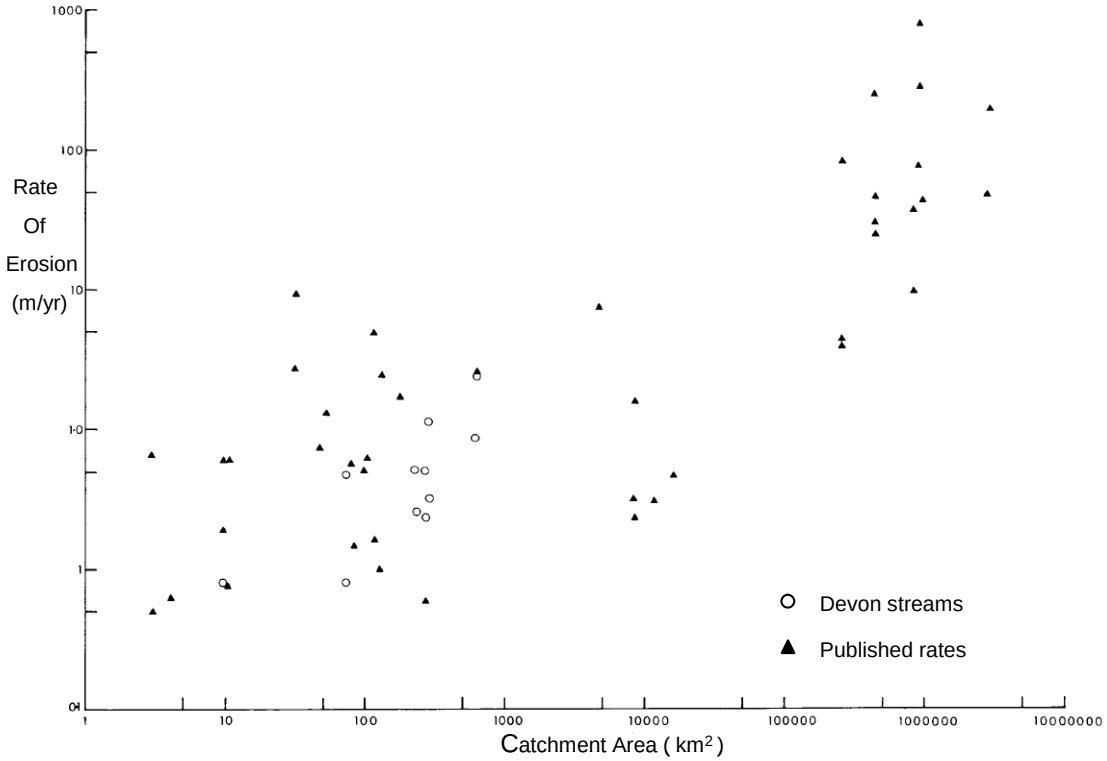

Figure 3.3 Relationships between Catchment Area and Erosion Rates (after Hooke 1980)

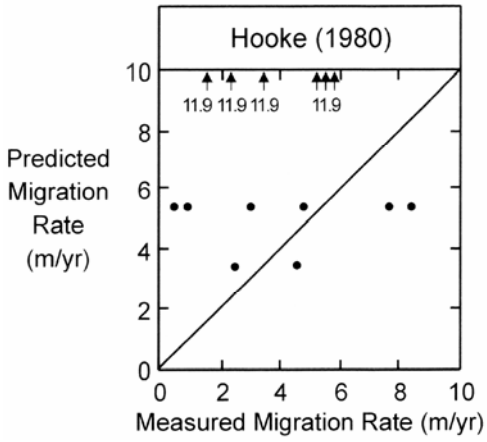

Figure 3.4 Predicted versus Measured Migration Rate using Hooke's Empirical Equation (Briaud et al. 2001a)

3.1.3 Brice (1982)

Brice believed that meander migration rate should be somehow related to the size of the stream. He employed the channel width for his empirical model as a characteristic parameter for the stream size, while Hooke (1980) selected the drainage basin area that is an indirect measure of stream size. The database for the analysis, as shown in Figure 3.5, consists of erosion rates in 36 nationwide streams in the US. The proposed formula to predict meander migration rate is as follows:

$$Y = 0.01B \tag{3.3}$$

Where, Y = mean erosion rate, (m/yr)

B = channel width, (m)

The additional data points were added to Figure 3.5 by Briaud et al. (2001a), and the predicted migration rates for the selected rivers in their evaluation study were compared with the measured values in Figure 3.6. It clearly indicates that Brice's empirical equation seriously under-estimates the erosion rates in other rivers. This implies that his model is too simple to be applied to the other cases because he correlated migration rate with only one parameter, channel width.

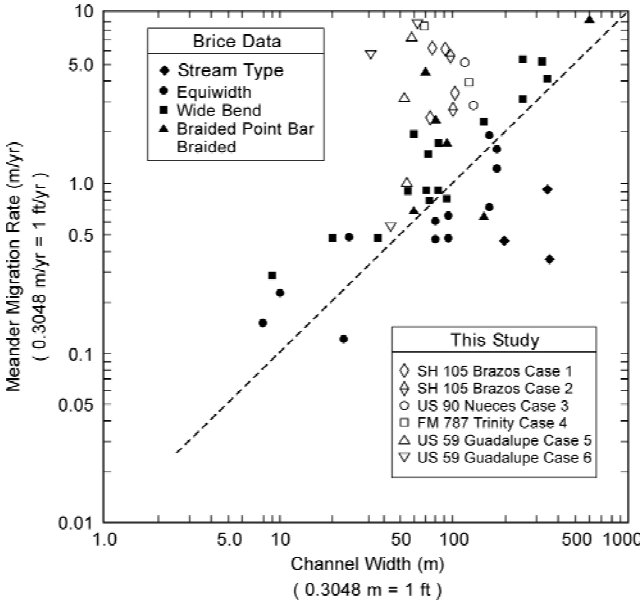

Figure 3.5 Relationships between Migration Rate and Channel Width (Brice 1982; Briaud et al. 2001a)

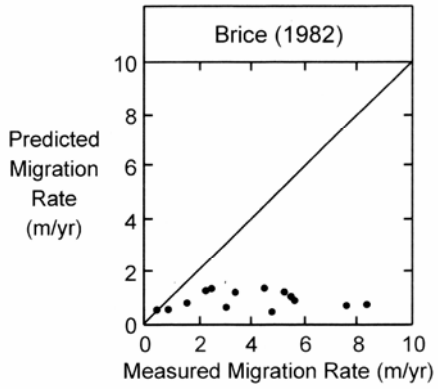

Figure 3.6 Predicted versus Measured Migration Rate using Brice's Empirical Equation (Briaud et al. 2001a)

3.1.4 Nanson and Hickin (1983)

Nanson and Hicken presented the lateral migration rate of a river as a function of the ratio of radius of curvature of a bend (r_c) to channel width (b). This correlation was

based on the field data for the Beatton River and other rivers in Canada. Figure 3.7 shows the relationship between the normalized channel migration rate (*Mr/b*) and the ratio of radius of curvature to channel width (r_c/b). The additional data points from a previous study (Briaud et al. 2001a) were plotted together. According to the plot, the maximum migration rate occurs when the ratio of radius of curvature to channel width (r_c/b) is about 3. Analysis of river meanders using an energy approach (Leopold and Langbein 1966, Chang 1984) supported this idea. A river does the least work in turning a curved bend when the ratio of radius of channel curvature to channel width becomes 3. In the range of $r_c/b < 3$, as the radius of curvature decreases, migration rate tends to decrease drastically. In the range of $r_c/b > 3$, as the radius of curvature increase, migration rate tends to decrease, but gradually. The data from Nanson and Hickin (1983) fit roughly to the following relations (Odgaard 1987):

$$\begin{aligned} Mr(m/year) &= 0.2(r_c/b) \qquad for\,(r_c/b) < 3 \\ Mr(m/year) &= 2.0(r_c/b)^{-1} \quad for\,(r_c/b) \geq 3 \end{aligned} \tag{3.4}$$

Where, Mr = mean erosion rate, (m/year)

b = channel width, (m)

r_c = radius of curvature, (m)

Although their approach has been very popular to other researchers, the data in the figure are widely scattered. It is therefore quite hard to get the best fit line. Furthermore, the other important parameters such as flow velocity and soil properties were not considered, which can be a serious limitation of their approach. The previous evaluation study of the existing technique for prediction of meander migration by Briaud

et al. (2001a) is an example to show such limitations on the application to other rivers where a similar scattering problem between predicted and measured migration rate is shown in Figure 3.8.

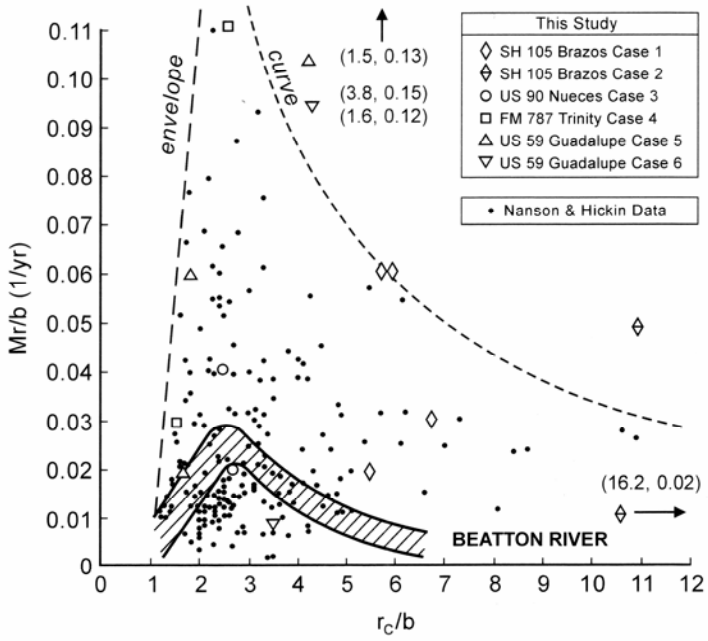

Figure 3.7 Relationships between Migration Rate and Geometry (Nanson and Hickin 1983, 1986; Briaud et al. 2001a)

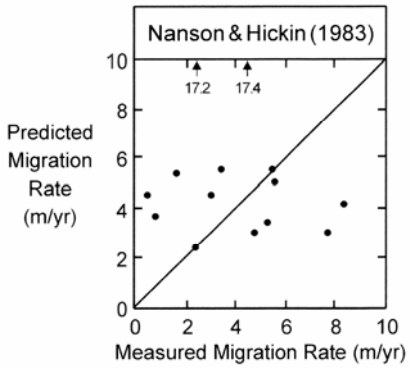

Figure 3.8 Predicted versus Measured Migration Rate using Nanson and Hickin's Empirical Equation (Briaud et al. 2001a)

3.1.5 Blondeaux and Seminara (1985)

Blondeaux and Seminara developed a 2-D model of flow and bed topography in a sinuous erodible channel. They examined the mechanism of the meander loop development by using the proposed model. Their analysis and comparison with experimental data appears to support that alternate-bar formation and bed amplification (i.e. meander loop) are dominated by two different mechanisms: instability and resonance, respectively. These two mechanisms are not totally independent, however, but are somewhat correlated to each other. They reported that a 'resonance' mechanism can occur when the values of the relevant parameters are within a optimum range to strengthen the swinging tendency of the meandering bends.

3.1.6 Odgaard (1987)

Odgaard adopted the bend theory (Ikeda et al. 1981), in which the rate of bank erosion is proportional to the difference between the near-bank depth-averaged mean velocity and the reach-averaged mean velocity at bank full discharge, and this is expressed as follows:

$$v = e(\bar{u}_b - u) \tag{3.5}$$

Where, v = bank erosion rate, (m/year)

e = erosion constant

$\bar{u}_b$ = near-bank depth-averaged mean velocity, (m/s)

u = reach-averaged mean velocity, (m/s)

He used his meander flow model (Odgaard 1986) to calculate the near-bank depth-averaged mean velocity. Then, he attempted to correlate the erosion rate with

various channel characteristics: width, depth, curvature, arc angle of channel centerline, channel slope, friction factor, and degree of vegetation on the banks. This analysis was based on the collected data for two different rivers in Iowa: East Nishnabotna River and Des Moines River. Figure 3.9 shows the comparison results between the measured and predicted erosion rate in East Nishnabotna River. Note that the erosion constant *e* is 6.4×10^{-7} for no or light vegetation case (Figure 3.9(a)) and *e* is 3.2×10^{-7} for heavy vegetation case (Figure 3.9(b)).

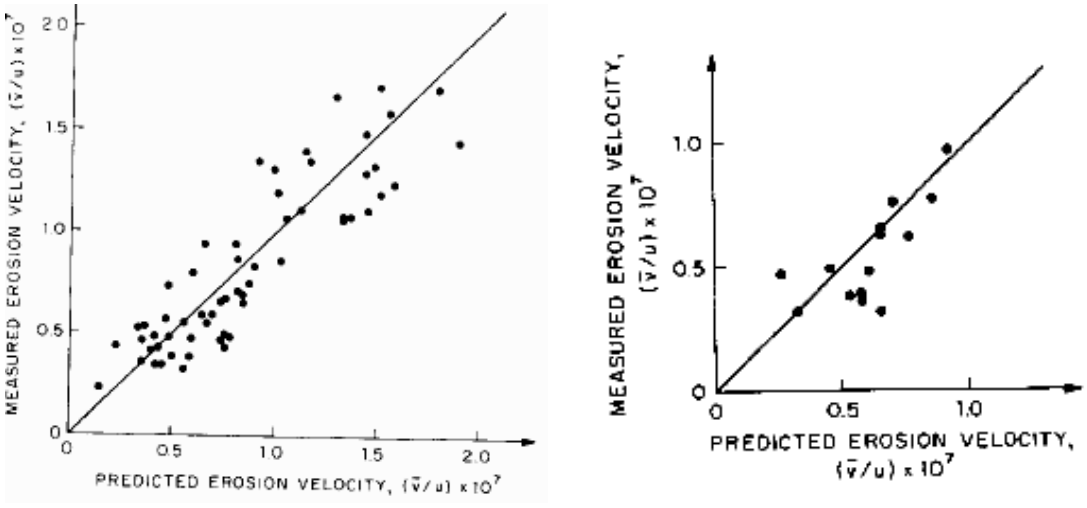

(a) No or Light Vegetation (b) Heavy Vegetation

Figure 3.9 Measured versus Predicted Erosion Rate in East Nishnabotna River (Odgaard 1987)

3.1.7 Biedenharn et al. (1989)

Biedenharn et al. investigated the behavior of meandering bends on the Red River, particularly the reaches between Shreveport, LA, and Index, AR. A total of 160 meandering bends, along approximately 150 miles, were examined, and the average

annual erosion rate were correlated with the ratio of radius of curvature of a bend (R) to channel width (W) as Nanson & Hicken (1983) did for their empirical approach. Figure 3.10 shows the result of the analysis of collected data, and there is a reasonably good agreement with the data from Nanson and Hicken (1986).

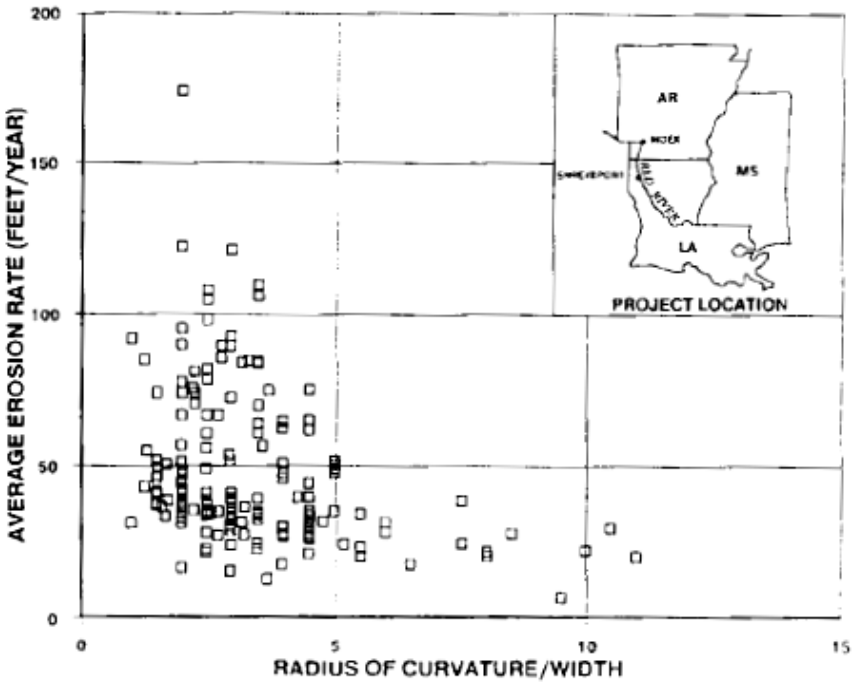

Figure 3.10 Average Annual Erosion Rate versus *R*/*W* (Biedenharn et al. 1989)

3.1.8 Hudson and Kesel (2000)

Hudson and Kesel investigated channel migration and morphology of meandering bends for the lower Mississippi River for the period from 1877 to 1924. They tried to correlate the migration rate with the ratio of radius of curvature of a bend (R) to channel width (W). Figure 3.11 shows the results of data analysis, and the shape of plotted data looks little different from the previously reported plot by Nanson and Hickin

(1983); the maximum migration in the lower Mississippi River occurs where R/W is about 1.0. The authors explained this deviation in terms of homogeneity of sediment materials. The previous model (Nanson and Hickin 1983) is based on data from homogeneous flood-plain deposits which allows the channel to migrate in a more free way, while this model is based on data from heterogeneous flood-plain deposits including the existence of high erosion resistive clay plugs. This study supports that an empirical model for prediction of meander migration merely based on a correlation with a single parameter, without considering the other site-specific conditions, is hardly a general solution.

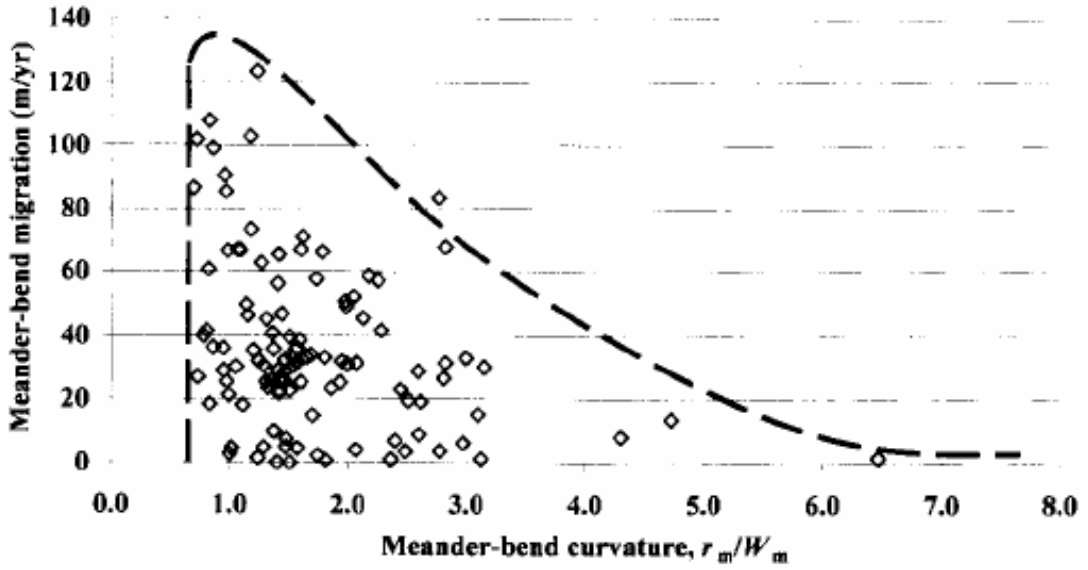

Figure 3.11 Model of Channel Curvature and Migration in Lower Mississippi River (Hudson and Richard 2000)

3.1.9 Darby et al. (2002)

Darby et al. developed a comprehensive numerical model to simulate bank erosion and channel migration in meandering rivers. Their model consists of three sub-models for flow, sediment transport, and bank erosion. One of unique features in this model is that the model can simulate the deposition of collapsed bank material and its removal from the toe of the bank by the flow. The model was evaluated by using two sets of flume tests data and one set of actual river data. The results are promising, but they generally underestimate the bank migration rates, which is undesirable.

3.1.10 Abad and Garcia (2006)

Abad and Garcia (2006) developed the RVR MEANDER program as a handy toolbox to assist the prediction of meander migration. This program is based on their model for the evolution of meandering rivers (Abad and Garcia 2004). There are two sub-modules in this model. One sub-module (statistical module) estimates primary parameters of the meandering channel such as sinuosity, migration rate, fattening, and skewness automatically by comparing input geometries at three different times (Figure 3.12). Another sub-module (migration module) simulates a plan form evolution (migration) based on the bend theory (Ikeda et al. 1981) where the bank erosion rate is proportional to the difference between the near-bank depth-averaged mean velocity and the reach-averaged mean velocity (Figure 3.13).

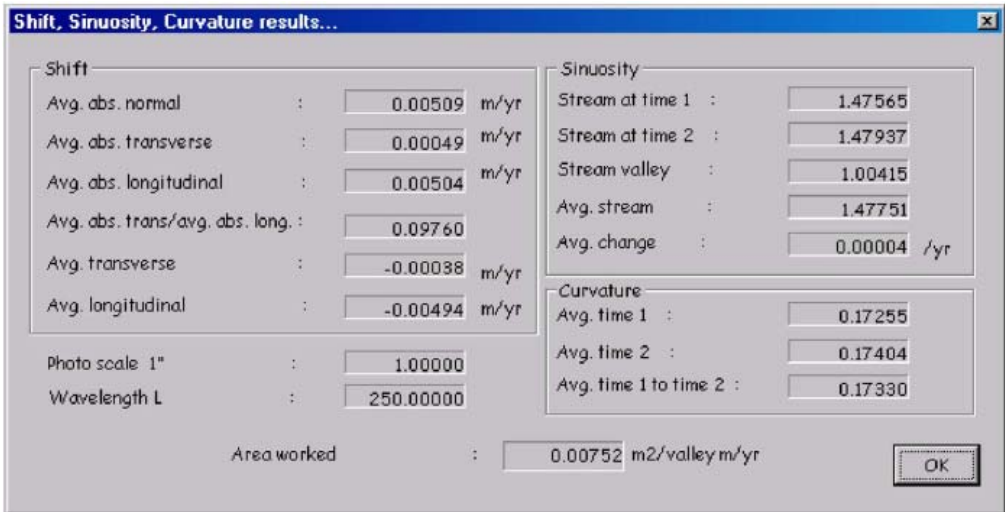

Figure 3.12 Statistical Module (Abad and Garcia 2006)

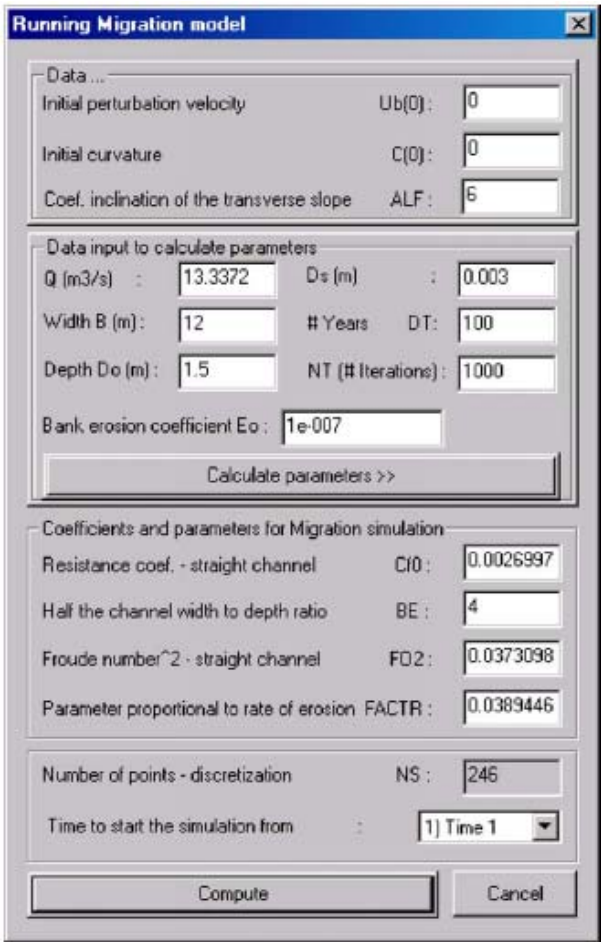

Figure 3.13 Migration Module (Abad and Garcia 2006)

Two versions of the program were developed: stand-alone Microsoft Windows-based and geographical information system (GIS)-based versions. The stand-alone version was written in Microsoft Visual C++ and Microsoft Foundation Classes (MFC). The geometry input can be done by typing manually, utilizing a spreadsheet, or importing from an ArcMap-DXF file.

The GIS-based version was written in Microsoft Visual C++ and MFC like the stand-alone version. In addition, Visual Basic and the ArcObjectsTM Developer Kit were used as well. The user can import the river geometry data from existing GIS line data within ESRI ArcMap. An example result of the prediction of a meandering river is shown in Figure 3.14.

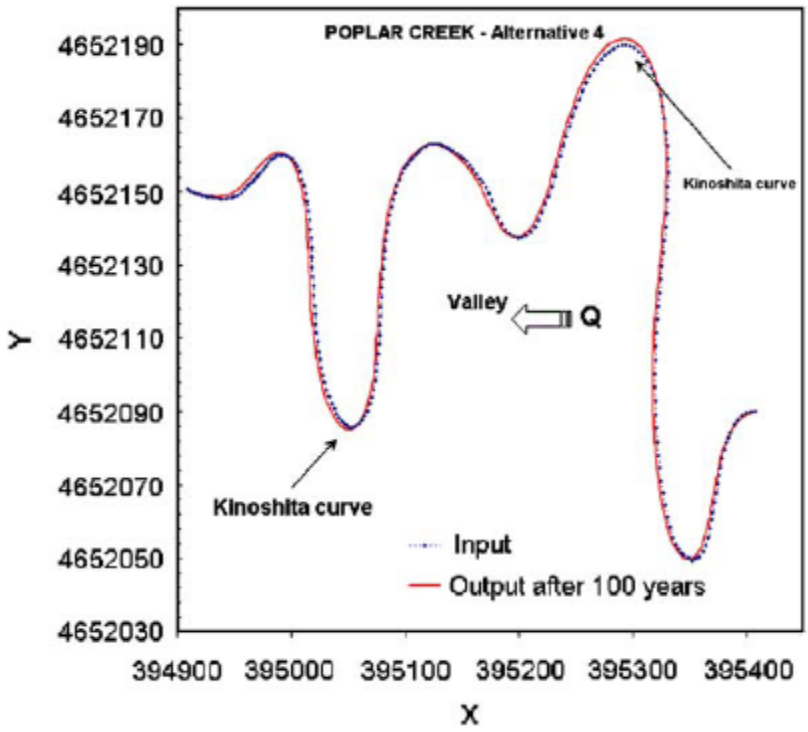

Figure 3.14 Output of Plan form Migration (Abad and Garcia 2006)

3.2 MEANDER MIGRATION FLUME TESTS

There is not much literature available about the experimental study of meander migration, especially flume tests in an erodible bed. This is because it commonly requires a significant amount of effort to prepare the physical model in a flume, as well as an extremely high cost. A few valuable previous works based on the experimental study related to meander migration are reviewed and summarized in the following sections. Once this research on meander migration in clay, based on a large-scale flume tests, are published, very valuable information will be provided to many engineers.

3.2.1 Friedkin (1945)

The most remarkable set of flume tests on behavior of self-formed meandering rivers in a large-scale flume, 36 m (120 ft) long and 11.4 m (38 ft) wide, was conducted by the U.S. Army Corps of Engineers (Friedkin 1945) as shown in Figure 3.15. They conducted these flume tests in different conditions to investigate the effect of discharge, angle of attack, bed slope, initial cross-section, material types, and not feeding sand at the entrance. The studies were not based on a quantitative approach but rather on a qualitative approach.

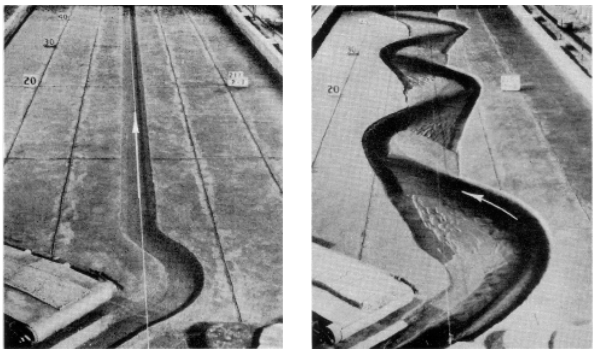

(a) Initial Condition (b) After 4 hours

Figure 3.15 Photos from Sand Flume Test with Feeding Sand at the Entrance (Friedkin 1945)

The effect of not feeding sand at the entrance to balance the sediment transport was not noticeable at the beginning of the test. The lack of sediment supply at the entrance of the channel gradually caused the channel to flatten with decreasing velocity, slowly progressing downstream as shown in Figure 3.16.

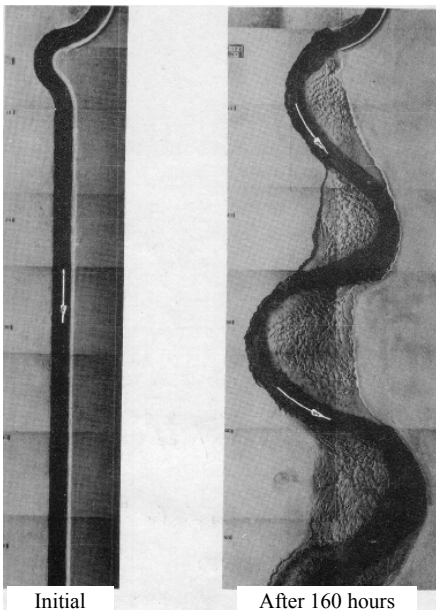

Figure 3.16 Photos from Sand Flume Test without Feeding Sand at the Entrance (after Friedkin 1945)

The size of the simulated meandering bends in the tests depends on the discharge and on the axial slope as shown in Figure 3.17 and Figure 3.18. From the tests, it is seen that the higher the discharge or axial slope, the bigger the bends. This trend is reasonable since both discharge and slope are function of the energy of a stream.

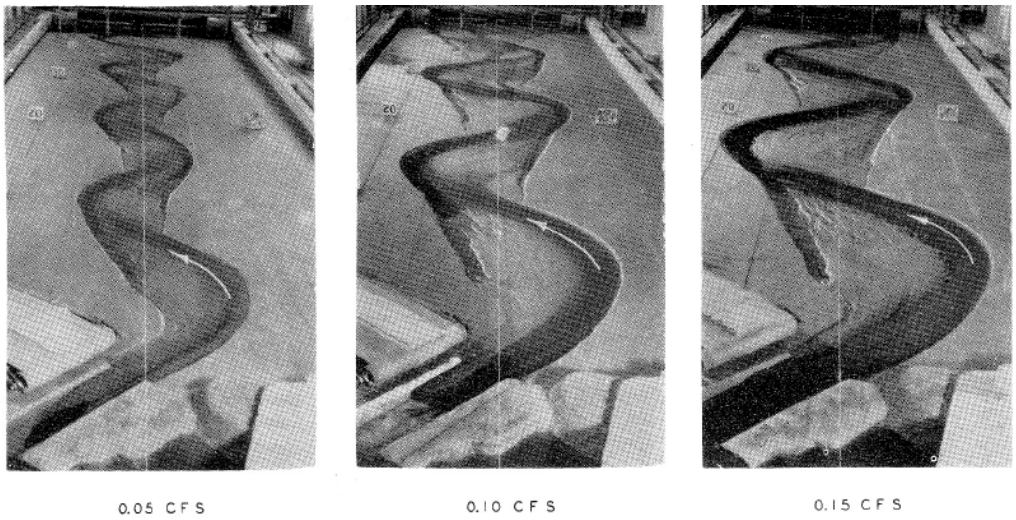

Figure 3.17 Effect of Discharge on the Size of Bend (Friedkin 1945)

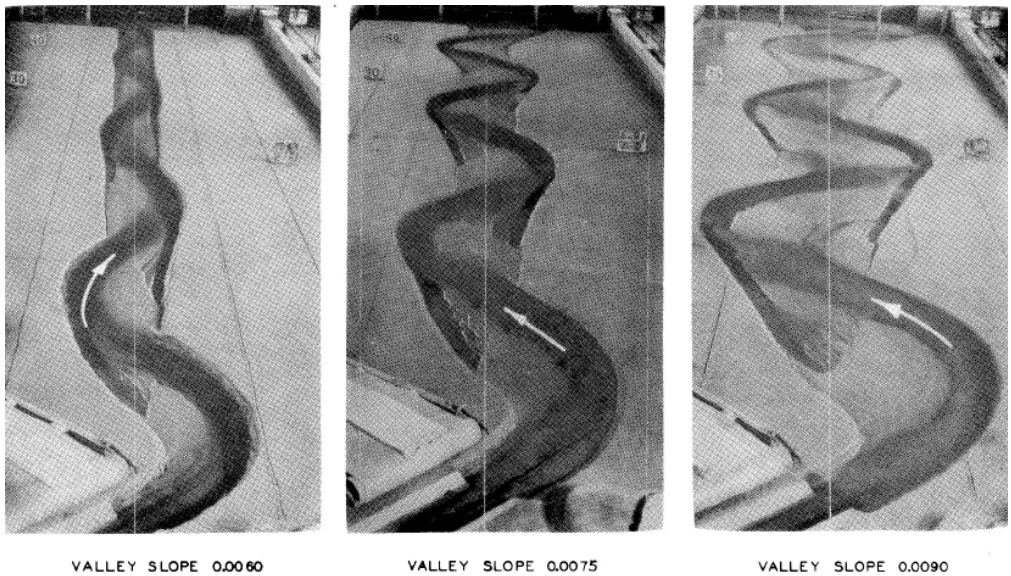

Figure 3.18 Effect of Valley Slope on the Size of Bend (Friedkin 1945)

The effects of changes in the initiating angle of attack were studied by varying angles from 30° to 45°, and then to 60° (see Figure 3.19). All other conditions were the same. It is quite obvious that the larger attack angle created the larger meandering bend.

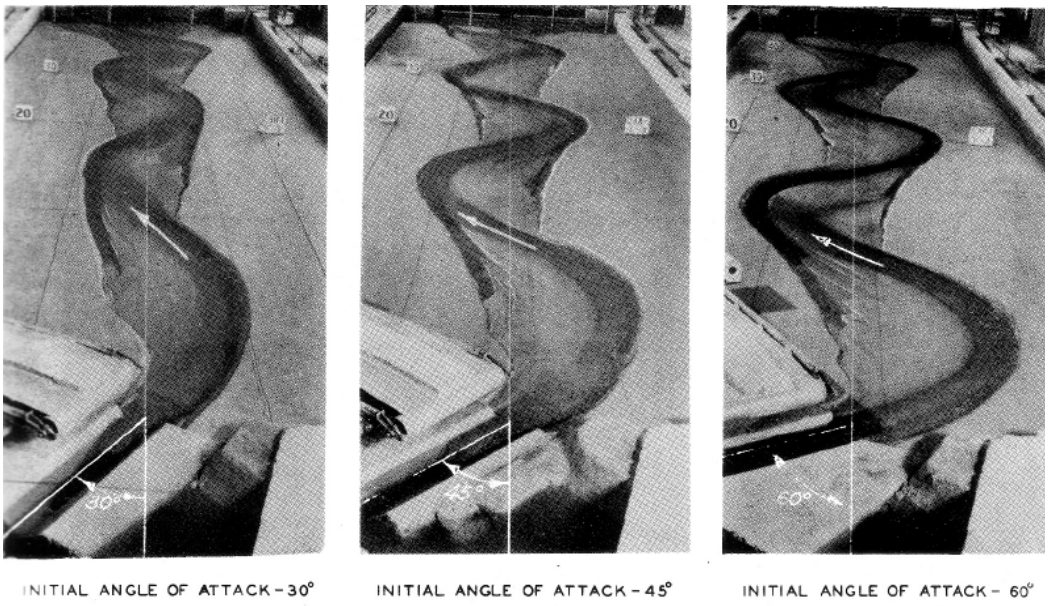

Figure 3.19 Effect of Attack Angle on the Size of Bend (Friedkin 1945)

3.2.2 Schumm and Khan (1972)

Schumm and Khan examined the behavior of the model channel in a flume with respect to slopes and sediment loads. It was found that sediment loads are strongly related to slopes and that channel pattern changes dramatically when slope and sediment load exceed their threshold values. At a low slope and sediment load, the channel tends to keep the original pattern, and at a very high slope and sediment load, the channel altered to a braided channel. The meandering channel pattern can be produced only if the channel meets the required criteria: slope and sediment load are higher than the threshold

values, but lower than the upper bound values in which a braided channel is developed. These trends are illustrated in Figure 3.20 by plotting channel sinuosity versus slopes from the experimental results, in which sinuosity is defined as the ratio of channel or thalweg length to the straight line distance along the flume.

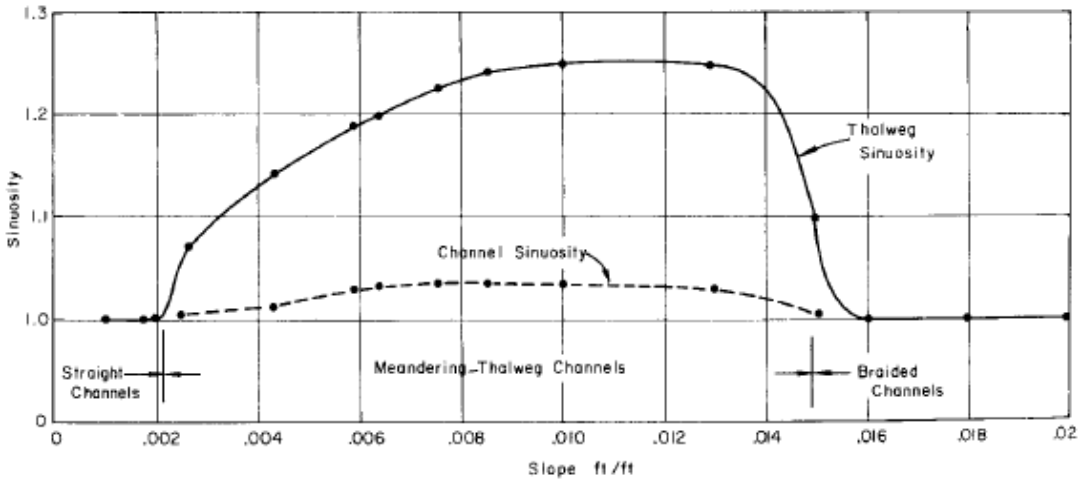

Figure 3.20 Relation between Slope and Siuosity (Schumm and Khan 1972)

3.2.3 Nakagawa (1983)

Nakagawa investigated the effect of the different boundary conditions at the wetted perimeter on the channel meandering by conducting a series of flume tests. He proposed that the shear stress distribution in the transverse direction is one of the primary parameters affecting channel meandering. Based on the experimental results, it was found that there is a prerequisite criterion in terms of a ratio of two shear forces at the channel bottom and bank to initiate river meandering. When the ratio of the total shear force along the channel bottom to that at the bank is lower than 0.2, the channel will meander.

A total of five flume tests as shown in Table 3.2 were performed in a concrete flume which was 25 m (83.3 ft) long and 2 m (6.7 ft) wide. The flume was filled with sand 30cm (1 ft) deep except for the very beginning of the upstream. After leveling the sand surface to a designed slope, an initial channel was carved by a sand scraper. A constant-head tank connected to the entrance of the flume provided the desired constant flow rate, and a magnetic flow meter was installed to measure the flow rate. The sand with a median grain diameter d_{50} = 0.43 mm was used in the tests, and its specific gravity is about 2.65. There seemed to be no sediment supply at the entrance of the flume. Figure 3.21 shows a schematic diagram of the experimental setup.

Table 3.2 Hydraulic Parameters in Flume Tests (after Nakagawa 1983)

	Experiment No.						
Parameter	1	2	3	4		5	
Froude No.	0.50	0.44	0.61	1.21	2.18	1.60	1.45
Mean flow velocity (cm/s)	20.2	17.0	30.1	31.8	37.4	32.8	36.7
Mean water depth (cm)	1.7	1.5	2.5	0.7	0.3	0.43	0.65
Elapsed time (min)	20	43	32	20	20	20	20
Long. distance (m)	3.7	8.0	4.0	2.0	2.0	2.0	2.0

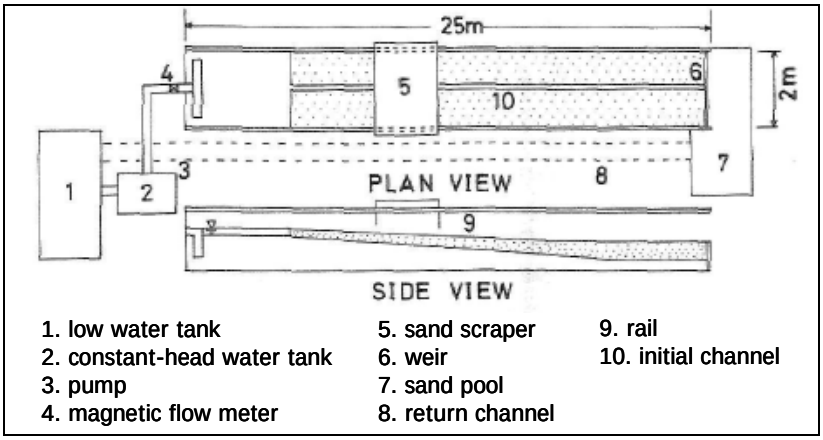

Figure 3.21 Schematic Diagram of the Flume Setup (after Nakagawa 1983)

Figure 3.22 shows the dimensions of the initial trapezoidal cross-section and the boundary conditions for each case. As seen in the figure, only the first test was conducted in a fully erodible-bed, and the other three tests (Exp. 2, 3, and 4) were done in a partially erodible-bed where either the lateral or vertical erosion could occur. The photos taken during the first test are shown in Figure 3.23. A propagation phenomenon is clearly observed in the later stage at t = 305 min, where the amplitudes of the meandering bends are getting bigger progressing from the upstream to the downstream. This might be due to the lack of sediment supply as reported by a previous study (Friedkin 1945).

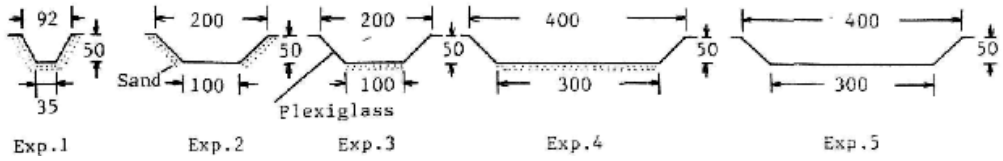

Figure 3.22 Dimensions of the Cross-sections and Boundary Conditions (Nakagawa 1983)

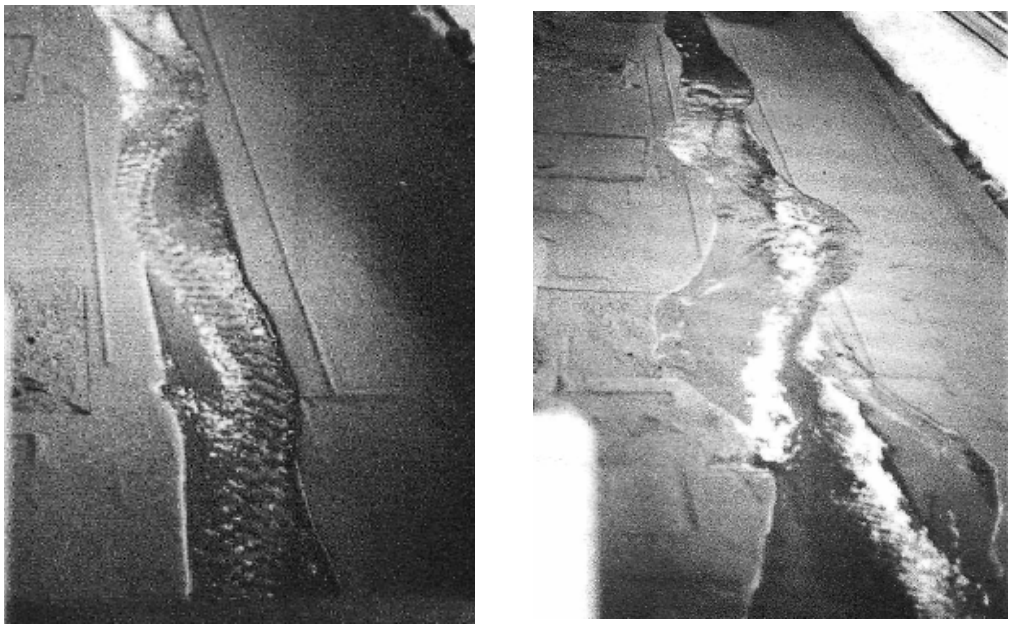

(a) After 91 min (b) After 305 min

Figure 3.23 Photos from Flume Test (Nakagawa 1983)

3.2.4 Smith (1998)

A meandering river is common in natural rivers, but it is quite difficult to reproduce well defined and highly sinuous meandering channels in physical model tests (Smith 1998). Smith used a small-scale flume with a mixture of light, fine grained sediment to simulate meandering streams. A total of three experiments were conducted with different combinations of rock flour, diatomaceous earth, kaolinite, cornstarch, calcined white China clay as shown in Table 3.3. The first case, in which a mixture of diatomaceous earth and calcined white China clay was used, turned out to be the most successful test.

The flume tests were performed in a tilting flume, 3 m (10 feet) long, and 1.2 m (4 feet) wide. The water circulation system consisted of a small pump, collection tank at

the downstream. The flow rate was determined by measuring the volume of water for a specific duration. After mixing the different materials as predetermined, it was moistened and leveled. A straight initial channel was carved, and the slope was adjusted. A sediment supply at the upstream was fed at approximately 12 hours intervals. Note that the sediment was fed not continuously but intermittently, and a noticeable effect of sediment supply was not observed during the experiments.

Table 3.3 Experimental Parameters of the Stream Flow (after Smith 1998)

	DE + CWC	Cornstarch + CWC	Rock flour + Kaolinite
Flow rate (ml/s)	9	35	45
Slope	0.015	0.020	0.025
Flow velocity (cm/s)	15 – 20	18 – 22	18 – 25
Mean water depth (cm)	~ 0.5	~ 0.5	~ 0.7
Froude No.	0.68 – 0.91	0.82 – 1.00	0.69 – 0.95
Reynolds No.	750 – 1000	900 – 1100	1250 - 1750

Note: DE = diatomaceous earth, CWC = calcined white China clay

The photos taken during the first test are shown in Figure 3.24. It was reported that channel migration had slowed after 250 hours, and the channel seemed to reach an equilibrium status after 500 hours, which means almost no change in the plan form was observed after 250 hours. In fact, this conforms to the proposed hyperbolic model in our research. Figure 3.25 shows the typical sequence of meander development observed during his flume tests.

(a) Broad View (flow runs from up to bottom)

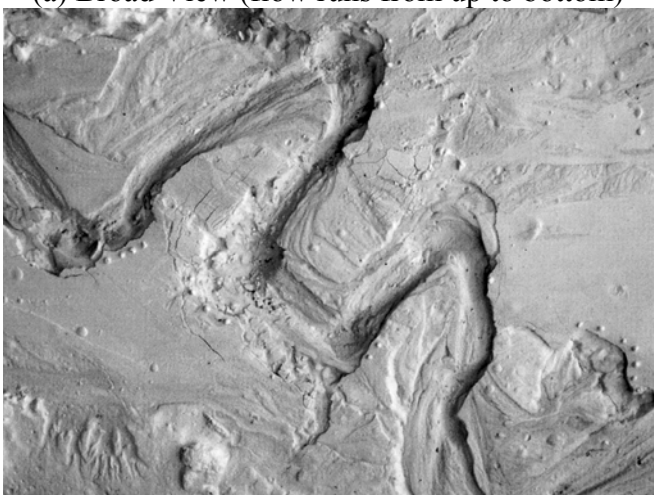

(b) Detailed View (flow runs from left to right)

Figure 3.24 Photos from Flume Test (Smith 1998)

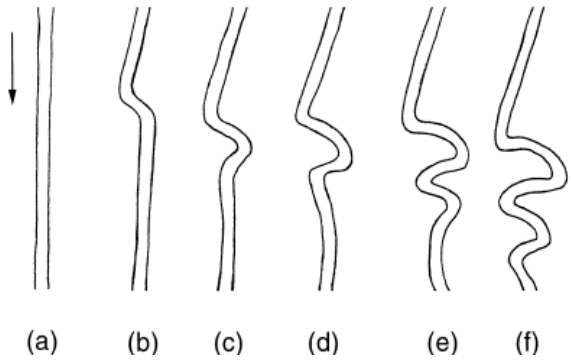

Figure 3.25 The Sequence of Meander Development (Smith 1998)

3.2.5 Nagata et al. (2000)

Nagata et al. developed a numerical model to examine bed deformation and bank-line movement in 2D plan form. The 2D continuity and momentum balance equations were solved to obtain the unsteady open channel flow, filed in a moving boundary-fitted coordinate system. To predict the movement of the bank-line associated with erosion, a sediment transport model was developed based on the theory of non-equilibrium sediment transport reported by Nakagawa and Tsujimoto (1980). An intermittent bank erosion model (Hasegawa 1981) was employed to model the bank collapse and deposition.

Laboratory experiments were conducted to verify the proposed model. They used a tilting flume, 10 m (33 feet) long, 1 m (3.3 feet) wide and 0.2 m (0.7 feet) deep, as shown in Figure 3.26. The initial meandering channel plan forms were designed to be a sine-generated curve with 2 m (6.6 foot) wavelength and a 30° attack angle at the entrance of the channel. A trapezoidal cross-section was used for the initial condition with 14 cm (5.5 inch) in bottom width, 30 cm (11.8 inch) in top width, and 4 cm (1.6 inch) in bank height. A total of four wavelengths were prepared, but the measurement data from the second wavelength portion from the upstream were used due to the disturbances near the entrance and exit. The relatively uniform sand, with d_{50} of 1.42 mm, was used, and sediment was fed manually at the entrance of the upstream during the experiments. The plan form variations at several different time steps were measured by taking photographs. A point gauge and a laser bed profiler were used to measure bed profiles. Since the purpose of the flume tests was to validate their numerical model, no

specific relationship of meander migration from the experiments was proposed in this study.

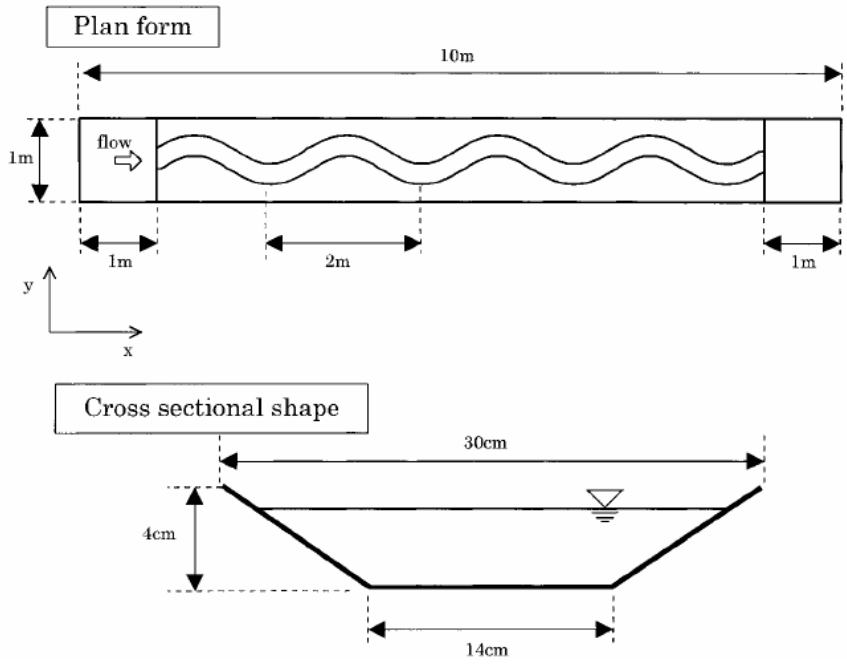

Figure 3.26 Experimental Setup (Nagata et al. 2000)

The calculated plan forms at the different time steps by the proposed model are compared with the experimental results in Figure 3.27; there is a reasonable agreement. Figure 3.28 demonstrates the accuracy of the model regarding the temporal profiles of the cross-sections by plotting the calculated and observed results together. The simulated results follow a similar pattern of the cross-sectional change in the measured data.

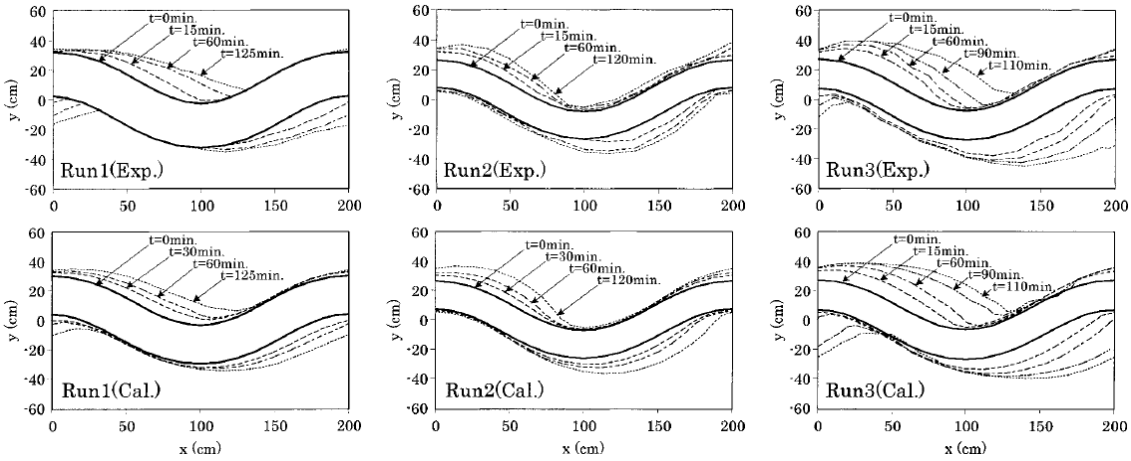

Figure 3.27 Temporal Changes in Plan Forms (Nagata et al. 2000)

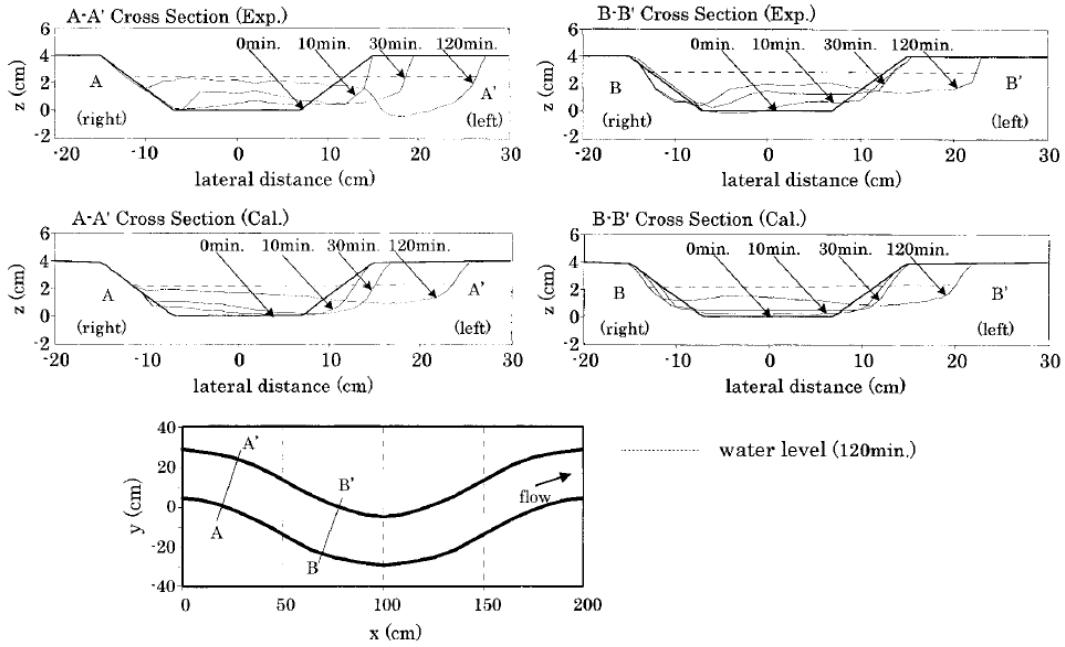

Figure 3.28 Temporal Changes in Cross-Sectional Profiles (Nagata et al. 2000)

3.3 RISK ANALYSIS FOR MEANDER MIGRATION

Nowadays probabilistic risk analysis is a popular approach in many engineering fields to estimate the probability of failure or to evaluate the confidence level associated

with any prediction result. The past relevant works by other researchers with regard to risk analysis for the soil erosion problem were studied and summarized.

3.3.1 Briaud et al. (2003)

Briaud et al. (2003) developed the SRICOS-EFA method to predict the scour depth in clay as a function of time in a probabilistic way. Future hydrographs (daily discharge versus time) are a main input parameter to run their model. Since future hydrographs are unknown, and it is not realistic to make a deterministic prediction, they developed a new technique to generate equally possible future hydrographs in a probabilistic manner. The frequency distribution curve for all the floods in a historical hydrograph for a given duration are first populated, then the distribution is randomly sampled, and finally a future hydrograph for the prediction period is generated. Note that this future hydrograph has the same mean and standard deviation as the past hydrograph. This process is repeated to generate 10,000 different sets of future hydrographs. A final scour depth at the end of the design life is calculated according to each hydrograph. These 10,000 final depths of scour are then plotted to create a frequency distribution plot with a mean and standard deviation as shown in Figure 3.29.

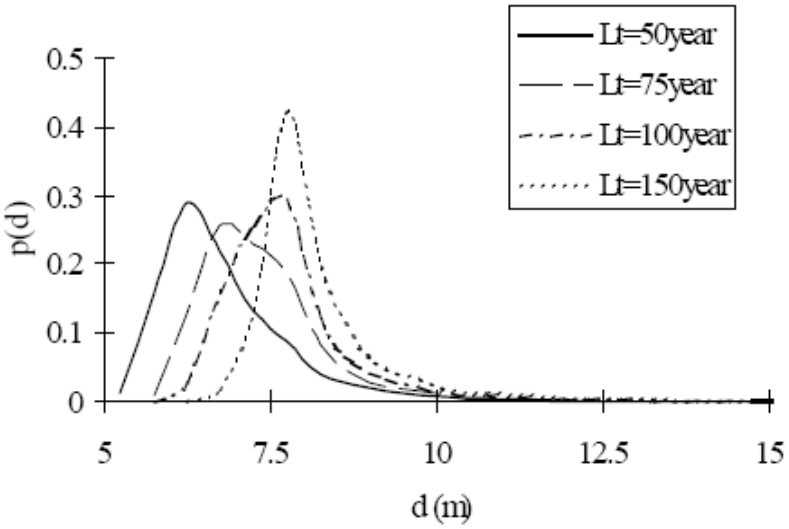

Figure 3.29 Probability Distribution of Scour Depth, *d*, for Different Lengths of the Project Life, L_t (Briaud et al. 2003)

This analysis can be used to estimate the probability of exceedance R associated with the choice of different design values of scour depth and project lives. By definition, R is the probability that the design conditions are exceeded during the life of the structure. From the probability distribution of d (Figure 3.29) it is possible to determine the cumulative distribution function (CDF) of d (Figure 3.30). R is then estimated as the probability of exceedance. This analysis provides a statistical framework that can be used in a cost-benefit study of bridge foundation design.

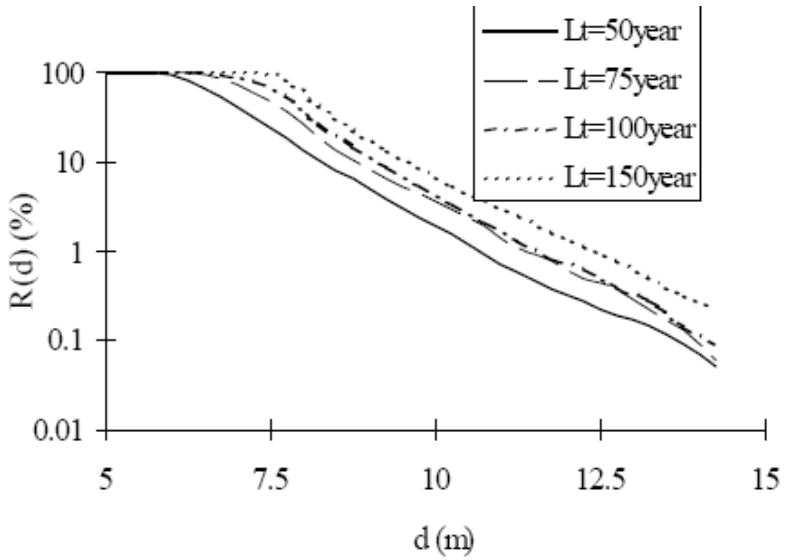

Figure 3.30 Risk Associated with Different Design Values of the Final Scour Depth, *d*, and Different Lengths of the Project Life, L_t (Briaud et al. 2003)

3.3.2 Lagasse et al. (2003, 2004a, 2004b)

Lagasse et al. (2003, 2004a, 2004b) conducted National Cooperative Highway Research Program (NCHRP) research Project 24-16. The final outcomes from this research were a stand-alone handbook for predicting stream meander migration using historical aerial photos, maps, and the computer program, "The Data Logger and Channel Migration Predictor". Their methodology is based on time-sequence maps and an extrapolation technique. First, circles that represent a meandering bend at three different times are fitted, as shown in Figure 3.31(a). Then, the direction of new migration can be determined by extrapolating the previous direction of movement (Figure 3.31(b)). Finally, the new location of the center and the magnitude of the radius are linearly extrapolated with respect to time (Figure 3.32). The equations for the extrapolation are Eqs. 3.6A to 3.6C.

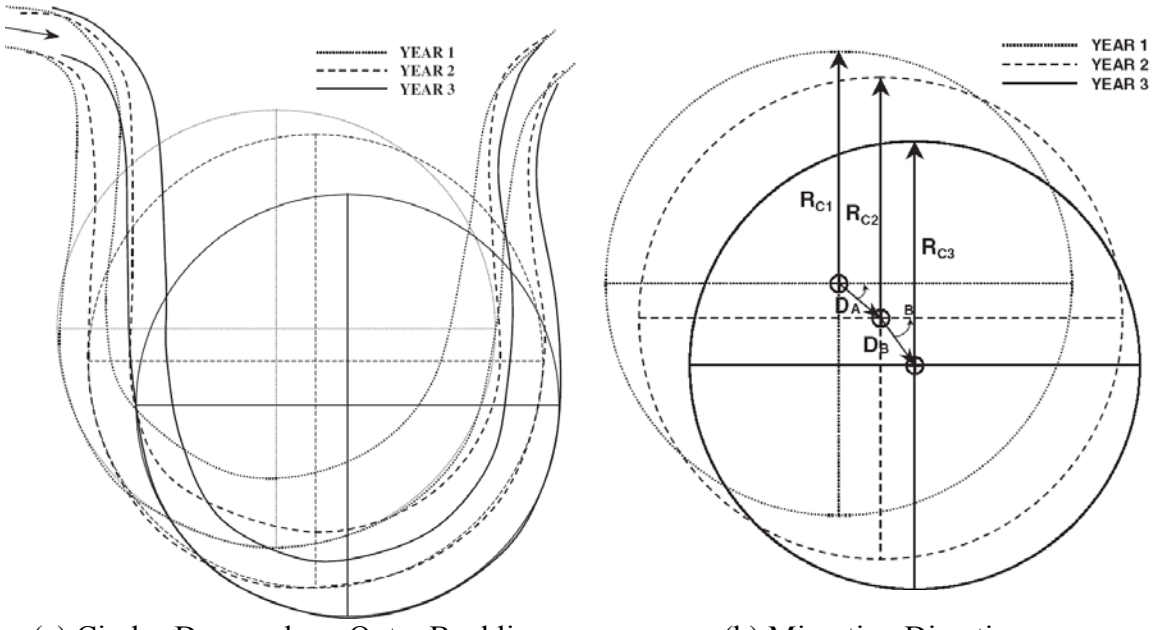

(a) Circles Drawn along Outer Bankline (b) Migration Direction

Figure 3.31 Time-Sequence Maps and Extrapolations (Lagasse et al. 2004b)

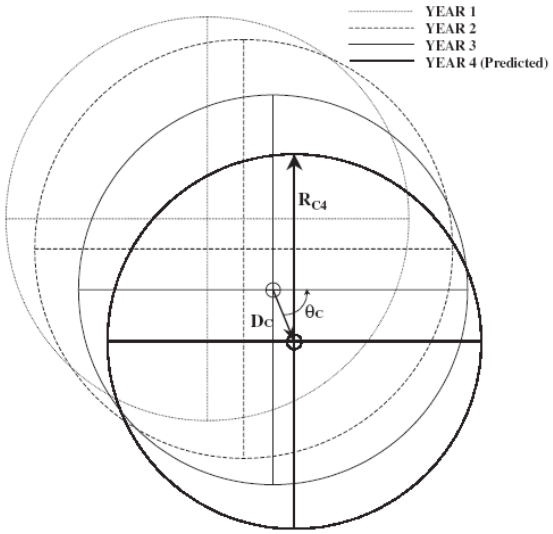

Figure 3.32 Predicted Position and Radius of Curvature of the Circle that Defines the Outer Bank of the Hypothetical Channel in Year 4 (Lagasse et al. 2004b)

$$R_{C4} = R_{C3} + \left[\left(\frac{(R_{C3} - R_{C2})}{(Y_B)} \right) (Y_C) \right] \tag{3.6A}$$

$$D_C = \left(\frac{(D_B)}{(Y_B)} \right) (Y_C) \tag{3.6B}$$

$$\theta_C = \left[\left(\frac{(\theta_B - \theta_A)}{(Y_B)} \right) (Y_C) \right] + \theta_B \tag{3.6C}$$

Briaud et al. (2001a) conducted a case study to evaluate this approach. A total of six sites were selected for the evaluation: Brazos River at SH 105 (two cases), Nueces River at US 90, Trinity River at FM 787, and Guadalupe River at US 59 (two cases). The result of the case study showed that it provided a reasonably satisfactory prediction of the radius of the meandering bend, but the direction of migration was predicted in the opposite direction to the historical data in some cases.

As part of this study, a database of measured bend migration was generated, and a statistical analysis was performed to develop guidance in estimating the normalized extension and translation migration with respect to the channel width for sites where aerial photos are not available. The procedures and guidance are given in the form of cumulative percentage plots. Two separate graphs produced from the case study are shown in Figures 3.33 and 3.34. There are four different categories of the channel such as Brice Class A, B_1, B_2, and C. For example, for meanders of the type Brice C sites, the probability of the normalized extension migration reaching 0.02 channel widths per year or less is 79 percent, according to Figure 3.33. For the same probability of 79 percent, the normalized translation migration, according to Figure 3.34, is 0.036 channel widths per year.

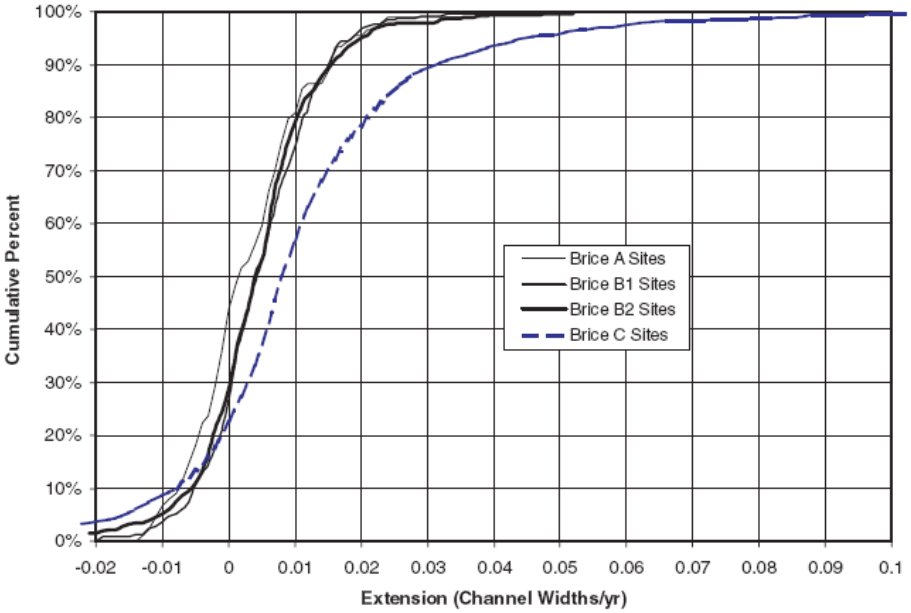

Figure 3.33 Cumulative Percentage of Extension Migration (Lagasse et al. 2004b)

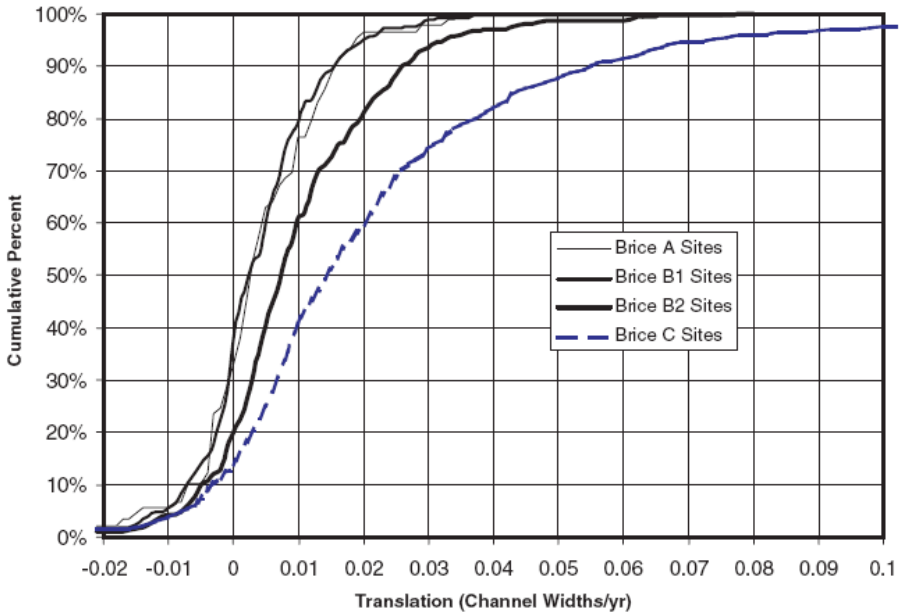

Figure 3.34 Cumulative Percentage of Translation Migration (Lagasse et al. 2004b)

Figure 3.35 shows example movements in percentages for a 30-year time period. This approach can be meaningful for sites in which historical records are not available.

The drawbacks of this method are that it cannot incorporate either a change in soil condition or a future hydrograph different from the past hydrograph. The advantages are its simplicity and its field-scale soil specifications.

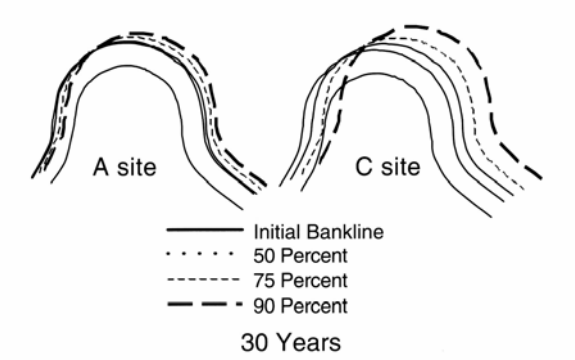

Figure 3.35 Example Movement Percentages for a 30-Year Time Period (Lagasse et al. 2004b)

CHAPTER IV

FLUME TEST IN CLAY

This chapter investigates channel meander migration in clay by conducting physical modeling in a large-scale flume. The approach is to vary each primary parameter obtained from dimensional analysis while keeping the remaining parameters constant. The effect and impact of each individual parameter on meander migration can then be examined to provide a basis for a parametric study.

4.1 DIMENSIONAL ANALYSIS

According to the physical considerations on meander migration phenomenon, the primary factors affecting the channel bank-line migration distance M of any point along the channel can be divided into four major categories: geometry, hydraulic condition, soil property, and the others not listed above. The parameters of geometry (Figure 4.1) consist of the channel width W, the radius of curvature of the channel R, the angle of the channel bend ϕ, and the channel bed slope s. The parameters of hydraulic condition are the fluid density ρ_w, the fluid viscosity μ_w, the average flow velocity U, and the water depth h. The parameter of soil property is the critical shear stress τ_c at which the bank erosion is initiated. The other parameters include external forcing, vegetation condition, and obstacles for the flow such as manmade structures, debris, etc. All of the parameters in the first three categories, as well as gravitational acceleration g, are considered in this research. The relationship between these parameters is formulated as:

$$M = f_0(W,\ R,\ \phi,\ s,\ \rho_w,\ \mu_w,\ U,\ h,\ \tau_c,\ g) \tag{4.1}$$

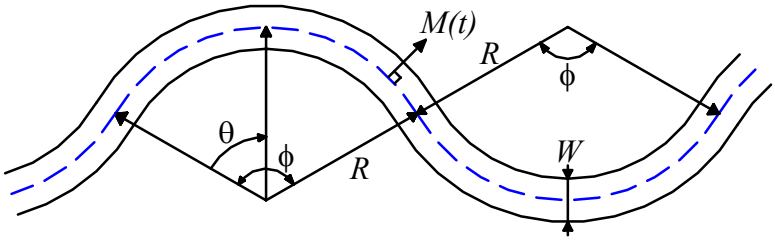

Figure 4.1 Channel Configurations

After the dimensional analysis, to calculate the migration distance M, the following relationship is obtained:

$$\frac{M}{W} = f_1\left(\frac{R}{W},\ \phi,\ Fr, s,\ Re,\ \frac{h}{W},\ \frac{\tau_c}{\rho_w U^2}\right) \tag{4.2}$$

Where,

Re = Reynolds Number = $\rho_w U h/\mu_w$

Fr = Froude Number = $U/(gh)^{1/2}$

The water depth depends on the flow rate and the channel bed slope in an open channel. If the flow rate and the cross-section are constant along the channel, a constant water depth is obtained by adjusting the channel bed slope. In other words, the channel bed slope is a dependent parameter of the flow rate and water depth. It is therefore ignored in the experimental study. Since the estimated Reynolds number in the experiments is larger than 15,000, the effect of fluid viscosity is minimal, so it can also be ignored (Munson et al. 2006). The dimensionless critical shear stress $\tau_c/\rho_w U^2$ is converted into the critical Froude number, Frc at which bank erosion is initiated. Removing the negligible parameters from the above, the equation is simplified to:

$$\frac{M}{W} = f_2\left(\frac{R}{W},\ \phi,\ Fr,\ Frc\right) \tag{4.3}$$

To predict the meander migration distance along the channel, it is necessary to move the whole channel point by point. In other words, a new parameter that represents the arbitrary location of interest within a certain channel bend should be included. The additional parameter θ, which varies from 0 to ϕ, is employed to denote the position along the channel. Finally, the equation from dimensional analysis is expressed as:

$$\frac{M}{W} = f_3(\frac{\theta}{\phi}, \frac{R}{W}, \phi, Fr, Frc) \tag{4.4}$$

4.2 EXPERIMENTAL SETUP

The meander experiments in clay were conducted in a large basin located on the second floor of the Hydromechanics Laboratory at Texas A&M University (Figure 4.2). The experimental setup consisted of these parts: test flume with the water circulation system, flow meter calibration, data measurement system, and soil.

4.2.1 Test Flume Setup

The basin in the Hydromechanics Laboratory is 22.0 m (72.6 feet) long, 10.0 m (33 feet) wide, and 0.9 m (3 feet) deep. The basin was filled with approximately 200 tons of sand left from the previous flume tests (Yeh 2007) in sand. Sand was used in order to not only save on clay cost but also to minimize the maintenance effort of keeping moisture on the clay.

For each case, a guide channel in the sand bed was carved to put the clay banks along the predetermined channel and to form the channel geometry. To reduce the scale effect, the channel was designed to maximize the scale ratio while containing at least three curved bends. A straight channel was connected to each end of the curved channel with a transition, which is a curved bend of one-half of the bend angle, ϕ. The straight

section was kept long enough so the flow became fully developed before it entered the first curved bend. The initial cross section of the channel is of rectangular shape with a width of 60.0 cm (23.6 inches) and a depth of 12.0 cm (4.7 inches) (Figure 4.3 (d)). Plywood plates were laid at the bottom of the channel so only the banks would erode.

Figure 4.2 Experimental Setup in the Hydromechanics Laboratory

During the first pre-test with a trapezoidal cross section of the channel (Figure 4.3 (a)), almost no erosion was observed on the side walls along the channel. Thus, no lateral movement of the river occurred, as shown in Figure 4.4. Instead, erosion of the bottom of the channel was observed. This is attributed to the relatively low shear stress on the walls as compared to the higher shear stress on the bottom of the channel.

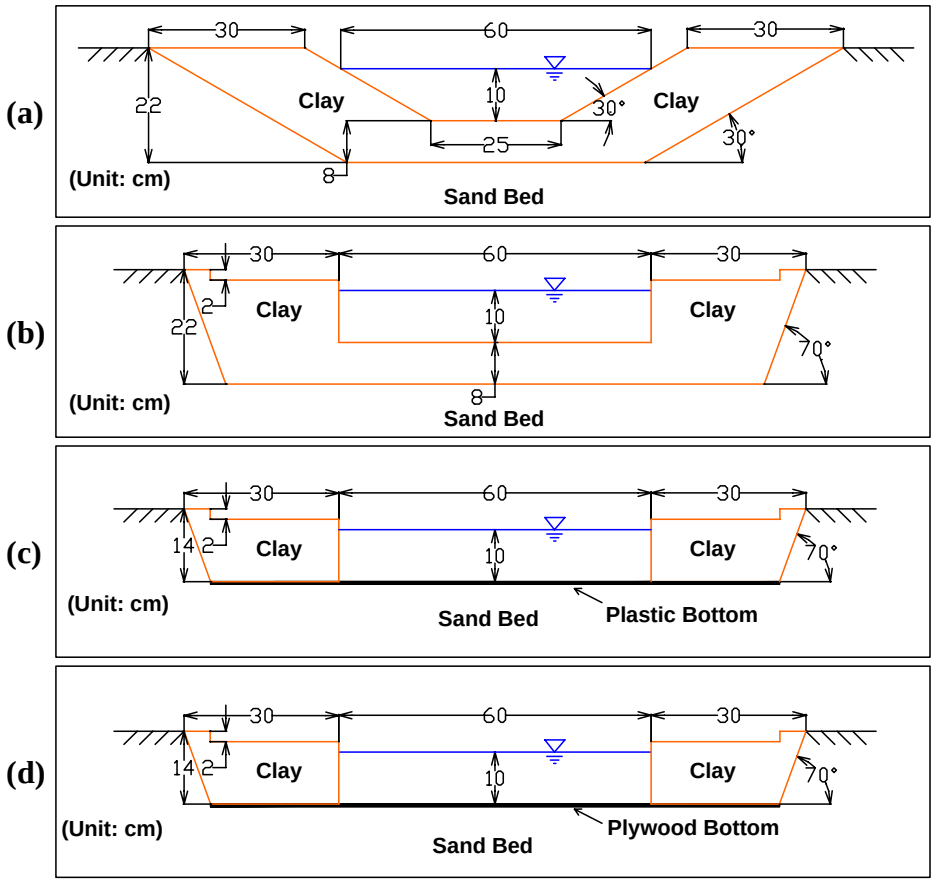

Figure 4.3 Trial Cross Sections: (a) Case 01, (b) Case 02, (c) Case 03, and (d) Case 04 (Finally Adapted Cross Section)

(a) t = 0 hr (b) t = 20 hr

Figure 4.4 Photos of Clay Test Case 01 (R/W = 4, ϕ = 120°, Fr = 0.50)

In the second pre-test, the cross-sectional shape was changed from a trapezoidal to a rectangular channel which had vertical walls on both sides. This increased the shear stress on the side walls so that the lateral movement of the river could be simulated (Figure 4.3 (b)). This test did induce side wall erosion along the channel, but there was still excessive bottom erosion as well, as shown in Figure 4.5. A huge amount of bottom clay was required to accommodate this bottom erosion. Since the clay cost and preparation time for the bottom layer were prohibitive, a non-erodible bottom such as a thin plastic sheet was used.

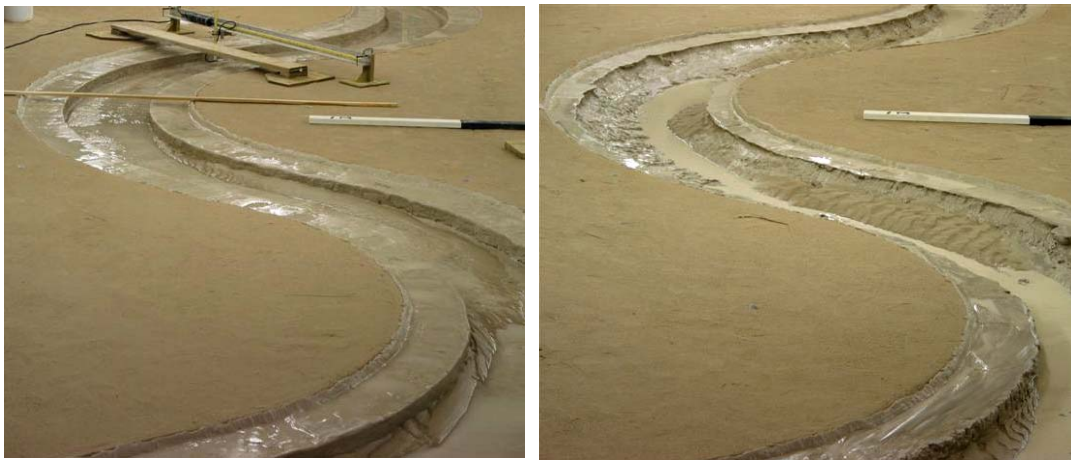

(a) t = 6 hr (b) t = 106 hr

Figure 4.5 Photos of Clay Test Case 02 (R/W = 4, ϕ = 120°, Fr = 0.50)

In the third pre-test, the bottom material was changed to the plastic sheets (Figure 4.3 (c)) while keeping the vertical walls on both banks. It was found that the roughness of the plastic was too low compared to that of the clay. As a result, local flow velocity on the bottom increased, causing vibration of the plastic and turbulent flow (Figure 4.6). Therefore, the bottom layer was replaced with treated plywood to match the roughness of clay and increase the stiffness to avoid excessive vibration (Figure 4.3 (d)).

(a) t = 0 hr (b) t = 184 hr

Figure 4.6 Photos of Clay Test Case 03 (*R/W* = 6, ϕ = 65°, *Fr* = 0.50)

To investigate the impact of a non-erodible channel bottom with respect to magnitude of migration distance, the measurement data from Case 02 (erodible bottom) are compared with those from Case 07 (non-erodile). The only difference between these two cases is the bottom condition, where the radius-to-width ratio R/W is 4 and the bend angle ϕ is 120° in both cases. It is found that the channel with non-erodible bottom produces somewhat larger migration than the channel with erodible bottom, which means the prediction results, based on the non-erodible bottom condition, will be conservative. The comparison results of two cases are shown in Figure 4.7. The measurement data from Case 02, however, is available only for the early stage during the test, and thus this conclusion might be applicable only for the early stage.

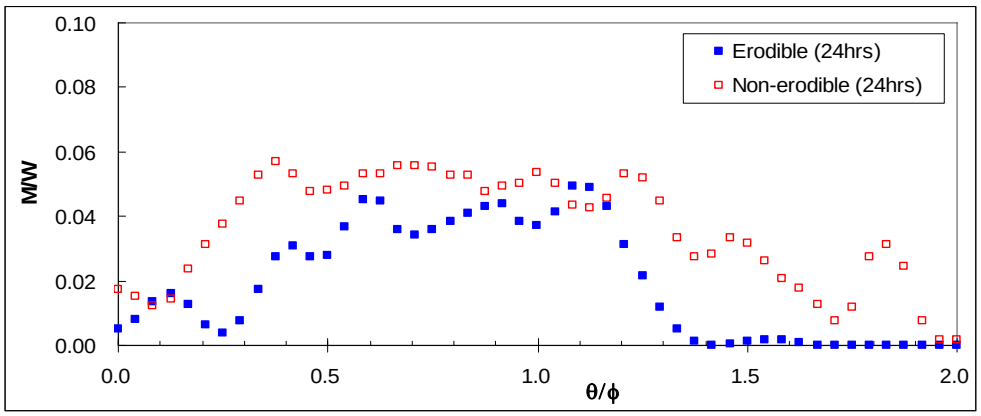

(a) Right Bank

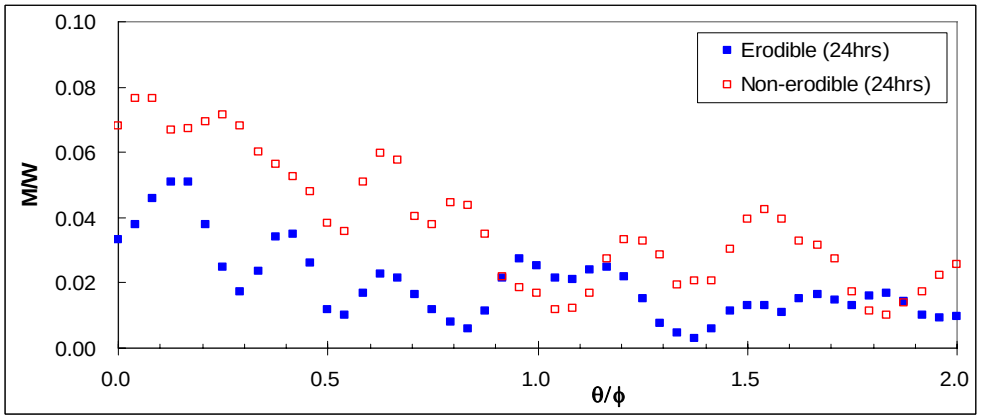

(b) Left Bank

Figure 4.7 Migration Distance in Erodible versus Non-erodible Bottom

The channel slope was carefully controlled by adjusting the slope of the sand bed to maintain a constant initial water depth of h = 10 cm (3.9 inches) along the channel with a maximum discrepancy less than 1.0 cm (0.4 inch) which corresponds to 10 percent of the design depth in each test case. The water circulation system consisted of a pump, a constant-head water tank, a piping system, a sump in the basement, a clay channel, and two reservoirs before the entrance of the channel and after the exit of the channel. A sluice gate after the downstream reservoir controlled the water depth in the channel.

The pump was located on the ground floor, while the basin was on the second floor. Water pumped from the sump tank in the basement into the constant-head water tank through the piping system which then flowed into the clay channel passing the upstream reservoir (Figure 4.8). The function of the upstream reservoir was to minimize turbulence before water flow into the clay channel. A 3-inch PVC diverting pipe in the constant-head water tank eliminated the excessive pumping capacity. In addition, a 3-inch PVC overflow pipe, located at about 3/4 of the height of the water tank, kept the elevation head constant. The water from the water tank was supplied through two PVC pipes (3-inch and 4-inch) to maximize the amount of water supply into the upstream reservoir. Since the 3-inch pipe was kept fully open during the experiments, there was no need for a flow meter. One flow meter was installed on the 4-inch pipe, however, to be able to adjust the amount of water.

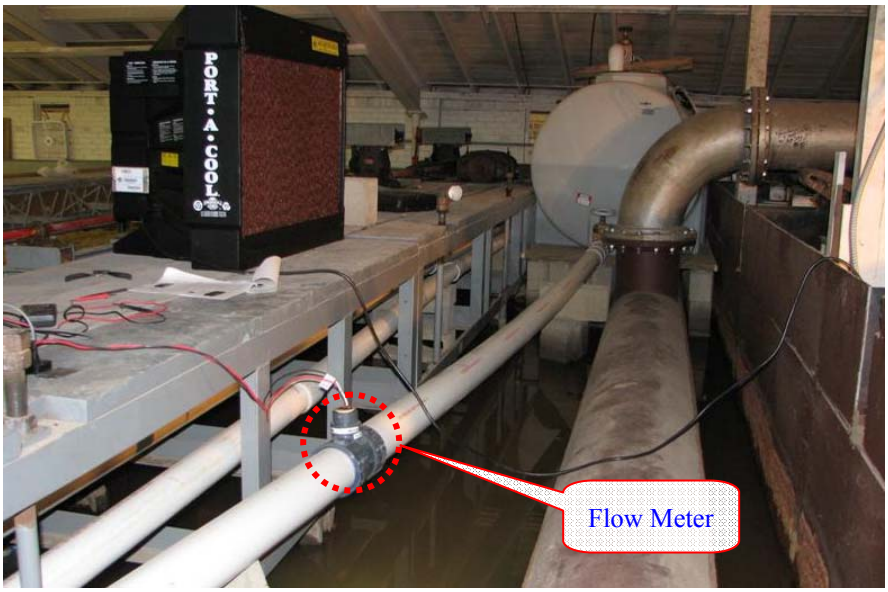

Figure 4.8 Upstream Reservoir and Water Tank

4.2.2 Flow Meter Calibration

The flow meter is a device to measure the flow rate. The flow meter used in this study consisted of two components: a flow sensor and a flow transmitter (Figure 4.9). The flow sensor was spliced to the 4-inch PVC pipe. It had an impeller inside the sensor so that it could generate a low impedance wave signal which was transmitted with a frequency proportional to the flow rate. The transmitter then converted the signal from the sensor to a linear analog signal. A digital multi-meter was connected to the transmitter to read the output current. A calibration curve showing the relationship between the actual flow rate inside the pipe in gallons per minute (GPM) and the output current in milliampere (mA) from the transmitter was needed.

(a) Flow Sensor (b) Flow Transmitter

Figure 4.9 Flow Meter for 4-inch PVC Pipe (source: www.dataindustrial.com)

The best way to calibrate the flow meter is to conduct the calibration not for the flow meter itself but for the installed water circulation system in the basin instead. This

method ensures the most accurate result for the specific setup condition of the water supply system. The procedures of the calibration of the flow meter are as follows:

1. Calibrate the volume of the upstream reservoir by using a bucket that has a known volume.
2. Adjust the flow rate to a certain level and record the output current (mA).
3. Filled the upstream reservoir with water and record the required time so that the flow rate (GPM) can be calculated.
4. Repeat steps 2 and 3 several times with a different flow rate each time.

The calibration results are plotted on Figure 4.10; the linear trend line was used to adjust the flow rates for the experiments in the basin. Note that the full capacity of the 3-inch pipe (150GPM), which was kept fully open during the experiments, should be added to the flow rate from this trend line to get the total flow rate.

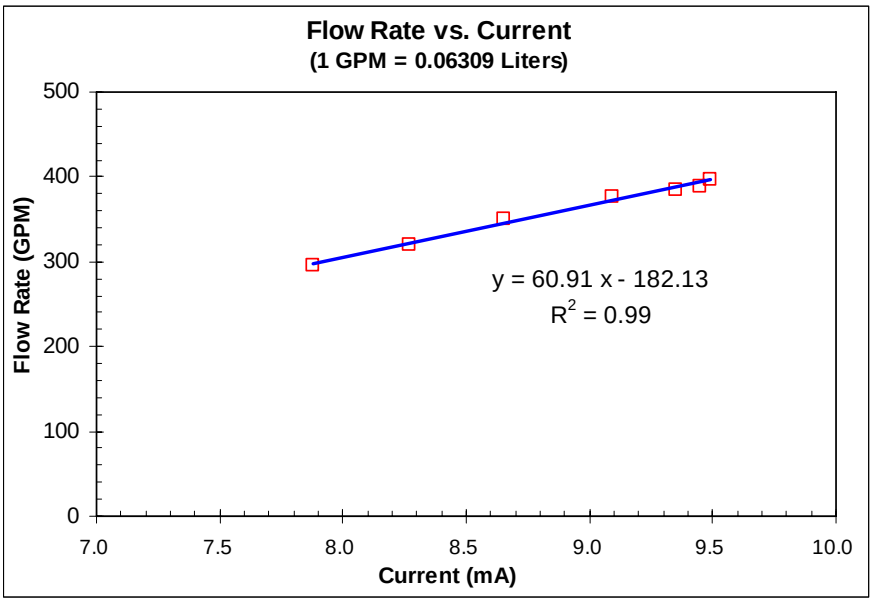

Figure 4.10 Calibration of the Flow Meter – Calibration Curve

4.2.3 Measurement of Geometry and Flow Velocity

Data acquisition during the test included water depth, geometries of the bank-lines, water surface elevation profile, and water velocity. Water depth was measured at the channel center line using a ruler. For the geometry of two bank-lines, a laser coordinate-measurement system was used, as shown in Figure 4.11. Before this laser system was selected, digital photogrammetry was considered for the geometry data acquisition because it has been frequently used as a surface monitoring tool in fluvial research in both flume and natural river channel studies (Lane et al. 2001). There were two major issues with employing this technique, however, including a high cost to setup the necessary equipment in a large-scale flume and reflection problems due to the water surface. As a result, a laser coordinate system was designed instead. In this system, an instrument bridge spanning the flume over the test section was used to mount the laser. Two coordinate scales were installed: one on the side wall of the flume for the x direction, and one on the instrument bridge for the y direction. Once the bridge moved to a pre-designated x-coordinate position, the y-coordinate was obtained by sliding the carrier on the bridge to the interfaces between the clay banks and water. The measurement error in this system is 1.0 cm which is 1.7 % of the initial channel width.

The water surface elevations were measured for several designated cross sections at certain time intervals. A plumb bob and a digital level measured the changes in water surface elevation throughout the tests, as shown in Figure 4.12. An analog multi-meter connected to two electrical wires detected current changes between the plumb bob and the wires through the ground when the tip of the plumb bob touched the water surface. In

addition, a digital level was used to take readings of relative changes in the elevation from a scale attached to one of the wires. This system avoided possible extensive calibration work since all readings are independent of the measurement locations. The measurement error for water surface elevation is 1.0 mm which is 1.0 % of the initial water depth.

Figure 4.11 Carrier with Laser Sliding on the Bridge for Transverse Coordinate (*y*-direction) Measurement

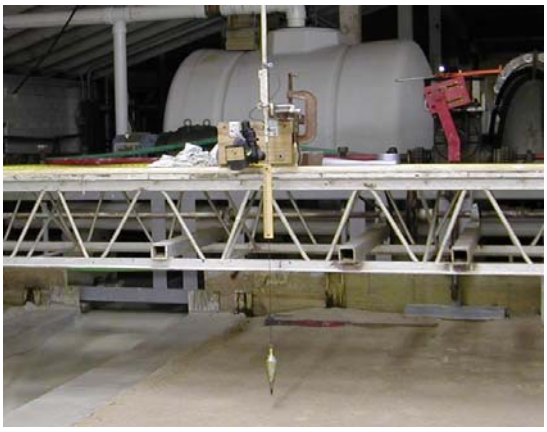

(a) Attached Scale and Plumb Bob

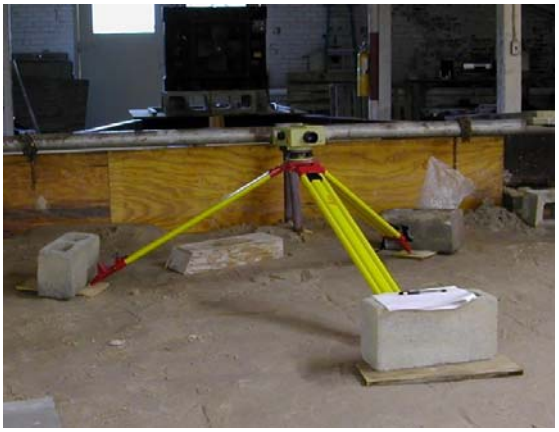

(b) Digital Level

Figure 4.12 Carrier with Laser Sliding on the Bridge for Transverse Coordinate

Acoustic Doppler velocimetry (ADV) uses the acoustic Doppler Effect to measure the water velocity by measuring the velocity of small particles in the water (Lane et al. 1998). It has been widely used to measure the velocity of water in every type of hydraulic research, and it can also be used to estimate turbulence characteristics (Nikora and Goring 1998). In this study, a 2-D ADV measuring the velocity in two orthogonal components (longitudinal and transversal direction) was adapted because it could allow closer access to a channel bottom than a 3-D one. Its accuracy is 1.0 % of measured velocity and the applicable velocity range is from 1.0 mm/s to 2.5 m/s. The main use of the ADV was to obtain the average flow velocities by measuring the velocity at the center of the selected cross-sections along the channel. At a certain time step, more extensive velocity measurements were performed to obtain the 2-D velocity maps at the same cross-sections to get a better understanding of the flow patterns. For this purpose, the ADV probe was installed on a frame on which a tape measure was attached to trace the location of the measurement points within the channel (Figure 4.13).

(a) ADV Probe

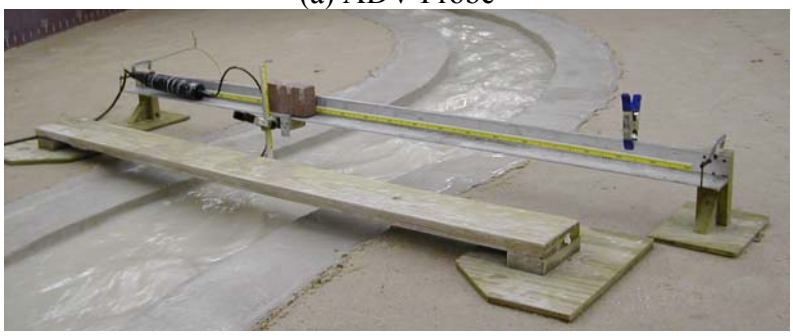

(b) Installed ADV Probe on a Frame

(c) Data Acquisition Computer Connected to ADV Probe

Figure 4.13 Water Velocity Measurement Instrument

4.3 Clay Properties

The maximum mean velocity from the water supply system was about 55.0 cm/s due to the limited height of the water tank (525 gallons). Therefore, a more erodible clay type was chosen to initiate the erosion process under the experimental setup. “Grande”

clay is the most erodible clay type among the available clays from the clay supplier (located in Austin), so it was used for all the flume tests

4.3.1 Index List

Grain size distribution analysis, including a hydrometer test for the Grande clay, was carried out according to the ASTM standard D422: Standard Test Method for Particle-Size Analysis of Soils. The result is shown in Figure 4.14.

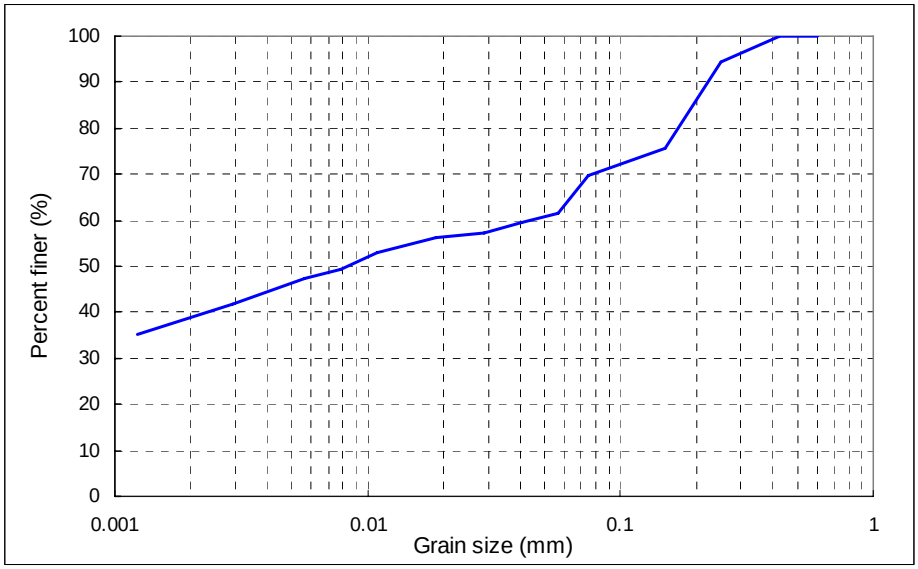

Figure 4.14 Grain Size Distribution Curve of Grande Clay

4.3.2 Engineering Properties

Geotechnical tests were conducted according to the ASTM standard D4318 (Standard Test Methods for Liquid Limit, Plastic Limit, and Plasticity Index of Soils) to obtain the engineering properties of Grande clay. The obtained properties are tabulated in Table 4.1. The vane shear test was also conducted to obtain its undrained shear strength, and the result is shown in the table.

Table 4.1 Geotechnical Properties of Grande Clay

Liquid Limit (LL)	Plastic Limit (PL)	Plastic Index (PI)	Shear Strength (kPa)
28.4%	14.5%	13.9%	8.2

4.3.3 Erosion Properties

Seed et al. (2006) defines erodibility, not as a single number, but rather as a relationship between the erosion rate and the hydraulic shear stress. This relationship is named the erosion function, and can be obtained by conducting the EFA (Erosion Function Apparatus). The EFA was developed to measure the erodibility of a soil sample for predicting the scour depth at bridge piers (Briaud et al. 1999). The test results include the relationships of the soil erosion rate (mm/hr) with the mean velocity (m/s) and the shear stress (Pa). The results of the EFA test for Grande clay are shown in Figures 4.15 and Figure 4.16. From the figures, the critical Froude number *Frc* is estimated as 0.38. The critical Froude number is the minimum Froude number that initiates the bank-line erosion in the tests.

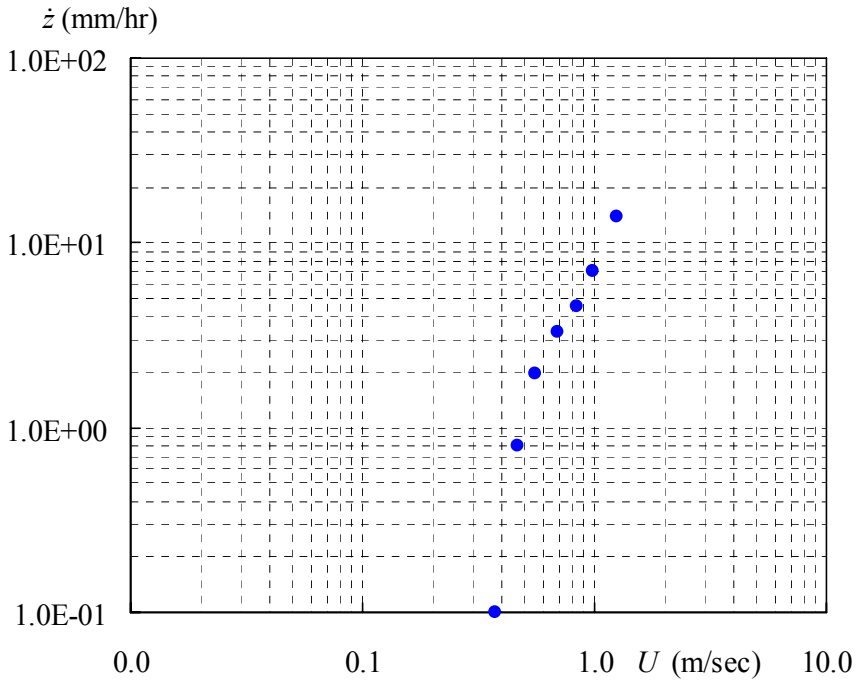

Figure 4.15 Erosion Rate versus Velocity from the EFA Test

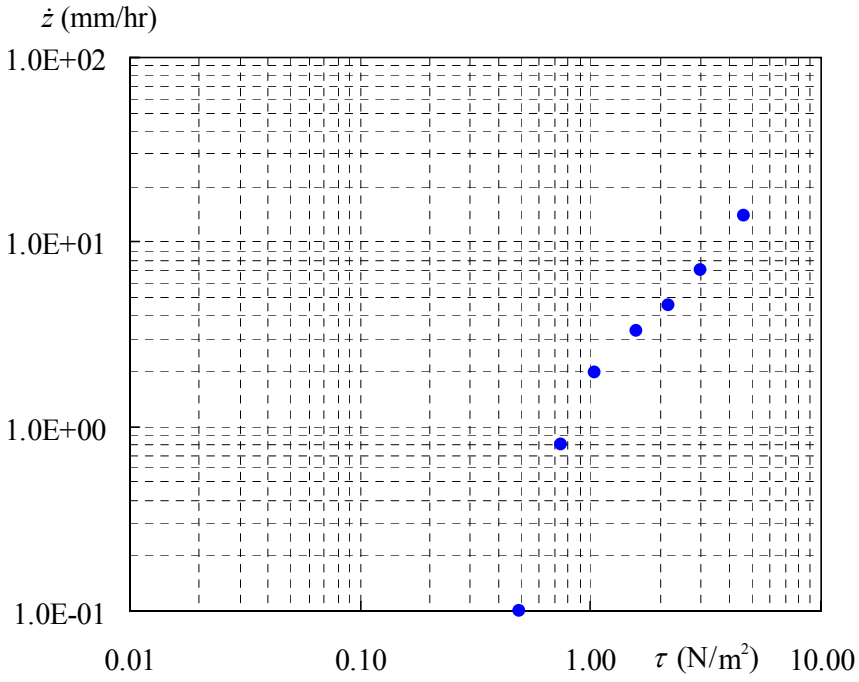

Figure 4.16 Erosion Rate versus Shear Stress from the EFA Test

4.4 FLUME TEST MATRIX

A total of eight flume tests cases were conducted with the parameters shown in Table 4.2. The first three cases are the preliminary tests performed for finding the optimal experimental conditions regarding the slope of the channel and the cross-sectional shape. After the preliminary tests, five cases were conducted to vary the radius-to-width ratio R/W and the bend angle ϕ. The geometries of the channel for all cases are plotted in Figure 4.17. Note that the parameters in Table 4.2 refer to the initial test conditions and do not reflect later changes. A constant Froude number in the tests was used for all cases because the critical Froude number is very high and the margin to increase the flow rate is minimal due the laboratory conditions. Furthermore, it was found from the previous tests in sand that the Froude number effect on the maximum meander distance is insignificant (Yeh 2007).

Table 4.2 Test Matrix in Clay Tests

Case No.	*R/W*	ϕ	*Fr*	*Fr-Frc*
01	4	120˚	0.50	0.12
02	4	120˚	0.50	0.12
03	6	65˚	0.50	0.12
04	4	65˚	0.50	0.12
05	6	65˚	0.50	0.12
06	2	65˚	0.50	0.12
07	4	120˚	0.50	0.12
08	4	220˚	0.50	0.12

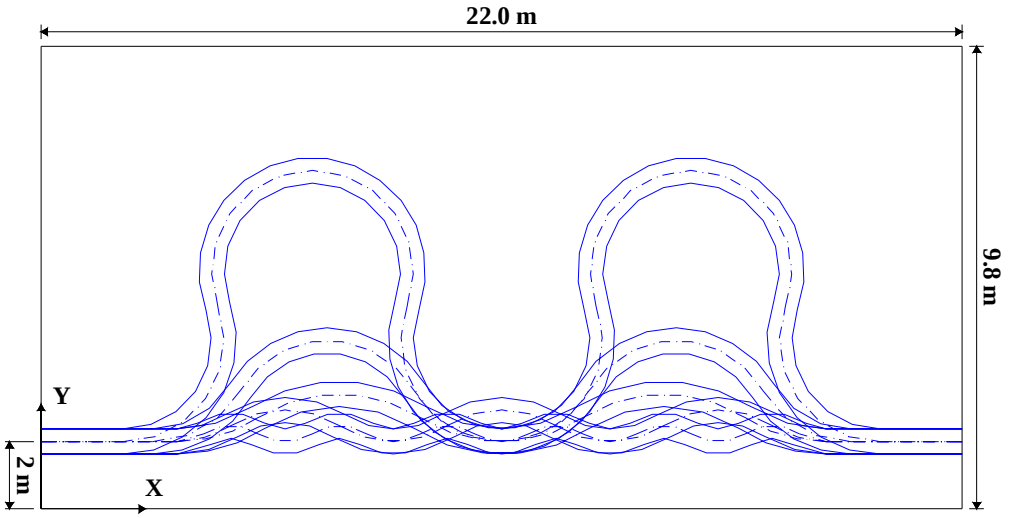

Figure 4.17 Sketches of Plan Forms of All Test Cases

4.5 FLUME TEST PREPARATION

The required channel slope for maintaining a constant water depth along the channel varies case by case since it mainly depends on the geometry of the channel. Therefore, the first step in test preparation is leveling the sand bed. This step includes drawing two reference lines on each flume side wall marking the bed level, flooding the entire test area, and leveling the sand bed by draining water gradually. Once the leveling work was done, the water inside the sand was drained. To make the sand bed more stable, a couple of holes were dug and the water was then pumped out. Subsequently, the contour of the guide channel in the sand bed was drawn, and the sand channel was carved using a mold and shovels. Figure 4.18 shows the carved guide channel in the sand bed.

Figure 4.18 Carved Guide Channel in the Sand Bed

Plywood plates were cut according to the shape of the guide channel and laid on the bottom of the channel. This means only the banks were erodible. The Grande clay was delivered in blocks of 25 cm (9.8 inches) × 18 cm (7.1 inches) × 18 cm (7.1 inches). Each block was in a sealed plastic bag. The clay blocks were laid on both sides of the channel using a wooden mold placed on the middle of the channel (Figure 4.19). The finished clay banks were covered with soaked cloths to maintain moisture inside the clay. The cloths were sprayed frequently to retain moisture until the tests started. A series of photos for the step by step procedures is shown in Appendix A.

Figure 4.19 Laying the Clay Blocks along the Channel

4.6 FLUME TEST PROCEDURES AND MEASUREMENTS

All the flume tests in clay were conducted according to the following procedure:

1. Measure the initial geometry of both bank-lines (left and right).
2. Turn on the pump and adjust the flow rate to the predetermined value.
3. Adjust the sluice gate to obtain the desired constant water depth of 10 cm (3.9 inches) in the channel.
4. Take pictures of the initial running conditions.
5. Measure the initial water velocity on several predetermined stations.
6. Measure the water surface elevation along the channel.
7. At the next time step, take pictures of the running conditions and shut down the experiment.
8. Measure the geometry of both bank-lines.
9. Take pictures of the drained channel.
10. Re-start the experiment and measure the water velocity, the water depth, and water surface elevation.
11. Repeat steps 7 to 10 until the experiment is completed.
12. After the experiment is finished, measure the cross-sectional profiles.

For each case, the primary measurements were the geometry of the bank-lines, the water velocity, the water depth, and the water surface elevation. Note that the typical cross-sectional profile along the eroded channel has a concave bank wall on the outer bank as shown in Figure 4.20. In this situation, the right bank-line location was

measured at the deepest spot along the concave wall, otherwise there was no erosion seen from the measurement at the interface with the water surface.

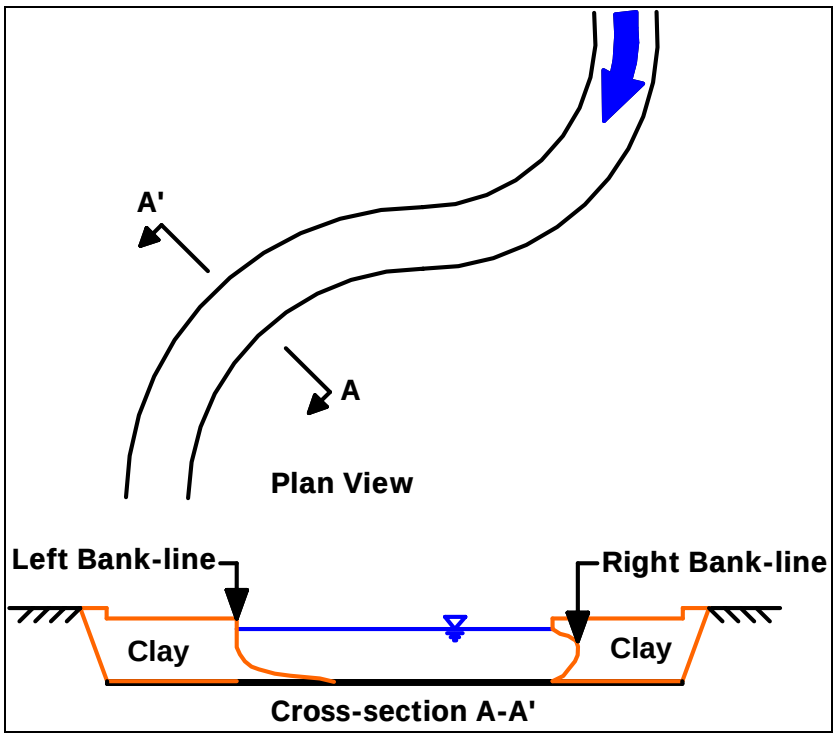

Figure 4.20 Definition of Bank-line in Flume Tests

4.7 TEST RESULTS

The photos taken during each flume test and all the test results are shown in Appendix B and C, respectively. The test results of case 08 are presented in this chapter as an example case. Two photos in Figure 4.21 show the initial and final conditions of the test. In the photos, most parts of the outer banks were eroded, while the inner banks were mostly intact. This phenomenon can be clearly seen in Figure 4.22 which represents the measured initial geometry and final geometry on both bank-lines.

(a) Initial Condition at t = 0 hr

(b) Final Condition at t = 336 hr

Figure 4.21 Photos of Clay Test Case 08 (R/W = 4, ϕ = 220°, Fr = 0.50)

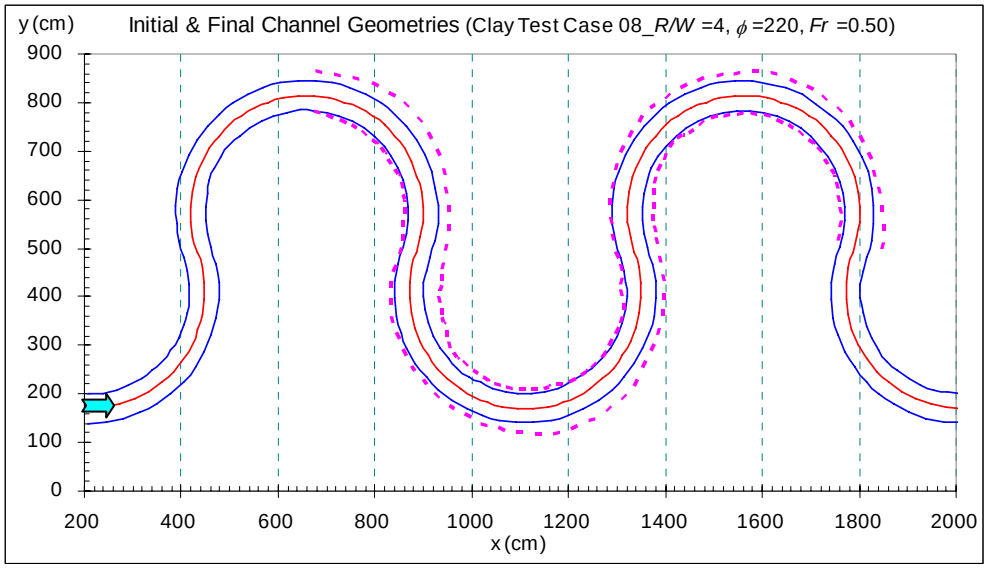

Figure 4.22 Channel Geometry at the Initial Stage and Final (336 hr) Stage (Clay Test Case 08)

The plan form evolution of the second and third bends at several different time steps is shown in Figure 4.23. The figure shows that the channel bank-line expands laterally and translates downstream. In other words, the channel migration contains two components: cross-valley movement and down-valley movement. The bank-line movement begins from the first half of the leading outer bend ($0.0 < \theta/\phi < 0.5$) and ends on the second half of the following inner bend ($1.5 < \theta/\phi < 2.0$). The maximum movement occurs behind the apex of the outer bend ($\theta/\phi = 0.5$), which indicates a phase lag to the channel curvature. Both right and left banks have a similar but alternate erosion pattern.

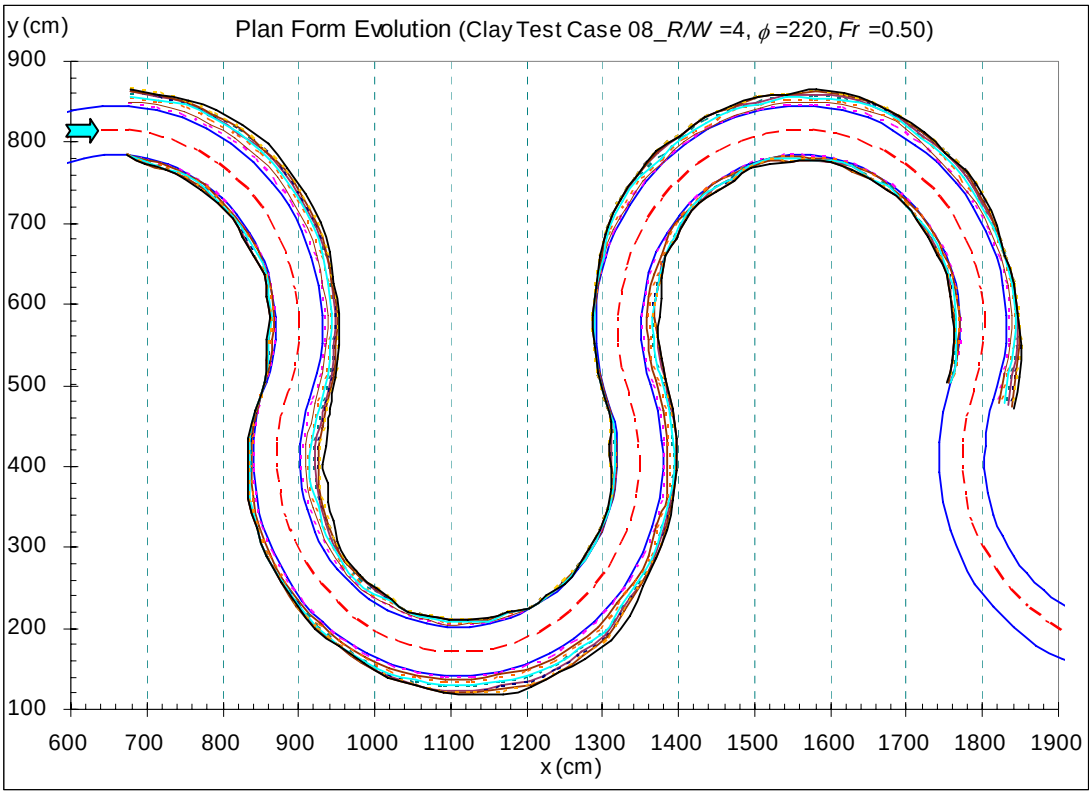

Figure 4.23 Plan Forms Evolution at *t* = 0, 24, 48, 72, 96, 120, 150, 180, 210, 240, and 336 hr (Clay Test Case 08)

Three cross-sectional profiles looking downstream at stations 1, 4, and 6 are plotted in Figure 4.24. The locations of these stations are shown in Figure 4.25. Most erosion occurred in the outer banks as expected. The coarse particles in the Grande clay deposited along the inner banks in the channel, although the amount was relatively small in comparison with that in the sand flume tests (Yeh 2007). Note that Grande clay contains approximately 30 % fine sand particles as shown in the grain size distribution curve. Therefore, some heavy sandy particles deposited at the inner banks where the flow velocity is relatively lower, while the finer particles were suspended in the water and carried downstream along the channel.

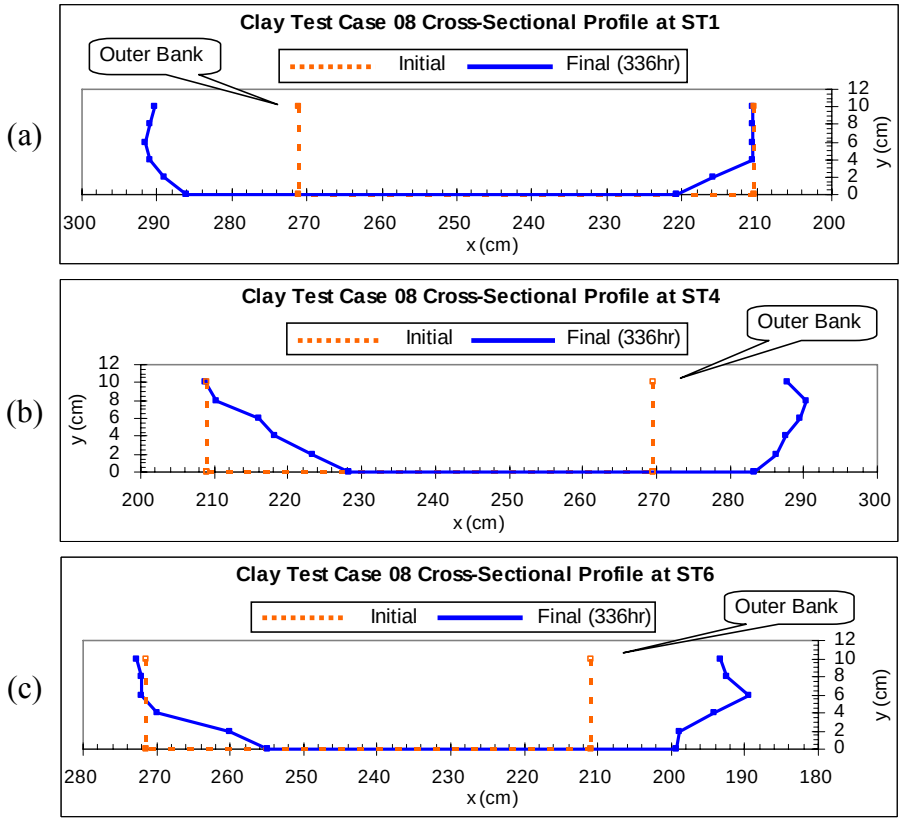

Figure 4.24 Evolution of Cross-Sectional Profiles at Three Stations

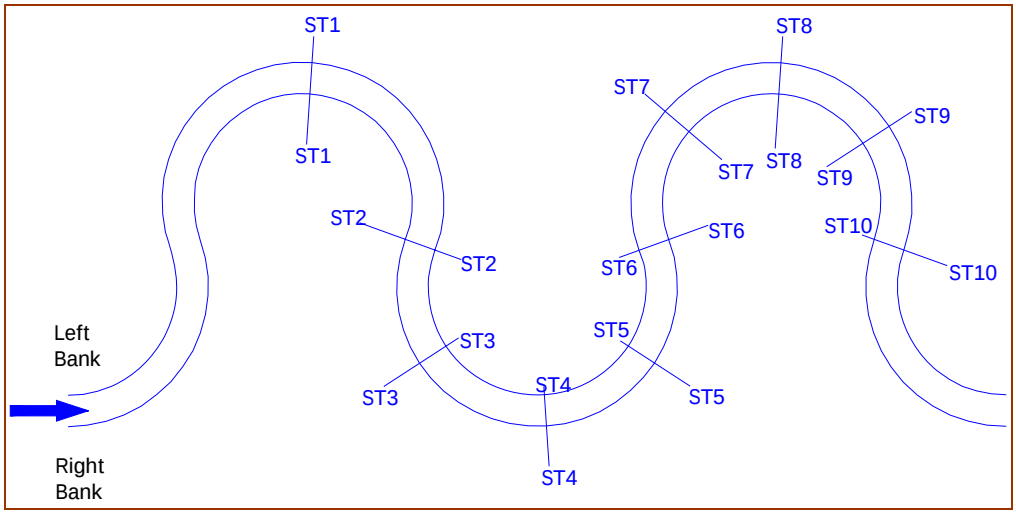

Figure 4.25 Locations of the Predetermined Stations

The mean velocities in different time intervals at the predetermined stations are shown in Figures 4.26. In this study, the mean velocity U is obtained in two methods: 1. Direct measurement at the center of the cross-section using the ADV; 2. For the given flow rate, the cross-sectional area is estimated from the geometry measurement and then the mean velocity is calculated as $U = Q/A_w$, with A_w being the wetted cross-section area. The mean velocities from the two methods are often quite different each other. This is because the mean velocity by ADV measurement is the local velocity at the middle of the cross-section, meaning it can be quite sensitive to the measurement location. Therefore, the mean velocity estimated as $U = Q/A_w$ would be more reasonable representation of the average flow velocity in the channel.

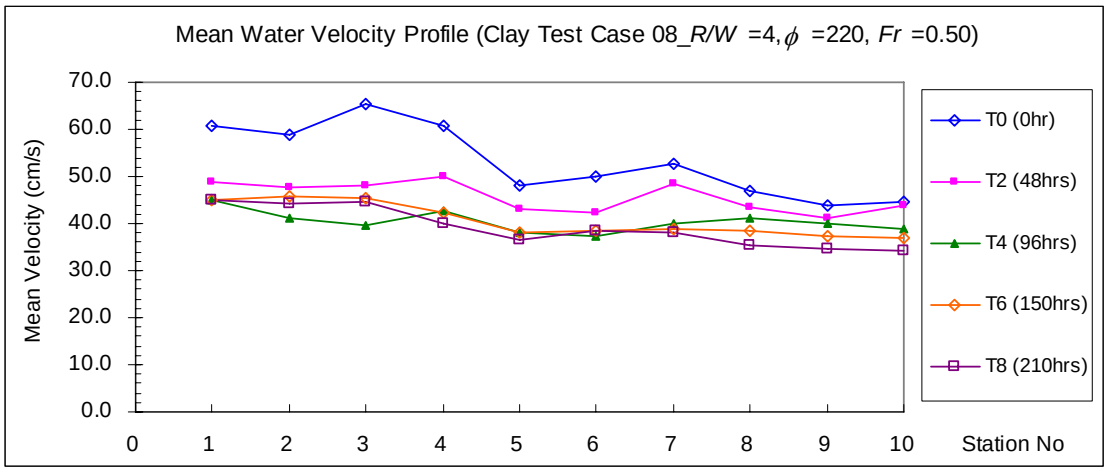

(a) Direct Measurement by ADV

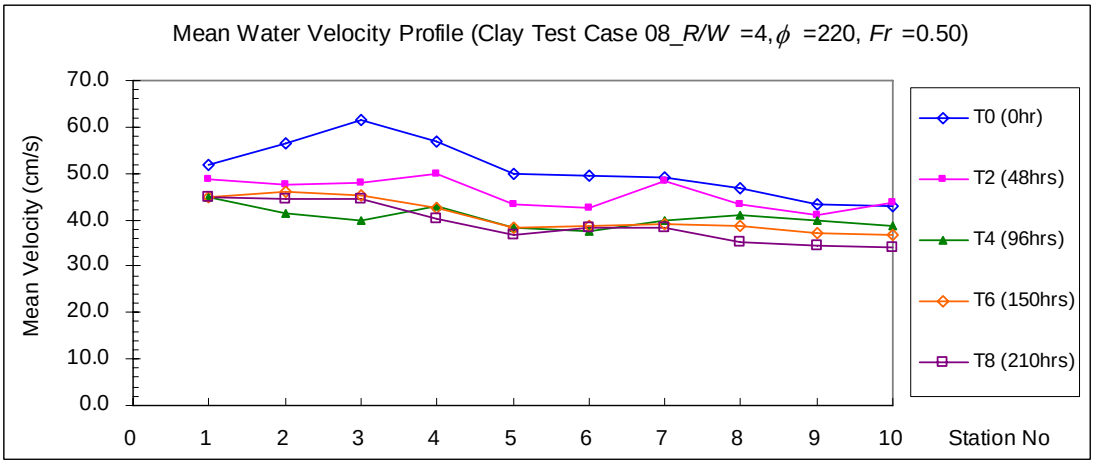

(b) Calculated by the Equation of Continuity ($U = Q/A_w$)

Figure 4.26 Mean Velocity Profile (Clay Test Case 08)

The measured water elevations in different time intervals at the predetermined stations are shown in Figures 4.27. The water elevation H_w was measured at the middle of the cross section along the channel. The water surface elevations decreased as the bank-line erosion process continued.

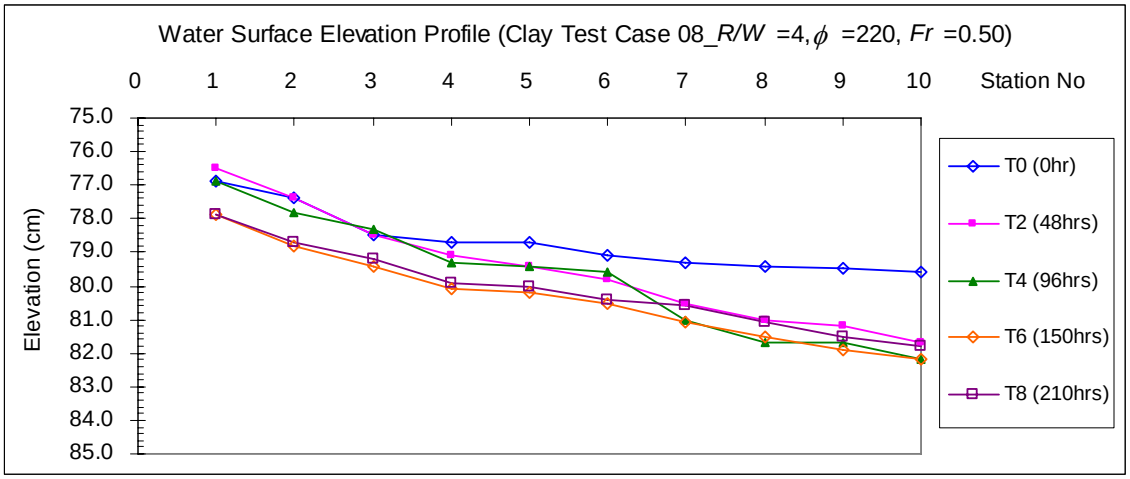

Figure 4.27 Water Surface Elevation Profile (Clay Test Case 08)

The longitudinal surface velocity profiles measured by using ADV at the beginning of the flume test (Case 08) are plotted in Figure 4.28. It successfully shows that the maximum longitudinal velocity along the second bend is gradually shifting from left to right bank (i.e. inner bank to outer bank). In general, this trend in the measured velocities matches well to the simulated free surface velocities by 3-D numerical simulation as shown in Figure 4.29.

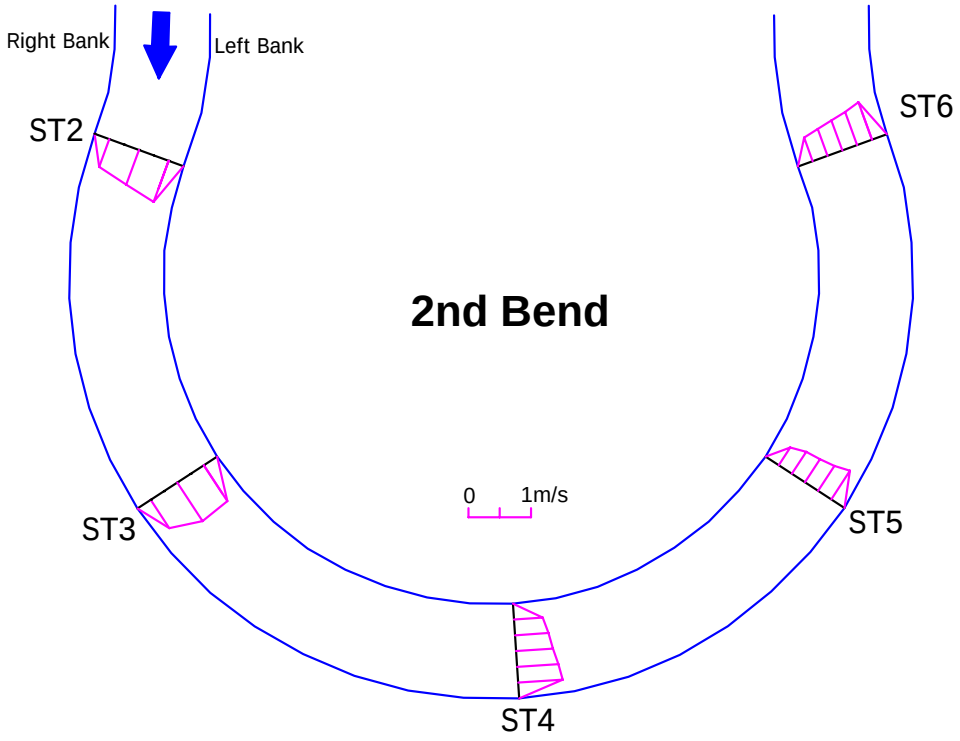

Figure 4.28 Longitudinal Surface Velocity Profiles at T0 (Clay Test Case 08)

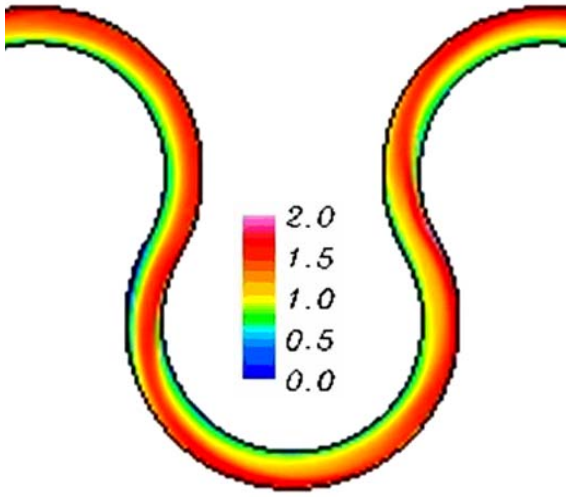

Figure 4.29 Free Surface Velocity Profiles from Numerical Simulation (after Briaud et al. 2007)

The longitudinal and transversal velocity profile at the predetermined station, ST4, is shown in Figure 4.30. The secondary flow pattern is clearly detected in the measurement result (Figure 4.30(b)). The measured velocity profiles for other stations and at different time steps are included in Appendix C.

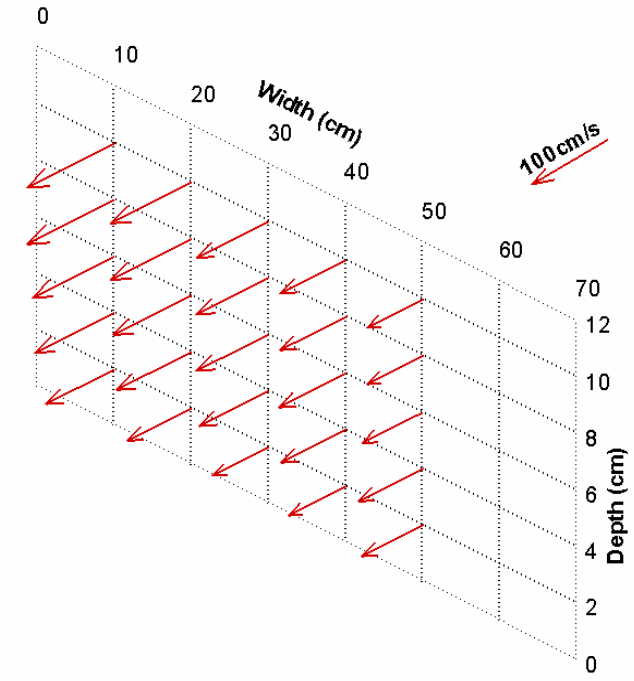

(a) Longitudinal Velocities

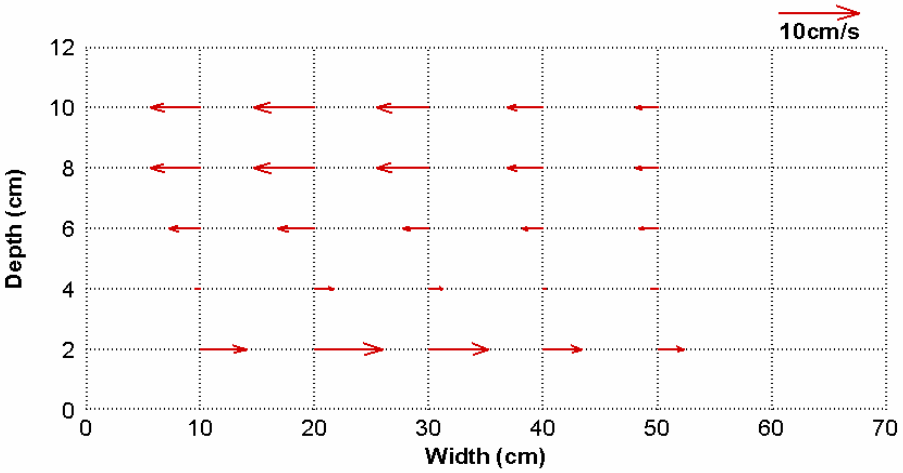

(b) Transversal Velocities

Figure 4.30 Initial Velocity Profiles at ST4 (Clay Test Case 08)

CHAPTER V

DATA ANALYSIS OF FLUME TEST RESULTS

The flume test results are analyzed to propose two equations for maximum migration distance and initial migration rate. A hyperbolic model is chosen to model meander migration process with respect to time, and the experimental data is fitted with this model to get the spatial distributions of two target variables (M_{max} and $\dot{M}_i$) along the channel. Then, the appropriate forms of the distribution functions are proposed to describe the spatial distributions. Finally, the multiple regression technique is applied to estimate the unknown coefficients in the proposed equations.

5.1 DATA DEDUCTION FOR MAXIMUM MIGRATION DISTANCE

The channel migration distance is defined in the normal direction to the initial channel bank-line. During the flume tests, it was observed that the channel migration rate had its maximum value at the beginning of each test, which means that the channel was eroded quickly within a short period of time. However, as the water continued to erode the channel banks, the migration rate decreased gradually, expecting a maximum value of the migration distance when the time is infinite (i.e. equilibrium state). The measured migration distance at a cross section on the right bank is shown in Figure 5.1 as an example, and it clearly shows the aforementioned behavior. The experimental data points are fitted with a hyperbolic function as follows:

$$M = \frac{t}{a + bt} \tag{5.1}$$

Where,

M = channel migration distance, (cm)

t = time, (hr)

a = constant in which 1/a is the initial migration rate, $\dot{M}_i$ (cm/hr)

b = constant in which 1/b is the maximum migration distance, M_{max} (cm)

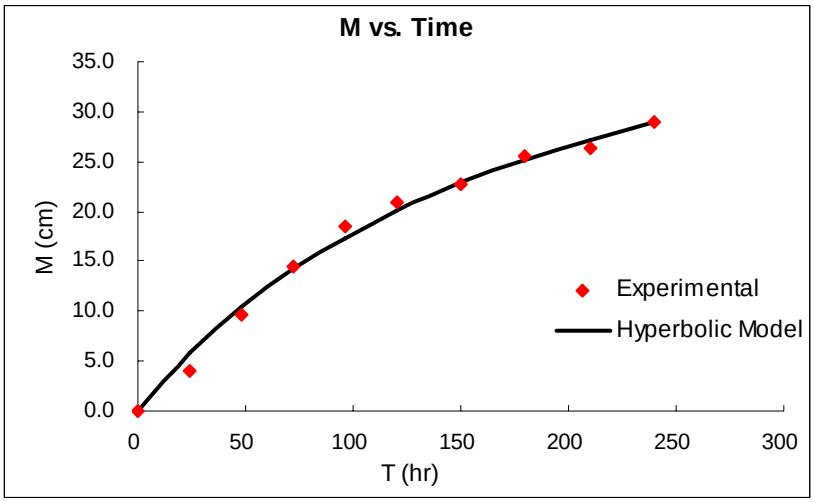

Figure 5.1 Migration Distance versus Time in Clay Test Case 08 (R/W = 4, ϕ = 220°, Fr = 0.50, θ/ϕ = 0.69)

Alternatively, the t/M can be plotted against the measurement time, and then the data can be fitted with a linear equation as shown in Figure 5.2. The advantage of this method is that the scattering data, particularly at the very beginning stage, can be easily identified and thus discarded in the fitting process. The source of these scattered data points might be non-homogeneity of the clay condition between the surface and inner portion of the clay banks. In other words, the surface of the clay bank was more likely to be dried out than the inner part during the preparation of the test setup, although water was sprayed regularly all over the clay banks. This drying could decrease the erosion rate at the beginning of the test. Consequently, all the experimental data are checked by

plotting the t/M versus time graphs, and then those scattering data at the early time steps are discarded in analyzing the experimental data.

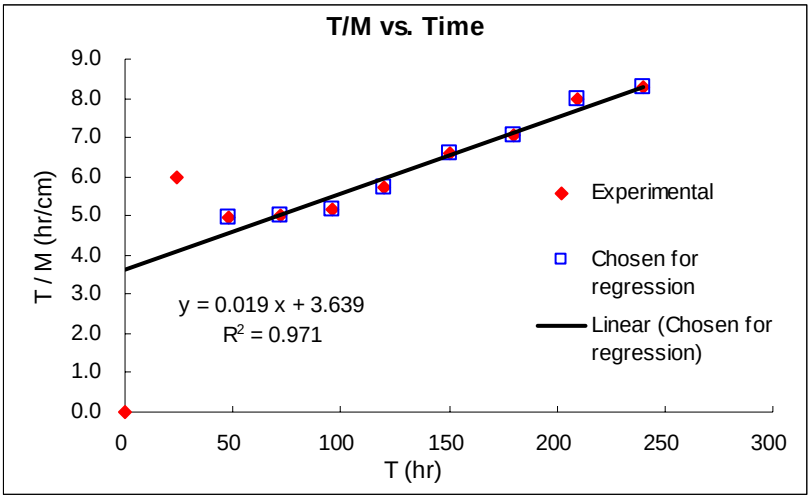

Figure 5.2 *T/M* versus Time in Clay Test Case 08 (*R/W* = 4, ϕ = 220°, *Fr* = 0.50, θ/ϕ = 0.69)

The maximum migration distance M_{max} at each cross section along the channel is obtained by curve fitting the measured data points using the hyperbolic function as described above. After curve fitting at every point along the channel (i.e. obtain M_{max} value for each point), the spatial distribution of the maximum migration distances are obtained. A 3-point moving average technique is applied to smooth out the distribution because there are some noisy values of M_{max} along the channel. The maximum migration distances are then normalized by the initial channel width W, as shown in Figure 5.3 (Clay Test Case 08).

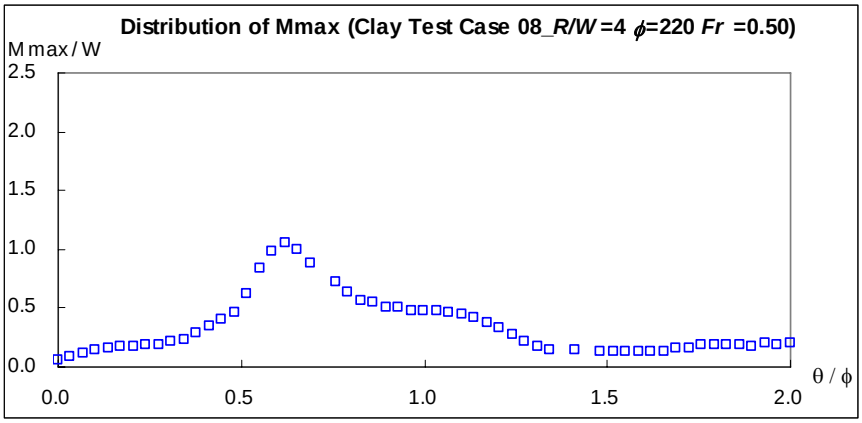

Figure 5.3 M_{max} Distributions along the Channel for Clay Test Case 08

A 3-D numerical simulation result (Briaud et al. 2007) indicates that the secondary flow is fully developed from the second bend. In the experiments, measurement data are taken from the second bend to the third bend in order to ensure that the fully developed secondary flow in the channel is accounted for, and that the backwater effect from the channel exit can be negligible. The result shows that M_{max} along the channel has a peak value behind the channel apex ($\theta/\phi = 0.5$), which means there is a phase lag to the channel curvature. The typical shape of the M_{max} distribution in the flume tests turns out to be a skewed bell shape, unlike a Gaussian distribution which has a symmetrical bell shape. To accommodate this skewness, the Pearson IV distribution function is employed to formulate the M_{max} values along the channel:

$$\frac{M_{\max}}{W} = a \frac{\left[1+\frac{\left(\frac{\theta}{\phi}-\frac{ce}{2d}-b\right)^2}{c^2}\right]^{-d} \exp\left[-e\left(\tan^{-1}\left(\frac{\frac{\theta}{\phi}-\frac{ce}{2d}-b}{c}\right)+\tan^{-1}\left(\frac{e}{2d}\right)\right)\right]}{\left(1+\frac{e^2}{4d^2}\right)^{-d}} \qquad (5.2)$$

where a is the maximum value of M_{max}/W, θ/ϕ is the normalized angle, b is the location (in terms of θ/ϕ) of the maximum value, c and d are the coefficients controlling the bandwidth of the bell-shaped distribution, and e is the coefficient controlling the skewness of the distribution. It turns out that the Pearson IV function can represent the distribution of M_{max} well in all the cases as shown in Figure 5.4.

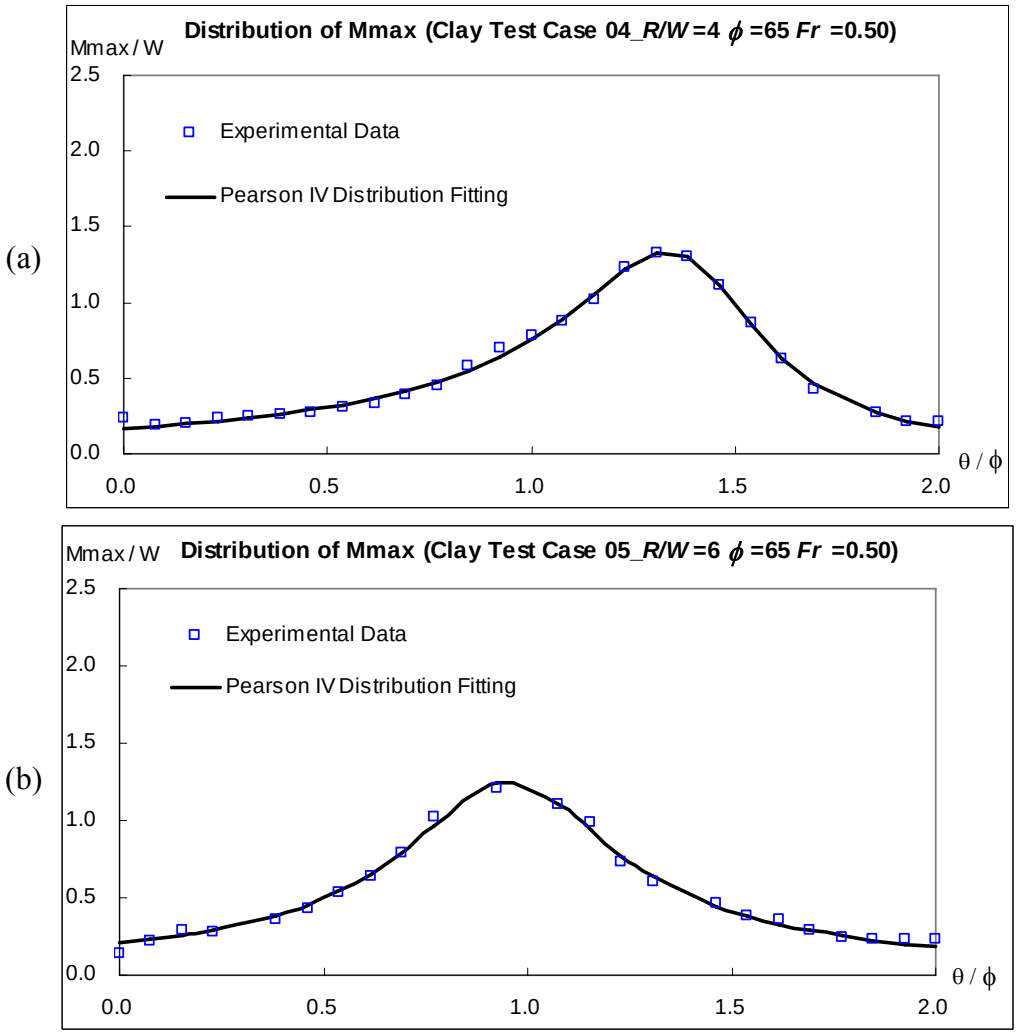

Figure 5.4 Experimental Data and Fitted Curve for M_{max}

(c)

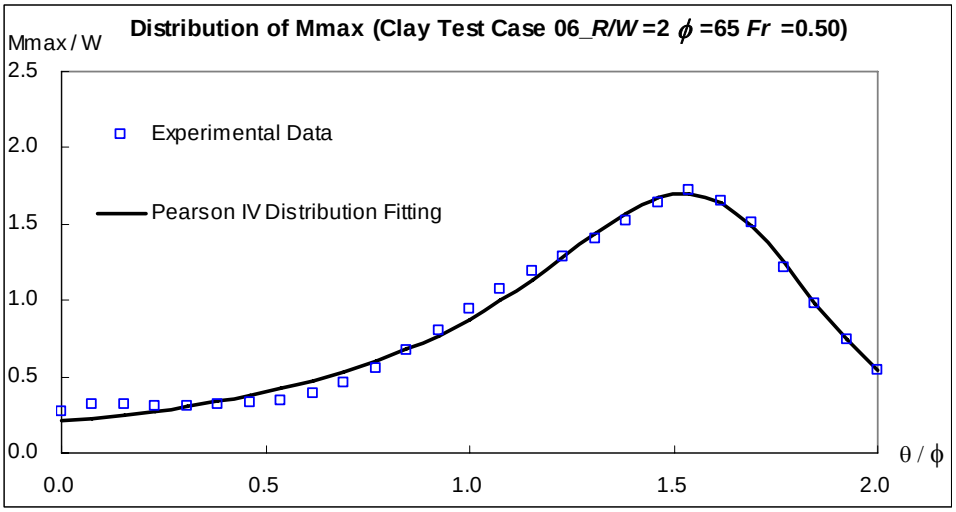

(d)

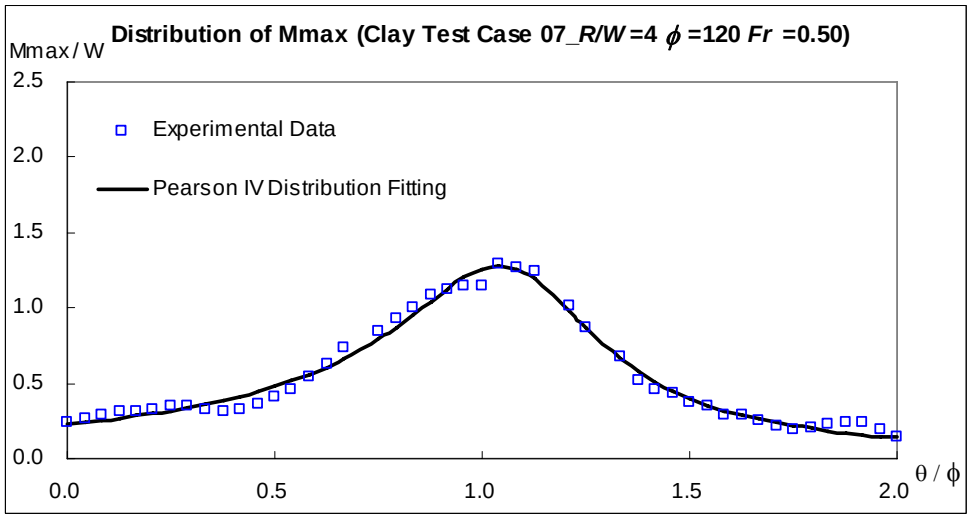

(e)

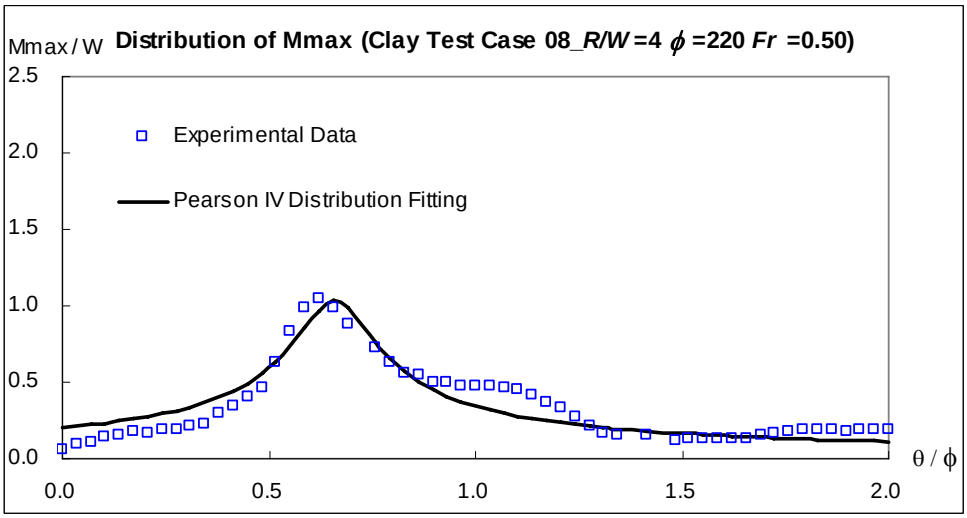

Figure 5.4 Continued

5.2 PROPOSED EQUATIONS FOR MAXIMUM MIGRATION DISTANCE

There are five undetermined coefficients in the proposed prediction equation for M_{max} (Eq. 5.2). These coefficients are found by correlating the measurements with the three controlling parameters, R/W, ϕ, and $Fr\text{-}Frc$. Based on physical considerations and observations, the near-bank velocity in a cross section has a stronger relationship with the channel migration than the mean velocity. Therefore, a correction factor, β that represents the magnitude of the near-bank velocity in terms of the mean velocity, is employed in the analysis. A 3-D numerical simulation result (Briaud et al. 2007) shows that the correction factor β is affected by the channel radius curvature R. In other words, if the approaching velocity is the same, the centrifugal force in a small R/W channel generates a larger near-bank velocity than that in a large R/W channel. The following simple equation, based on the numerical simulation results, is used to estimate the correction parameter β with respect to R/W:

$$\beta = \frac{1}{R/W} + 1 \tag{5.3}$$

According to Eq. 5.3, the near-bank velocity in the channel, when $R/W = 2$, is 1.5 times larger than the mean velocity. If the channel is less sinusoidal (e.g. $R/W = 6$), it becomes 1.2 times larger than the mean velocity. Since the correction factor β is used in the analysis, two other controlling parameters, R/W and $Fr\text{-}Frc$, can be incorporated as a single parameter (i.e. $\beta Fr\text{-}Frc$), where the effect of R/W is embedded in the correction factor β.

The correlations between the five coefficients and $\beta Fr\text{-}Frc$ are shown in Figure 5.5. The result shows the maximum peak value of M_{max} occurs at $\beta Fr\text{-}Frc = 0.37$ where

R/W = 2, and it decreases as $\beta Fr\text{-}Frc$ decreases (Figure 5.5 (a)). This means a channel has the largest maximum migration distance M_{max} when R/W = 2. The similar conclusion has been reported by various researchers (Nanson and Hickin1983, 1986; Biedenharn et al. 1989; Hudson and Richard 2000), even though their concern is the relationship between average migration rate and R/W. The coefficient b increases as $\beta Fr\text{-}Frc$ increases, meaning that the peak location of M_{max} moves downstream as R/W increases (Figure 5.5 (b)). This indicates that the following inner bend may have a greater migration rate and migration distance as a result of phase lag. The coefficient c has a relatively small variation in all the cases shown in Figure 5.5 (c). The coefficient d increases as $\beta Fr\text{-}Frc$ increases, as shown in Figure 5.5 (d), which implies that meander migration in a channel with a large $\beta Fr\text{-}Frc$ (or small R/W) occurs over a longer channel length along the outer bank-line. The skewness, controlled by the coefficient e in the M_{max} distribution, reaches maximum value at $\beta Fr\text{-}Frc$ = 0.37 (R/W = 2), and it decreases as $\beta Fr\text{-}Frc$ decreases (Figure 5.5 (e)). Note that the shape of the M_{max} distribution becomes more symmetric when $\beta Fr\text{-}Frc$ = 0.20 where R/W = 6.

(a)

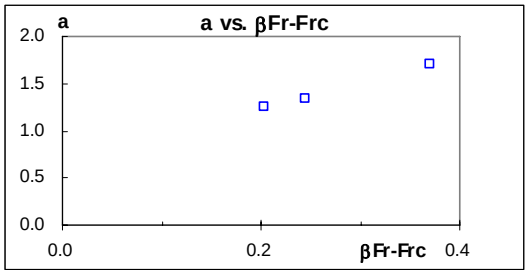

(b)

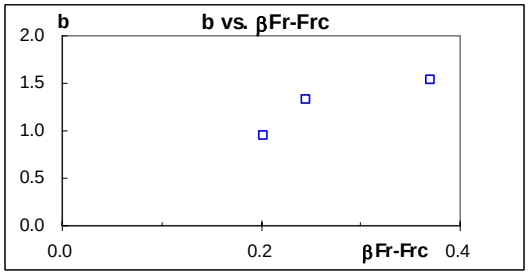

Figure 5.5 Five Coefficients in the Pearson IV Equation for M_{max} vs. ($\beta Fr\text{-}Frc$)

(c)

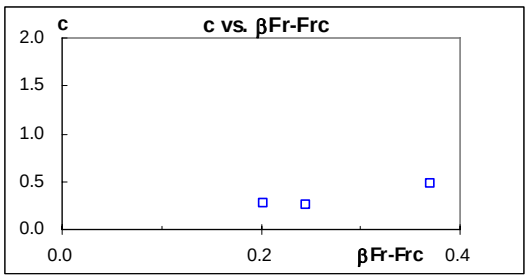

(d)

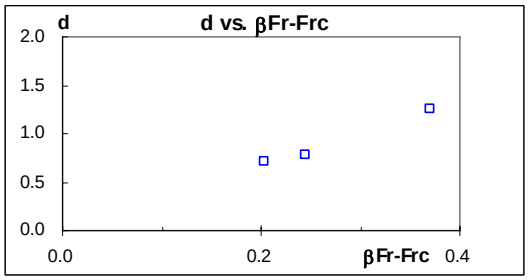

(e)

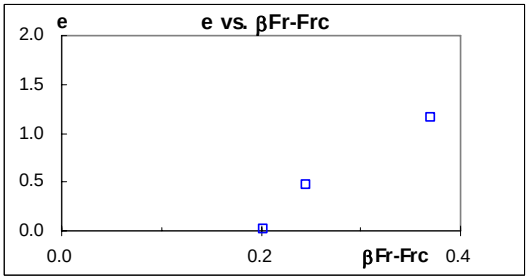

Figure 5.5 Continued

The distribution of M_{max} is also affected by the channel bend angle ϕ, as shown in Figure 5.6. As ϕ increases, the peak value of M_{max} decreases, which means a longer flow path along the meandering bend with a bigger bend angle reduces the magnitude of migration (Figure 5.6 (a)). The coefficient b decreases as ϕ increases, which means that the peak location of M_{max} moves upstream as ϕ increases (Figure 5.6 (b)). The coefficient c is somewhat constant for all of three cases as shown in Figure 5.6(c), but the coefficient d decreases as ϕ increases, as shown in Figure 5.6(d). This means that the migration in a channel with a large ϕ occurs over a localized channel length along the outer bank-line, while a small ϕ produces a meander migration over a longer channel length. The skewness in the M_{max} distribution also shows a similar trend; it reaches maximum value at $\phi = 65°$ and decreases as ϕ increases (Figure 5.6 (e)). Note that the distribution becomes more symmetric when ϕ reaches 220°.

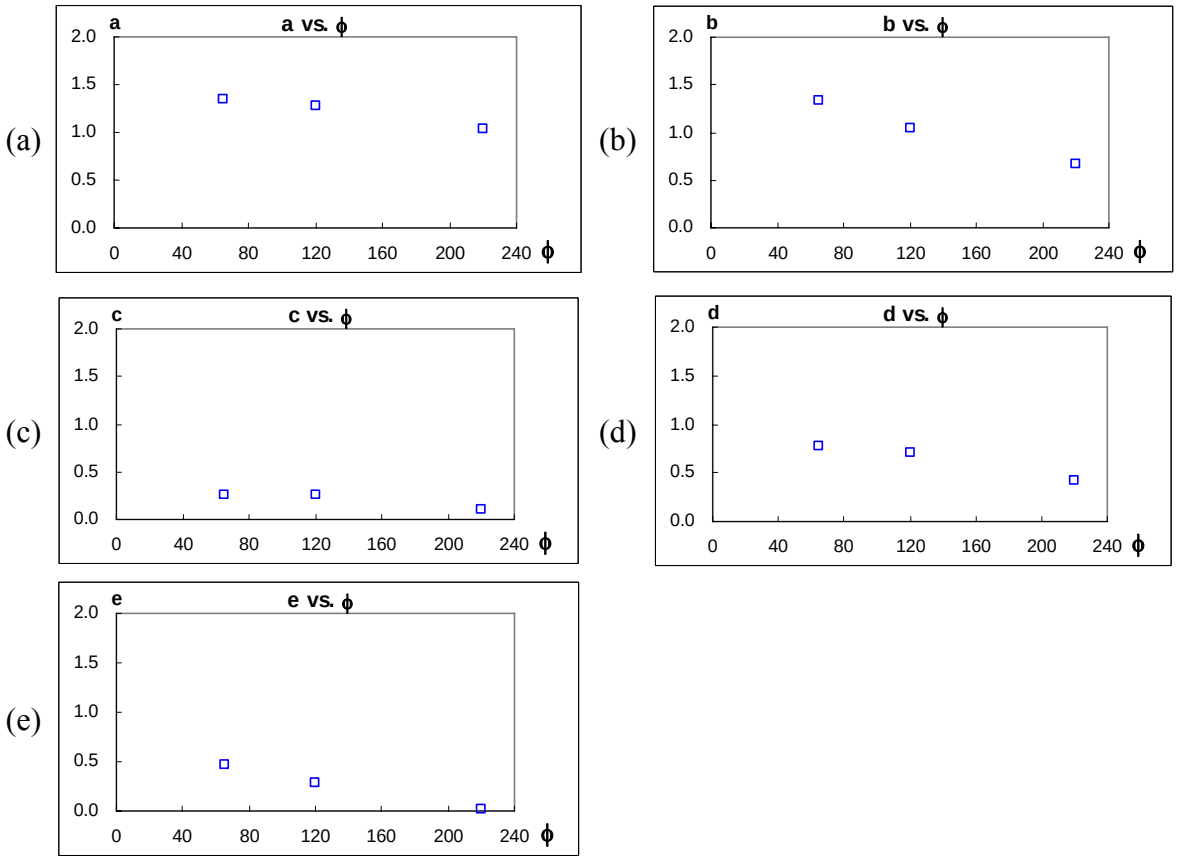

Figure 5.6 Five Coefficients in the Pearson IV Equation for M_{max} vs. ϕ

According to Figure 5.5 and Figure 5.6, each of the five coefficients in the M_{max} equation is a function of $\beta Fr\text{-}Frc$ and ϕ (Eqs. 5.4-5.8), and can be obtained using multiple regression analysis with the experimental data.

$$a = K_a\left(g\left(\beta Fr - Frc\right)\right)^{A_a}\left(\ g\left(\phi\right)\right)^{B_a} \tag{5.4}$$

$$b = K_b\left(g\left(\beta Fr - Frc\right)\right)^{A_b}\left(\ g\left(\phi\right)\right)^{B_b} \tag{5.5}$$

$$c = K_c\left(g\left(\beta Fr - Frc\right)\right)^{A_c}\left(\ g\left(\phi\right)\right)^{B_c} \tag{5.6}$$

$$d = K_d\left(g\left(\beta Fr - Frc\right)\right)^{A_d}\left(\ g\left(\phi\right)\right)^{B_d} \tag{5.7}$$

$$e = K_e\left(g\left(\beta Fr - Frc\right)\right)^{A_e}\left(\ g\left(\phi\right)\right)^{B_e} \tag{5.8}$$

Where,

K_i, A_i, *and* B_i *are unknown, and* $i = a$ *to* e

The final form of the prediction equation with these five coefficients in the Pearson IV distribution function is as follows:

$$\frac{M_{max}}{W} = a\frac{\left[1+\dfrac{\left(\dfrac{\theta}{\phi}-\dfrac{ce}{2d}-b\right)^2}{c^2}\right]^{-d}\exp\left[-e\left(\tan^{-1}\left(\dfrac{\dfrac{\theta}{\phi}-\dfrac{ce}{2d}-b}{c}\right)+\tan^{-1}\left(\dfrac{e}{2d}\right)\right)\right]}{\left(1+\dfrac{e^2}{4d^2}\right)^{-d}} \tag{5.9}$$

Where,

$$a = 2.456\left(-2.267\left(\beta Fr - Frc\right)+2.539\right)^{0.970}\phi^{-0.210} \quad (\text{for } R/W < 2.0)$$

$$a = 2.456\left(2.735\left(\beta Fr - Frc\right)+0.688\right)^{0.970}\phi^{-0.210} \quad (\text{for } R/W \geqq 2.0)$$

$$b = 20.671\left(\beta Fr - Frc\right)^{0.685}\phi^{-0.449}$$

$$c = 0.214\exp[3.325\left(\beta Fr - Frc\right)-0.00696\phi]$$

$$d = 0.457\exp[3.420\left(\beta Fr - Frc\right)-0.00403\phi]$$

$$e = 2.000\left[1.868Ln\left(\beta Fr - Frc\right)+3.0338\right]^{0.827}\left[-0.380Ln\left(\phi\right)+2.0763\right]^{0.913}$$

Note: $\beta = \dfrac{1}{R/W}+1$, $b = 1.5$ (for R/W<2.0), and $e = 0$ (for R/W >6 or ϕ >220°)

5.3 DATA DEDUCTION FOR INITIAL MIGRATION RATE

The initial migration rate $\dot{M}_i$ at each cross section along the channel is obtained by the same curve fitting for the maximum migration distance M_{max} as described above. In fact, the initial migration rate is 1/a in Eq. 5.1, which is the initial slope of the fitted

hyperbolic curve in Figure 5.1 or the reciprocal of the y-intercept in Figure 5.2. Like the spatial distribution of the maximum migration distance shown in Figure 5.3, a similar spatial distribution of the initial migration rate is obtained. The initial migration rates, normalized by the mean velocity U, are shown in Figure 5.7 (Clay Test Case 08).

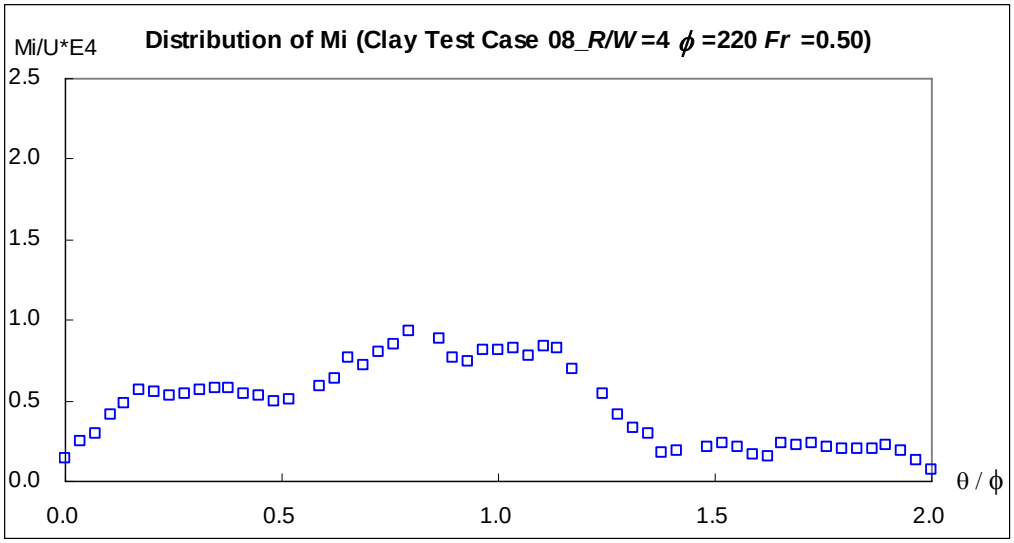

Figure 5.7 $\dot{M}_i$ Distributions along the Channel for Clay Test Case 08

The result shows that $\dot{M}_i$ along the channel has its peak value behind the channel apex (θ/ϕ = 0.5), which means there is also a phase lag to the channel curvature as it exists in the M_{max} distribution. The typical shape of the obtained $\dot{M}_i$ distribution seems to be similar to that of M_{max} distribution, and thus the same type of function, Pearson IV (Eq. 5.2), is employed to formulate the $\dot{M}_i$ along the channel. Figure 5.8 shows the regression results of spatial $\dot{M}_i$ distributions for every case.

(a)

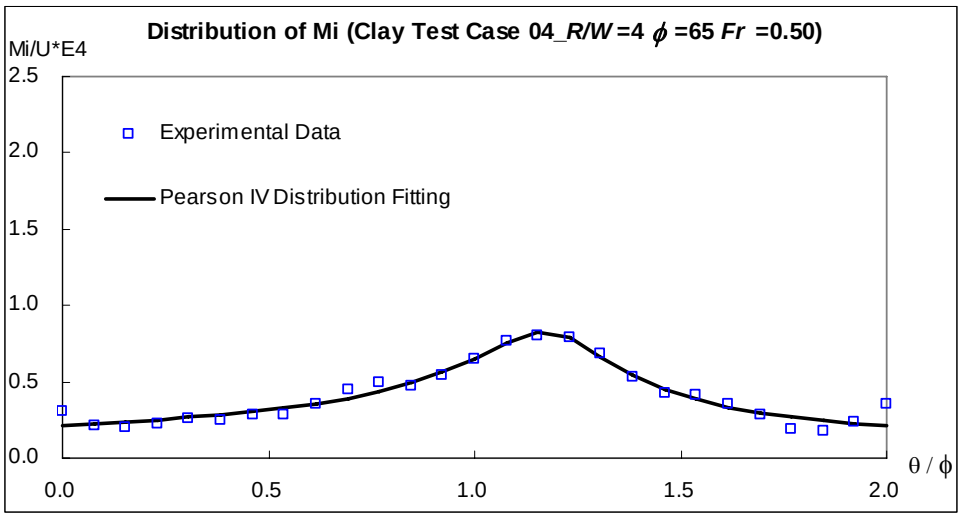

(b)

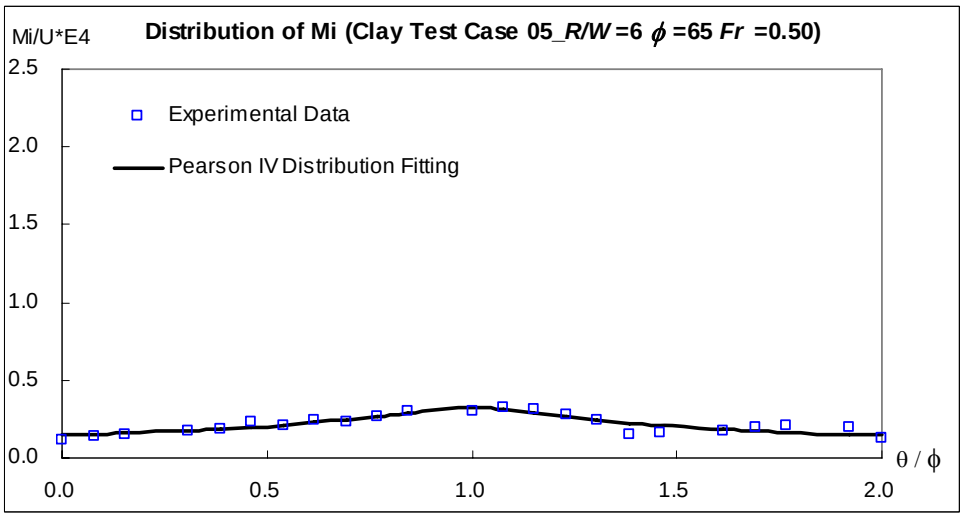

(c)

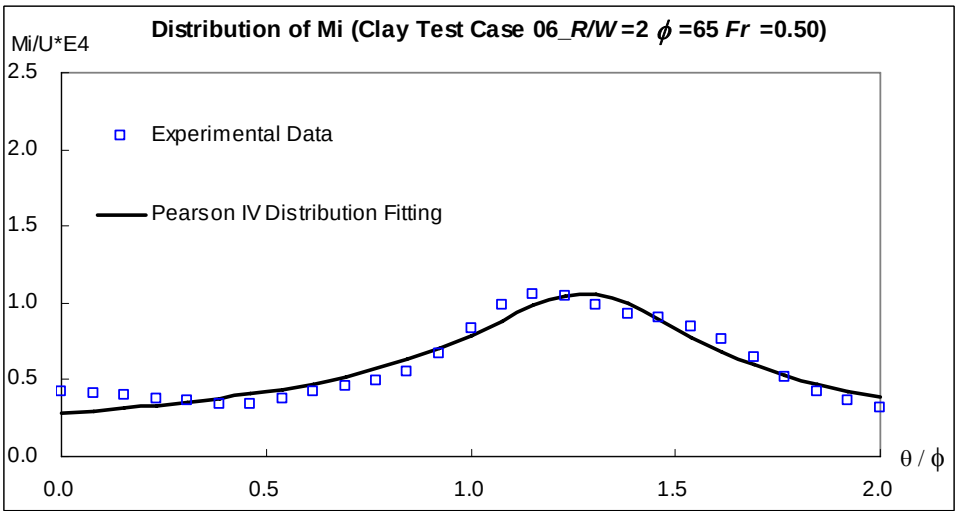

Figure 5.8 Experimental Data and Fitted Curve for $\dot{M}_i$

(d)

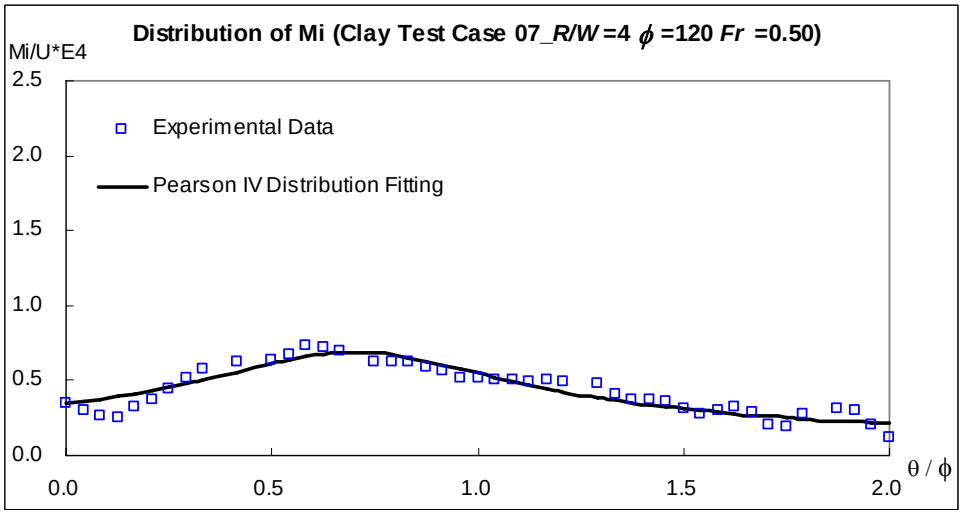

(e)

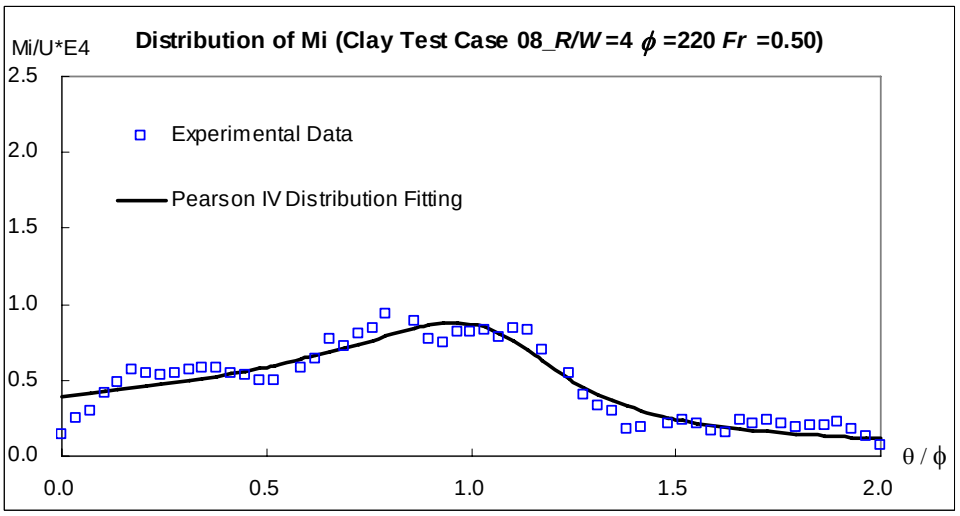

Figure 5.8 Continued

5.4 PROPOSED EQUATIONS FOR INITIAL MIGRATION RATE

There are five undetermined coefficients in the proposed prediction equation for $\dot{M}_i$ (Eq. 5.2). These coefficients are found by correlating the measurements with the three controlling parameters, R/W, ϕ, and Fr-Frc. In fact, as described above, the effect of R/W is embedded in the correction factor β, and thus those coefficients are correlated with two dominant parameters: βFr-Frc and the bend angle ϕ.

The correlations between the five coefficients and *βFr-Frc* are shown in Figure 5.9. The result shows the maximum peak value of $\dot{M}_i$ occurs at *βFr-Frc* = 0.37, where *R*/*W* = 2 and it decreases as *βFr-Frc* decreases, following the same trend of M_{max} (Figure 5.9 (a)). The coefficient *b* increases as *βFr-Frc* increases, which mean that the peak location of $\dot{M}_i$ moves downstream as *R/W* increases, like in M_{max} (Figure 5.9 (b)). This indicates that the following inner bend may have a greater initial migration rate as a result of phase lag. The coefficient *c* has a relatively small variation in all the cases shown in Figure 5.9 (c). The coefficient *d* increases as *βFr-Frc* increases, as shown in Figure 5.7 (d), which indicates that meander migration in a channel with a large *βFr-Frc* (or small *R/W*) occurs over a longer channel length along the outer bank-line. The skewness, controlled by the coefficient *e* in the $\dot{M}_i$ distribution, has a relatively small variation in all the cases, as shown in Figure 5.9 (e).

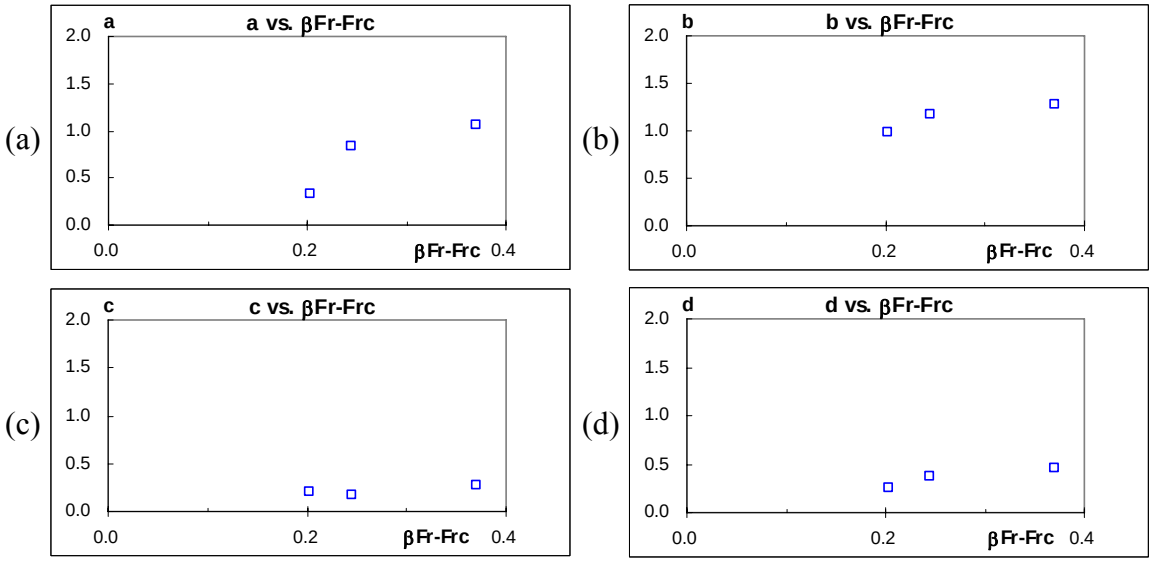

Figure 5.9 Five Coefficients in the Pearson IV Equation for $\dot{M}_i$ vs. (*βFr-Frc*)

(e)

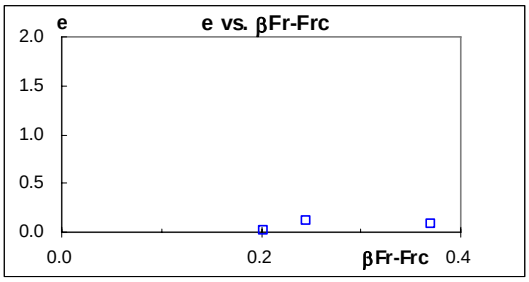

Figure 5.9 Continued

The distribution of $\dot{M}_i$ is also influenced by the channel bend angle ϕ, as shown in Figure 5.10. The coefficient a is somewhat constant for all of three cases, as shown in Figure 5.10(a). The coefficient *b* decreases as ϕ increases until the bend angle becomes 120°, which means that the peak location of $\dot{M}_i$ moves downstream as ϕ increases (Figure 5.10(b)). However, it shows a relatively constant value beyond the bend angle of 120°. The coefficients *c* and d are approximately proportional to the bend angle ϕ, as shown in Figures 5.10(c) and 5.10(d). However, the coefficient d increases more rapidly than the coefficient c, which means that the migration in a channel with a small ϕ occurs over a localized channel length along the outer bank-line, while a large ϕ produces meander migration over a longer channel length. The skewness in the $\dot{M}_i$ distribution shows a nearly constant trend; the effect of bend angle ϕ seems to be minimal, unlike the M_{max} distribution.

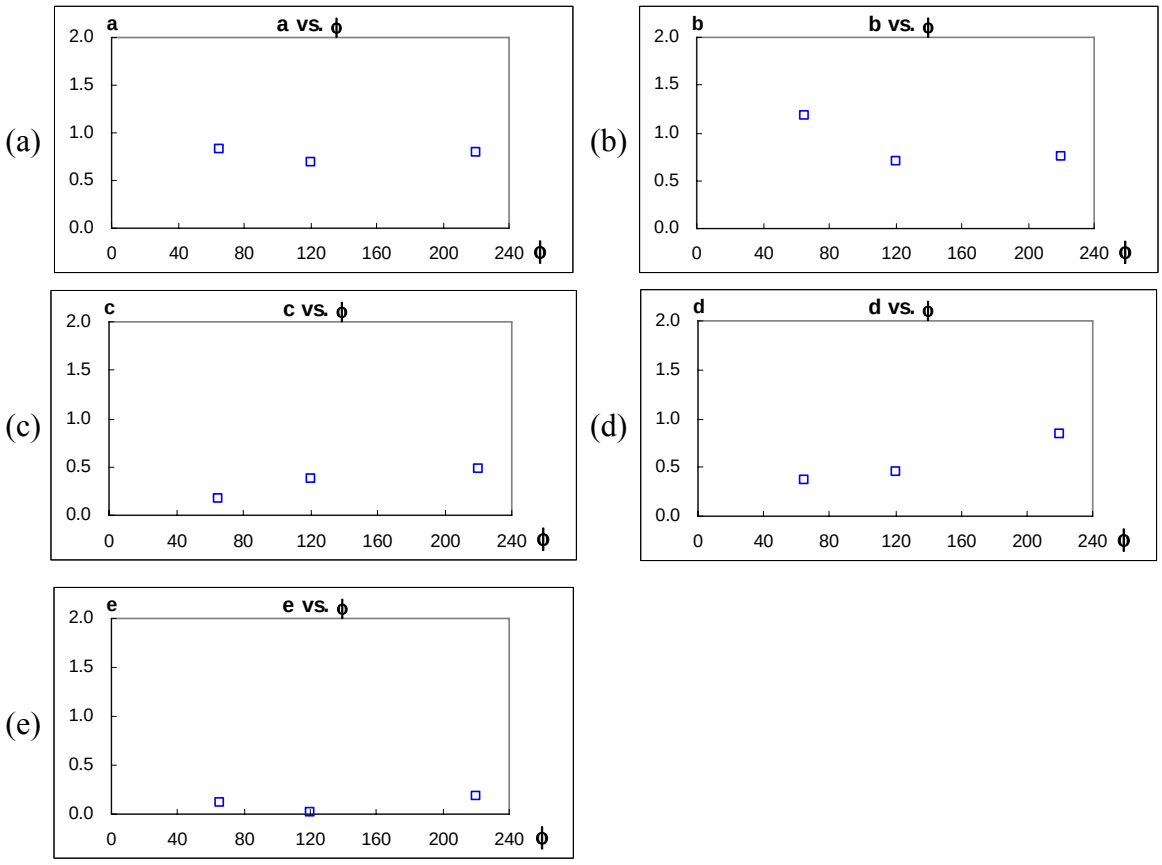

Figure 5.10 Five Coefficients in the Pearson IV Equation for $\dot{M}_i$ vs. ϕ

Based on the analysis results in Figure 5.9 and Figure 5.10, each coefficient in the $\dot{M}_i$ equation is a function of βFr-Frc and ϕ, and the types for their own functions can be obtained using regression analysis with the experimental data. The final form of the prediction equation with these five coefficients in the Pearson IV distribution function can be expressed as follows:

$$\frac{\dot{M}_i}{U \cdot E4} = a \frac{\left[1 + \frac{\left(\frac{\theta}{\phi} - \frac{ce}{2d} - b\right)^2}{c^2}\right]^{-d} \exp\left[-e\left(\tan^{-1}\left(\frac{\frac{\theta}{\phi} - \frac{ce}{2d} - b}{c}\right) + \tan^{-1}\left(\frac{e}{2d}\right)\right)\right]}{\left(1 + \frac{e^2}{4d^2}\right)^{-d}} \quad (5.10)$$

Where,

$$a = 1.110\left(-1.413(\beta Fr - Frc) + 1.583\right)^{1.215} \qquad \text{(for } R/W < 2.0\text{)}$$

$$a = 1.110\left(1.121 Ln(\beta Fr - Frc) + 2.232\right)^{1.215} \qquad \text{(for } R/W \geqq 2.0\text{)}$$

$$b = 0.881\left[0.445 Ln(\beta Fr - Frc) + 1.740\right]^{1.209}\left[-0.00226(\phi) + 1.184\right]^{0.964}$$

$$c = 4.0459\left[0.507(\beta Fr - Frc) + 0.078\right]^{0.923}\left[0.260 Ln(\phi) - 0.906\right]^{0.884}$$

$$d = 3.251\left[0.311 Ln(\beta Fr - Frc) + 0.775\right]^{1.0944}\left[0.00308(\phi) + 0.143\right]^{1.028}$$

$$e = 8.286(\beta Fr - Frc)^{2.432}\left[0.0000229(\phi)^2 - 0.00614(\phi) + 0.417\right]^{0.748}$$

Note: $\beta = \frac{1}{R/W} + 1$, $b = 1.5$ (for $R/W \leqq 1.0$), and $e = 0$ (for $R/W > 6$)

5.5 VERIFICATION OF THE PROPOSED EQUATIONS

Once any prediction equation is developed based on the regression of the experimental data, it needs to be validated first with the same laboratory data, and then with full scale field data if available. If it does not produce a satisfactory precision for the same laboratory data used to generate the equation, there is no need to consider a full-scale verification study with filed data. Therefore, as the first step in the verification process, the proposed two equations for M_{max} (Eq. 5.9) and $\dot{M}_i$ (Eq. 5.10) were evaluated by predicting the flume test results.

By using Eq. 5.1, the meander migration along the channel in the flume tests was predicted, where *a* and *b* coefficients in the hyperbolic function are calculated by Eq. 5.9 and Eq. 5.10, respectively. For example, the prediction results for T5 (after 120 hrs) in case 06 are shown in Figure 5.11.

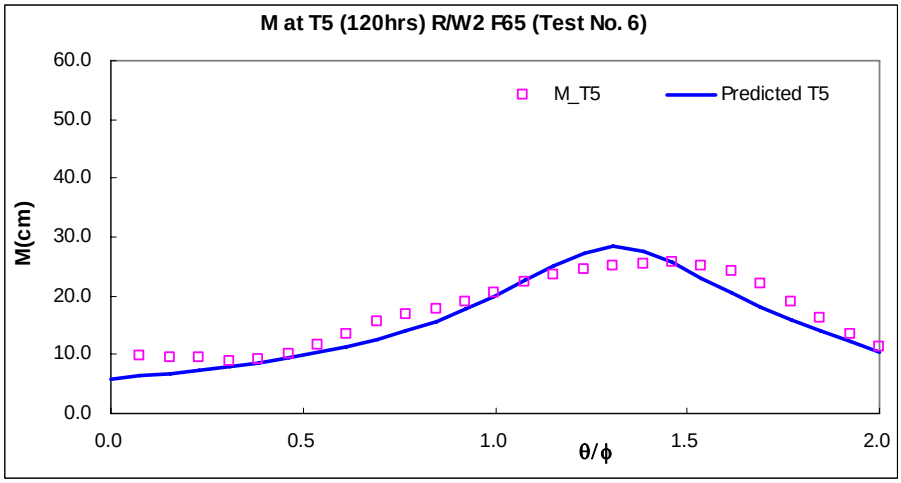

Figure 5.11 Predicted versus Measured Migration Distances in Clay Test Case 06

Root-mean-square errors between the measured and predicted migration distances are calculated and shown in Figure 5.12. The errors are normalized by the initial channel width *W*. Figure 5.12(a) shows the errors at the first measurement (T1) in each case, typically 24 hours after the tests started. This might be an alternative test for the predicted initial migration rates, and the averaged error along the channel is 0.049 (or 4.9 % of the initial channel width). Figure 5.12(b) shows the errors at the last measurement in each case, ranging from 180 to 240 hours after the tests started. This would be an alternative test for the predicted maximum migration distances, and the

averaged error along the channel is 0.046 (or 4.6 % of the initial channel width). This level of precision is quite satisfactory, considering that these tests are large-scale experimental data. Finally, Figure 5.12(c) shows the overall errors which include all the errors in every time step. The errors have an average value of 0.028 (or 2.8 % of the initial channel width), which is the best precision we can expect. In addition to the verification of the proposed equations against the laboratory data, a full-scale verification was done for the Brazos River at SH 105, which will be covered in a following chapter.

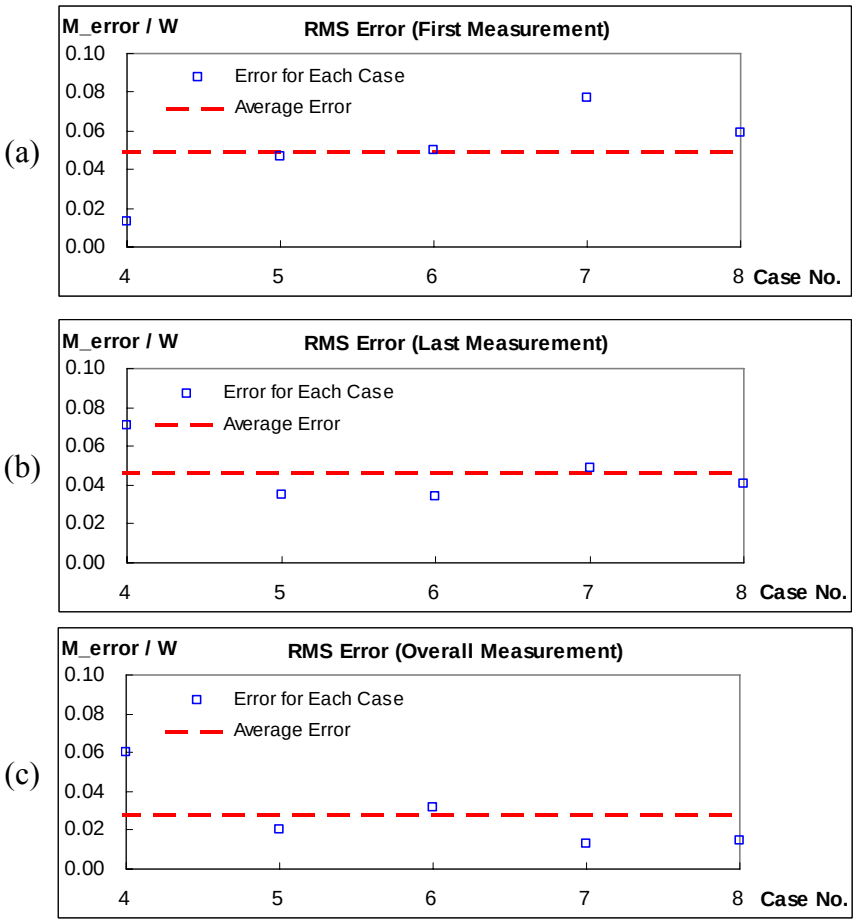

Figure 5.12 Estimated Root-mean-square Error of the Proposed Equations

CHAPTER VI

RISK ANALYSIS

6.1 INTRODUCTION

A meandering river migrates at a rate controlled by the shear stress at the interface between the water and the channel bank. The hydraulic shear stress imposed by the water is controlled by the velocity of the flow, which is dependent on the hydrograph of the river. Therefore, a meander migration prediction process must take the hydrograph of the river into account. This hydrograph is unknown, however, because it will occur in the future during the design life of the bridge or the highway embankment. Because it is not realistic to make a deterministic prediction of a future hydrograph, it is more desirable to make predictions of many equally-possible hydrographs in a probabilistic manner. Each hydrograph corresponds to a different predicted position of the meandering river, and a probabilistic post-process provides a probability that the river will move to a given location at a given time.

6.2 FUTURE HYDROGRAPH

A new methodology to generate a future hydrograph was developed (Wang 2006), and it is based on the statistical properties of the past hydrograph data: the past hydrograph (Figure 6.1) is assumed to be log-normally distributed, as shown in Figure 6.2., and it fits the original distribution of the hydrograph reasonably well. Then, the required statistical parameters (such as the mean and standard deviation of the given hydrograph) are retrieved from the fitted distribution, and the equally-possible future

hydrograph is then generated by using a random number generation technique. Detailed information can be found in Wang's dissertation (2006).

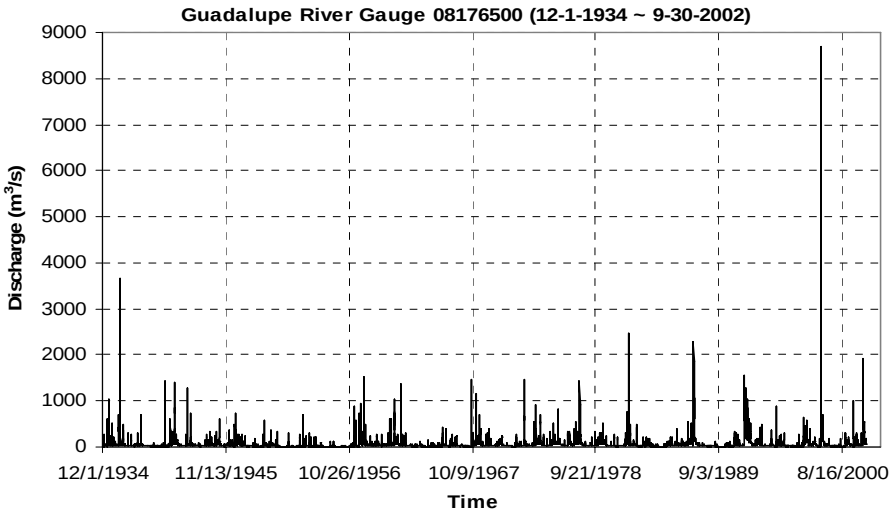

Figure 6.1 Hydrograph of Guadalupe River Gauge Station 08176500 (Wang 2006)

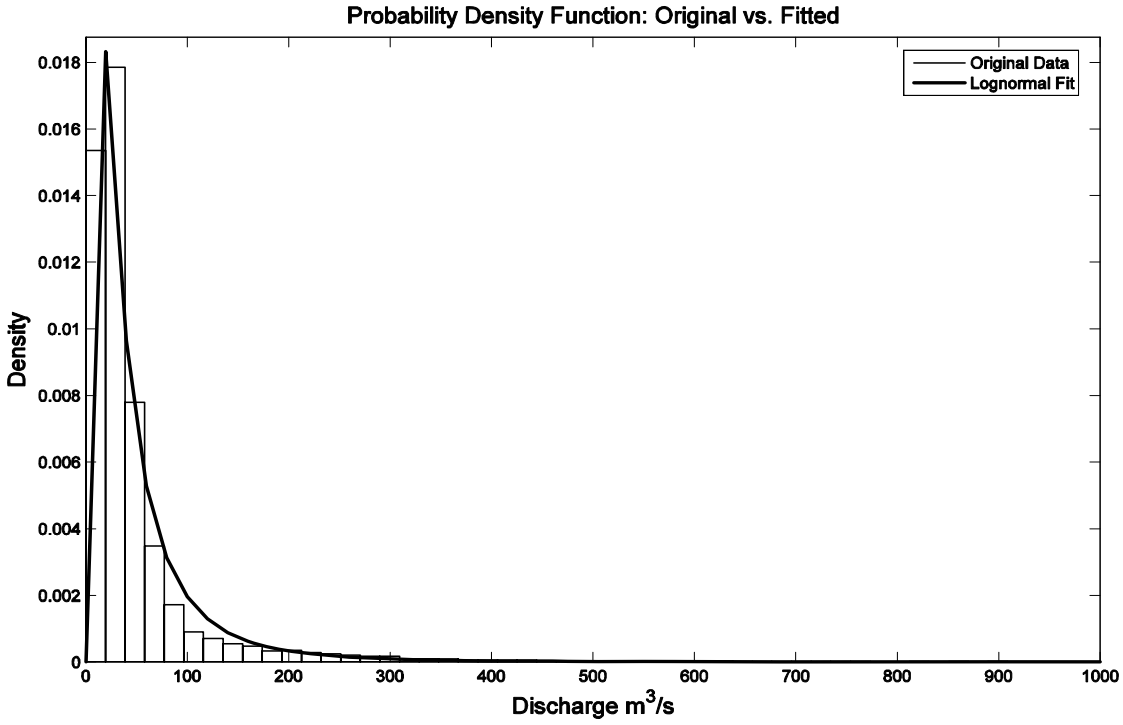

Figure 6.2 PDF of Original Data and Fitted Distribution for the Guadalupe River (Wang 2006)

6.3 CUMULATIVE DENSITY FUNCTION MAP

A large number of equally-possible future hydrographs are generated by the random number generating scheme, as described in the previous section. For each hydrograph, the MEANDER program predicts the migrated location of the river at the end of the project life. In other words, if 1,000 future hydrographs are generated, 1,000 rivers are simulated at the different locations according to each hydrograph, as shown in Figure 6.3. In the figure, the dotted line represents the initial geometry of the river and the solid lines are the predicted locations of the rivers after a given project life.

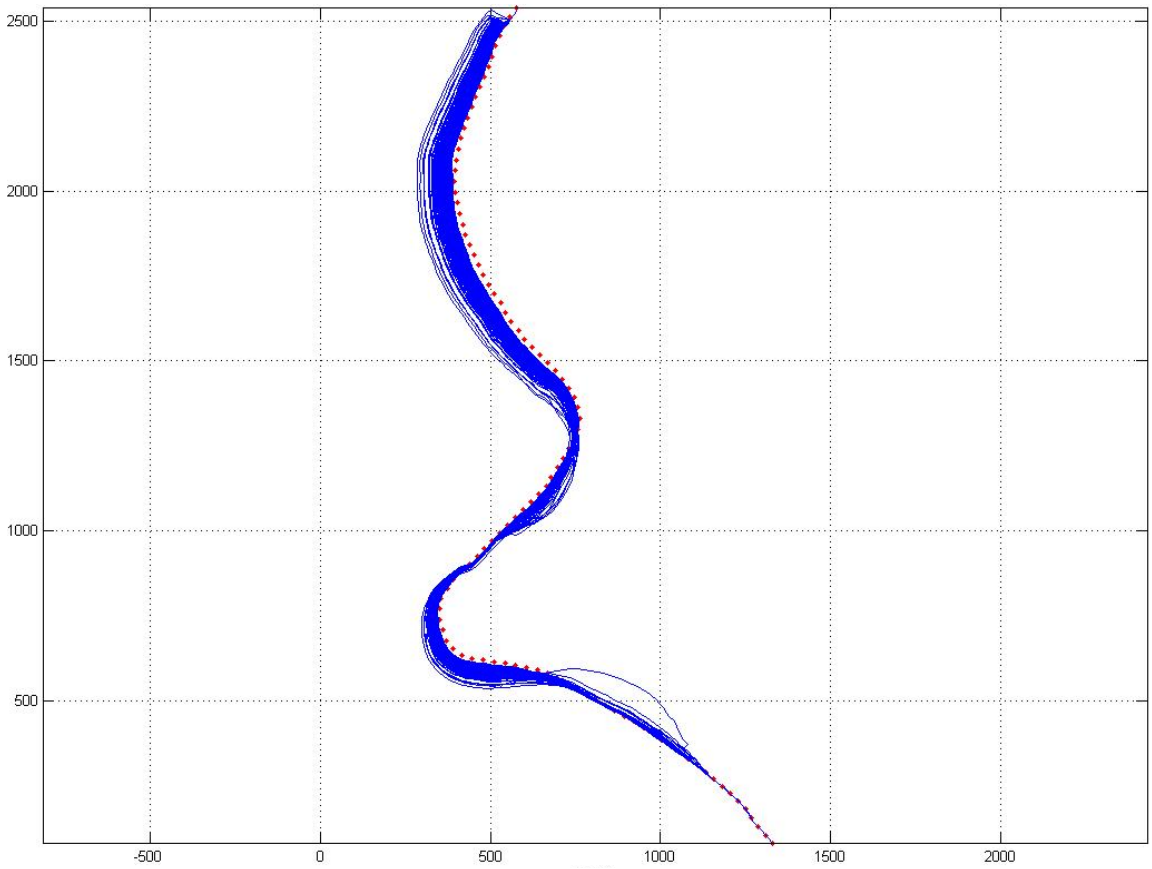

Figure 6.3 Generated Rivers According to the Future Hydrographs

Once a number of different river geometries are generated as shown above, a statistical post-processing scheme generates the probabilistic information of the prediction results: firstly, the cumulative density function map, which is a contour map, to delineate the probability associated with the predicted locations of the river. Secondly, cumulative density function graph is developed for a given bridge direction, which provides more detailed information about the migration distance along that direction.

An independent program module for this process using a relatively simple but quite reasonable approach was developed by using Matlab, and then incorporated into the MEANDER program. The new methodology of risk analysis in this study can be described by the following steps.

First, a number of reference lines are generated normal to the initial river geometry at every node point along the digitized channel, and then a number of small grids along each reference line are created as shown in Figure 6.4 and Figure 6.5. These reference lines and grids on the lines can be used as a domain for calculating the probabilities associated with the predicted locations of the river. The size of each grid is $0.1W$ and the length of the reference line is $4W$ in total, indicating that it is extended to $2W$ in both directions (i.e., right and left) from the initial river.

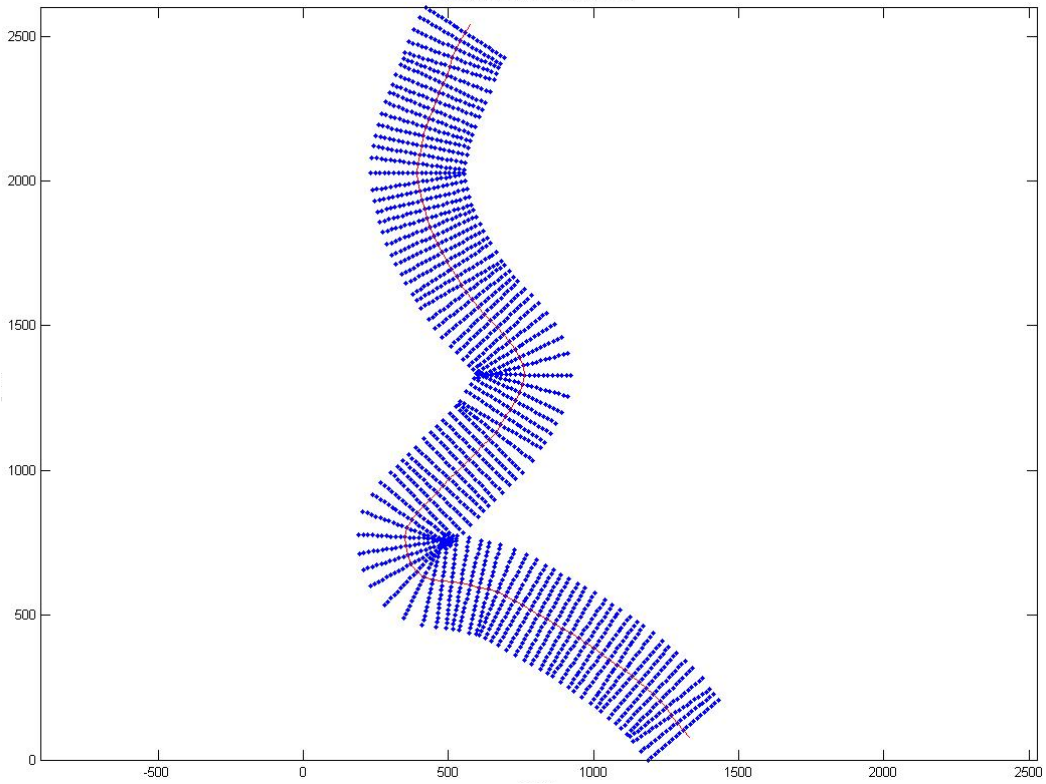

Figure 6.4 Generated Reference Lines along the Initial River

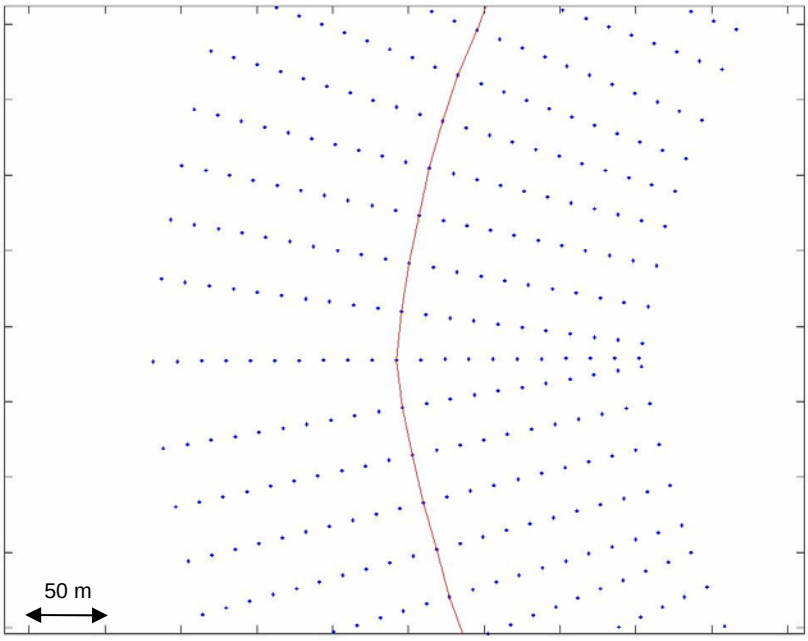

Figure 6.5 Detailed View of the Reference Lines

Second, the generated rivers from the previous step are superimposed on the simulated domain as shown in Figure 6.6. The numbers of crossings of the predicted rivers in each grid are counted and saved as a density value for that grid from the upstream direction to the downstream. This becomes the probability density function (PDF) for each reference line along the channel.

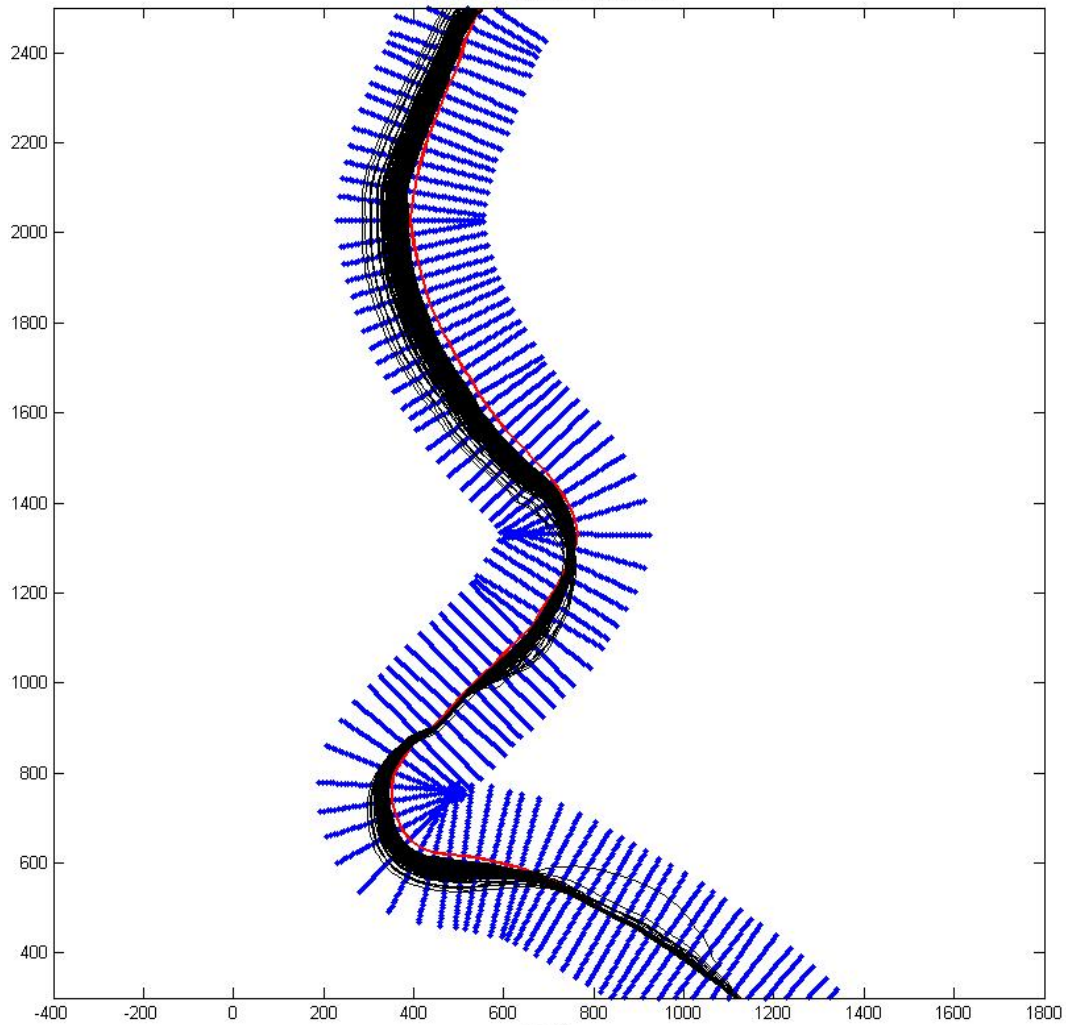

Figure 6.6 Superimposed Rivers on the Simulated Domain

Next, the cumulative distribution function (CDF) for each reference line can be calculated from the PDF obtained in the previous step, and a conceptual CDF is shown in Figure 6.7. All the points that have the same level of probability value (e.g., 1, 10, 30, and 50 percent) on every reference line along the river are then connected as shown in Figure 6.8. Each connected line represents a certain probability that the initial river will move to the location of that line or further at the end of project life (e.g., 75 years). A series of these lines with the initial geometry of the river can show the general trend of the meander migration of the river with the associated likelihood levels. This is called the CDF map, which is similar to a conventional contour map.

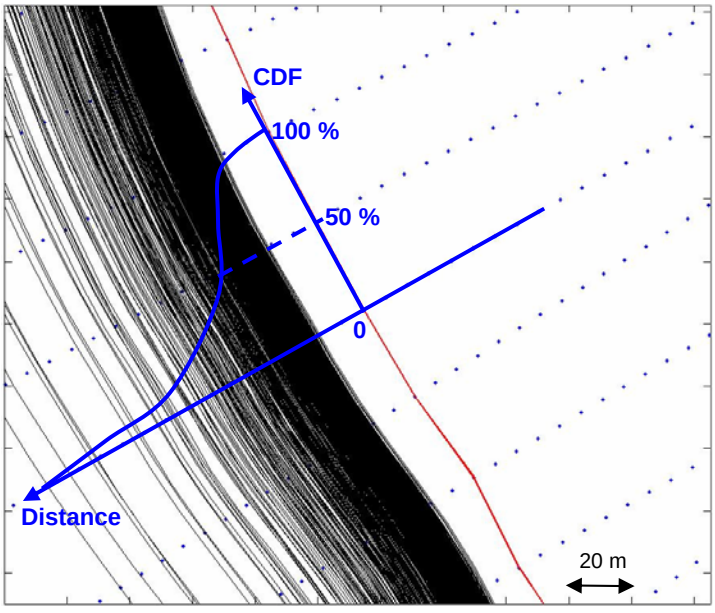

Figure 6.7 Conceptual CDF for a Reference Line on the Simulated Domain

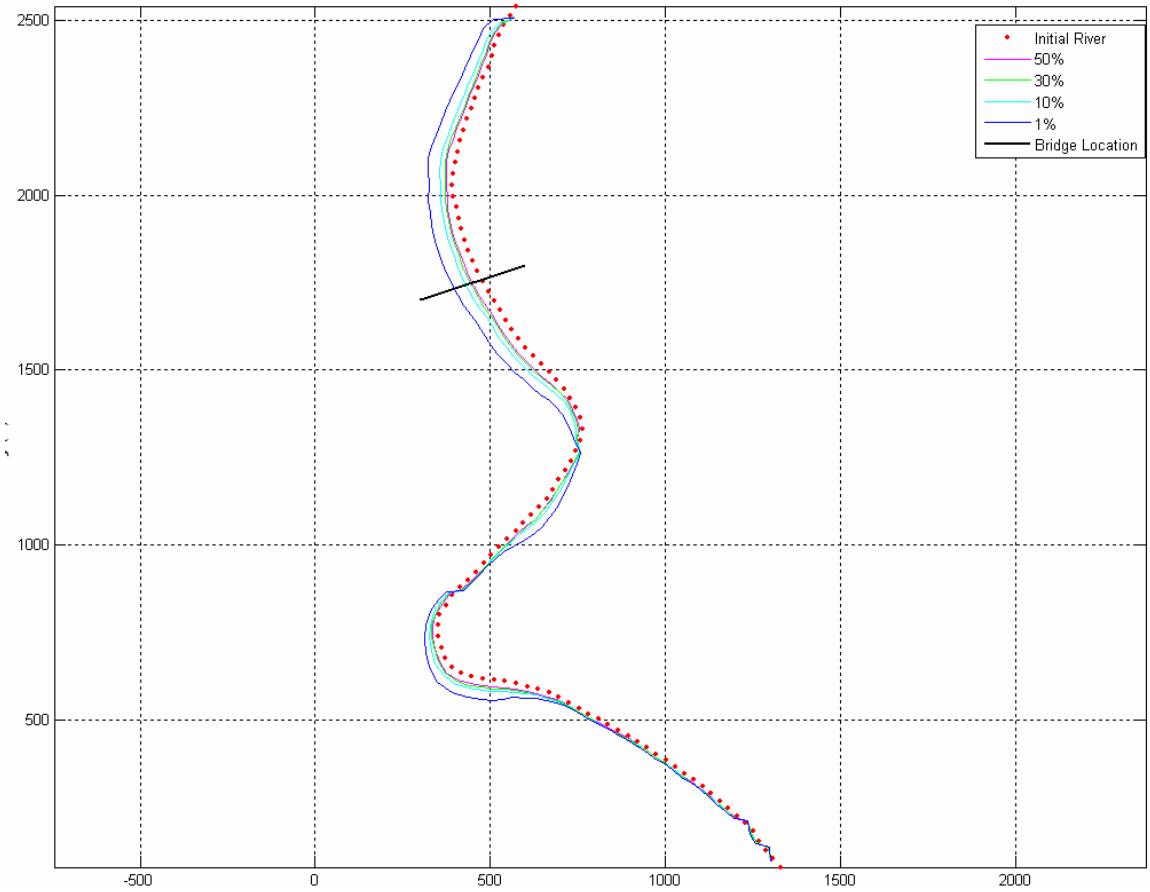

Figure 6.8 Cumulative Density Function Map

6.4 CUMULATIVE DENSITY FUNCTION FOR A GIVEN DIRECTION

As mentioned in the previous chapter, meander migration can undermine bridge piers, abutments, foundations of parallel highways, and cause loss of useful land. The common concern of these problems might be to know the bank movement at a specific location as well as direction (e.g. bridge direction) during a certain period of time. Although the CDF map provides the global picture of the predicted bank movement over the choosen period, it is often insufficient information regarding a specific location and direction. Therefore, a separate CDF graph for a given location and direction is

necessary to be a helpful tool from a practical standpoint. This CDF graph can be obtained by interpolating the saved density values on the CDF map: the x and y-coordinates of two end points of interest are specified as input data for the bridge location (Figure 6.8), and then the new CDF is calculated by interpolating the values of two adjacent points on each contour line associated with the different probability level (e.g. 50 % contour line). After repeating the interpolation for the other contour lines, a completed CDF graph for a given direction is obtained. This graph is plotted with a log scale on the y axis in a new screen so that the engineers can easily read the migration distance associated with a target risk level (e.g. 1 %) on the plot as shown in Figure 6.9. For example, the highlighted point in red can be interpreted as follows: there is a 1 percent probability that the river will move 82.5 m or further in the given direction over the design life of the bridge (e.g. 75 years).

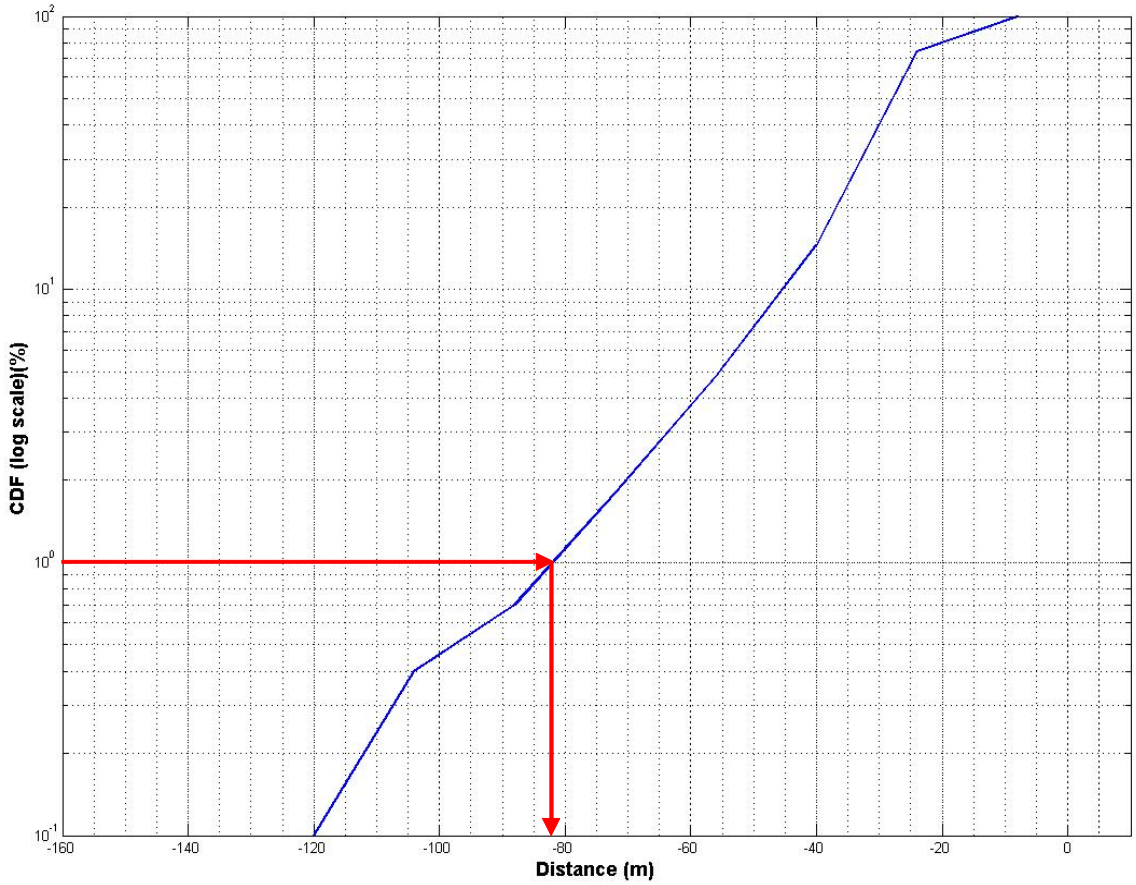

Figure 6.9 CDF Plot for a Given Bridge Direction

CHAPTER VII

FIELD VERIFICATION STUDY

7.1 INTRODUCTION

The program MEANDER is a final outcome of the research project (Briaud et al. 2007) to develop a new prediction method of meander migration based on the large-scale flume tests to establish the maximum migration distance equation, and numerical simulations to establish the maximum shear stress equation. All the components in the newly-developed methodology were implemented into this stand-alone program to provide the future users an automated prediction process. The obtained maximum migration distance equation from the experimental study in clay and the proposed risk analysis methodology were also implemented in the program. As a new method is developed based on the experimental study, it is inevitable to validate it by a verification study. This can be done through case studies with the field data and/or other available data resources. A verification study is extremely important for developing a new methodology because it helps to check whether the new method is applicable to the field cases with a certain level of accuracy. Since there is no applicable data on the experimental study of meander migration available, the field data obtained from a carefully chosen site, Brazos River at the SH 105 in Texas, is used for the field verification study.

7.2 BRAZOS RIVER AT SH 105

The SH 105 Bridge over the Brazos River near Navasota, Texas, is located about half a mile west of the intersection between SH 105 and FM 159 (Figure 7.1). The Brazos River joins with the Navasota River about one mile downstream from the bridge location. There is a meandering bend that approaches from the northeast several hundred meters upstream of the bridge crossing.

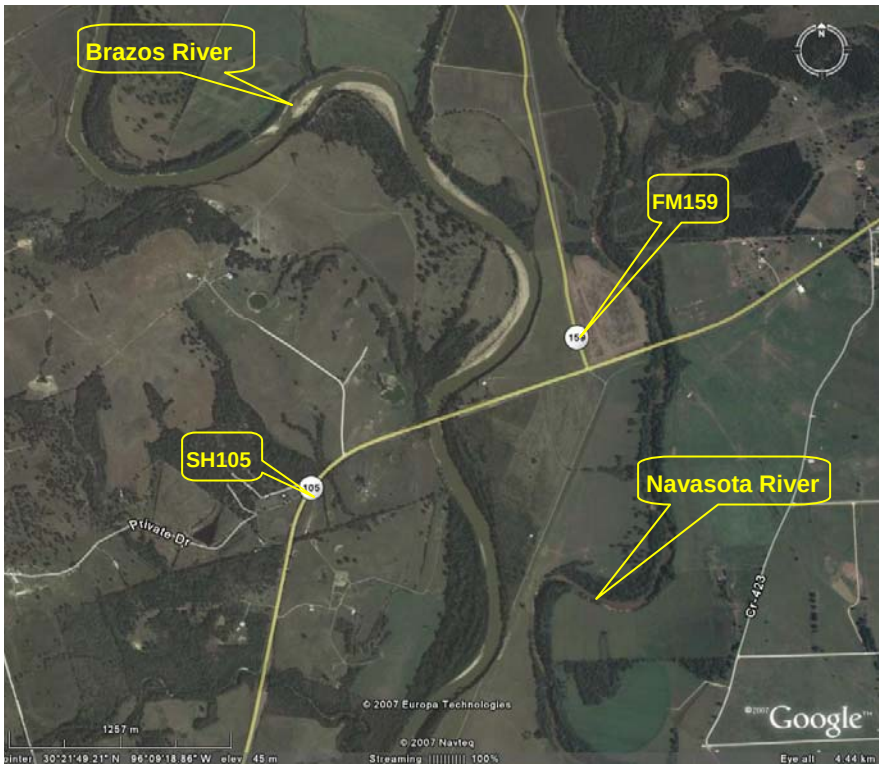

Figure 7.1 Brazos River Map (source: Google Earth 2007)

7.2.1 Site Description

The meander map (Figure 7.2) that was obtained from the 1981 and 1995 aerial photos and the Google satellite image (Google Earth 2007) shows the channel bank-line

movement of the Brazos River from 1981 to 2006. Note that the river geometry data from the satellite image was conservatively assumed as of 2006, because information about the date of the image is not available. During this period, the meandering bend at the upstream section of the bridge crossing moved approximately 98 m along the reference line which is the arrow in Figure 7.2. Moreover, the channel bank-line is expected to move continuously in the future. As a result, TxDOT has decided to replace the bridge to avoid a potential damage due to excessive bank erosion, and the new bridge is to be located about 228 m (760 ft) south of the old bridge.

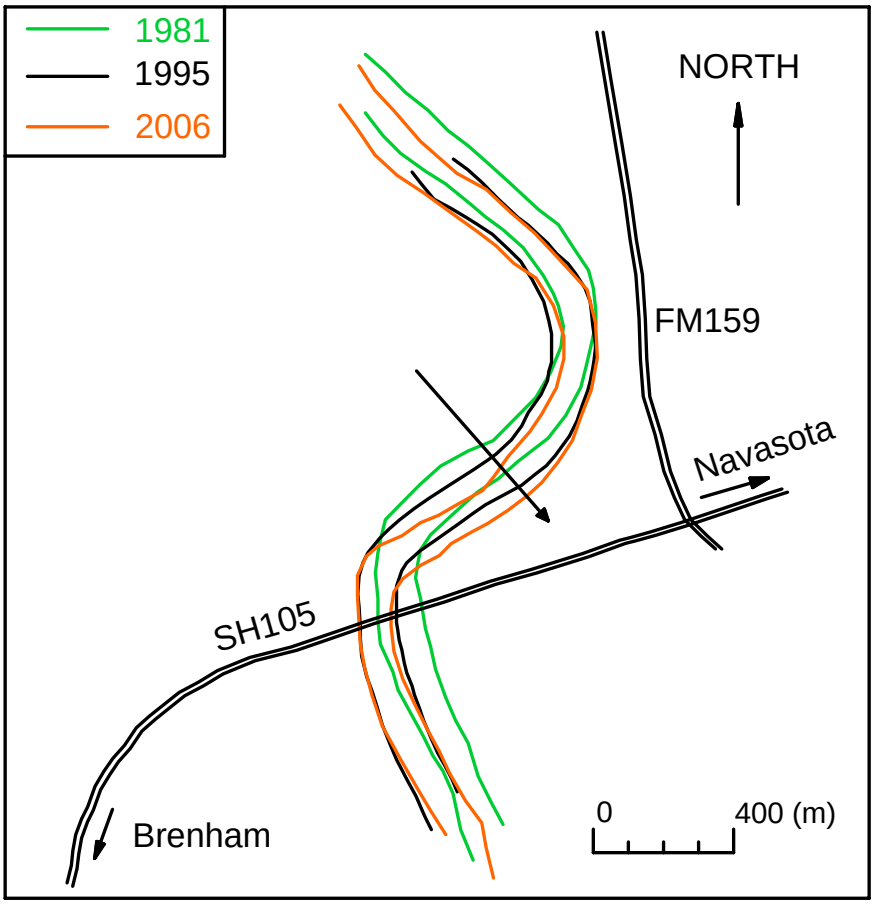

Figure 7.2 Brazos Meander Map

The channel profile of the Brazos River at the cross-section A-A' (Figure 7.3) has been measured periodically by the Bryan District (TxDOT). Figure 7.4 shows the channel profiles in 1951 and 2006 based on their measurement data. During this period, there was about 98 m of movements on both side banks due to erosion on the outer bank (west) and deposition on the inner bank (east). The cross-sectional profile data at the cross-section B-B', where much more serious movement occurred, is not available, and thus it needs to be assumed based on the information from the field visit and the channel profile at the bridge crossing. The best estimated channel profiles at this location are shown in Figure 7.5. As can be seen in Figure 7.5 (b), the outer channel bank-line (east) has moved towards the highway about 220 m during the same period.

Figure 7.3 Two Locations for Cross-sectional Profiles (source: Google Earth 2007)

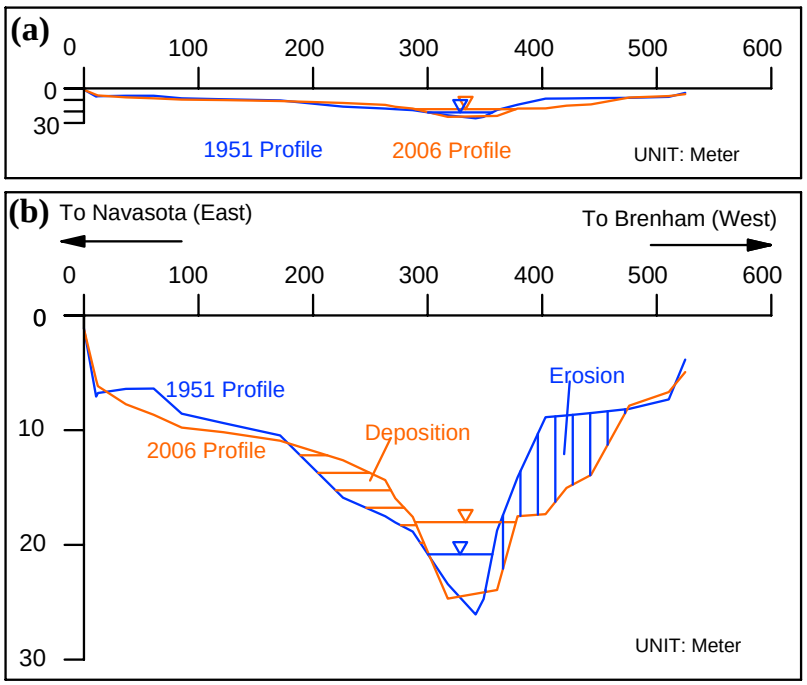

Figure 7.4 Cross-sectional Profiles at A-A': (a) To Scale, and (b) Not to Scale

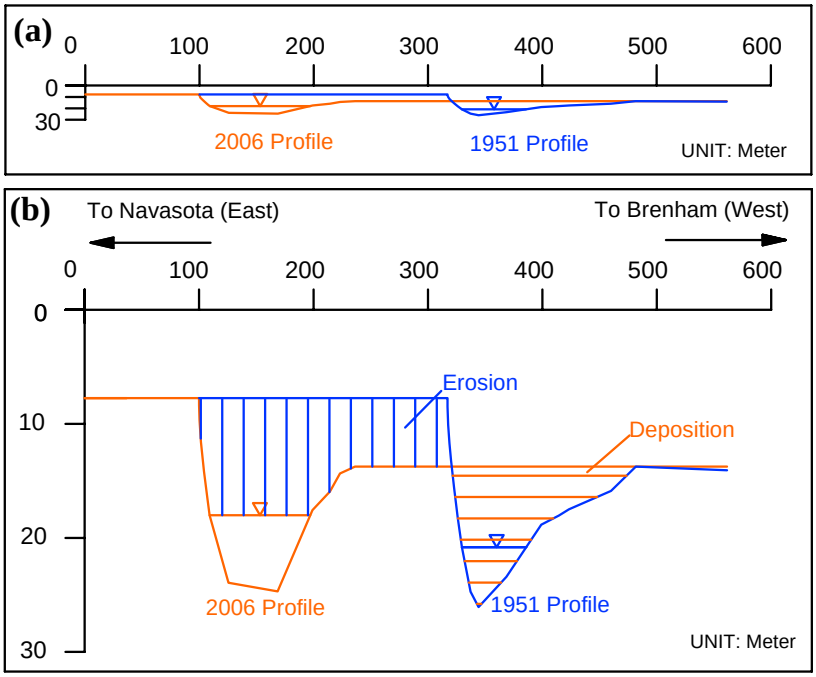

Figure 7.5 Cross-sectional Profiles at B–B': (a) To Scale, and (b) Not to Scale

The possible reason for two different levels of bank erosion on the meandering bend upstream and at the bridge crossing can be explained by looking at the site photos taken during the field visit in January 2007. As can be seen in Figure 7.6, there is heavy vegetation along the outer bank-line (left bank on the photo), and thus it can provide good protection against the erosion. Therefore, the total bank-line movement on this side could be less than that of the upstream bend, even if its geometric condition (sharp bend) is more susceptible to the meander migration. On the other hand, the upstream meandering bend has very little vegetation and its bank slope is quite steep, which indicates a higher potential for a mass failure initiated by undercutting due to the erosion. These unfavorable site conditions are clearly shown in Figure 7.7, and more photos are included in Appendix D.

Figure 7.6 Site Photo Taken on the SH 105 Bridge

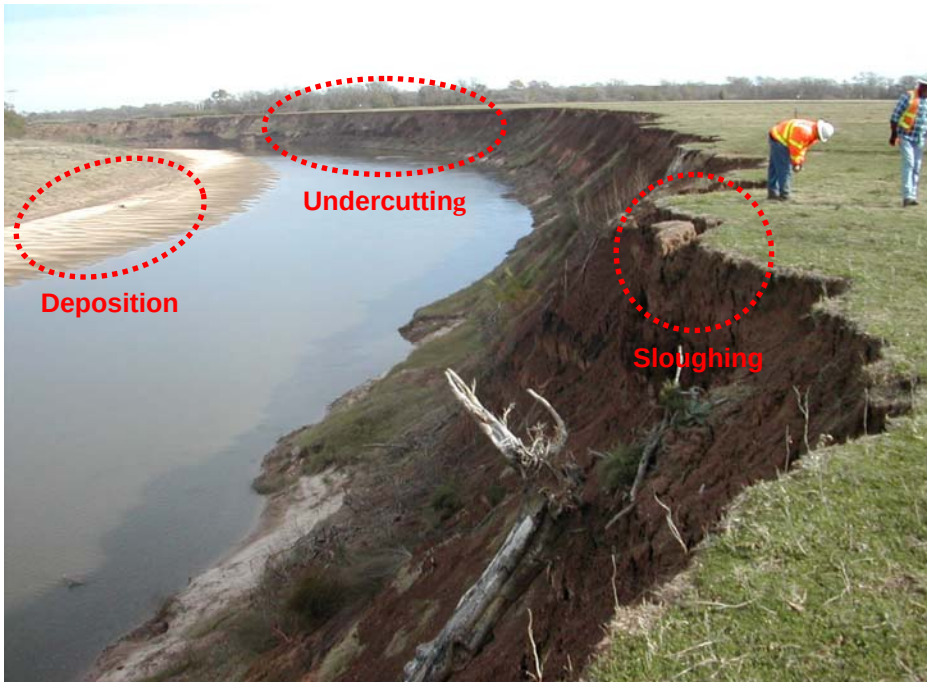

Figure 7.7 Photo of the Upstream Meandering Bend

7.2.2 Digitization of River Geometry

The geometry data for the Brazos River in 1981, 1995, and 2006 are prepared by digitizing the aerial photos and satellite image (Google Earth) with WinDIG (free software available at http://www.unige.ch/sciences/chifi/cpb/windig.html), as shown in Figure 7.8. If only a paper map or photo is available for the geometry data of the river, it needs to be converted to an electronic version before the digitization with the program. This can be done using a scanner if the map is not too big. There are two options to calculate migration in the MEANDER program: Bank Method and Centerline Method. The Bank Method uses two bank-lines (i.e. left and right) to describe the river, while the Centerline Method uses its centerline. In this study, the Centerline Method is used, and the digitized centerlines of the river in 1981, 1995, and 2006 are shown in Figure 7.9.

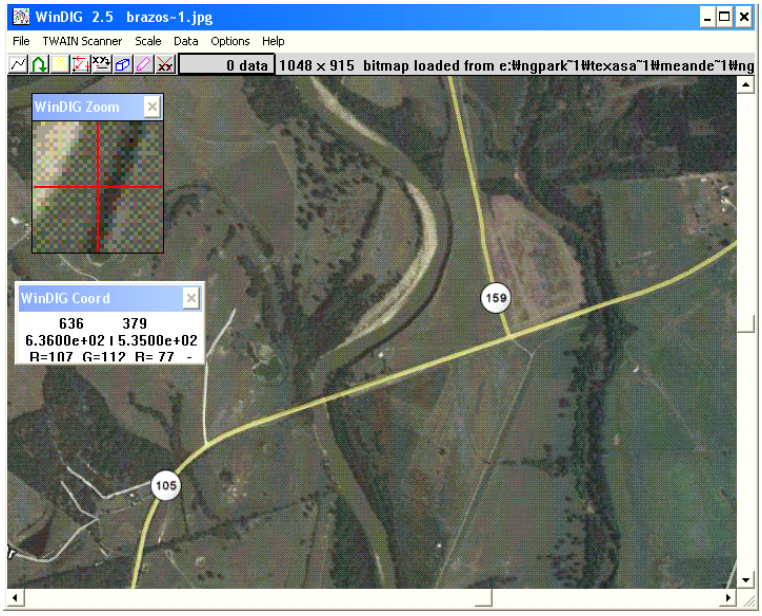

Figure 7.8 Digitized River Bank-lines with WinDIG

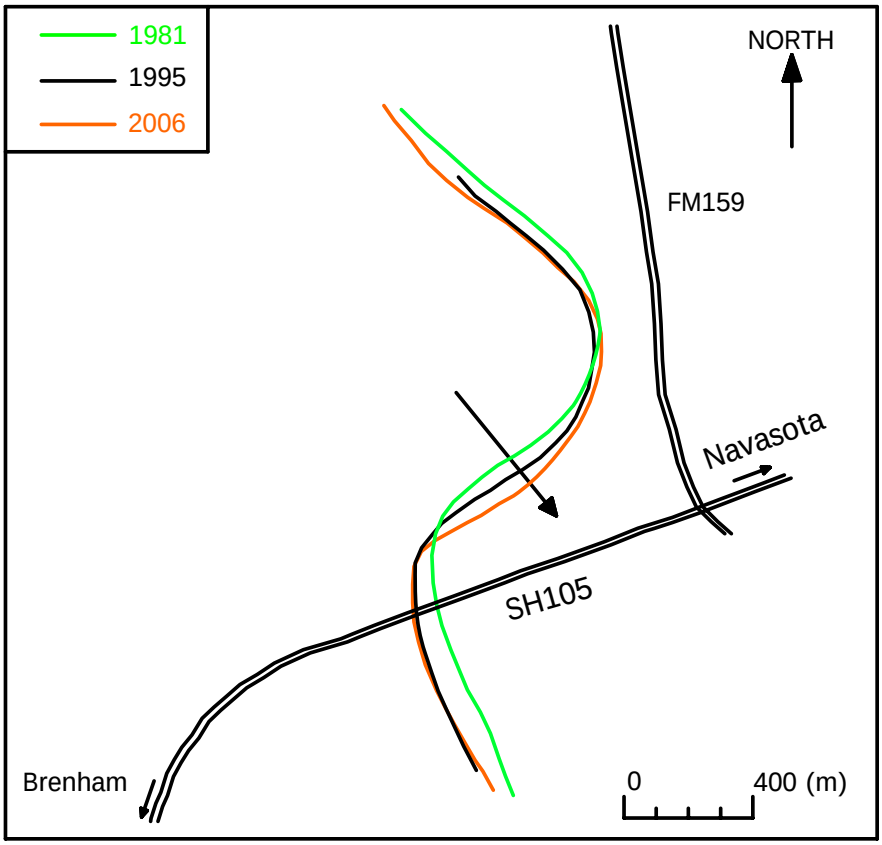

Figure 7.9 Hydrograph of Guadalupe River Gauge Station 08176500

7.2.3 Soil Sampling

A total of three sampling locations are selected based on the field visit and the history of meander migration in the past, and the exact boring locations are shown in Figure 7.3. Two locations are assigned along the upstream meandering bend because they experienced significant channel movement from 1981 to the present: B-1 on the apex of the bend and B-2 near the inflection point between the upstream bend and the bend at the bridge crossing. The last sampling location is the west bank of the river right under the SH 105 Bridge. The soil samples are taken every 10 feet (3 m) down to 50 feet (15 m) deep from the ground surface by using standard penetration tests (SPT) and Shelby tube samplers with a 3 inch (76.2 mm) outside diameter (Figure 7.10), which is required for EFA tests. The engineering soil properties are obtained in accordance with the standard of the American Society for Testing and Materials (ASTM) in the laboratory. The stratigraphies and the laboratory test results of B-1, B-2, and B-3 are shown in Figures 7.11, 7.12, and 7.13, respectively. The field boring logs are attached in Appendix E.

(a) Sampling Equipment (b) Samples

Figure 7.10 Photos of Sampling at the Site

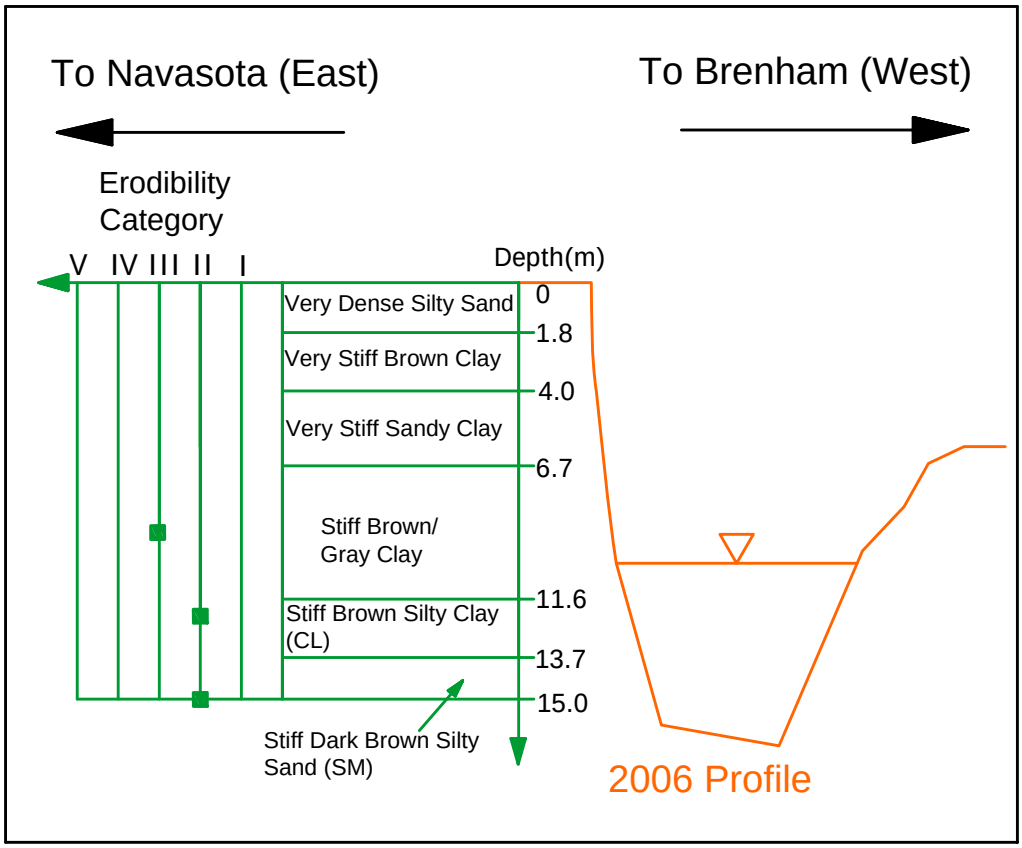

(a) Stratigraphy

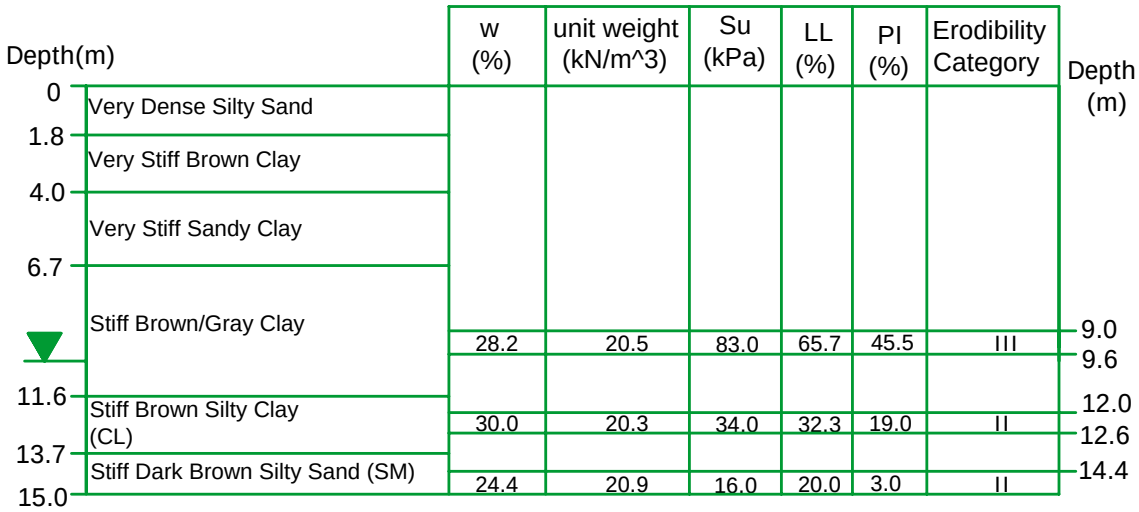

(b) Engineering Properties

Figure 7.11 Soil Layers at B-1

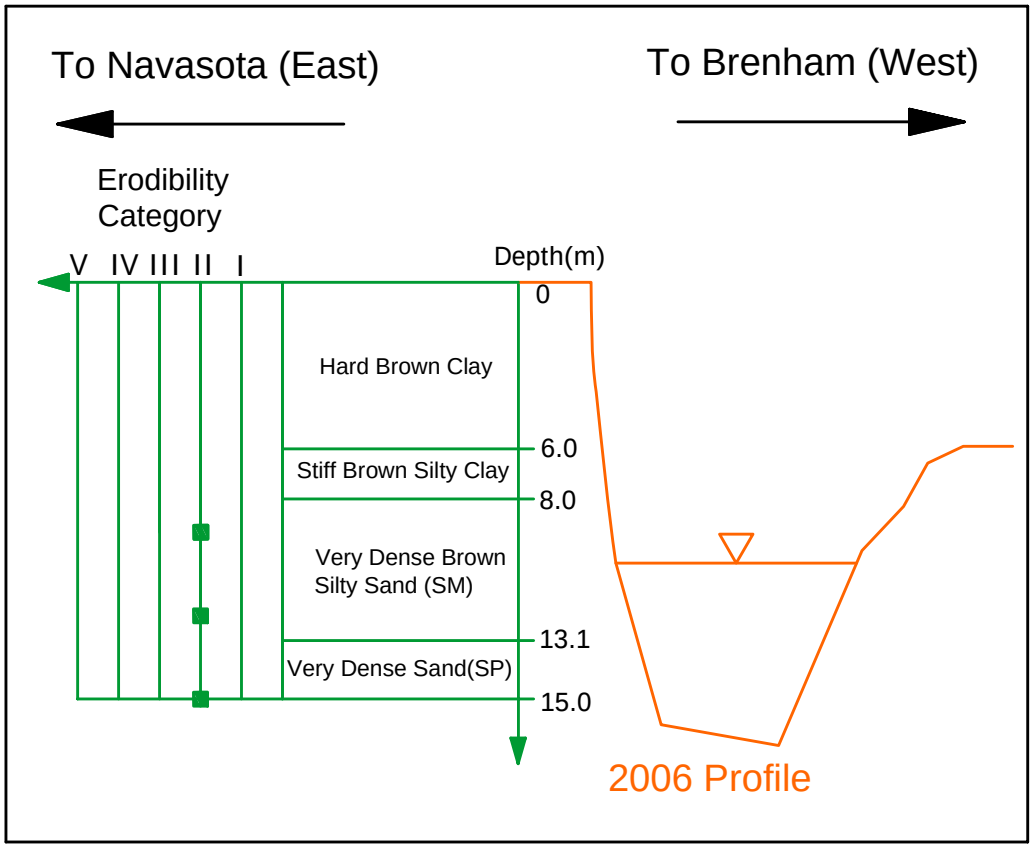

(a) Stratigraphy

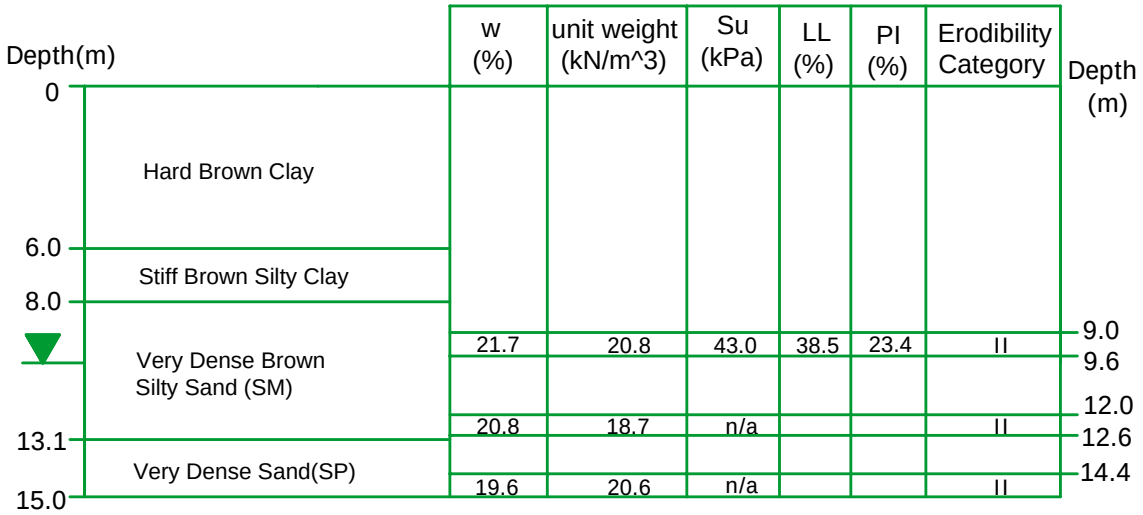

(b) Engineering Properties

Figure 7.12 Soil Layers at B-2

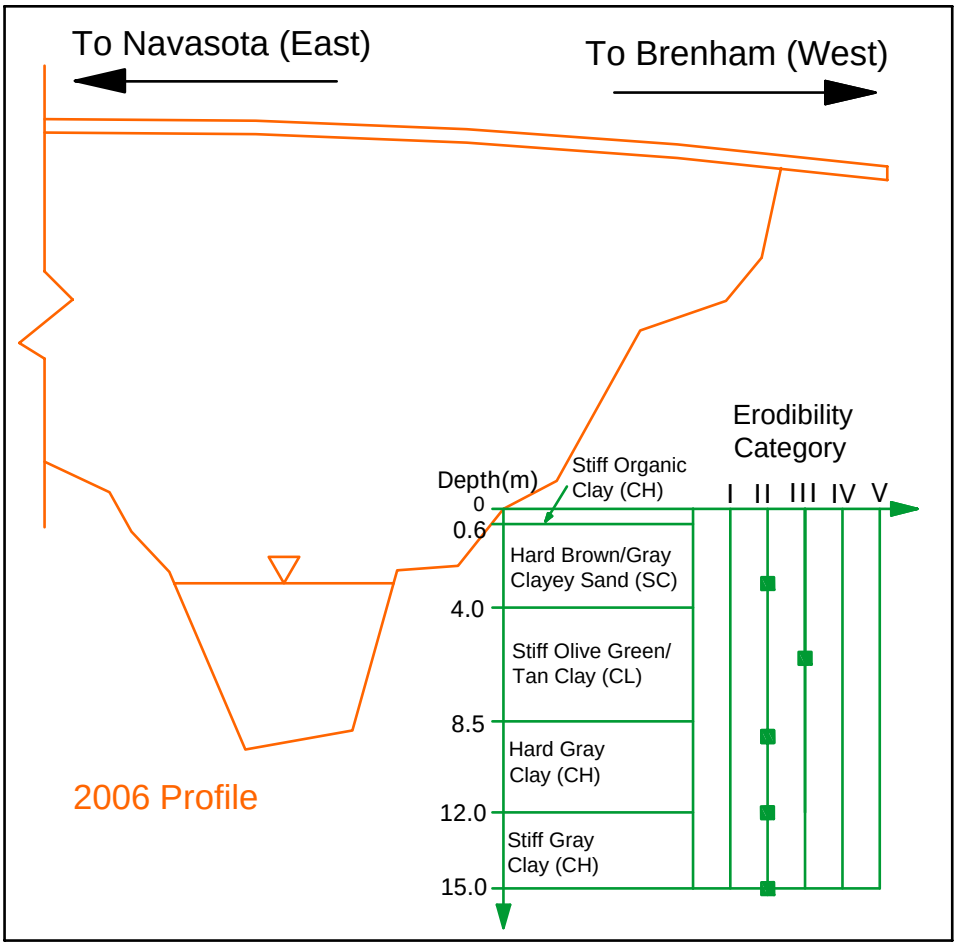

(a) Stratigraphy

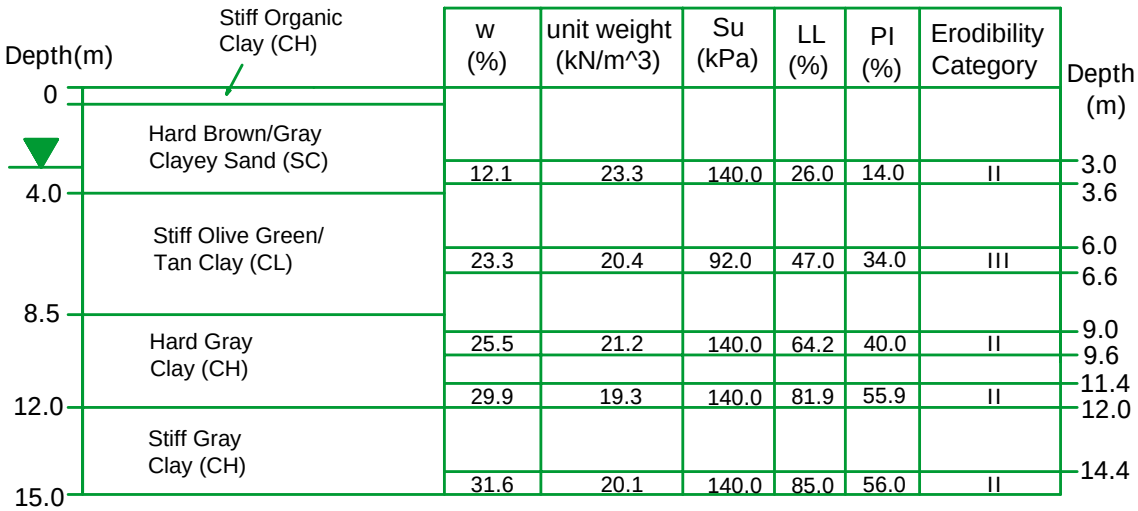

(b) Engineering Properties

Figure 7.13 Soil Layers at B-3

7.2.4 Erodibility from EFA Tests

The input data for the soil in the MEANDER program is the erosion function, which is the relationship between the erosion rate and the hydraulic shear stress applied by the water on the soil-water interface. This erosion function is obtained by performing an EFA Test on the selected Shelby tube samples from the site (Briaud et al. 2007). The EFA test results of these samples are shown in Figure 7.14, which are erosion rate versus shear stress curves. The test result designations are based on the boring number at the site and the depth interval over which the sample was taken. The red line in the figure is chosen as a representative erodibility input curve for the entire river reach, since the MEANDER program can only accommodate one erodibility input curve for the soil property. The reason for this selection is as follows. An in depth study of the meander erosion process at the site indicates that the bottom of the river bank of the upstream meandering bend is made of highly erodible sand, while the top of the river bank is made of less erodible fine grained soils. The sand is eroded; this creates undercutting of the overlying clay which sloughs in the river and is carried away. The erosion function which is selected is the one corresponding to the sand layer. Another type of the erodibility curve can be obtained from EFA tests: the erosion rate versus flow velocity curve, as shown in Figure 7.15.

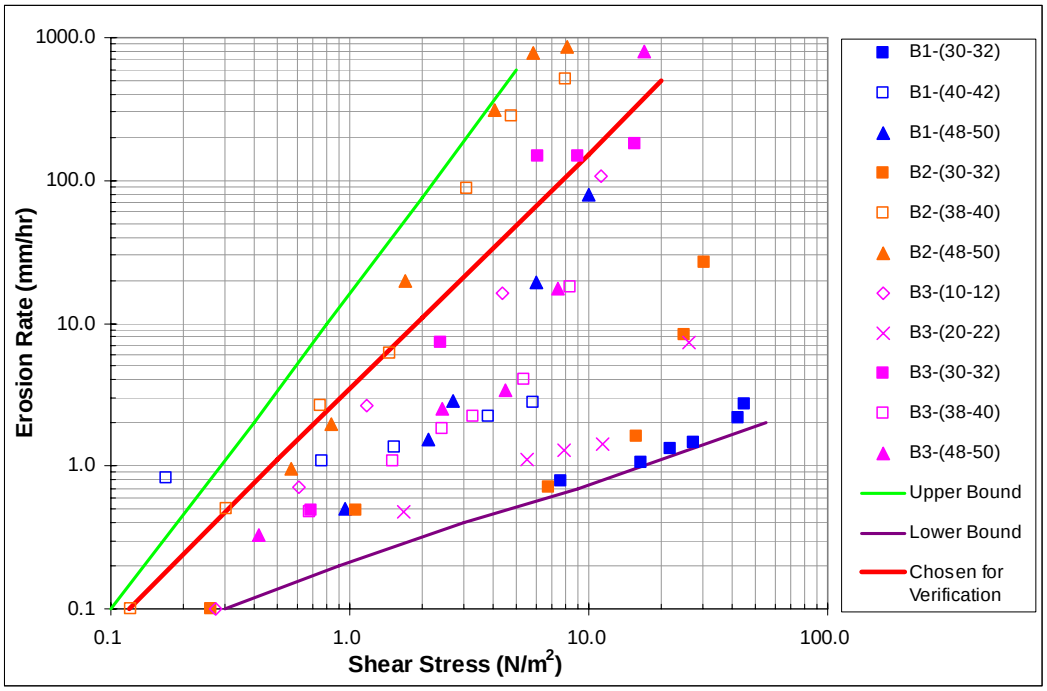

Figure 7.14 Erodibility Curves: Erosion Rate vs. Shear Stress

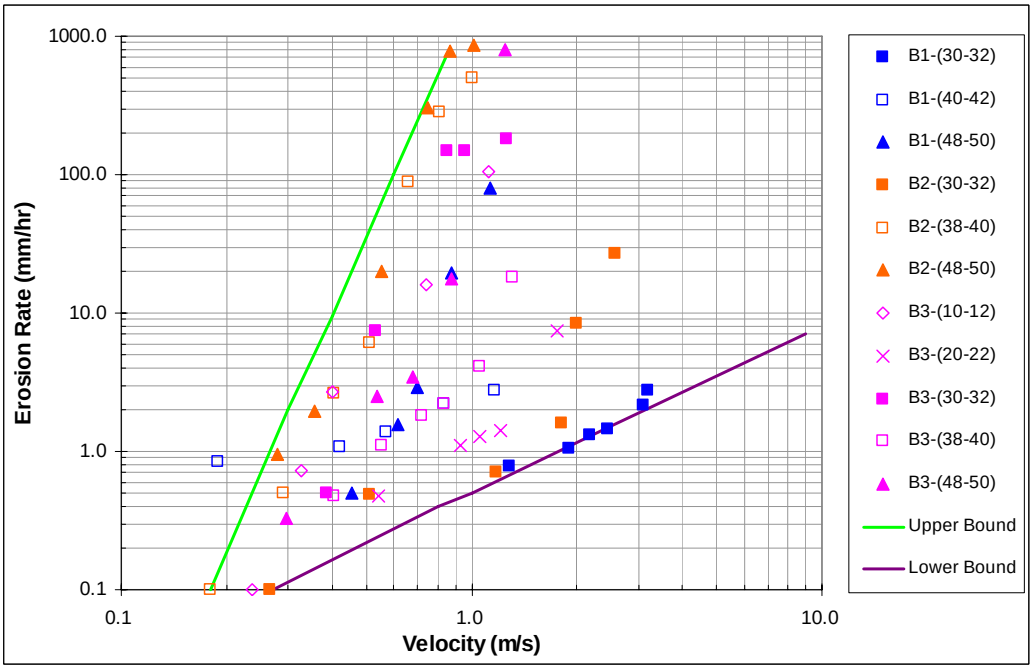

Figure 7.15 Erodibility Curves: Erosion Rate vs. Velocity

An erosion chart was developed to give a global interpretation of the EFA test results (Seed et al. 2006). This chart shows the erodibility curves in a way that categorizes the soils according to each erosion category: Category I is most erodible and Category V is most erosion resistant. The erosion chart for this study are populated with all EFA results, and it is shown in Figure 7.16.

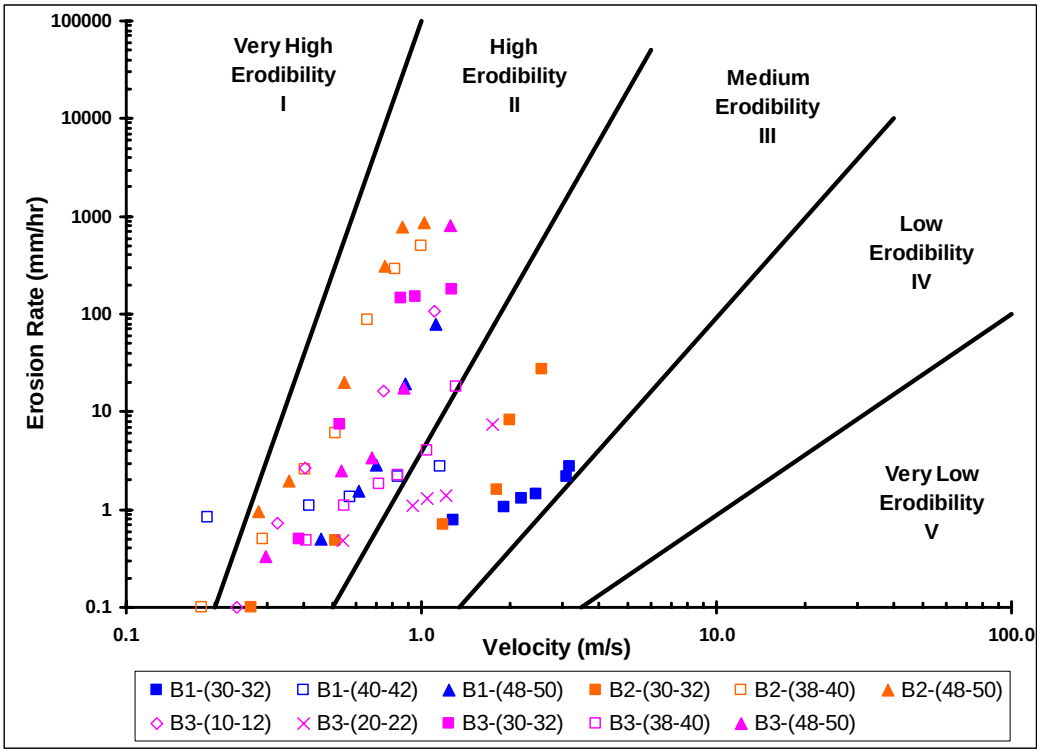

Figure 7.16 Erosion Chart with All EFA Test Results

7.2.5 Hydrograph

The nearest gauge station is found to be ST# 08110200 that used to be on the SH 105 Bridge (Figure 7.17). However, the available data from this station only covers for the period from 1965 to 1987. It seems to be closed in 1987. Therefore, the data from

other gauge stations on the upstream of the river needed to be used for the period from 1988 to 2006. The two other nearest gage stations on the upstream are found at approximately 80 km (50 miles) upstream in the channel lengthwise from the site, which are numbered as ST# 08108700 and ST# 08109000.

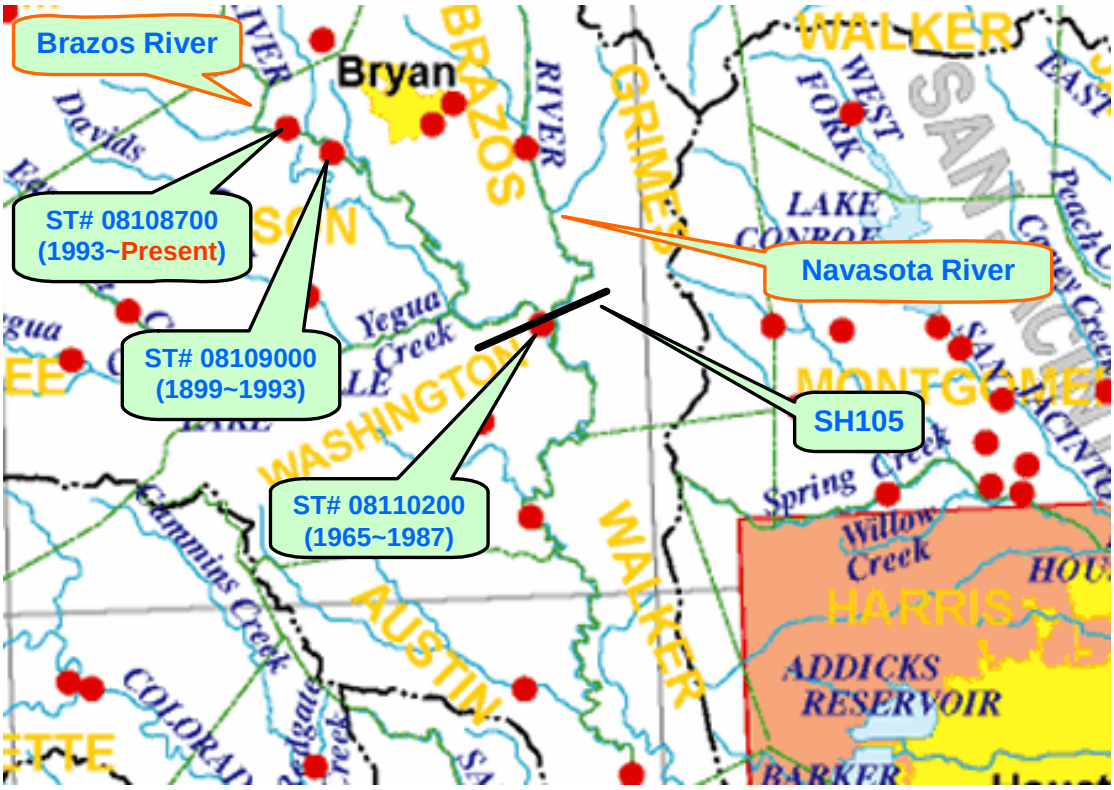

Figure 7.17 Locations of Gauge Stations along the Brazos River (http://pubs.usgs.gov)

Since the discharge hydrograph from the upstream can not be directly used for the downstream site, a calibration process is required to obtain a reasonable discharge hydrograph for the SH 105 Bridge site. The calibration is performed in the following way:

1. Populate a $Q_{downstream}/Q_{upstream}$ versus Q plot by using the discharge data of both downstream and upstream for the same period (Figure 7.18).
2. Estimate a boundary value between low and high discharge flow (600 m^3/s used in this study).
3. Select two correction factors in the two regions in a way that $Q_{downstream}$ is $Q_{upstream}$ multiplied by the correction factor.
4. Plot the corrected $Q_{upstream}$ with $Q_{downstream}$ to check whether these values reasonably match each other, especially for those peak values (Figure 7.19).
5. Repeat from step 2 to 4 if the match is not satisfactory.

The calibrated discharge hydrograph for the SH 105 Bridge site for the period from 1981 to 2006 is prepared as described above, and the results are shown in Figure 7.20. The maximum discharge during this period is 5243 m^3/s, which occurred in 1991.

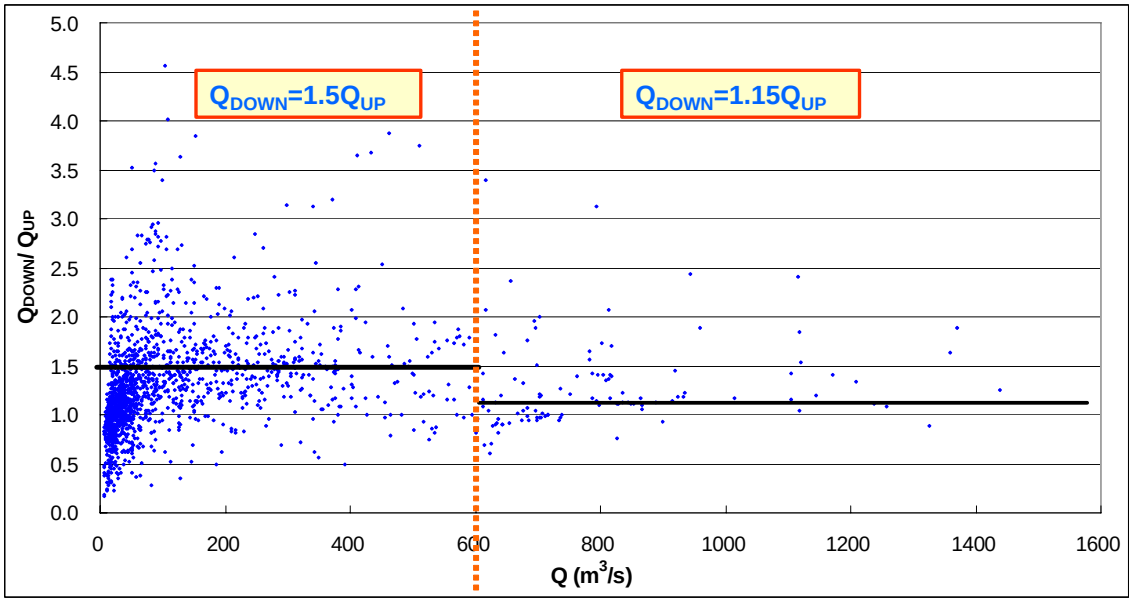

Figure 7.18 Comparison of Discharge between Upstream and Downstream

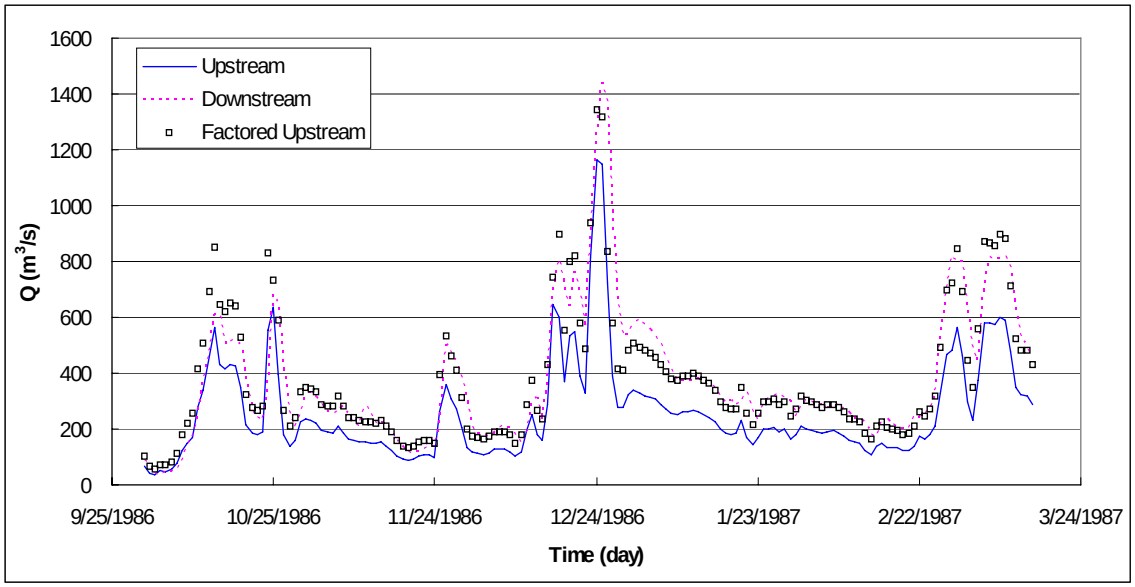

Figure 7.19 Calibration of the Upstream and Downstream Hydrographs

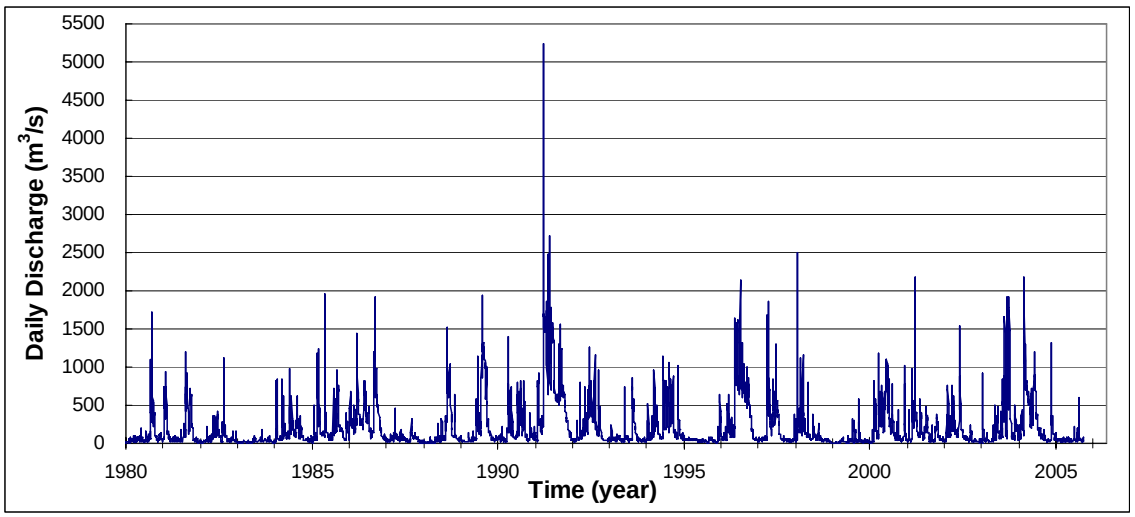

Figure 7.20 Discharge Hydrograph for the SH 105 Bridge Site

The site-specific curves of the relationships between the discharge versus velocity and the discharge versus water depth are obtained by the regression of the

measured data from the USGS website, and these are shown in Figure 7.21 and Figure 7.22, respectively. The discharge hydrograph can be converted to the velocity hydrograph and the water depth hydrograph by using these rating curves.

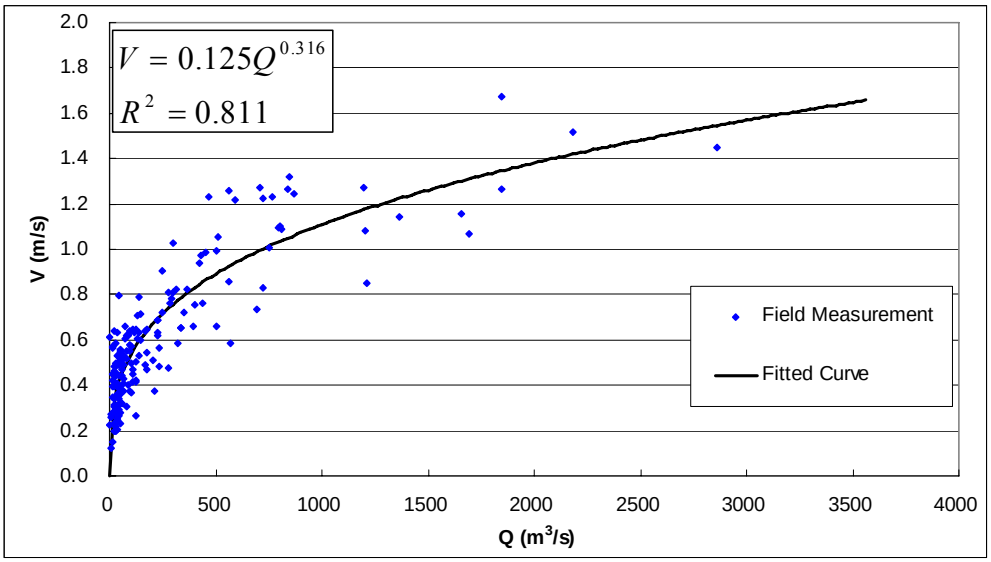

Figure 7.21 Relationship between Discharge and Velocity at the SH 105 Bridge

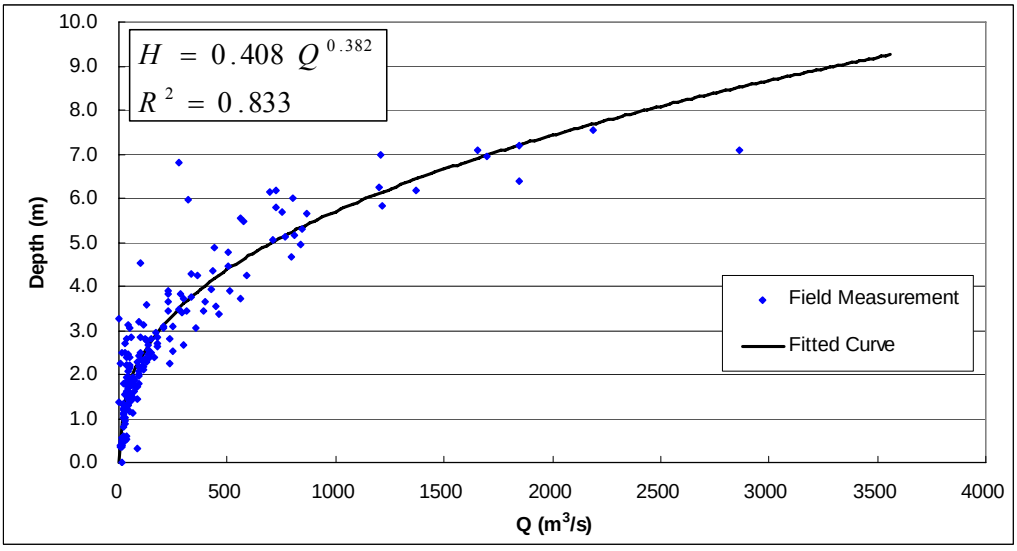

Figure 7.22 Relationship between Discharge and Water Depth at the SH 105 Bridge

7.3 DETERMINISTIC PREDICTION OF MEANDER MIGRATION

Prediction of meander migration on the Brazos River at the SH 105 was performed based on the input data described in the previous sections. The predicted locations of the Brazos River during the period from 1981 to 1995 and from 1981 to 2006 are shown in Figure 7.23 and Figure 7.24, respectively.

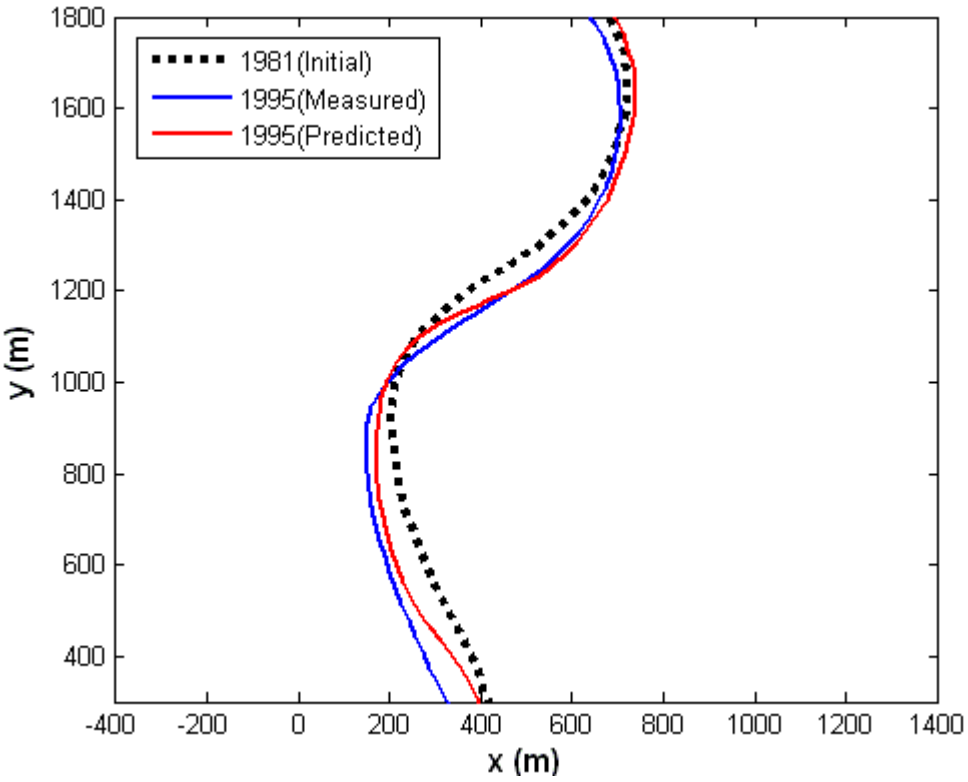

Figure 7.23 Predicted Location of the Brazos River (1981 ~ 1995)

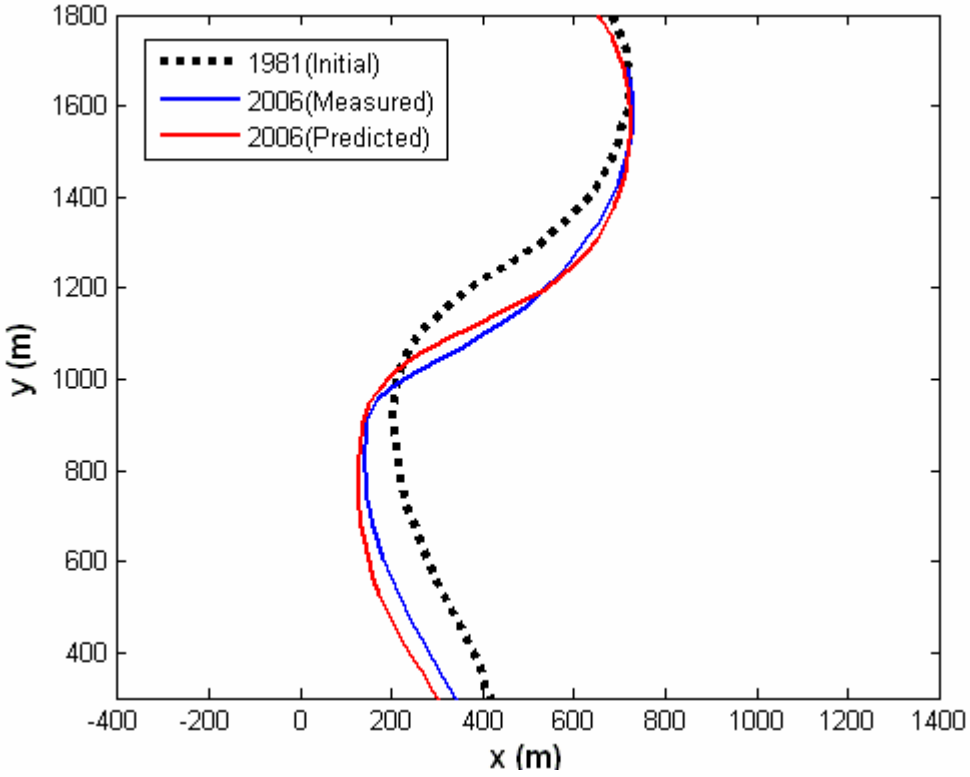

Figure 7.24 Predicted Location of the Brazos River (1981 ~ 2006)

The prediction results turned out to be reasonably accurate, especially for the channel movement on the upstream meandering bend. However, the channel movement towards the west bank at the SH 105 bridge crossing was somewhat over-estimated. There are three possible reasons for this: first, the prediction method can not consider the heavy vegetation along the outer bank-line. Second, a group of artificial rocks are found to be exposed above the ground surface, as shown in Figure 7.25, which was believed to be dumped as a countermeasure in the past. In fact, these natural and artificial countermeasures would provide significant protection against the erosion. Third, the input data for the soil properties in the prediction are based in the sand layer on the

upstream meandering bend, which is much more erodible than the actual soil at this location (i.e. clay).

a) Looking Upstream b) Looking Downstream

Figure 7.25 Heavy Vegetation and Dumped Artificial Rocks on the West Bank

The measured movements of the channel along the reference line, shown in Figure 7.9, are compared with the predicted movements in Figure 7.26(b). Figure 7.9(a) is the flow velocity hydrograph for the SH 105 Bridge site, which is converted from the discharge hydrograph (Figure 7.20) by using the rating curve, shown in Figure 7.21. The error between measured and predicted migration distance at 1995 is about 1 m, which is quite good. The predicted migration distance at 2006 is about 89 m, which is slightly lower than the measured value (i.e. 98 m). The error is equal to 7.5 % of the channel width which is approximately 120 m. This level of accuracy in the prediction of meander migration is the best precision we can expect.

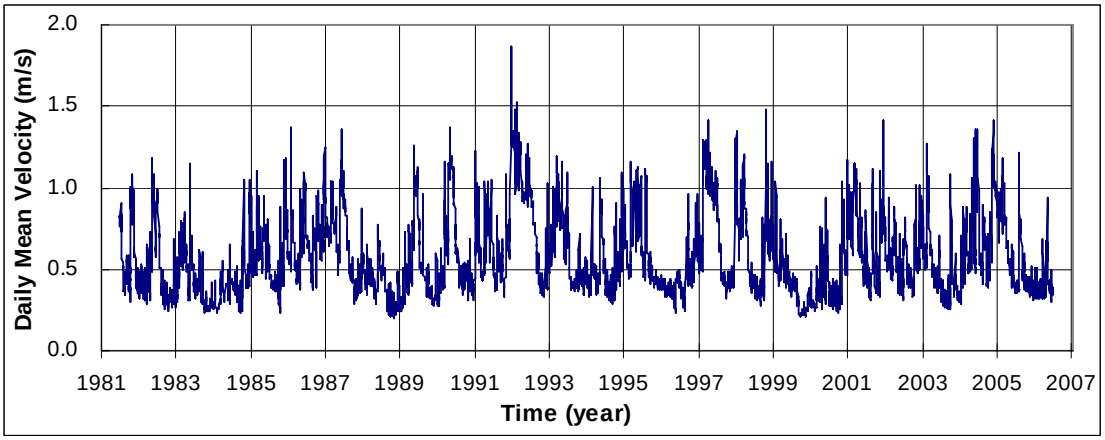

(a) Velocity Hydrograph

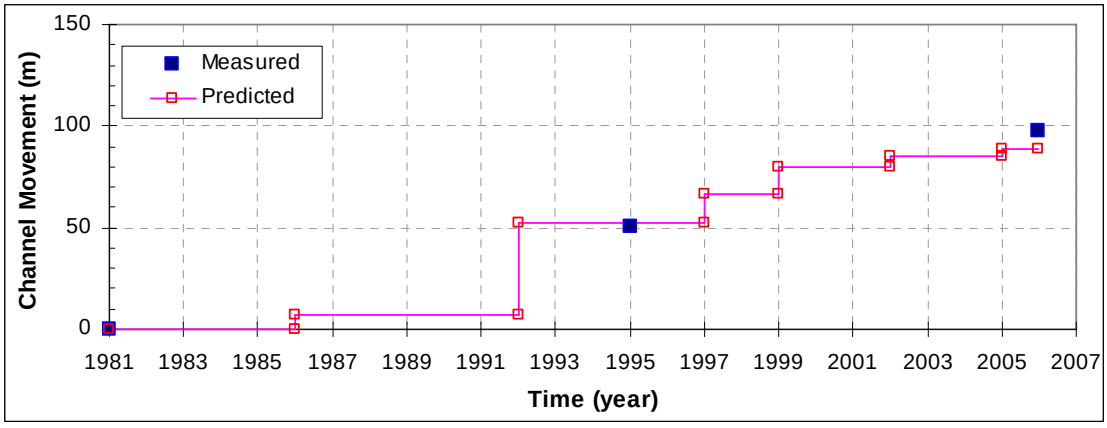

(b) Migration Distance

Figure 7.26 Measured vs. Predicted Migration Distance

7.4 PROBABILISTIC PREDICTION OF MEANDER MIGRATION

In addition to the deterministic prediction of meander migration on the Brazos River at the SH 105 in the previous section, a different type of prediction was conducted, which is a probabilistic prediction with the risk analysis option in the MEANDER Program. The prediction was done for the period from 1981 to 2006. A total of 1,000 equally-possible hydrographs were generated for the risk analysis. The prediction results

are shown in Figure 7.27, which contains 1,000 different predicted locations of the Brazos River.

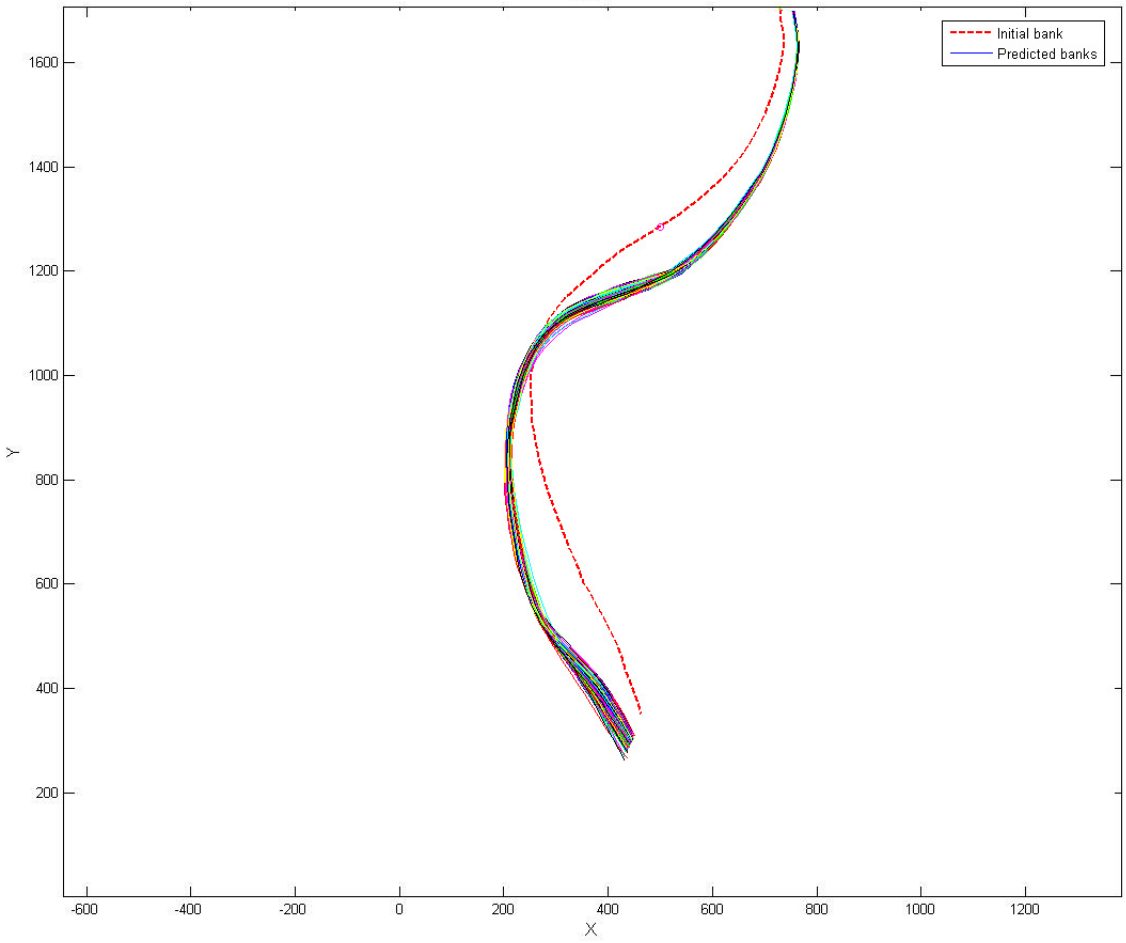

Figure 7.27 Predicted Locations of the Brazos River with the Risk Analysis (1981 ~ 2006)

Figure 7.28 shows the CDF map for those 1,000 locations of the predicted river. A series of contour lines with the initial geometry of the river shows the general trend of the meander migration of the river with the associated likelihood levels. However, it is hard to see the detailed information of the specific site, and thus a CDF plot was

generated for a given direction (i.e. reference line in Figure 7.9) in Figure 7.29 so that a corresponding migration distance to a certain risk level can be read from it. For example, if the target risk level is 1 %, the channel will move 108.5 m. In other words, the channel will migrate 108.5 m or further with 1 % probability of occurrence. The measured migration distance during this period is about 98 m shown in Figure 7.26(b), and this movement corresponds approximately to 70 % of risk level, which means there is 70% probability for the river will migrate 98 m.

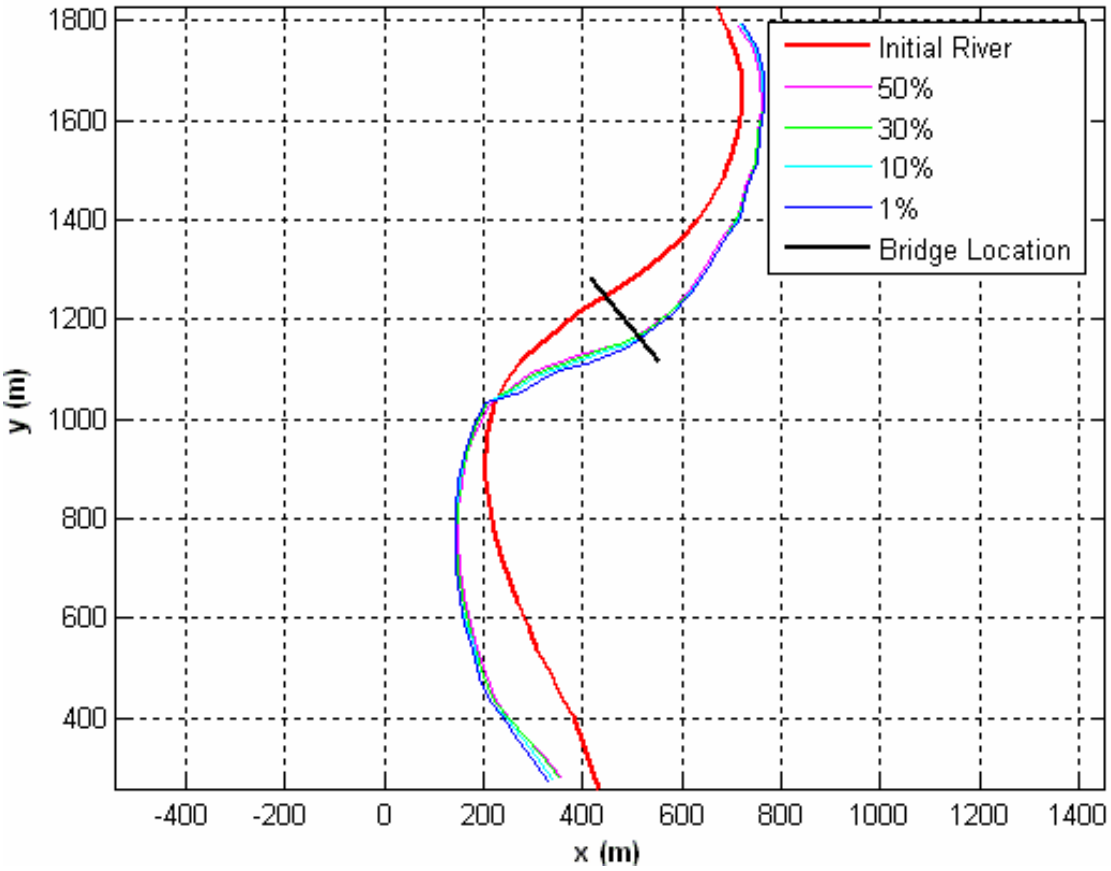

Figure 7.28 CDF Map for the Predicted Brazos River (1981 ~ 2006)

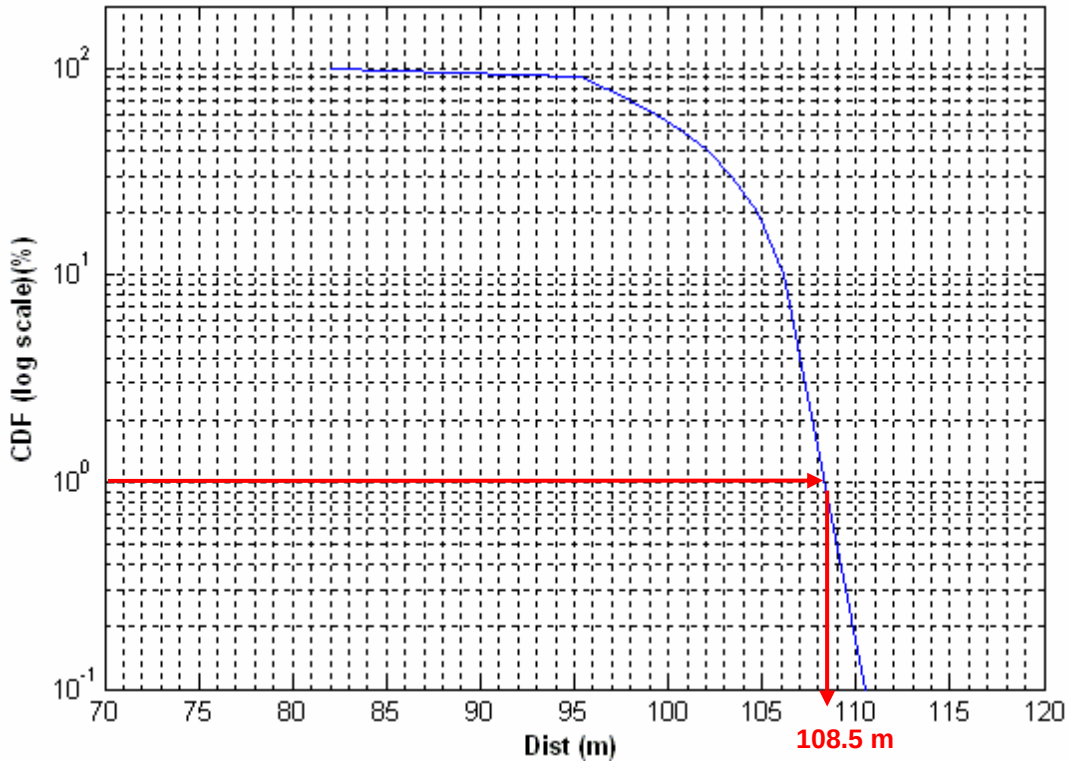

Figure 7.29 CDF Plot for the Given Direction (1981 ~ 2006)

CHAPTER VIII

CONCLUSIONS AND RECOMMENDATIONS

8.1 CONCLUSIONS

8.1.1 General

The purpose of this study is to improve the current approaches to predict meander migration, which currently have moderate or significant limitations regarding to their practical applications, as mentioned in the previous chapters. A more comprehensive approach has been developed by the research team at Texas A&M University, in which all of essential factors (i.e. soil, water, and geometry) affecting meander migration are taken into account. The particular objectives of this study are to develop a prediction equation of maximum migration distance based on the physical model tests, to develop a new methodology of risk analysis, and to conduct a verification study to evaluate the new prediction method in natural scale.

8.1.2 Meander Migration

Based on its sinuosity, the channel pattern of a river can be classified as straight, sinuous, meandering, or braided. A meandering river has its sinuosity larger than 1.5, and it can be characterized by a succession of alternating meander bends (Julien 2002). A transversal secondary circulation induced by a helical flow motion along a curved channel erodes the outer bank materials and transports them towards the inner bank. This causes a lateral shift of a meander bend. Since meander migration is a dynamic process at the interface between soil and water, the erosion (migration) rate depends on the flow

condition as well as erodibility of soil. Since the flow condition in a river is dependent on its geometric shape, the most essential influencing parameters are: soil, water, and geometry.

8.1.3 Literature Review

For a prediction method, three types of approaches are available: empirical equations, numerical models, and time-sequence maps and extrapolation, which is basically a modified empirical approach. Most empirical equations turn out to be too simple since meander migration is correlated with a hydraulic parameter. The time-sequence technique seems to be a quite reasonable approach, but its significant shortcoming is that the future flow condition needs to be assumed to be the same as the historical condition. Although numerical models can provide the extensive solution on the meander migration processes, their practical usage might be limited due to extensive calibration work.

From the literature review of flume experiments, it is found that Friedkin (1945) has conducted a comprehensive set of flume tests to simulate a self-formed meandering river. His qualitative study provides a tremendous insight into the experimental study in this research.

The risk analysis methodology developed by Briaud et al. (2003) provides a fundamental framework for the current research. However, a completely different scheme for the statistical post-processing of the predicted results is required because the concern in Briaud et al.'s study is the scour depth (i.e. 1-D problem), while meander

migration is a 2-D problem, which is a much more complicated target. As a result, a new scheme for this purpose is developed through this study to accommodate the 2-D aspect.

8.1.4 Flume Test in Clay

A total of eight flume tests have been conducted in a large basin located on the second floor of the Hydromechanics Laboratory at Texas A&M University, which includes the first three pre-tests. Based on the author's knowledge, these flume tests are the largest-scale tests for meander migration in clay in the world. However, a minimal number of test cases could be conducted in this study because the clay cost, preparation time, and required man power were prohibitive.

During the first pre-test with a trapezoidal cross section of the channel, we failed to simulate lateral movement due to the excessive bottom erosion. This was attributed to the relatively low shear stress on the walls compared to the higher shear stress on the bottom of the channel. In the second pre-test, the cross-sectional shape was changed from a trapezoidal to a rectangular channel to increase the shear stress on the side walls. This remedy did induce side wall erosion along the channel, but there was still excessive bottom erosion. To save a substantial expense in providing clay along the bottom of the channel, a non-erodible plastic sheet was used for the bottom in the third pre-test. After starting the test, we found that the roughness of the plastic was too low compared to that of the clay, which caused vibration of the plastic and turbulent flow as well. Finally, we settled on using treated plywood on the channel bottom to match the roughness of clay.

During each test, the following data were measured routinely: water depth, geometries of the bank-lines, water surface elevation profile, and water velocity. As

erosion continued, water depth decreased, the outer (concave) bank moved, the water surface elevation went down gradually, and the water velocity slowed down, anticipating that it will reach an equilibrium state when time is infinite.

8.1.5 Data Analysis of Flume Test Results

The test results of migration rate at each cross-section follow a hyperbolic function, and thus a hyperbolic model is adopted to model the migration process. The spatial distributions of the maximum migration distance and the initial migration rate turn out to follow the Pearson IV function, which can handle skewness of the bell-shaped distribution. The prediction equations of the initial migration rate and the maximum migration distance are obtained by using a multiple regression technique, and these are validated with the laboratory data. The averaged overall RMS error is estimated as 0.028 (or 2.8 % of the initial channel width), which is the best precision we can expect from a laboratory test.

Five coefficients in the M_{max} equation (Eq. 5.9) are determined by the regression analysis with a total of five valid flume tests results. They might be not enough data to obtain a more comprehensive set of the prediction equation of meander migration in clay, but the proposed equation in this study is still quite valuable, considering the scale of the experiments.

8.1.6 Risk Analysis

A new methodology to generate a future hydrograph is developed based on the statistical properties of the past hydrograph data (Wang 2006). A large number of future hydrographs are generated by random number generation, and these hydrographs have

the same probability of occurrence. For each hydrograph, the MEANDER program predicts the location of the river, and this will populate a distribution map of the predicted locations of the river. Then, a newly-developed algorithm written in Matlab calculates the cumulative density functions at every node point along the river from upstream to downstream. By connecting all the points along the river which have the same probability value, a contour map can be constructed to provide a general trend of meander migration with corresponding risk levels. Once a target direction, as well as location of a bridge, is specified, the specific prediction result for that particular location can be shown as a separate output.

8.1.7 Field Verification Study

A full-scale verification study has been performed to evaluate the applicability of the MEANDER program to the real field. The selected site for this study is the Brazos River at the SH 105 Bridge near Navasota, Texas. The predictions of the Brazos River are done for the periods from 1981 to 1995 and from 1981 to 2006. Comparison between predicted and measured movement show a reasonably good agreement.

The current version of the MEANDER program has some limitations on its applications. First, it can only accommodate a single erodibility input for the soil property, which means it can not consider the wide variation of non-homogeneous soil properties along a real river. Second, it is not able to simulate a self-formed meandering river (Friedkin 1945) that has an initially straight channel with a attack angle at the beginning of the channel.

8.2 RECOMMENDATIONS

A major part of the current research has been conducting large-scale flume tests and analyzing the experimental data to establish the prediction equation of meander migration. Although the scale of flume tests was large, several limitations could not be avoided, which include simplified test conditions, a small number of test cases, the use of a non-erodible channel bottom, the use of one discharge rate, and the use of one type of soil. Besides these limitations, the lack of more comprehensive full-scale verification studies might constrain the application of the new method to other sites. The followings are recommended for future research:

- Conduct more flume tests with a wider range of values of the controlling parameters, so that more data points are available for regression analysis to improve the current prediction equation of meander migration.
- Conduct flume test with a deep enough erodible clay bottom to accommodate excessive bottom erosion, in order to simulate a more realistic meandering channel. The data from these tests need to be compared with the data from the current research.
- Conduct flume tests with different types of clay or a mixture of sand and clay.
- The prediction method needs to be evaluated by a more comprehensive field verification study.

REFERENCES

Abad, J., and Garcia, M. H. (2004). "Conceptual and Mathematical Model for Evolution of Meandering Rivers in Naturalization Processes." *Proceedings of the 2004 World Water and Environmental Resources Congress: Critical Transitions in Water and Environmental Resources Management*, Salt Lake City, UT, USA, 2048-2057.

Abad, J., and Garcia, M. H. (2006). "RVR Meander: A Toolbox for Re-meandering of Channelized Streams." *Computers & Geosciences*, 32, 92-101.

Biedenharn, D. S., Combs, P. G., Hill, G. J., Pinkard Jr., C. F., and Pinkston, C. B. (1989). "Relationship between Channel Migration and Radius of Curvature on the Red River." *Proc., Int. Symp. on Sediment Transport Modeling*, New Orleans, LO, 536-541.

Blondeaux, P., and Seminara, G. (1985). "A Unified Bar-Bend Theory of River Meanders." *Journal of Fluid Mechanics*, 157, 449-470.

Briaud J.-L., Ting, F., Chen, H. C., Gudavalli, R., Perugu, S., and Wei, G. (1999). "SRICOS: Prediction of Scour Rate in Cohesive Soils at Bridge Piers." *Journal of Geotechnical and Environmental Engineering*, 125(4), 237-246.

Briaud J.-L., Chen H.-C., and Park S. (2001a). "Predicting Meander Migration: Evaluation of Some Existing Techniques." *Texas Transportation Institute Report No. 2105-1 for Texas Department of Transportation*, The Texas A&M University System, College Station.

Briaud J.-L., Chen H.-C., Edge W., Park S., and Shaw A. (2001b). "Guidelines for Bridges Over Degrading and Migrating Streams, Part 1: Synthesis of Existing Knowledge." *Texas Transportation Institute Report No. 2105-2 for the Texas Department of Transportation*, The Texas A&M University System, College Station.

Briaud J.-L., Ting, F., Chen, H. C., Cao, Y., Han, S. W., and Kwak, K. W. (2001c). "Erosion Function Apparatus for Scour Rate Predictions." *Journal of Geotechnical and Geoenvironmental Engineering*, 127(2), 105-113.

Briaud J.-L., Chen H.-C., Li, Y., Nurtjahyo, P, and Wang, J. (2003). "Complex Pier Scour and Contraction Scour in Cohesive Soils." *Texas Transportation Institute Report No. 24-15 for National Cooperative Highway Research Program*, The Texas A&M University System, College Station.

Briaud J.-L., Chen H.-C., Chang, K.-A., Chung, Y.-A., Park, N., Wang, W., and Yeh, P.-H. (2007). "Establish Guideline for Soils Properties-based Prediction of Meander Migration Rate." *Texas Transportation Institute Report No. 4378-1 for Texas Department of Transportation*, The Texas A&M University System, College Station.

Brice, J.C. (1977). "Lateral Migration of the Middle Sacramento River, California." *U.S. Geological Survey,* Water-Resources Investigations, 77-43.

Brice, J. C., and Blodgett, J. C. (1978). "Countermeasures for Hydraulic Problems at Bridges, Vol. I. Analysis and Assessment. (Final report. Jun 75 – Sep 78)." *Federal Highway Administration Report*, FHWA/RD-78/162.

Brice, J.C. (1982). "Stream Channel Stability Assessment." *Federal Highway Administration Report*, FHWA/RD-82/021.

Chang, H. H. (1984). "Analysis of River Meanders." *Journal of Hydraulic Engineering*, 110(1), 37-50.

Darby, S. E., Alabyan, A. M., and Van de Wiel, M. J. (2002). "Numerical Simulation of Bank Erosion and Channel Migration in Meandering Rivers." *Water Resources Research*, 38(9), 21-221.

Friedkin, J. F. (1945). "A Laboratory Study of the Meandering of Alluvial Rivers." *Technical Report*, U.S. Waterways Experiment Station, Vicksburg, MS.

Google Earth Beta v4.0.27XX (2007), Google Inc., Mountain View, CA.

Hasegawa, K. (1981). "Bank-erosion Discharge Based on a Non-equilibrium Theory." *Proc. Japan Society of Civil Engineers*, Tokyo, 316, 37-50 (in Japanese).

Hooke, J. M. (1980). "Magnitude and Distribution of Rates of River Bank Erosion." *Earth Surface Processes*, 5(2), 143-157.

Hudson, P. F., and Kesel, R. H. (2000). "Channel Migration and Meander-bend Curvature in the Lower Mississippi River Prior to Major Human Modification." *Geology*, 28(6), 531-534.

Ikeda, S., Parker, G., and Sawi, K. (1981). "Bend Theory of River Meanders. I: Linear Development." *Journal of Fluid Mechanics*, 112, 363-377.

Julien, P. Y. (2002). *River Mechanics*. 1st Edition, Cambridge University Press, Cambridge, United Kingdom.

Keady, D. M., and Priest, M. S. (1977). "The Downstream Migration Rate of River Meandering Patterns." *Proceedings, Mississippi Water Resources Conference*, Meeting 12th Mississippi Water Resources Conference, Jackson, MS, 29-34.

Lagasse, P. F., Spitz, W. J., and Zevenbergen, L. W. (2003). "A Methodology for Arcview Tools for Predicting Channel Migration." *ESRI, User Conference Proceedings*, San Diego, CA.

Lagasse, P. F., Spitz, W. J., Zevenbergen, L. W., and ZachMann, D. W. (2004a), "Methodology for Predicting Channel Migration." *Report for National Cooperative Highway Research Program Project 24-16*, Owen Ayres & Associates, Inc. Fort Collins, CO.

Lagasse, P. F., Spitz, W. J., Zevenbergen, L. W., and ZachMann, D. W. (2004b). "Handbook for Predicting Stream Meander Migration Using Aerial Photographs and Maps." *Report for National Cooperative Highway Research Program Project 24-16*, Owen Ayres & Associates, Inc. Fort Collins, CO.

Lane, S. N., Biron, P. M., Bradbrook, K. F., Butler, J. B., Chandler, J. H., Crowell, M. D., Mclelland, Richards, S. J., and Roy, A. G. (1998). "Three-Dimensional Measurement of River Channel Flow Processes Using Acoustic Doppler Velocimetry." *Earth Surface Processes and Landforms*, 23, 1247-1267.

Lane, S. N., Chandler, J. H., and Porfiri, K. (2001). "Monitoring River Channel and Flume Surface with Digital Photogrammetry." *Journal of Hydraulic Engineering*, 127(10). 871-877.

Leopold, L. B., and Langbein, W.B. (1960). "River Meanders." *Geological Society of America Bulletin*, 71, 769-794.

Leopold, L. B., and Langbein, W.B. (1966). "River Meanders." *Scientific American,* June, 60-70.

Morisawa, M. (1985). *Rivers.* 1st Edition, Longman, New York.

Munson, B. R., Young, D. F., and Okiishi, T. H. (2006). *Fundamentals of Fluid Mechanics*. 5th Edition, John Wiley & Sons, New York, 563.

Nagata, N., Hosoda, T., and Muramoto, Y. (2000). "Numerical Analysis of River Channel Processes with Bank Erosion." *Journal of Hydraulic Engineering*, 126(4), 243-252.

Nakagawa, H., and Tsujimoto, T. (1980). "Sand Bed Instability Due to Bed Load Motion." *Journal of Hydraulic Division*, 106(12), 2029-2051.

Nakagawa, T. (1983). "Boundary Effects on Stream Meandering and River Morphology." *Sedimentology*, 30, 117-127.

Nanson, G. C., and Hickin, E. J. (1983). "Channel Migration and Incision on the Beatton River." *Journal Hydraulic Engineering*, 109(3), 327-337.

Nanson, G. C., and Hickin, E. J. (1986). "A Statistical Analysis of Bank Erosion and Channel Migration in Western Canada." *Geological Society of America Bulletin*, 97(4), 497-504.

Nikora, V. I., and Goring, D. G. (1998). "ADV Measurements of Turbulence: Can We Improve Their Interpretation?" *Journal Hydraulic Engineering*, 124(6), 630-634.

Odgaard, A. J. (1986). "Meander Flow Model. I: Development." *Journal of Hydraulic Engineering*, 112(12), 1117-1136.

Odgaard, A. J. (1987). "Streambank Erosion along Two Rivers in Iowa." *Water Resources Research*, 23(7), 1225-1236.

Park, S. (2001). "Measured and Predicted Meander Migration near Four Highway Crossings in Texas." *M.E. Report*, Texas A&M University, College Station.

Schumm, S. A., and Khan, H. R. (1972). "Experimental Study of Channel Patterns." *Geological Society of America Bulletin*, 83, 1755-1770.

Seed, R. B., Bea, R. G., Abdelmalak, R. I., Athanasopoulos, A. G., Boutwell, G. P., Bray, J. D., Briaud**,** J.-L., Cheung, C., Cobos-Roa, D., Cohen-Waeber, J., Collins, B. D., Ehrensing, L., Farber, D., Hanemann, M., Harder, L. F., Inkabi, K. S., Kammerer, A. M., Karadeniz, D. Kayen**,** R.E., Moss, R. E. S., Nicks, J., Nimmala, S., Pestana, J. M., Porter, J. Rhee, K., Riemer, M. F., Roberts, K., Rogers, J. D., Storesund, R., Govindasamy, A. V., Vera-Grunauer, X., Wartman, J. E., Watkins, C. M., Wenk Jr., E., and Yim, S. C. (2006). "Investigation of the Performance of the New Orleans Flood Protection Systems in Hurricane Katrina on August 29, 2005, Volume I: Main Text and Executive Summary." *Report for National ScienceFoundation Grants Nos. CMS-0413327 and CMS-0611632*, The University of California, Berkeley, CA.

Smith, C. E. (1998). "Modeling High Sinuosity Meanders in a Small Flume." *Geomorphology*, 25, 19-30.

Wang, W. (2006). "A Hydrograph-Based Prediction of Meander Migration." Ph.D. Dissertation, Texas A&M University, College Station.

WinDIG 2.5 (2007), http://www.unige.ch/sciences/chifi/cpb/windig.html.

Wolman, W. G., and Leopold, L. B. (1957). "River Flood-plains-some Observations on Their Formation." U. S. Geological Survey Professional Paper, 282C, 87-109.

Yeh, P.-H. (2007). "Physical Models of Meander Channel Migration." Unpublished Ph.D. dissertation, Texas A&M University, College Station.

APPENDIX A

PHOTOGRAPHS OF THE PREPARATION

Figure A.1 Retrieving Clay from the Previous Test

Figure A.2 Filling the Sand Channel

Figure A.3 Leveling the Sand Bed

Figure A.4 Completion of Leveling Work

Figure A.5 Drawing the Contour of the Sand Channel

Figure A.6 Digging the Sand Channel

Figure A.7 Placing the Clay Banks and Covering with Wet Cloth

Figure A.8 Sprinkling the Clay Banks

Figure A.9 Completion of the Clay Channel

APPENDIX B

GALLERY OF FLUME TESTS

(a) Initial (b) Final (t = 20 hr)

Figure B.1 Clay Test Case 01 (R/W = 4, ϕ = 120˚, Fr = 0.50)

Figure B.2 Initial Condition of Clay Test Case 02 (*R/W* = 4, ϕ = 120˚, *Fr* = 0.50)

Figure B.3 Final Condition of Clay Test Case 02 (*t* = 106.5 hr)

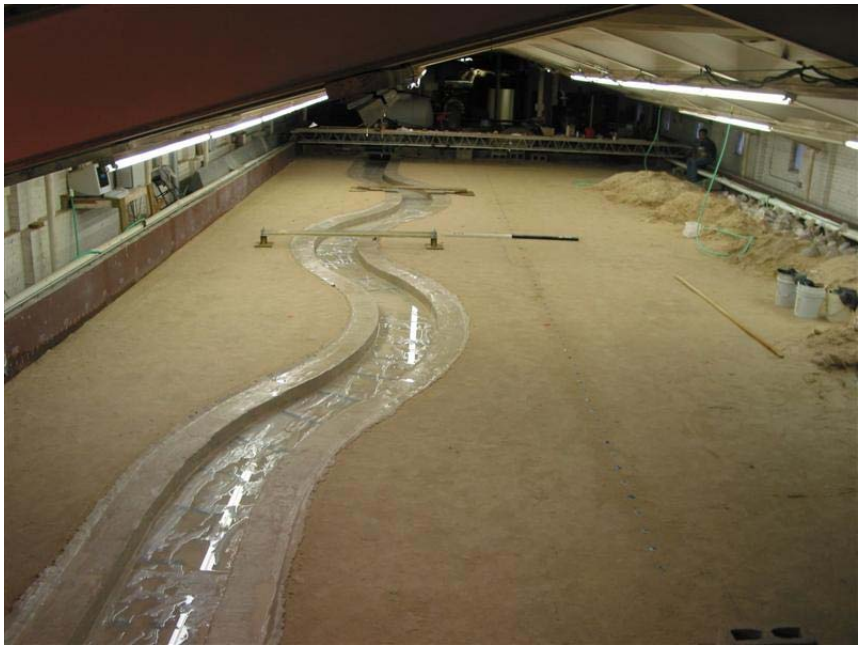

Figure B.4 Initial Condition of Clay Test Case 03 (*R/W* = 6, ϕ = 65˚, *Fr* = 0.50)

Figure B.5 Final Condition of Clay Test Case 03 (*t* = 163.5 hr)

Figure B.6 Initial Condition of Clay Test Case 04 (*R/W* = 4, ϕ = 65˚, *Fr* = 0.50)

Figure B.7 Final Condition of Clay Test Case 04 (*t* = 268 hr)

Figure B.8 Initial Condition of Clay Test Case 05 (*R/W* = 6, ϕ = 65˚, *Fr* = 0.50)

Figure B.9 Final Condition of Clay Test Case 05 (*t* = 184 hr)

Figure B.10 Initial Condition of Clay Test Case 06 (*R/W* = 2, ϕ = 65˚, *Fr* = 0.50)

Figure B.11 Final Condition of Clay Test Case 06 (*t* = 180 hr)

Figure B.12 Initial Condition of Clay Test Case 07 (*R/W* = 4, ϕ = 120˚, *Fr* = 0.50)

Figure B.13 Final Condition of Clay Test Case 07 (*t* = 192 hr)

Figure B.14 Initial Condition of Clay Test Case 08 (*R/W* = 4, ϕ = 220˚, *Fr* = 0.50)

Figure B.15 Final Condition of Clay Test Case 08 (*t* = 336 hr)

APPENDIX C

FLUME TEST RESULTS

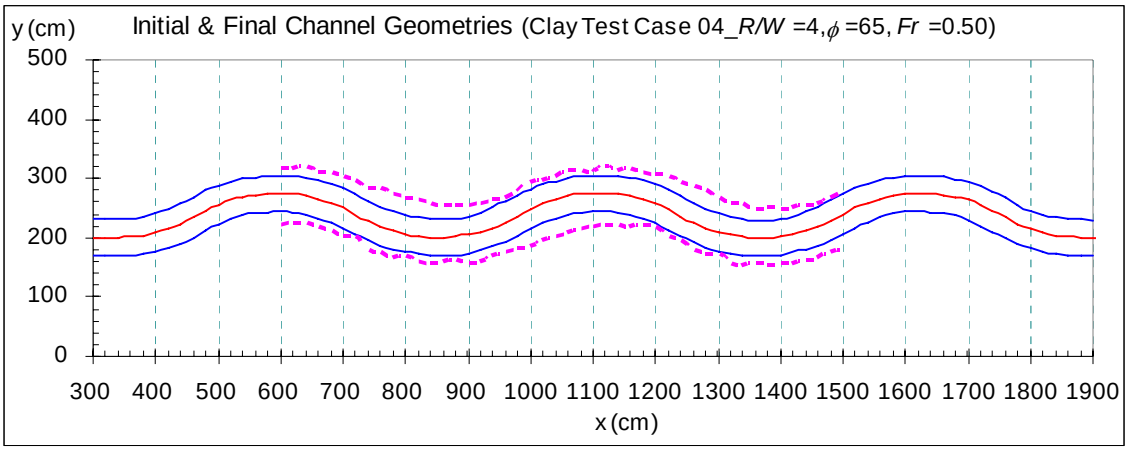

Figure C.1 Channel Geometry at the Initial and Final (268 hr) Stages (Clay Test Case 04)

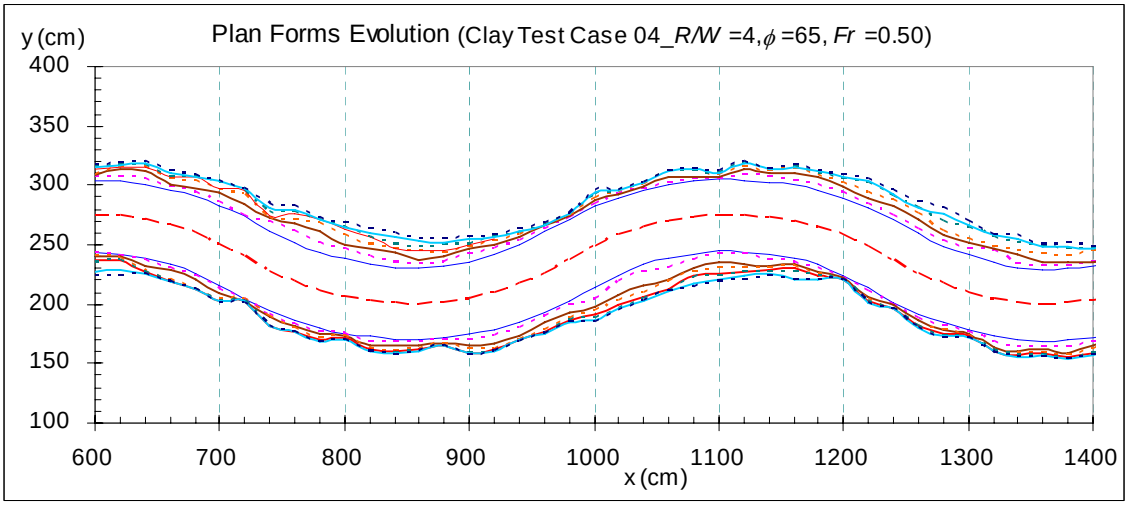

Figure C.2 Plan Forms Evolution at *t* = 0, 48, 96, 126, 156, 186, 220, and 268 hr (Clay Test Case 04)

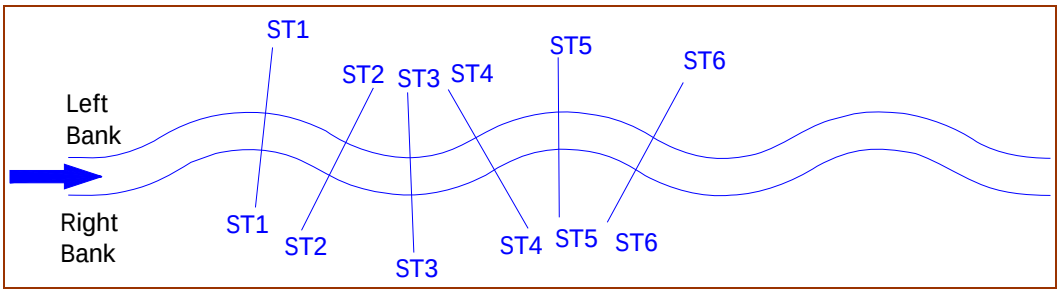

(a) Locations of the Predetermined Stations

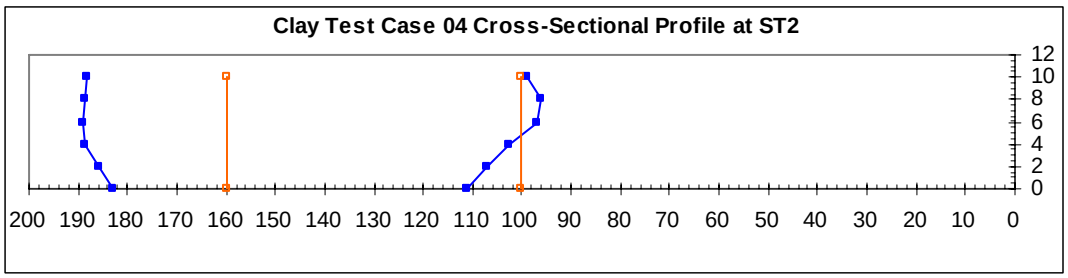

(b) Evolution of cross-sectional profile at station No. 2

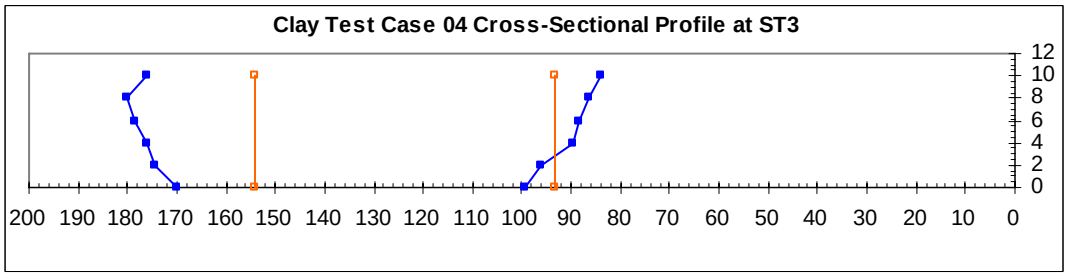

(c) Evolution of cross-sectional profile at station No. 3

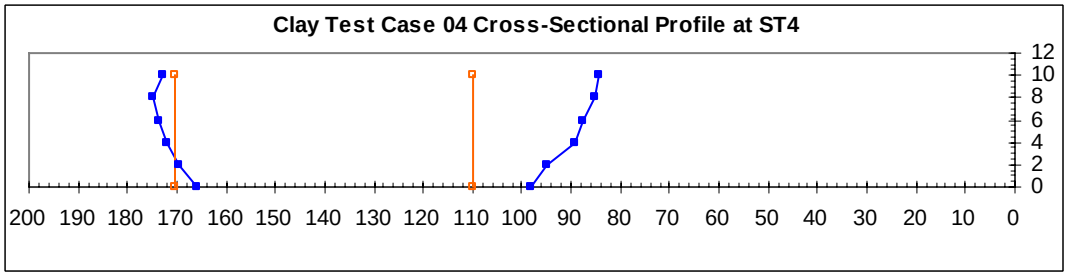

(d) Evolution of cross-sectional profile at station No. 4

Figure C.3 Cross-Sectional Measurement Results (Clay Test Case 04)

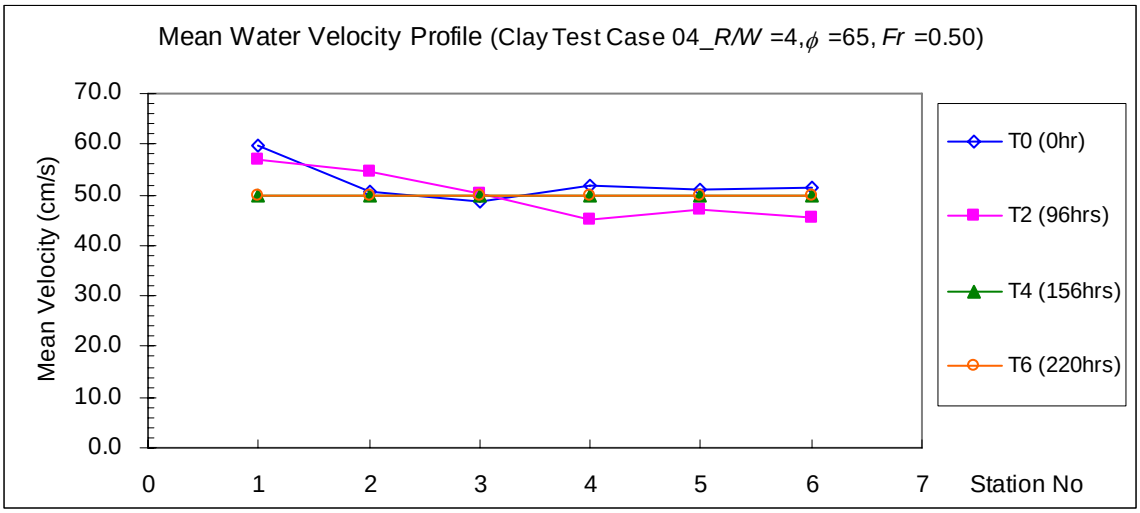

(a) Direct Measurement by ADV

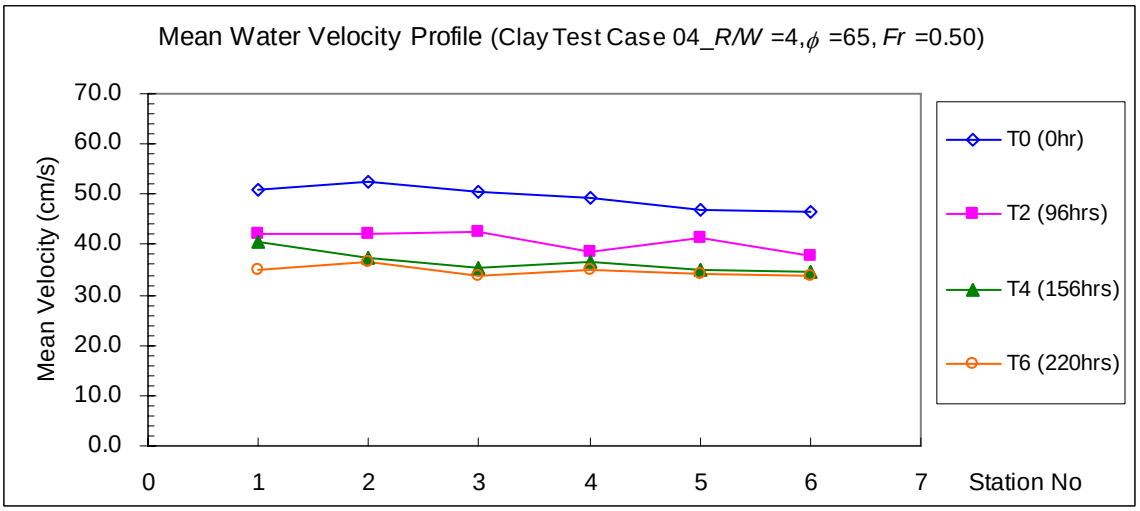

(b) Calculated by the Equation of Continuity ($U = Q/A_w$)

Figure C.4 Mean Velocity Profile (Clay Test Case 04)

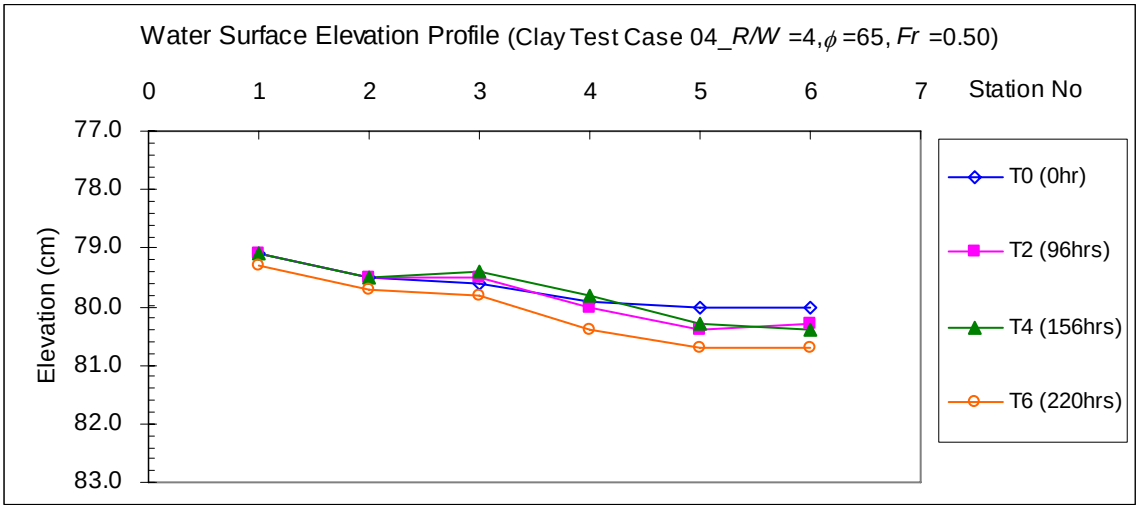

Figure C.5 Water Surface Elevation Profile (Clay Test Case 04)

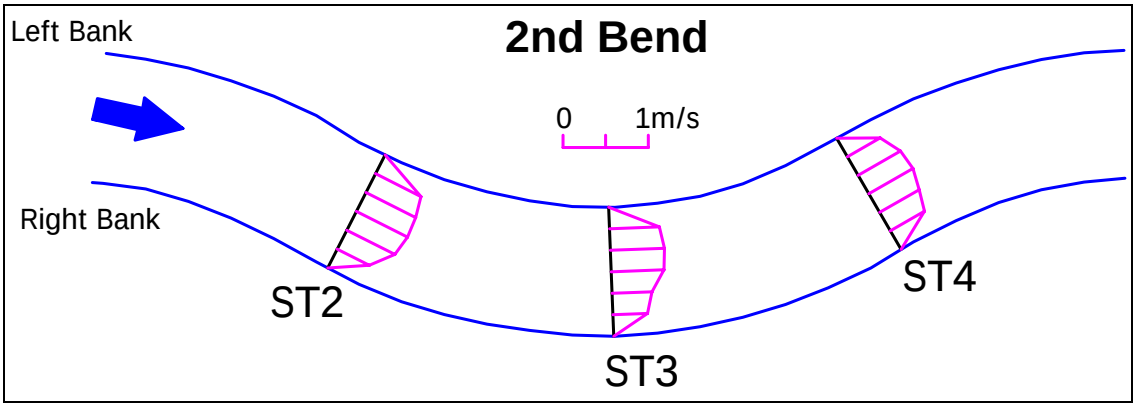

Figure C.6 Longitudinal Surface Velocity Profiles at T0 (Clay Test Case 04)

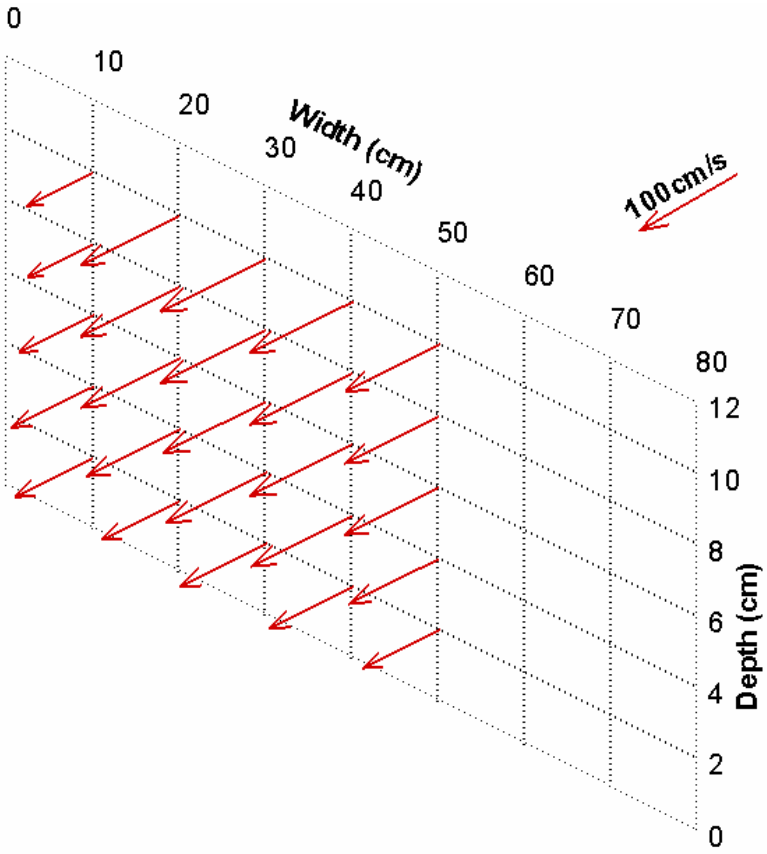

(a) Longitudinal Velocities

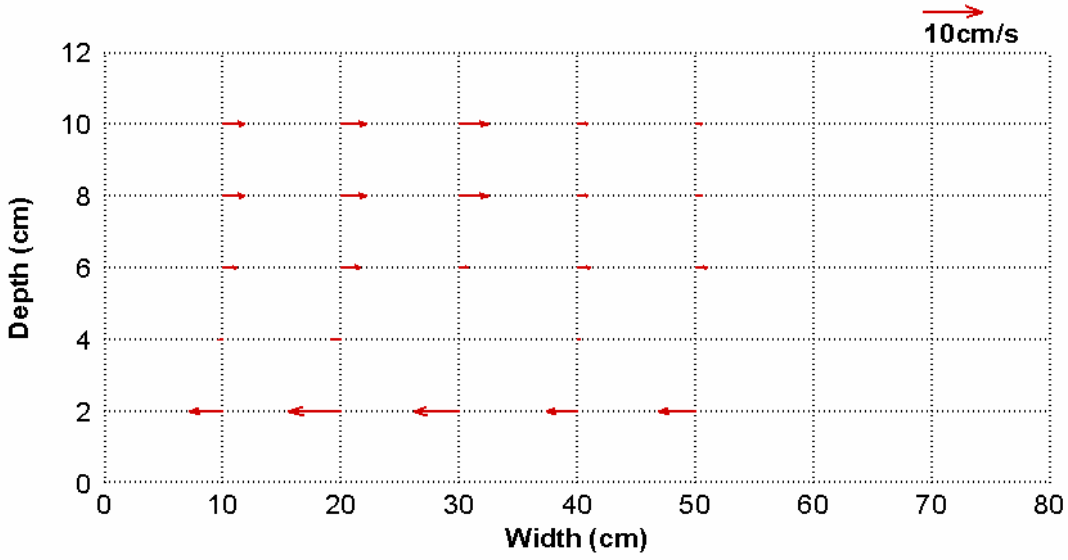

(b) Transversal Velocities

Figure C.7 Initial Velocity Profiles at ST2 (Clay Test Case 04)

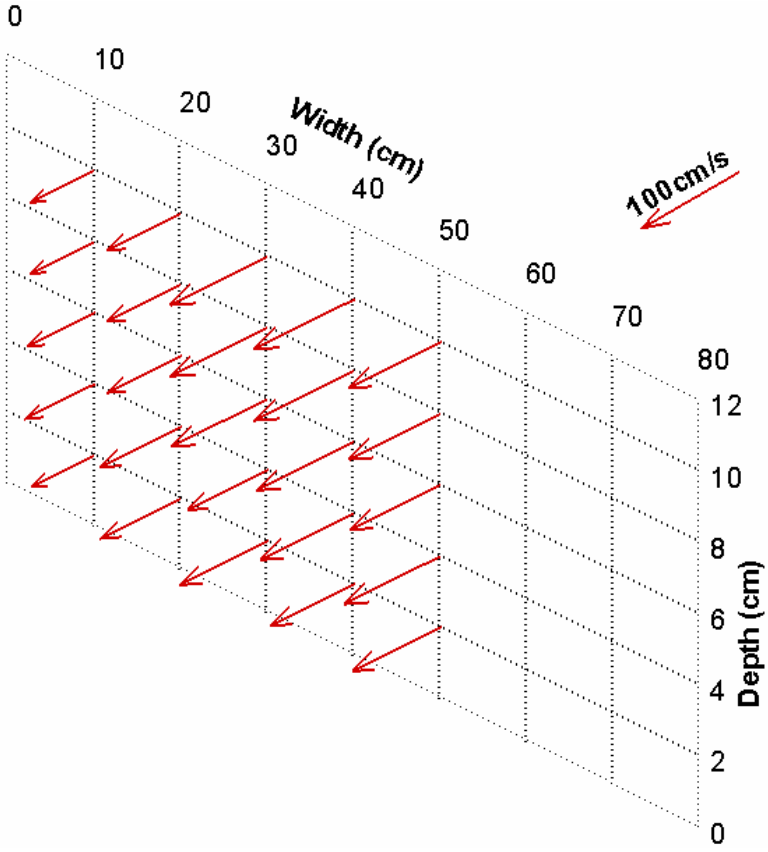

(a) Longitudinal Velocities

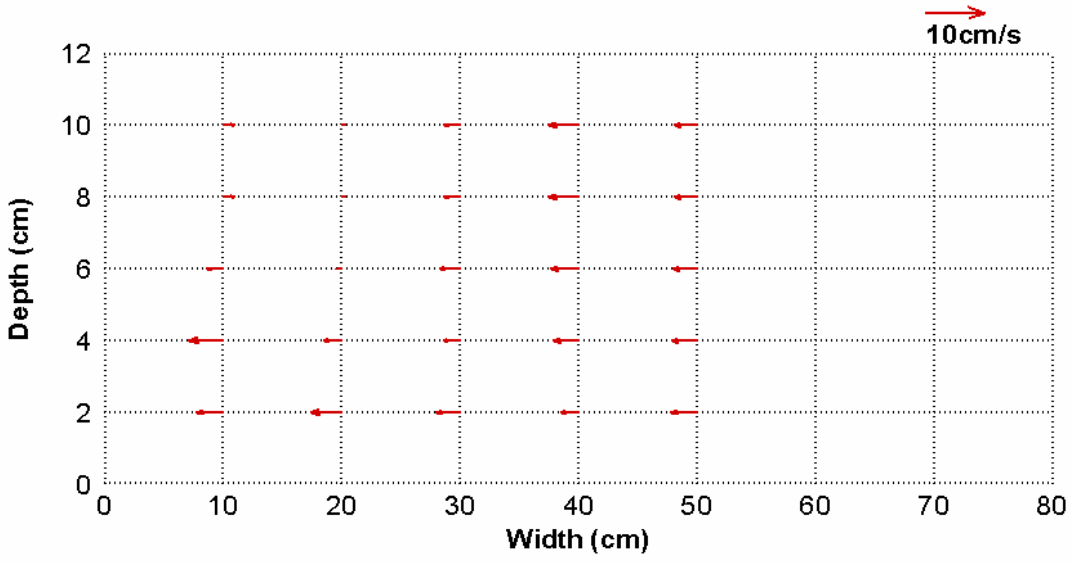

(b) Transversal Velocities

Figure C.8 Inital Velocity Profiles at ST3 (Clay Test Case 04)

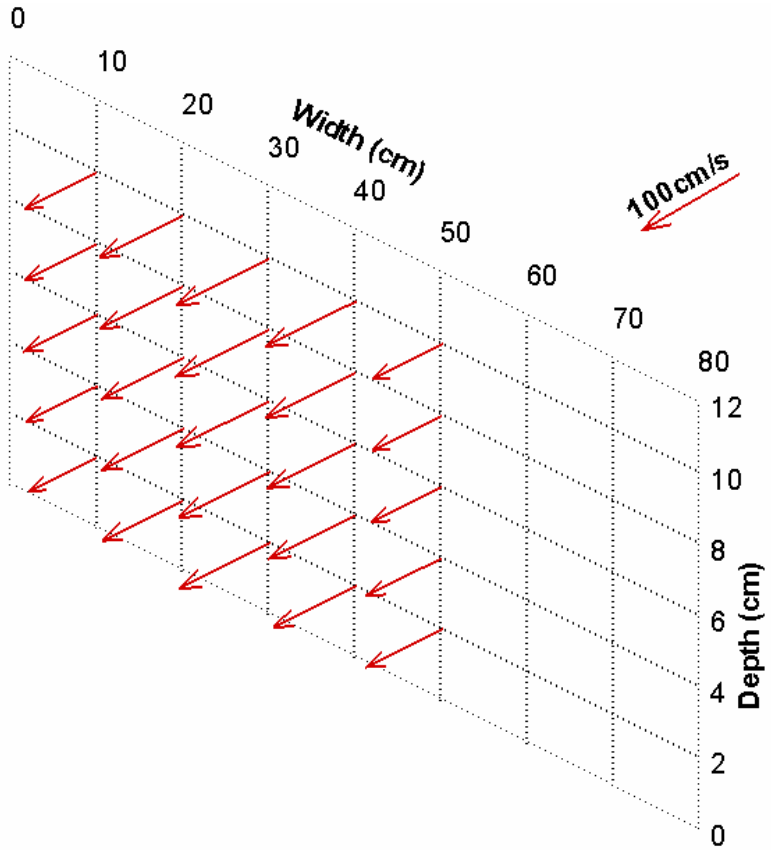

(a) Longitudinal Velocities

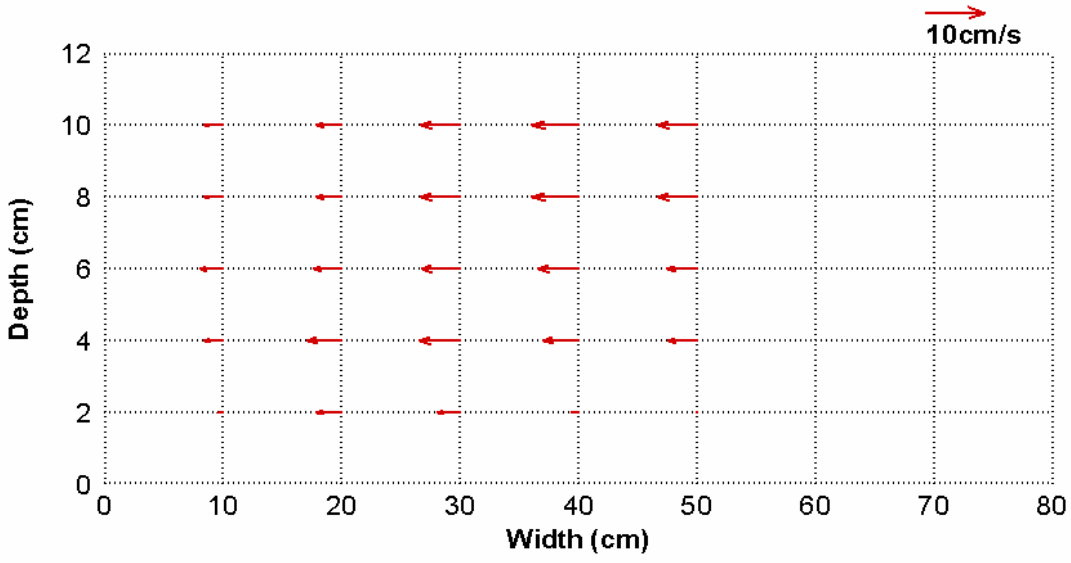

(b) Transversal Velocities

Figure C.9 Inital Velocity Profiles at ST4 (Clay Test Case 04)

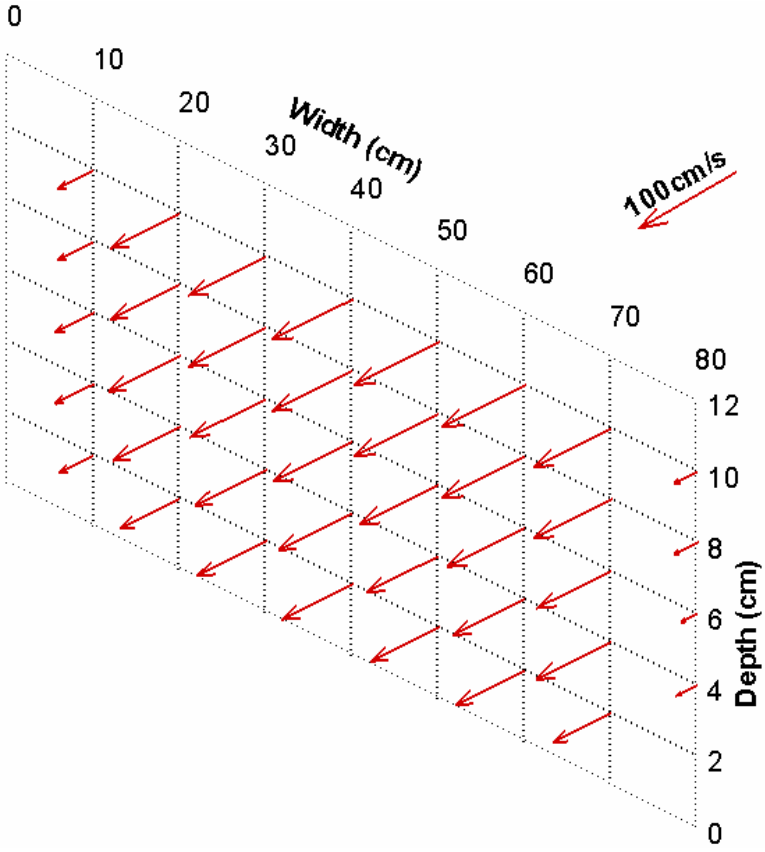

(a) Longitudinal Velocities

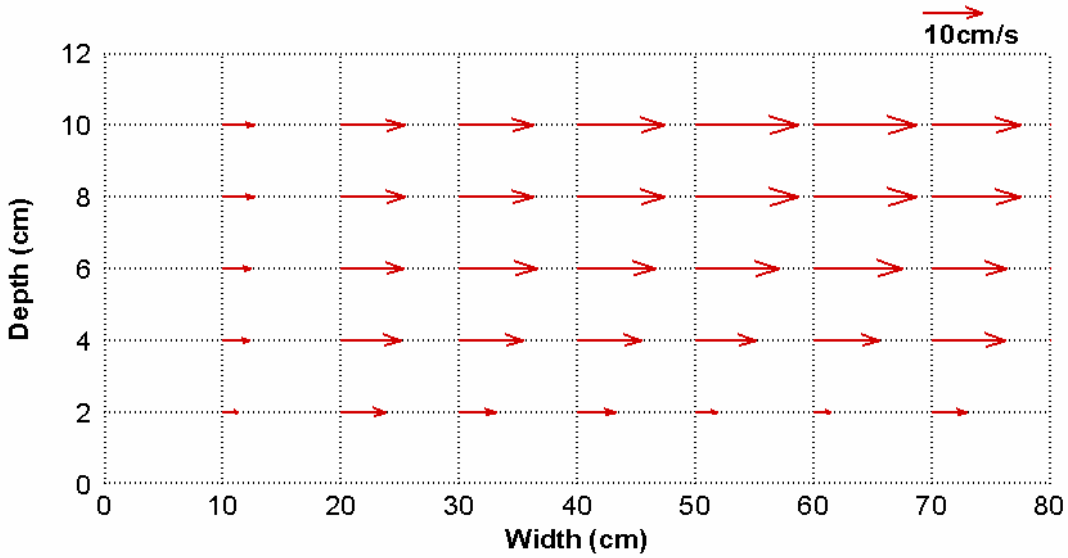

(b) Transversal Velocities

Figure C.10 Velocity Profiles at ST2 after 268 Hours (Clay Test Case 04)

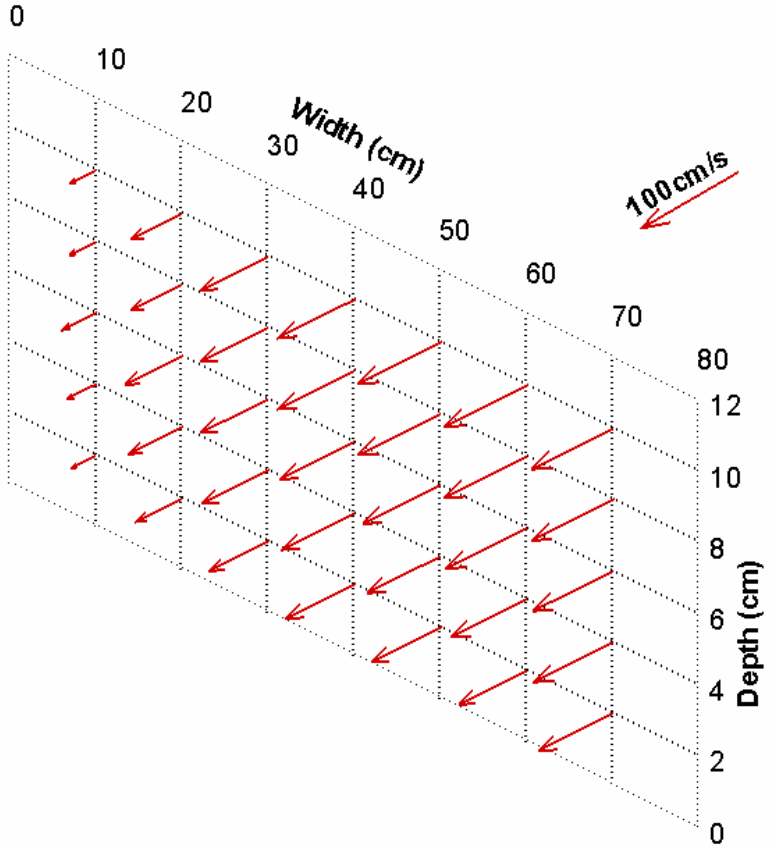

(a) Longitudinal Velocities

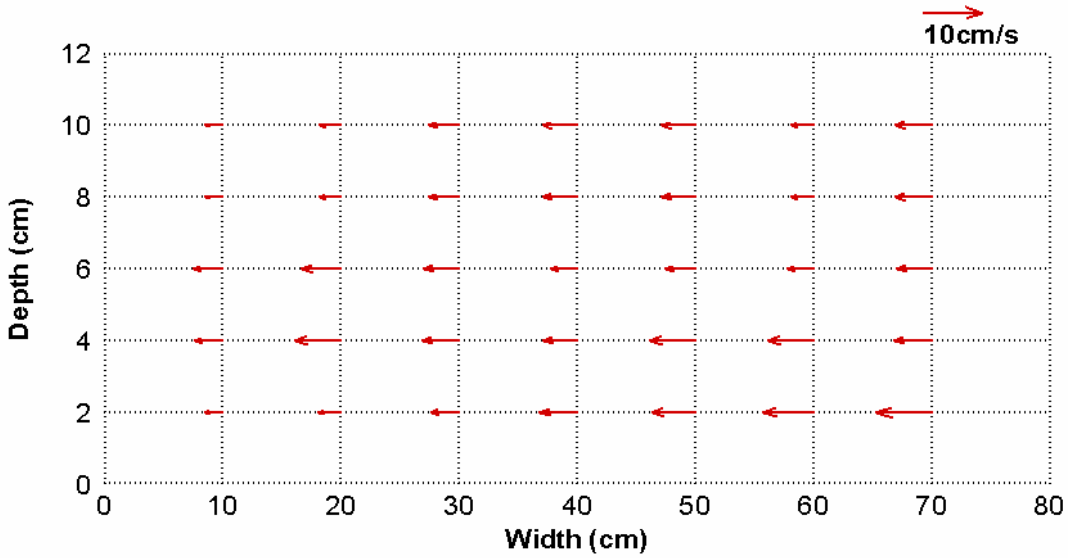

(b) Transversal Velocities

Figure C.11 Velocity Profiles at ST3 after 268 Hours (Clay Test Case 04)

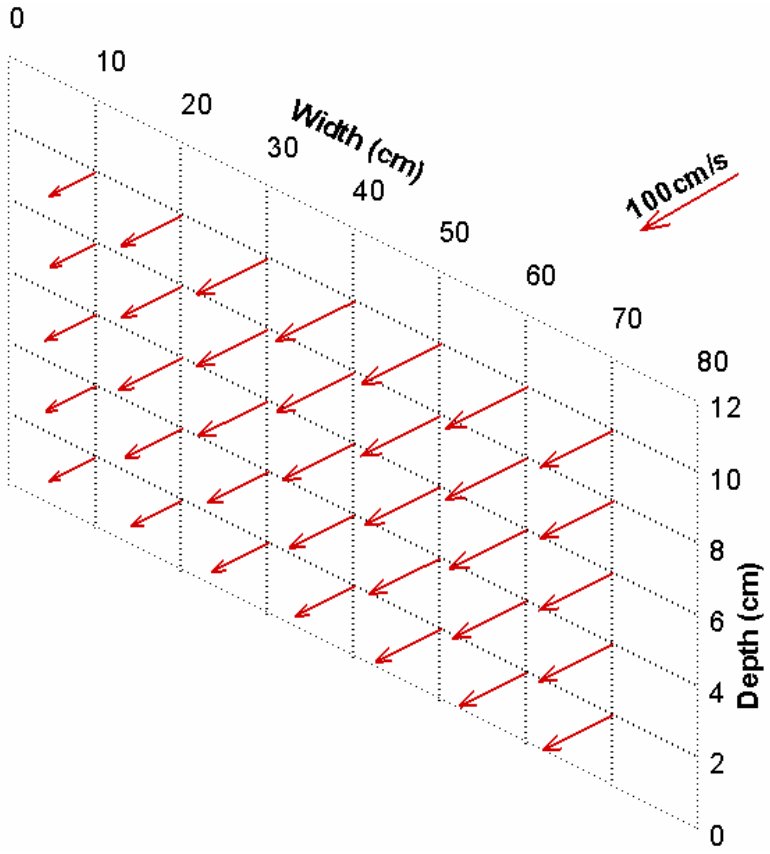

(a) Longitudinal Velocities

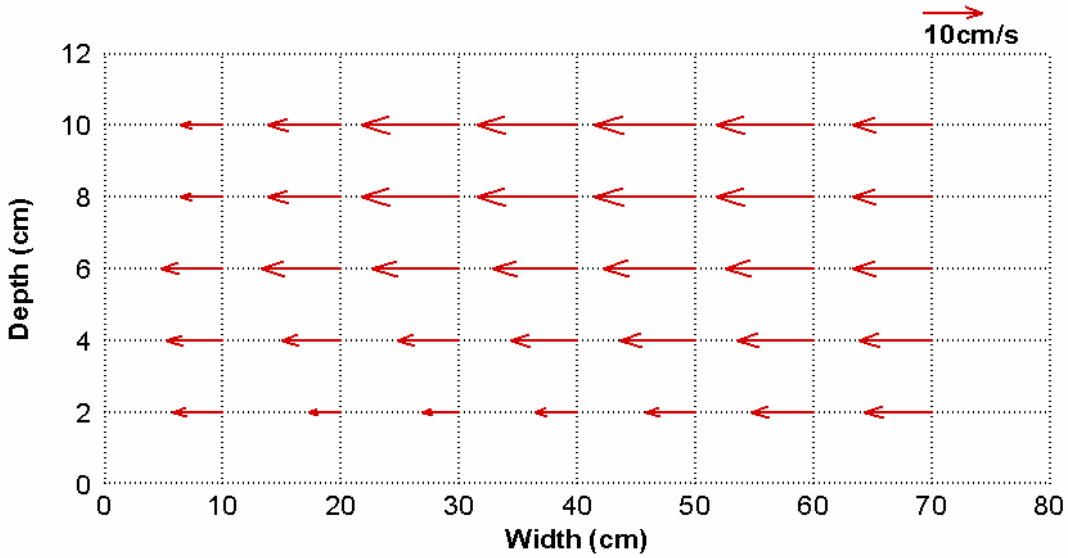

(b) Transversal Velocities

Figure C.12 Velocity Profiles at ST4 after 268 Hours (Clay Test Case 04)

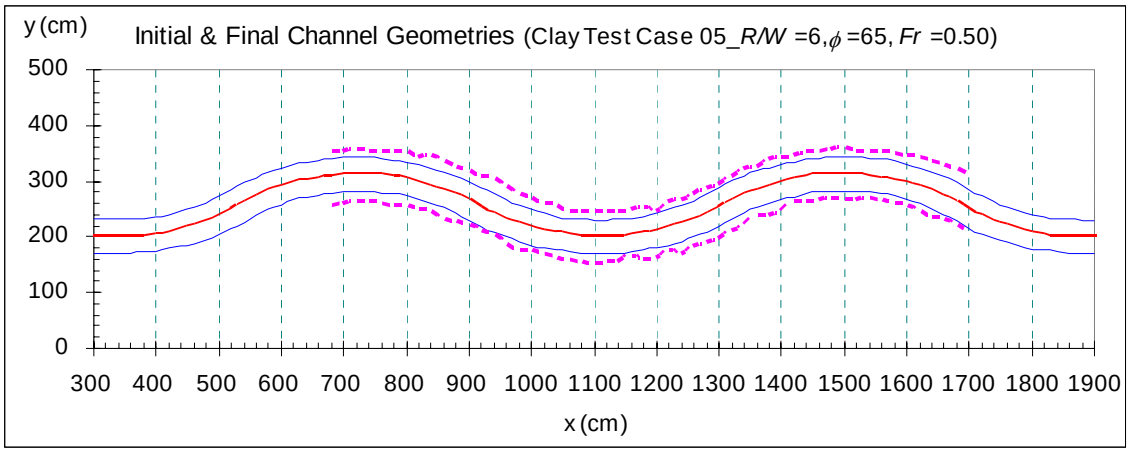

Figure C.13 Channel Geometry at the Initial and Final (260 hr) Stages (Clay Test Case 05)

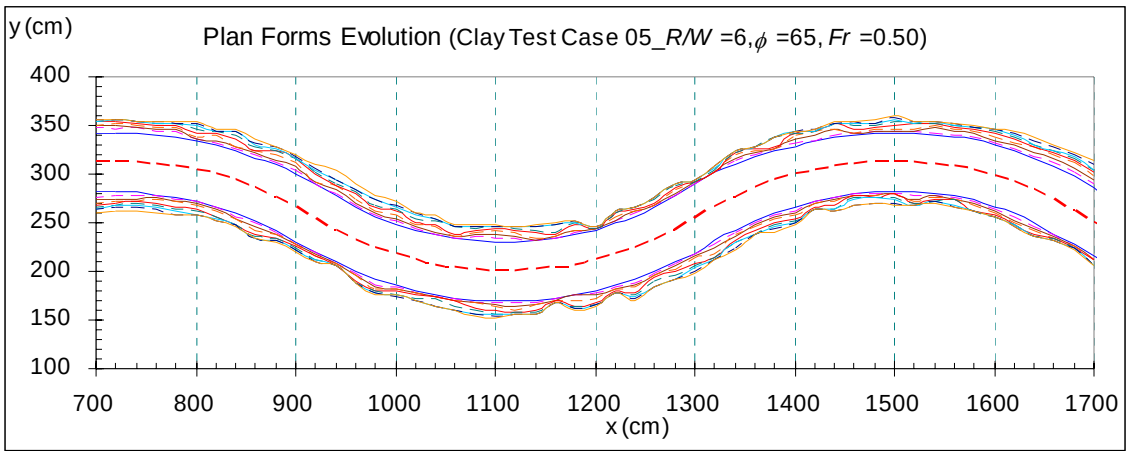

Figure C.14 Plan Forms Evolution at *t* = 0, 36, 60, 90, 120, 150, 184, 220, and 260 hr (Clay Test Case 05)

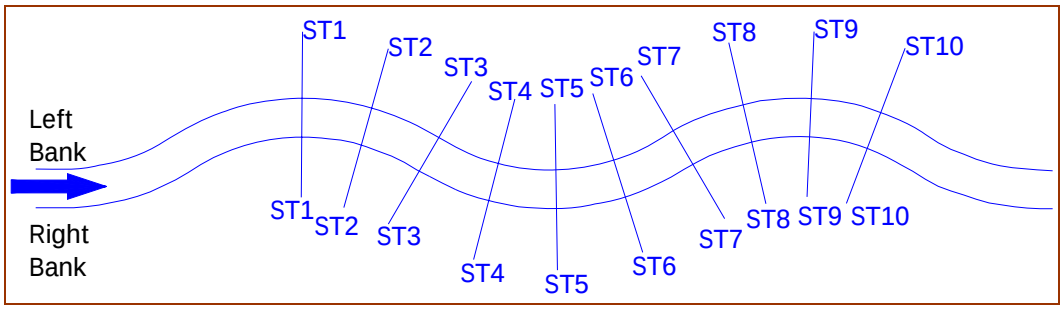

(a) Locations of the Predetermined Stations

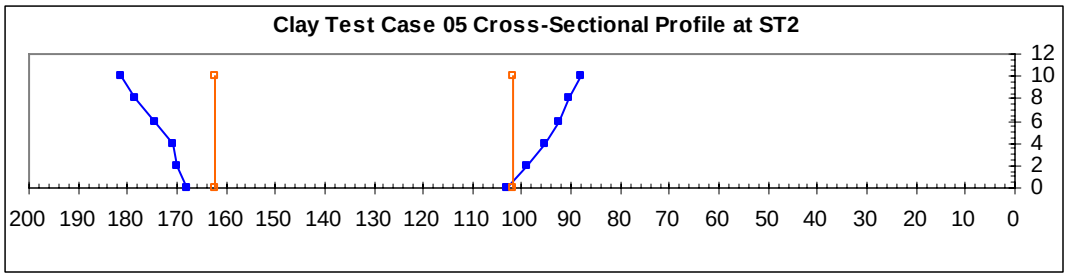

(b) Evolution of cross-sectional profile at station No. 2

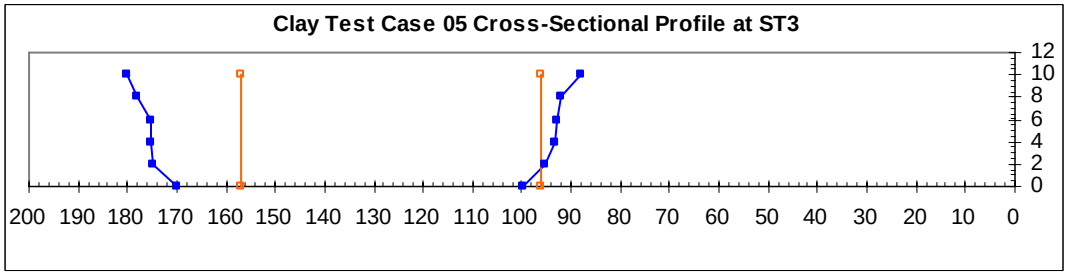

(c) Evolution of cross-sectional profile at station No. 3

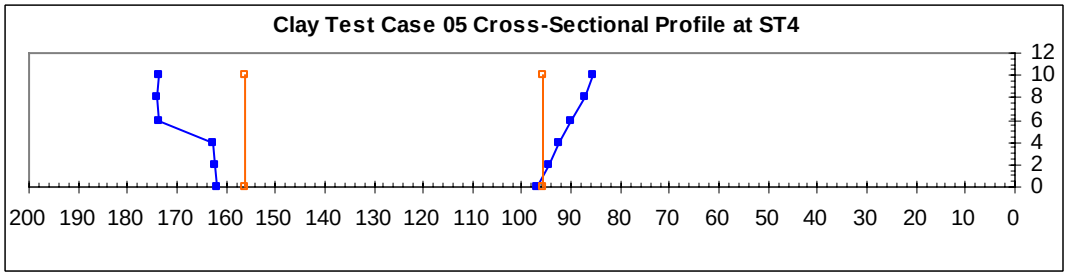

(d) Evolution of cross-sectional profile at station No. 4

Figure C.15 Cross-Sectional Measurement Results (Clay Test Case 05)

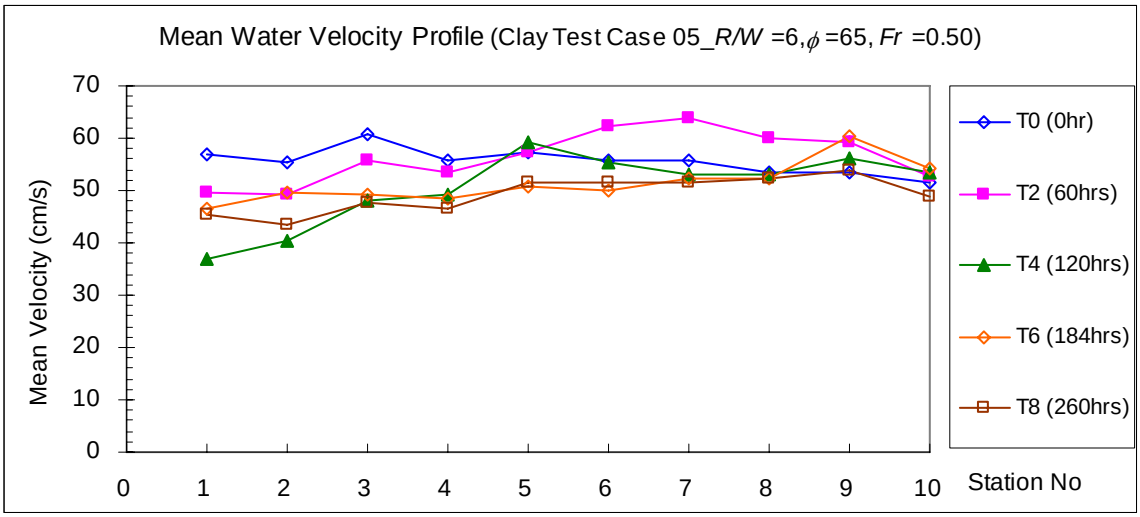

(a) Direct Measurement by ADV

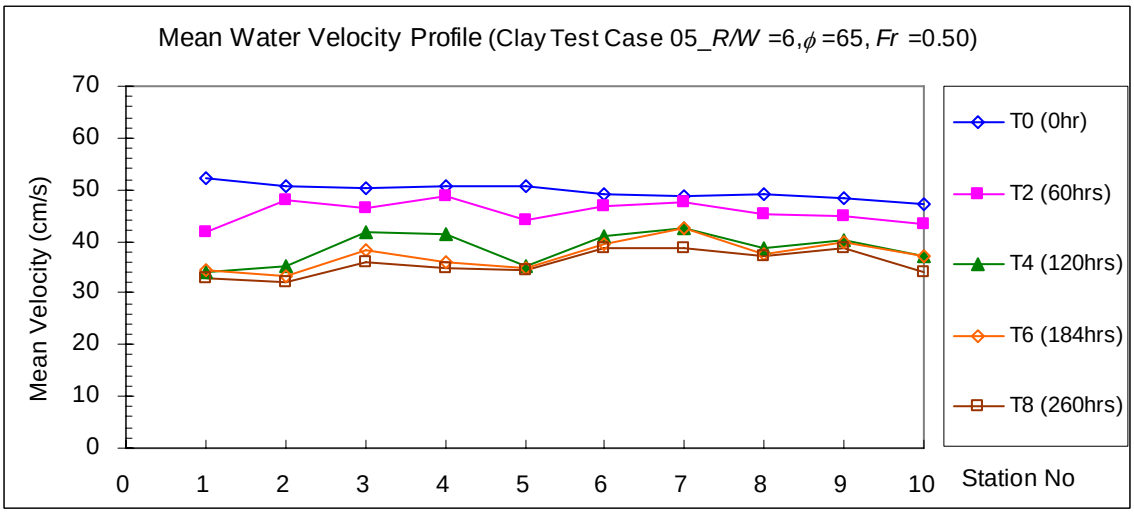

(b) Calculated by the Equation of Continuity ($U = Q/A_w$)

Figure C.16 Mean Velocity Profile (Clay Test Case 05)

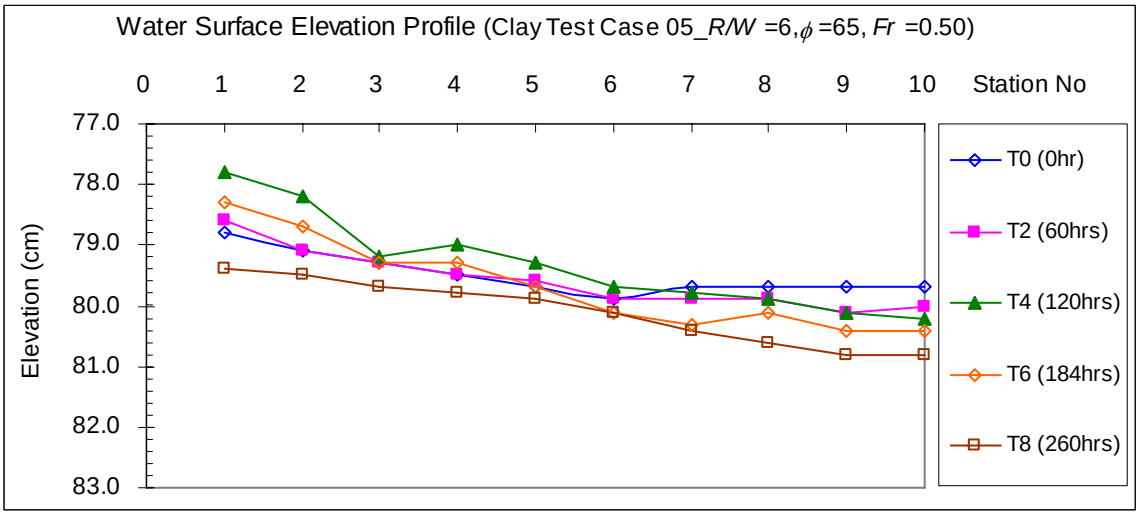

Figure C.17 Water Surface Elevation Profile (Clay Test Case 05)

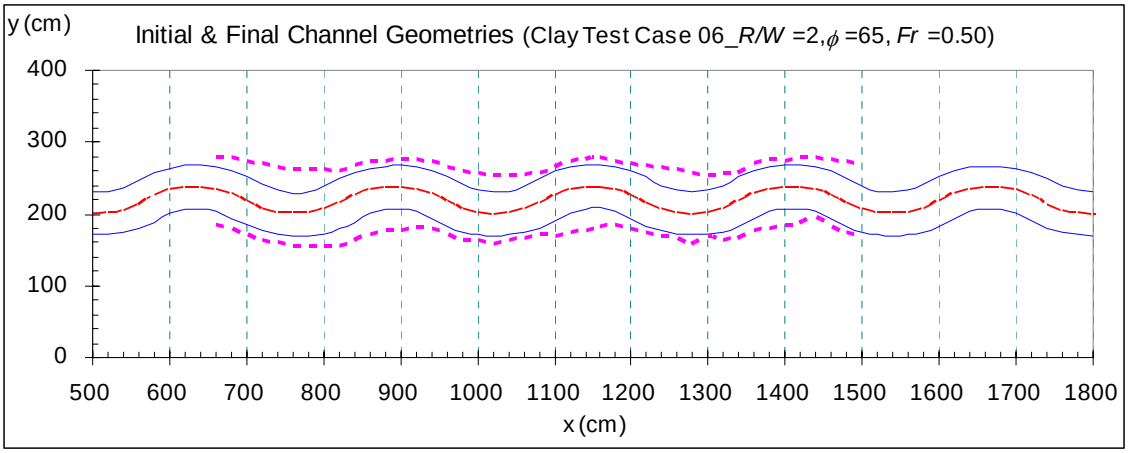

Figure C.18 Channel Geometry at the Initial and Final (192 hr) Stages (Clay Test Case 06)

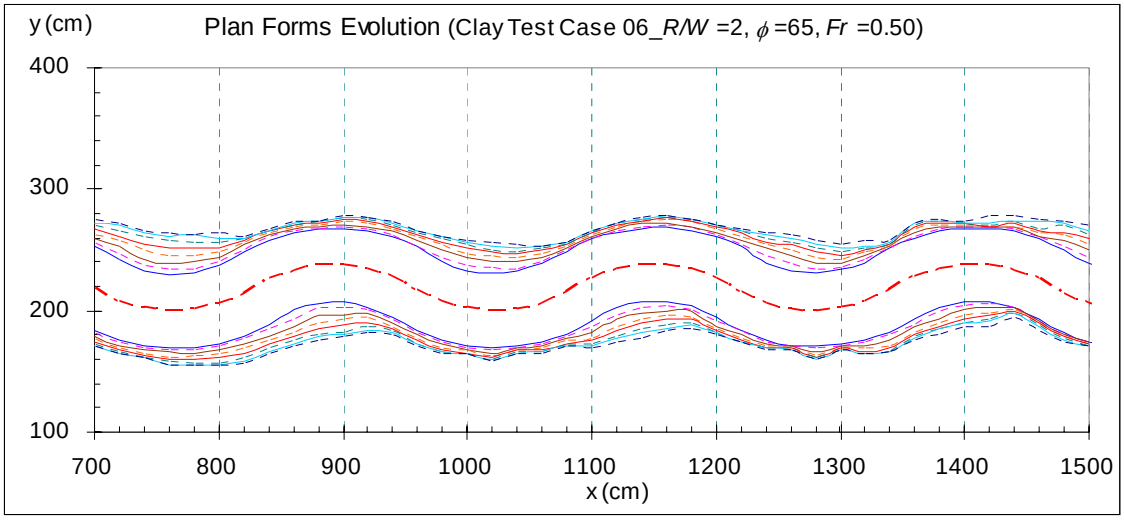

Figure C.19 Plan Forms Evolution at *t* = 0, 24, 48, 72, 96, 120, 144, and 180 hr (Clay Test Case 06)

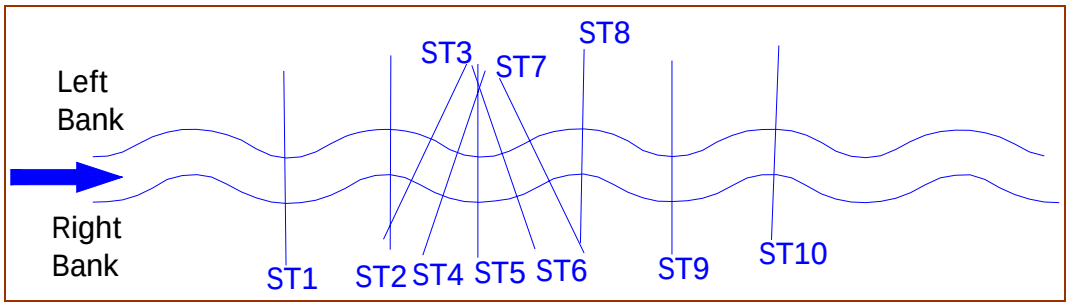

(a) Locations of the Predetermined Stations

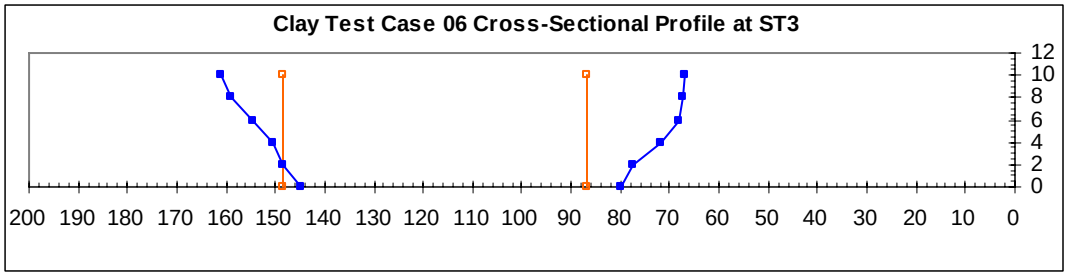

(b) Evolution of cross-sectional profile at station No. 3

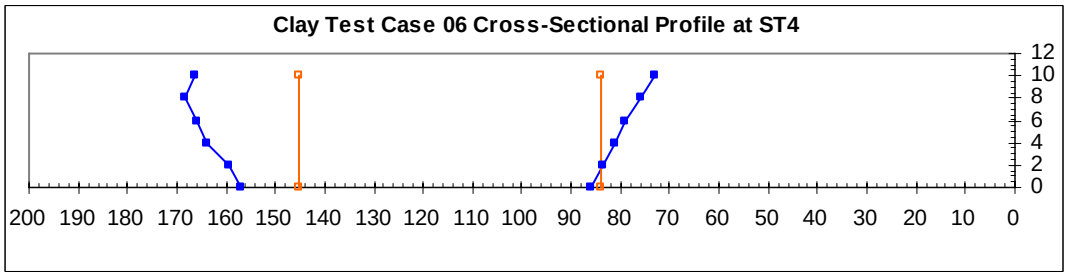

(c) Evolution of cross-sectional profile at station No. 4

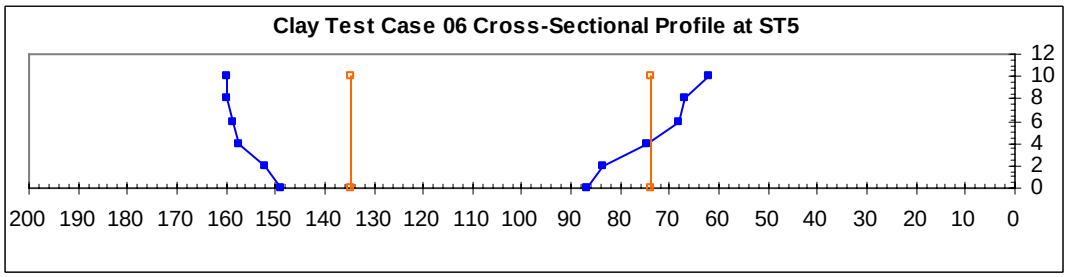

(d) Evolution of cross-sectional profile at station No. 5

Figure C.20 Cross-Sectional Measurement Results (Clay Test Case 06)

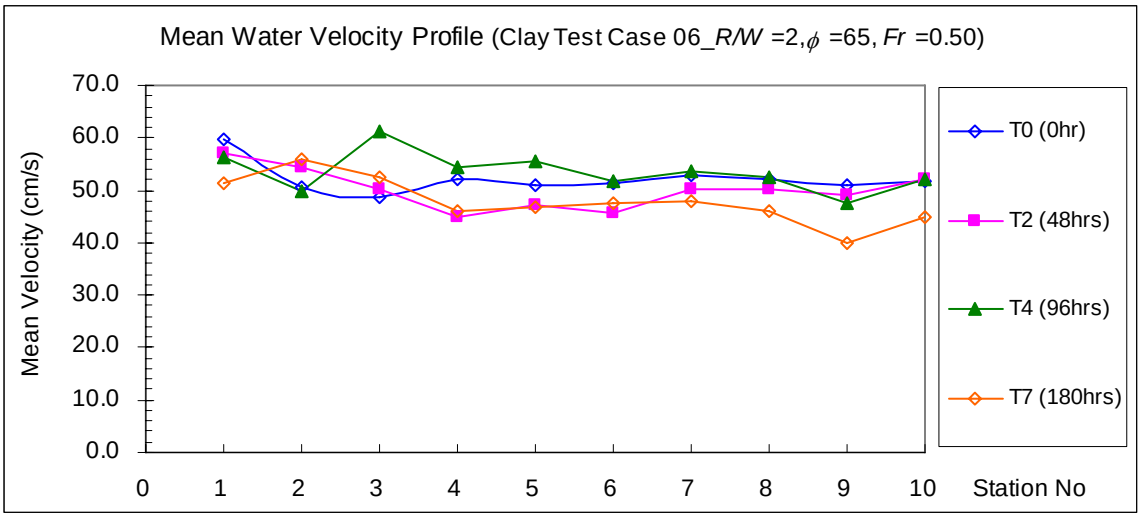

(a) Direct Measurement by ADV

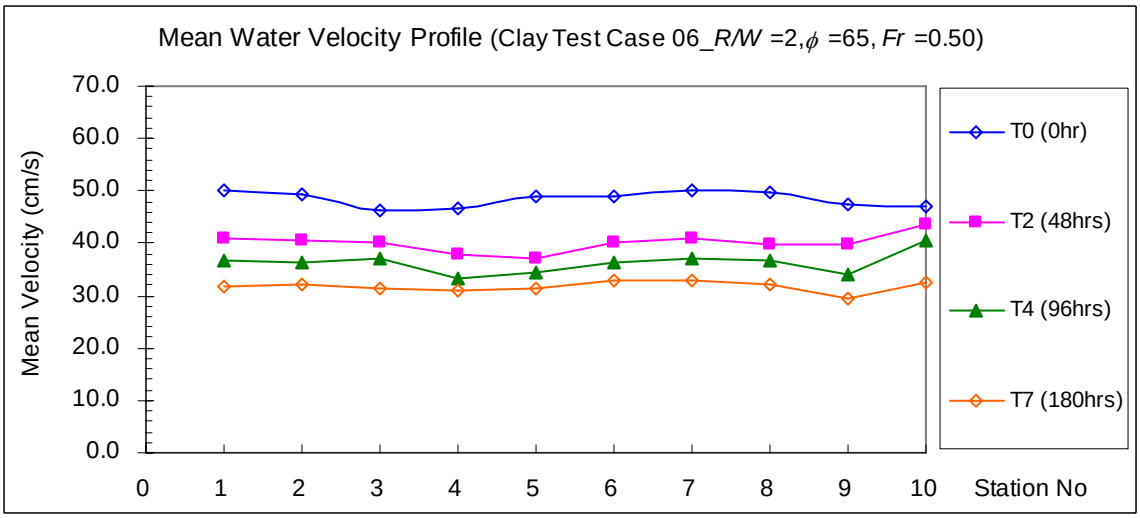

(b) Calculated by the Equation of Continuity ($U = Q/A_w$)

Figure C.21 Mean Velocity Profile (Clay Test Case 06)

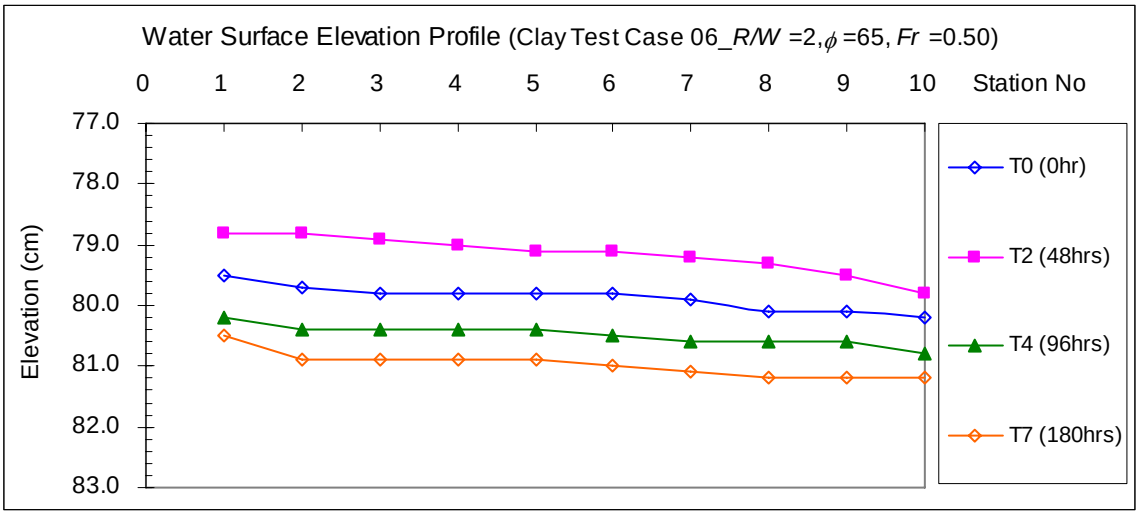

Figure C.22 Water Surface Elevation Profile (Clay Test Case 06)

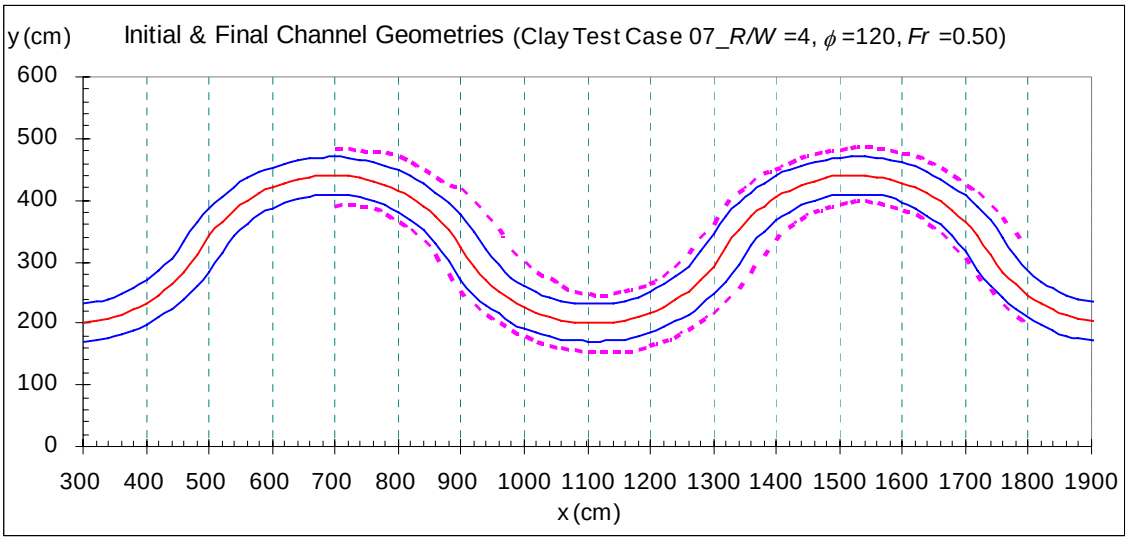

Figure C.23 Channel Geometry at the Initial and Final (192 hr) Stages (Clay Test Case 07)

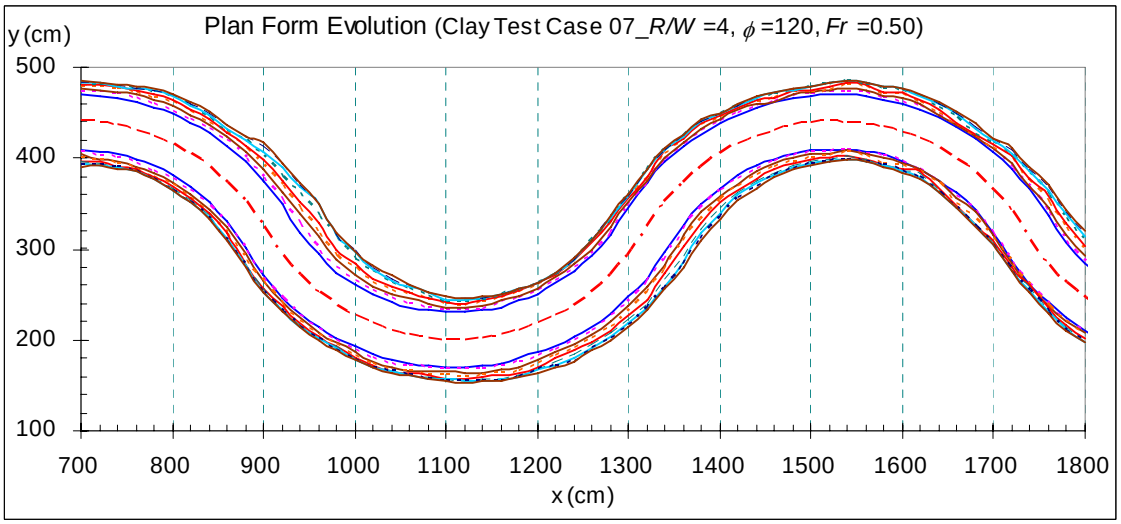

Figure C.24 Plan Forms Evolution at *t* = 0, 24, 48, 72, 96, 120, 144, 168, and 192 hr (Clay Test Case 07)

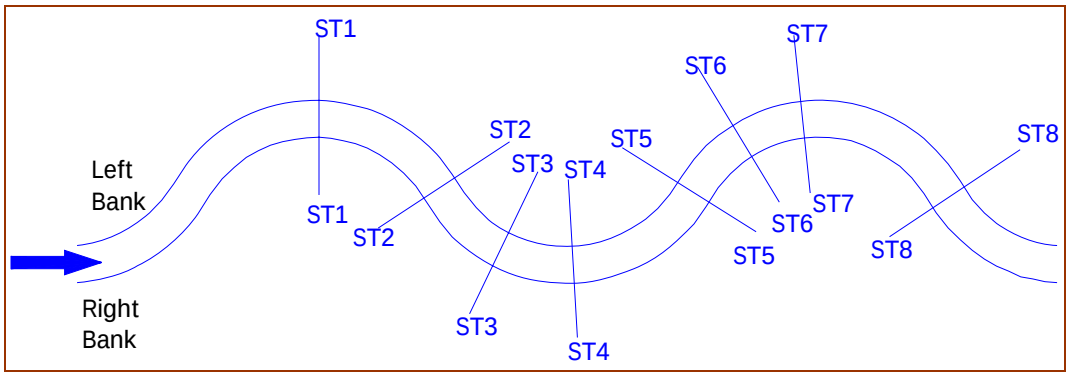

(a) Locations of the Predetermined Stations

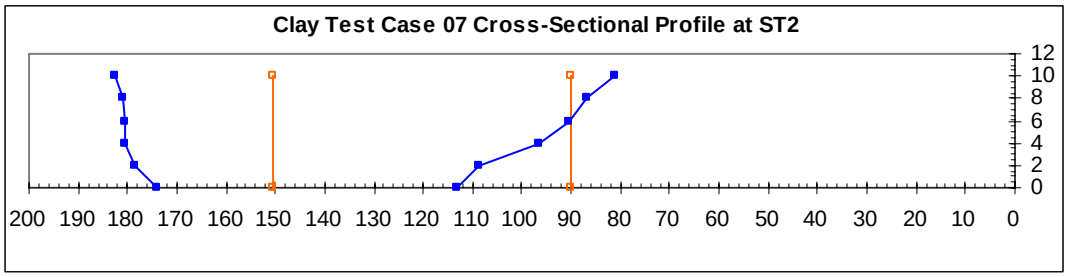

(b) Evolution of cross-sectional profile at station No. 2

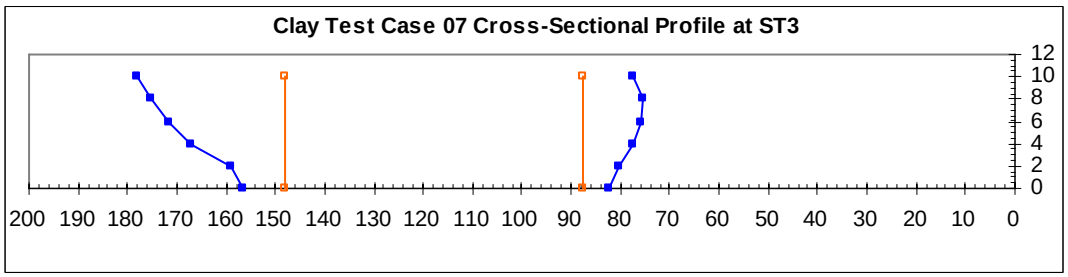

(c) Evolution of cross-sectional profile at station No. 3

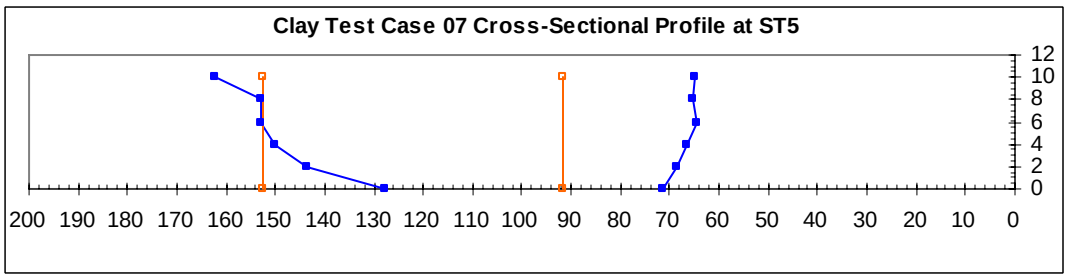

(d) Evolution of cross-sectional profile at station No. 5

Figure C.25 Cross-Sectional Measurement Results (Clay Test Case 07)

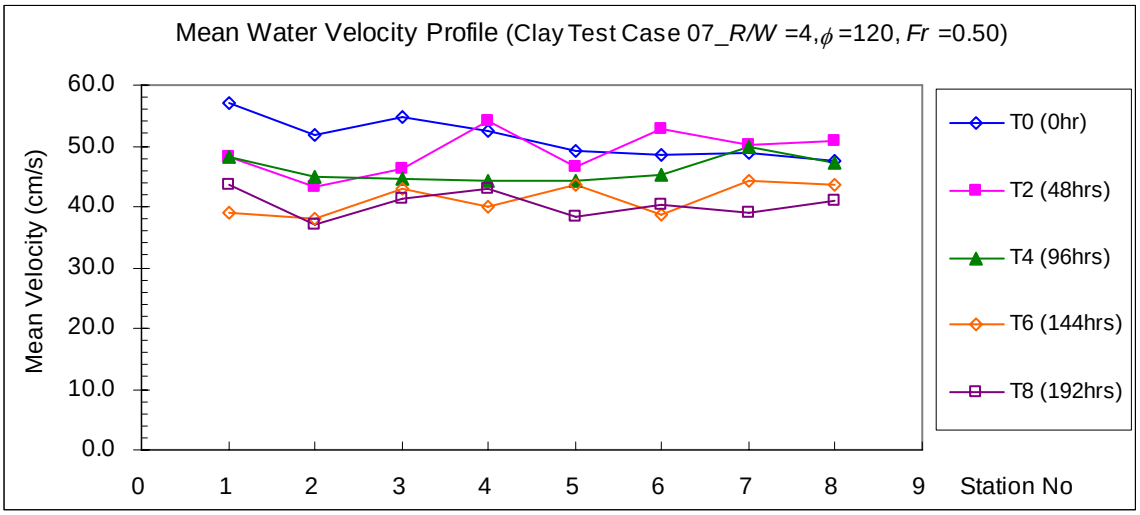

(a) Direct Measurement by ADV

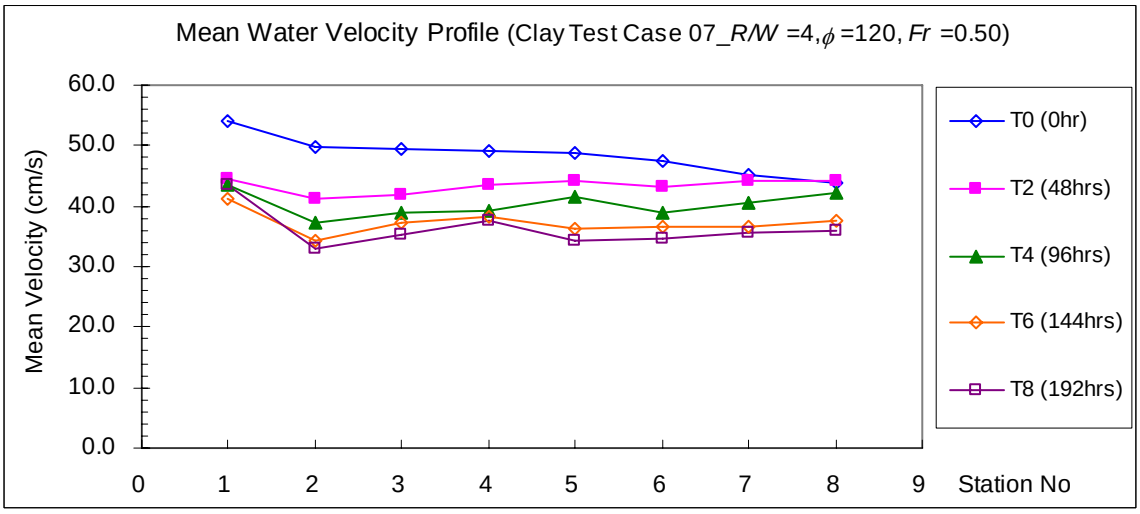

(b) Calculated by the Equation of Continuity ($U = Q/A_w$)

Figure C.26 Mean Velocity Profile (Clay Test Case 07)

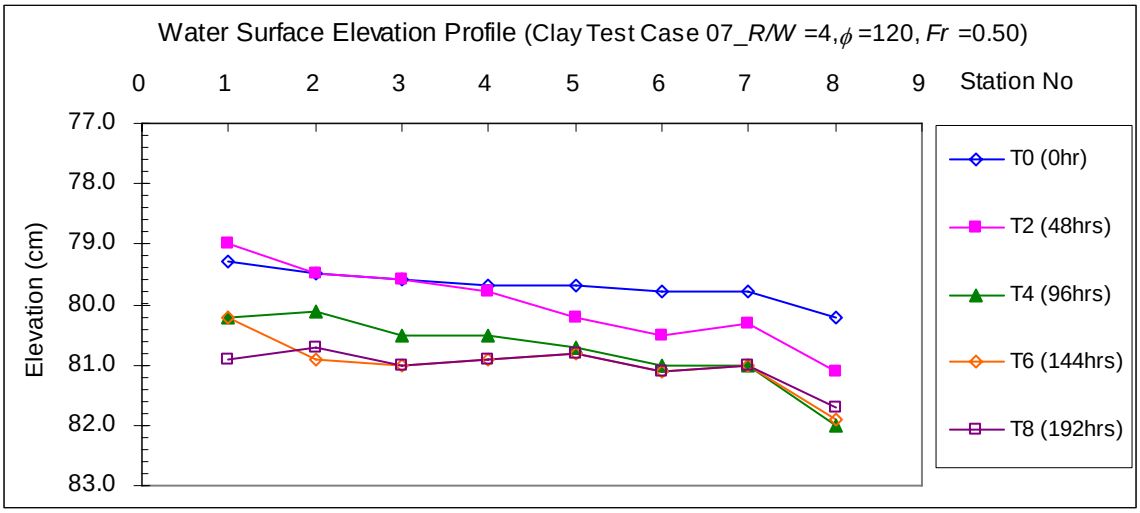

Figure C.27 Water Surface Elevation Profile (Clay Test Case 07)

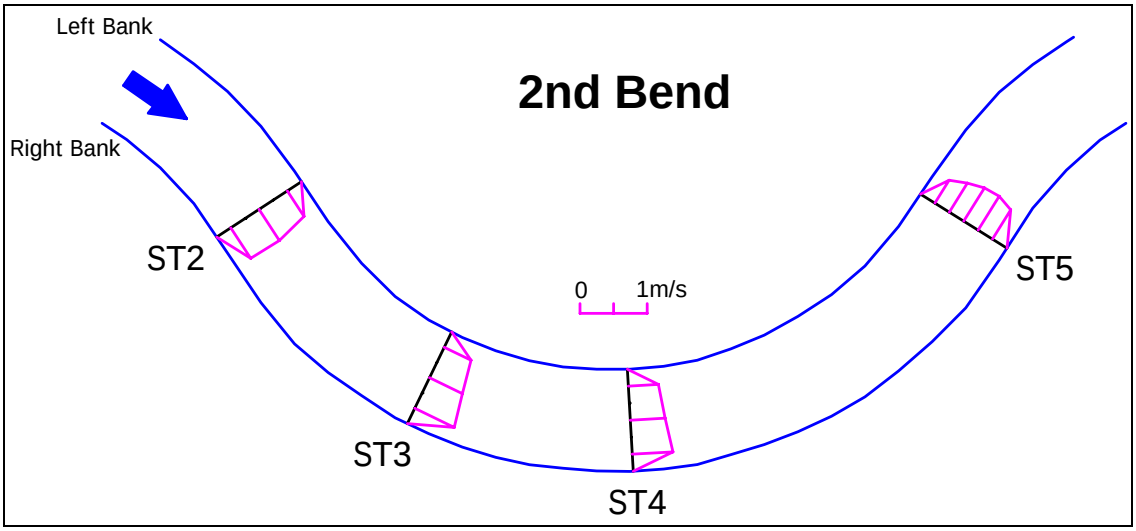

Figure C.28 Longitudinal Surface Velocity Profiles at T0 (Clay Test Case 07)

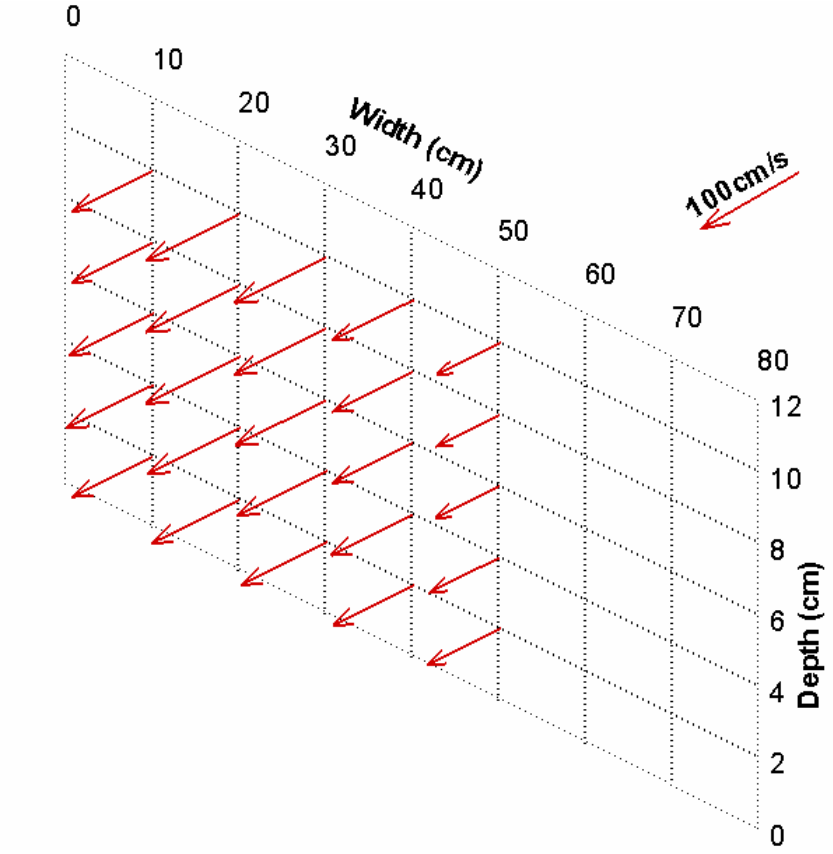

(a) Longitudinal Velocities

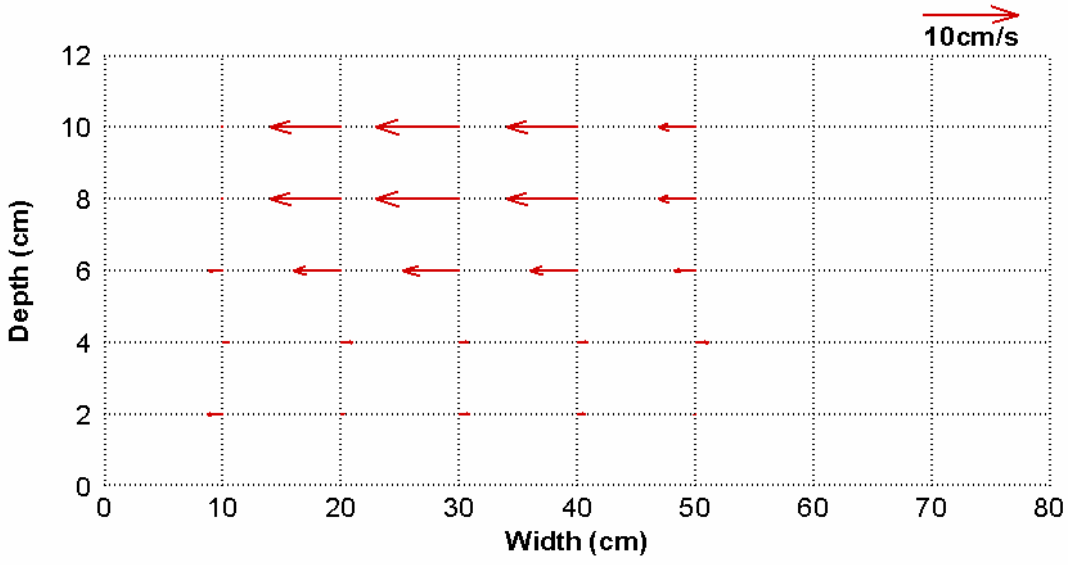

(b) Transversal Velocities

Figure C.29 Initial Velocity Profiles at ST5 (Clay Test Case 07)

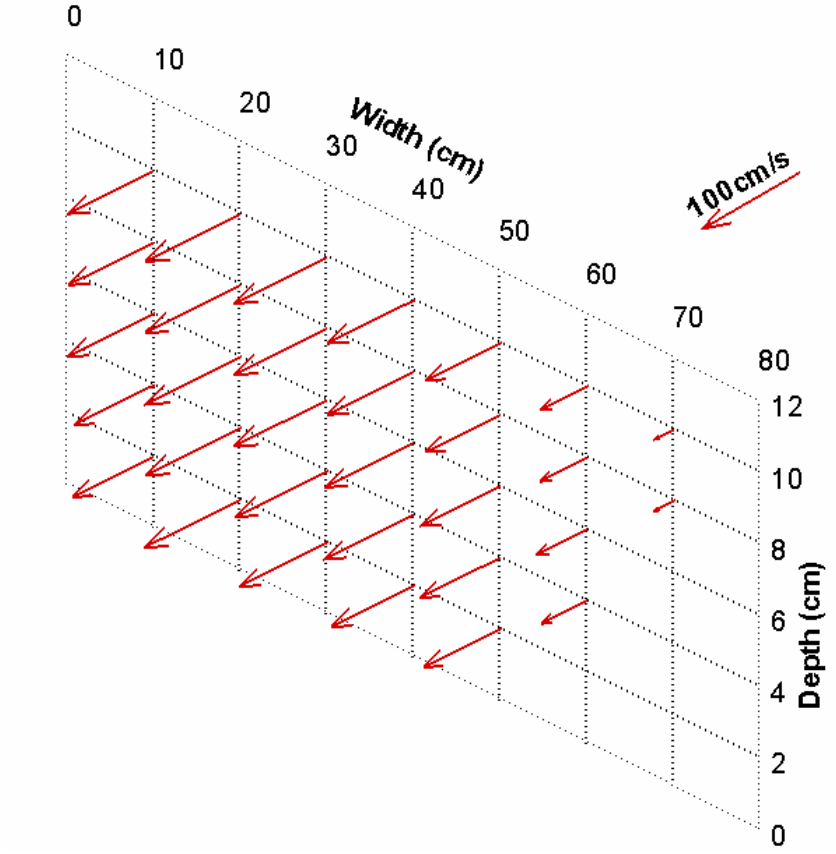

(a) Longitudinal Velocities

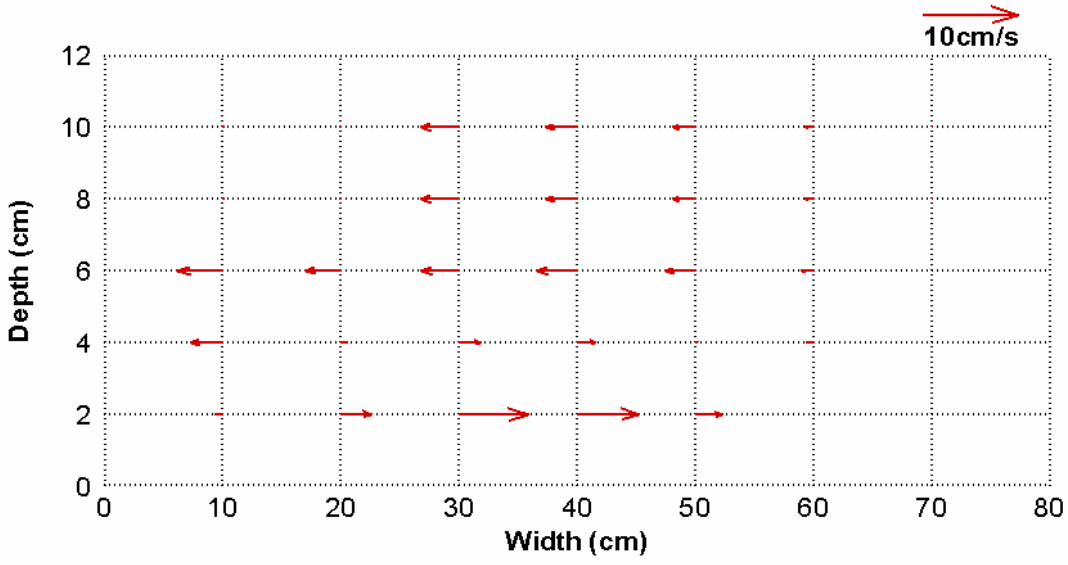

(b) Transversal Velocities

Figure C.30 Velocity Profiles at ST5 after 72 Hours (Clay Test Case 07)

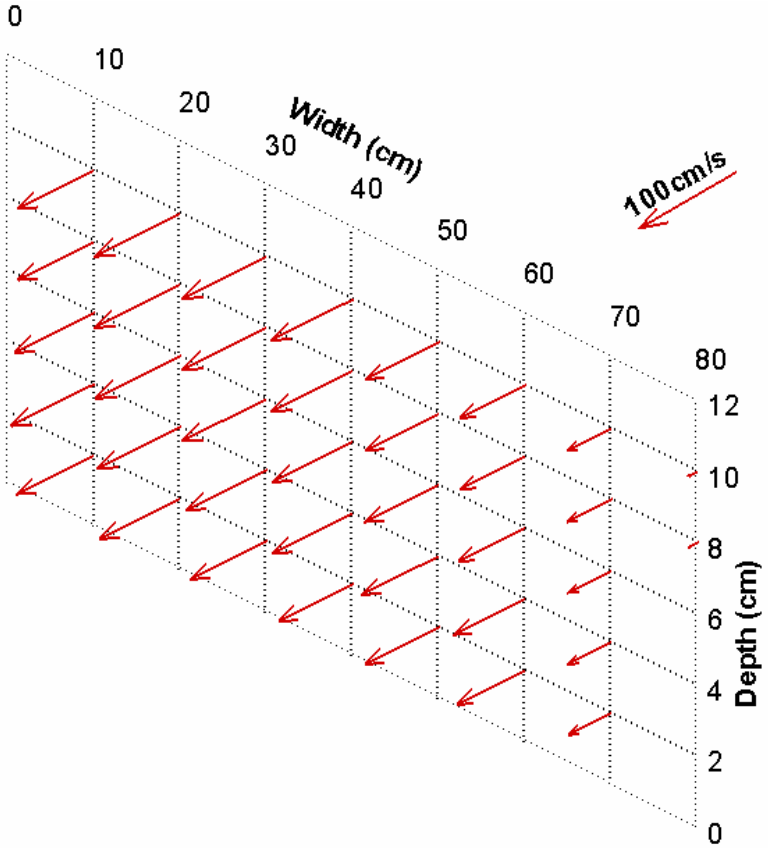

(a) Longitudinal Velocities

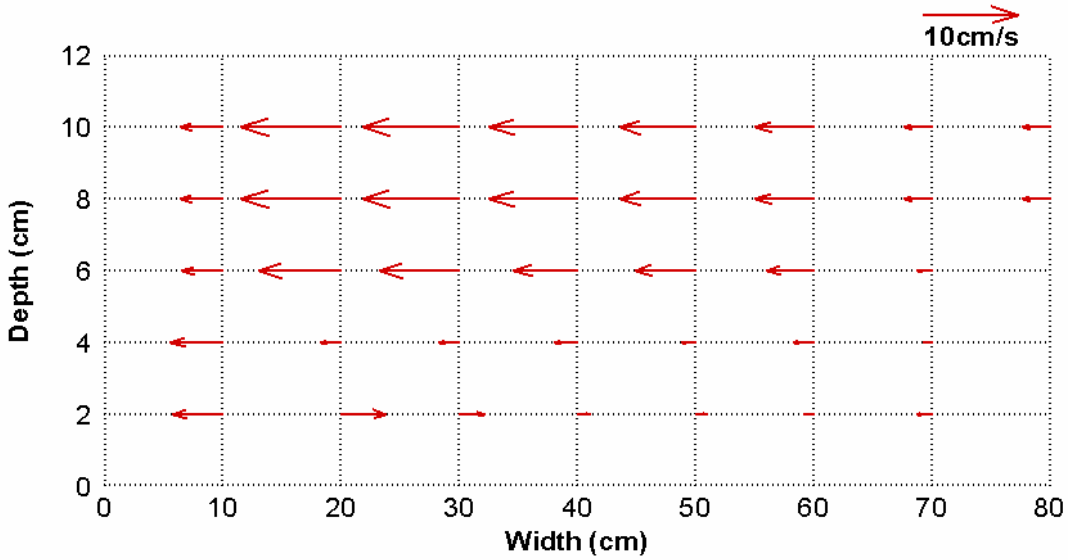

(b) Transversal Velocities

Figure C.31 Velocity Profiles at ST5 after 144 Hours (Clay Test Case 07)

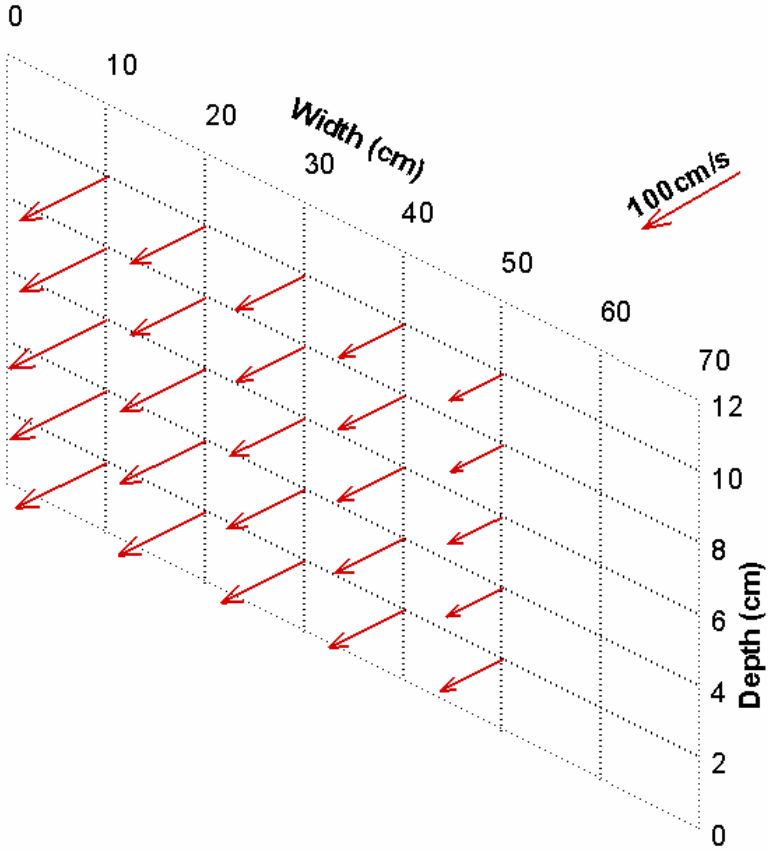

(a) Longitudinal Velocities

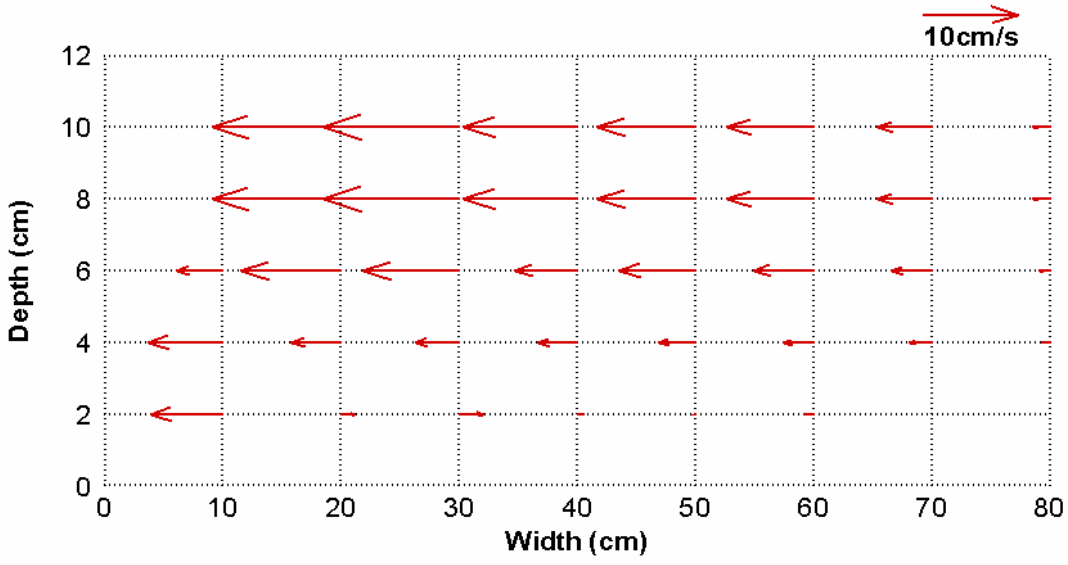

(b) Transversal Velocities

Figure C.32 Velocity Profiles at ST5 after 192 Hours (Clay Test Case 07)

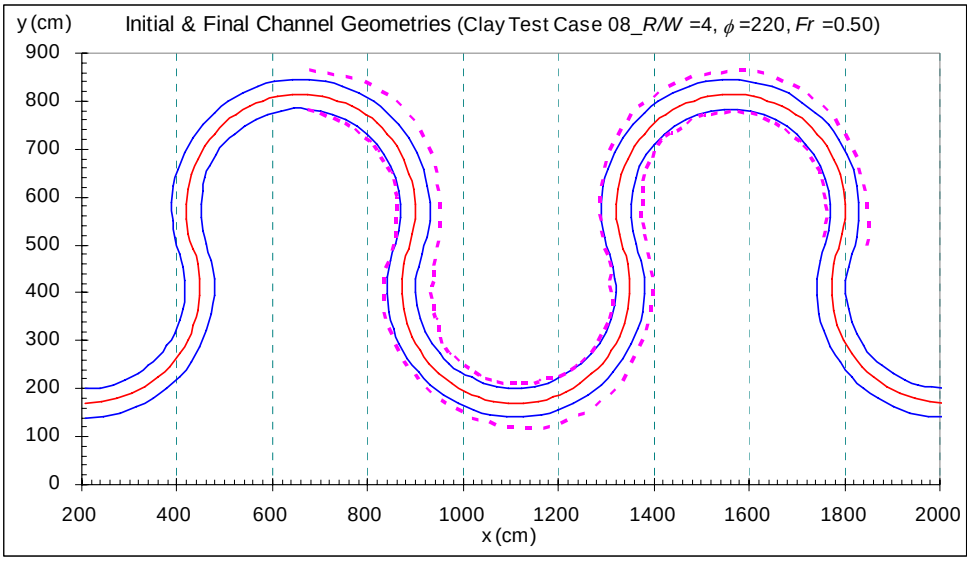

Figure C.33 Channel Geometry at the Initial and Final (336 hr) Stages (Clay Test Case 08)

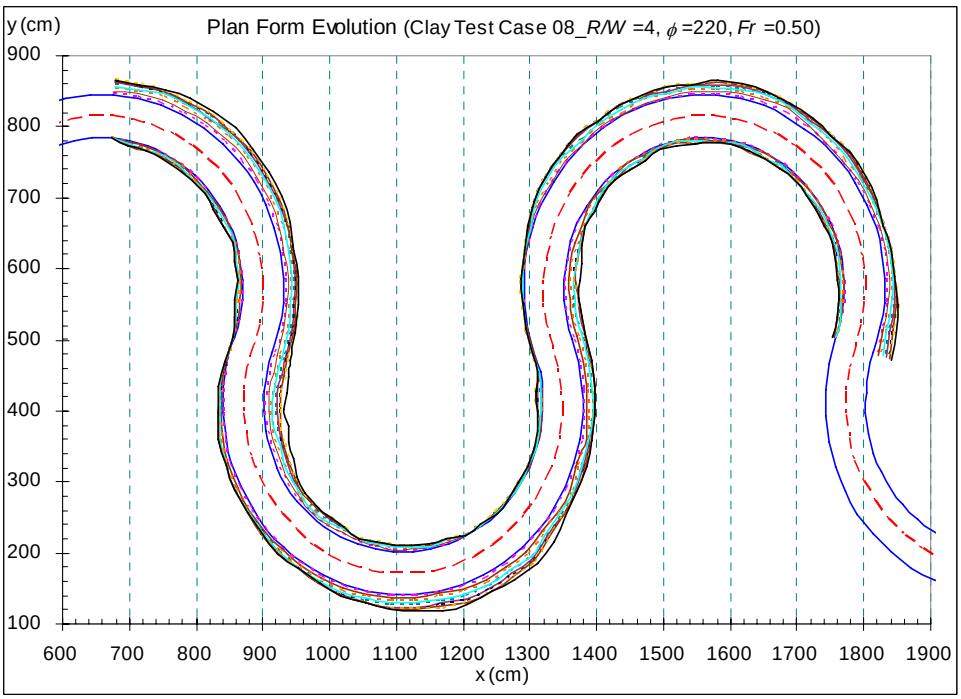

Figure C.34 Plan Forms Evolution at *t* = 0, 24, 48, 72, 96, 120, 150, 180, 210, 240 and 336 hr (Clay Test Case 08)

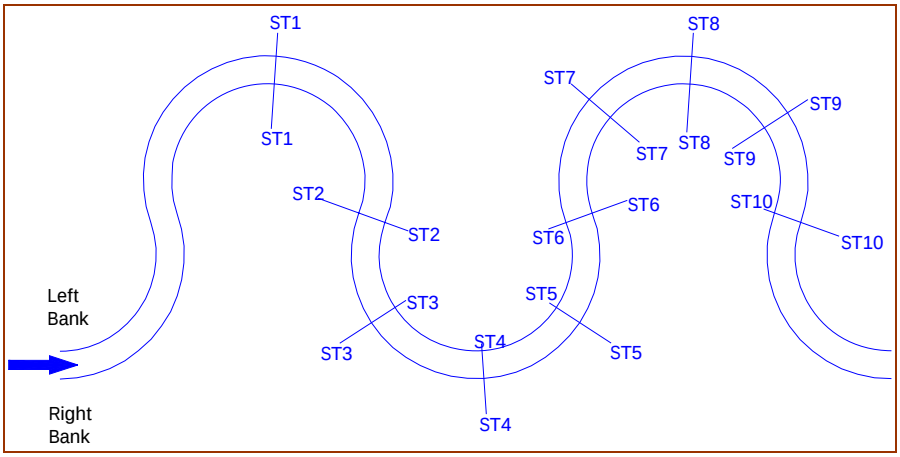

(a) Locations of the Predetermined Stations

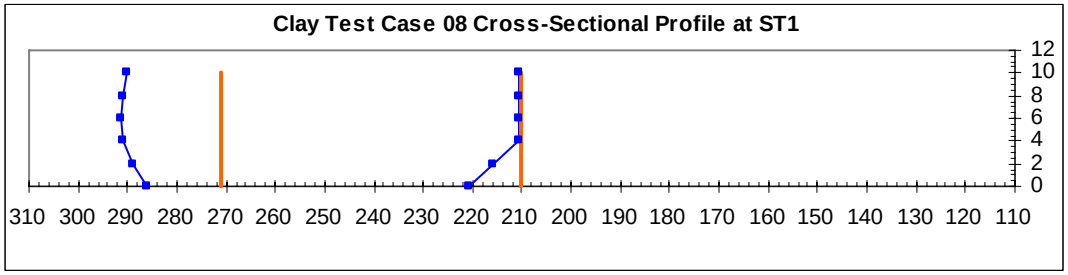

(b) Evolution of cross-sectional profile at station No. 1

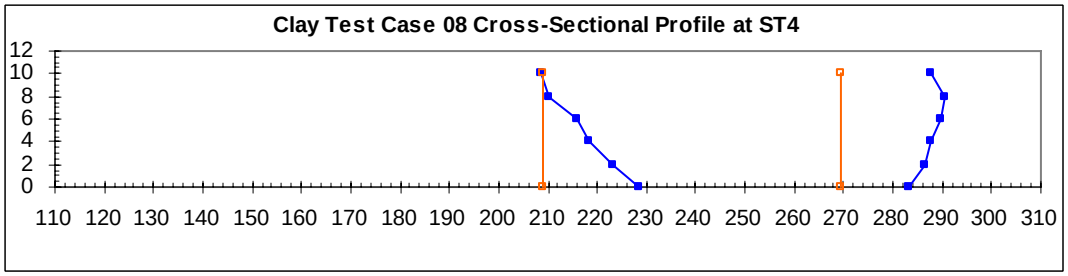

(c) Evolution of cross-sectional profile at station No. 4

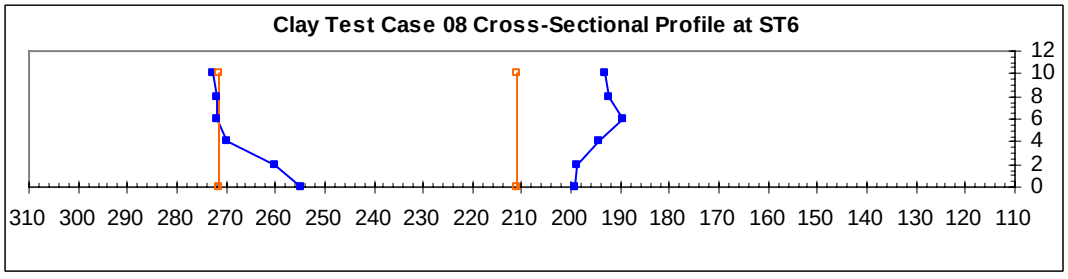

(d) Evolution of cross-sectional profile at station No. 6

Figure C.35 Cross-Sectional Measurement Results (Clay Test Case 08)

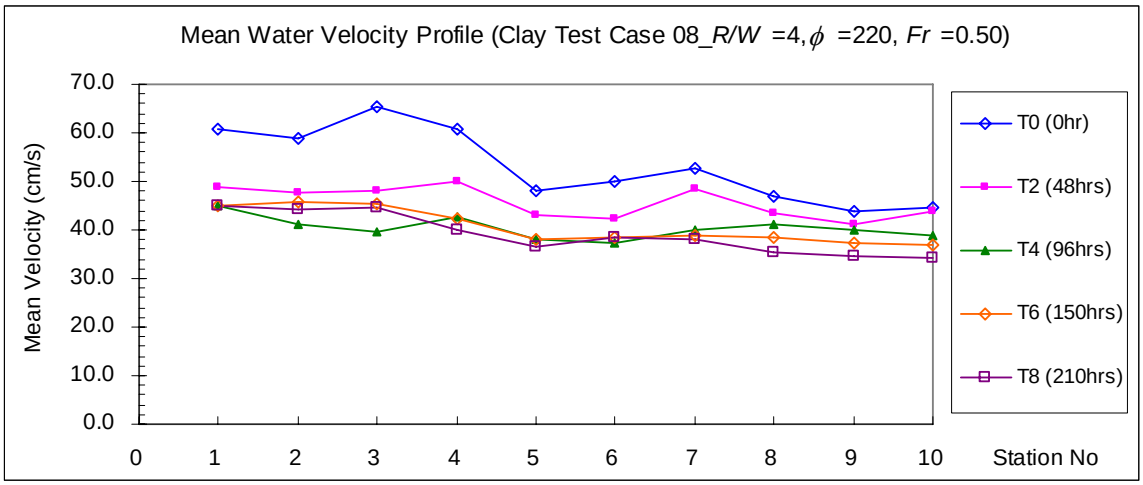

(a) Direct Measurement by ADV

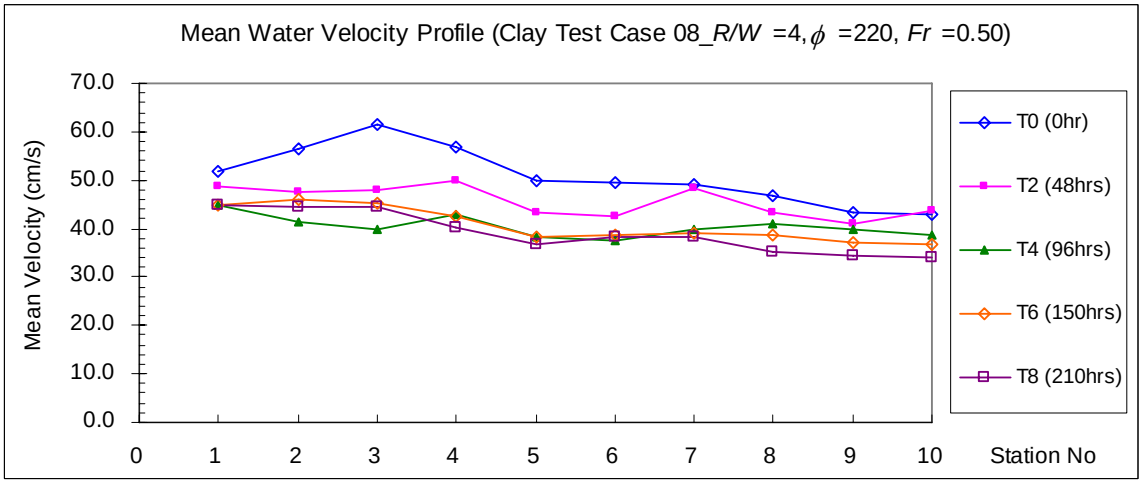

(b) Calculated by the Equation of Continuity ($U = Q/A_w$)

Figure C.36 Mean Velocity Profile (Clay Test Case 08)

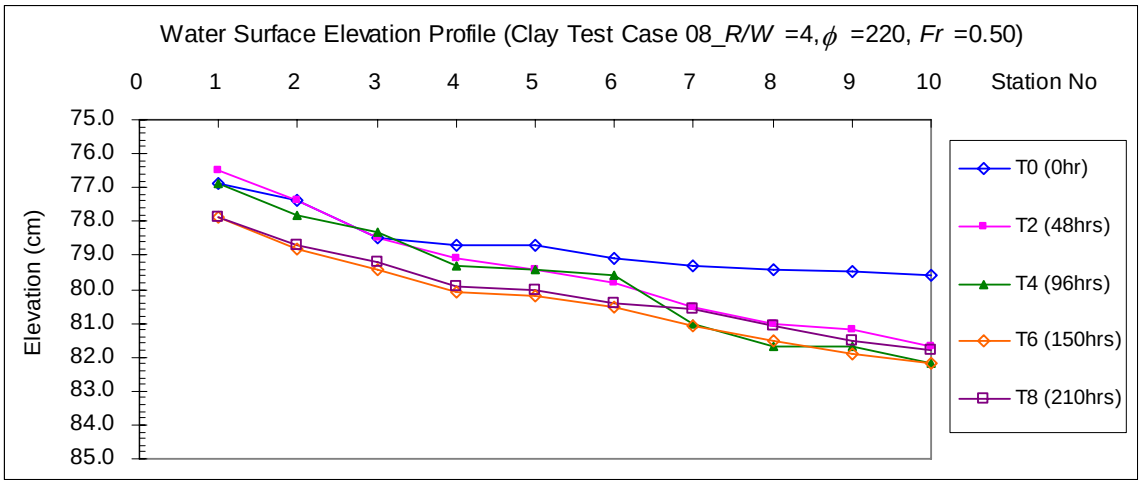

Figure C.37 Water Surface Elevation Profile (Clay Test Case 08)

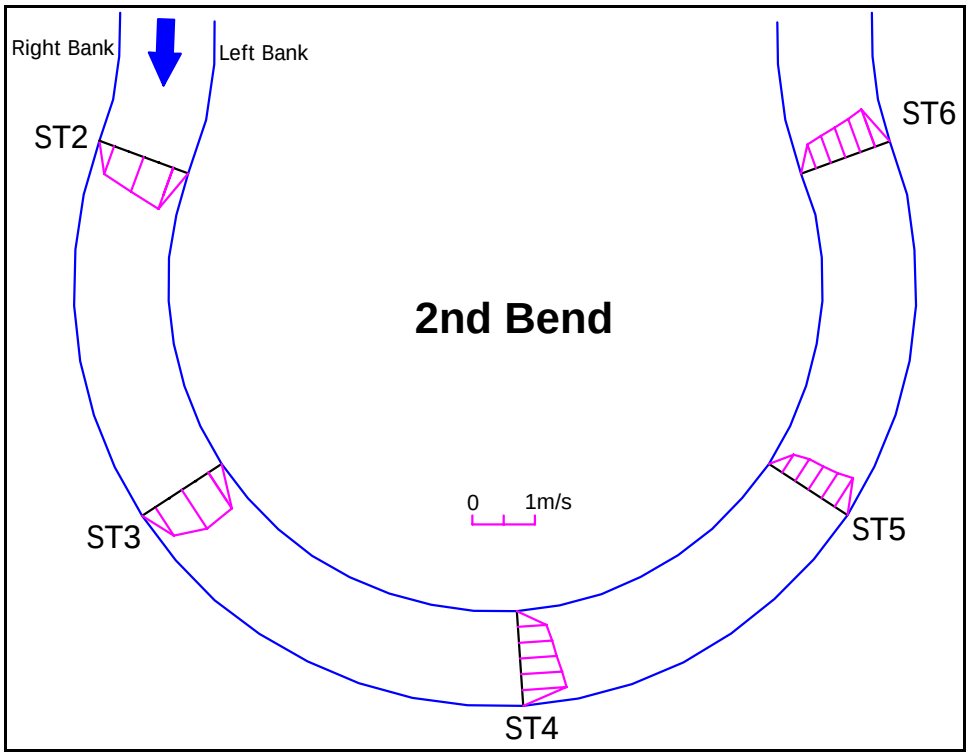

Figure C.38 Longitudinal Surface Velocity Profiles at T0 (Clay Test Case 08)

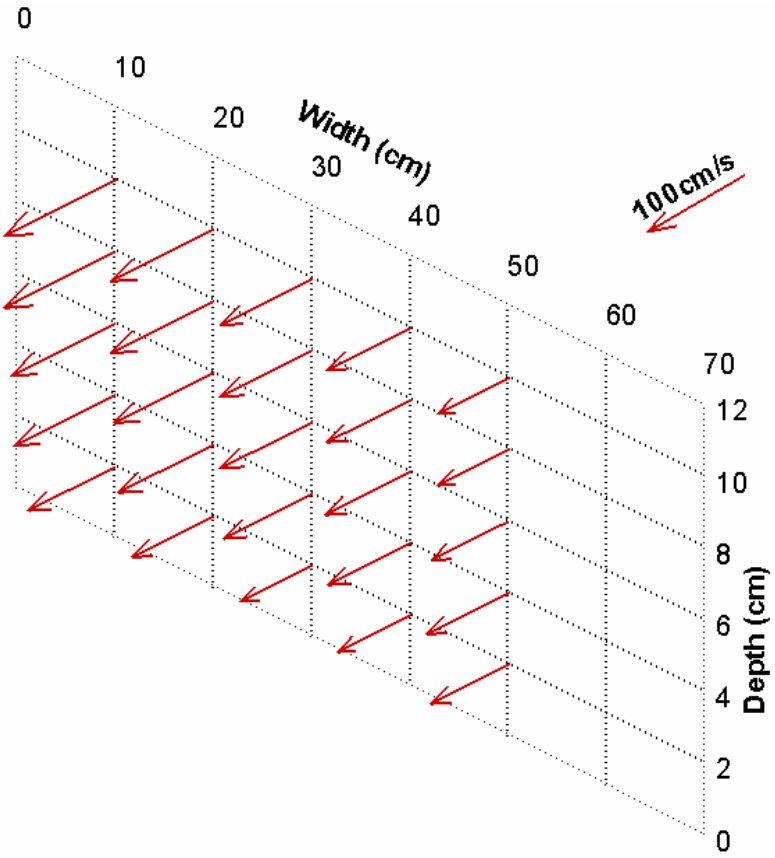

(a) Longitudinal Velocities

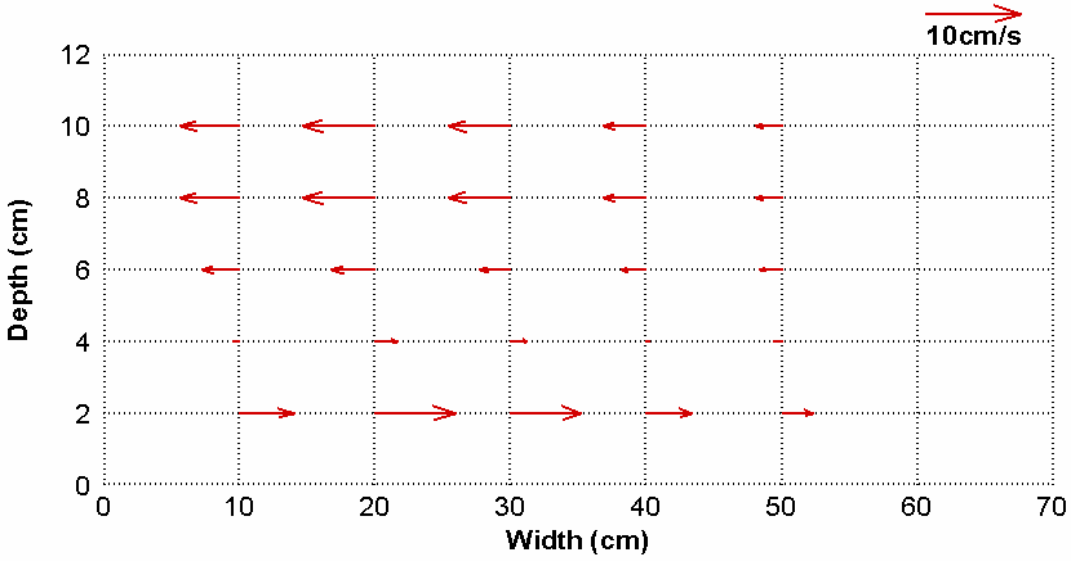

(b) Transversal Velocities

Figure C.39 Initial Velocity Profiles at ST4 (Clay Test Case 08)

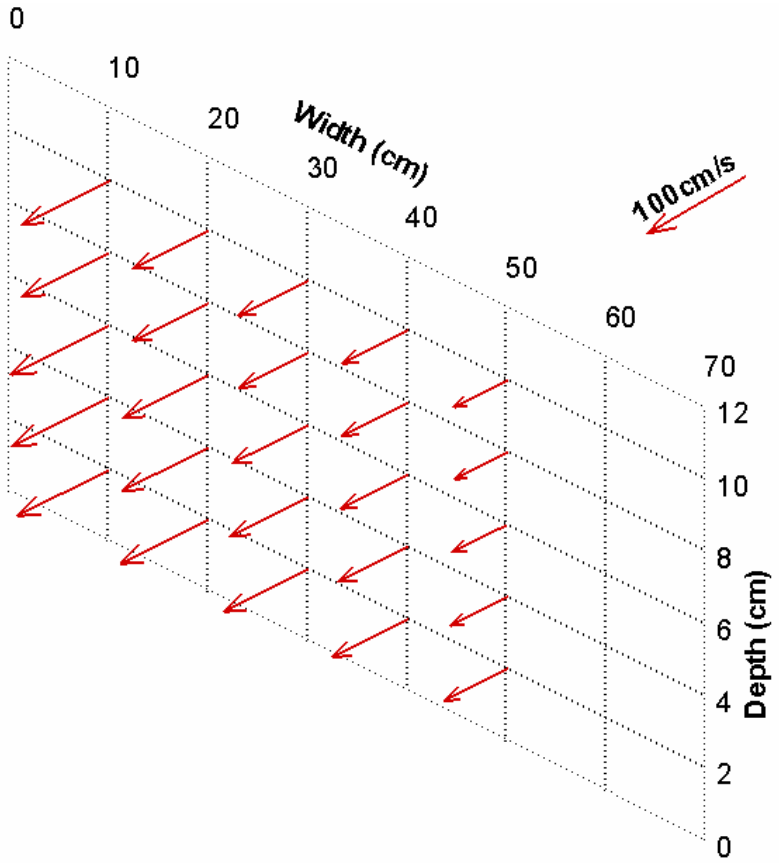

(a) Longitudinal Velocities

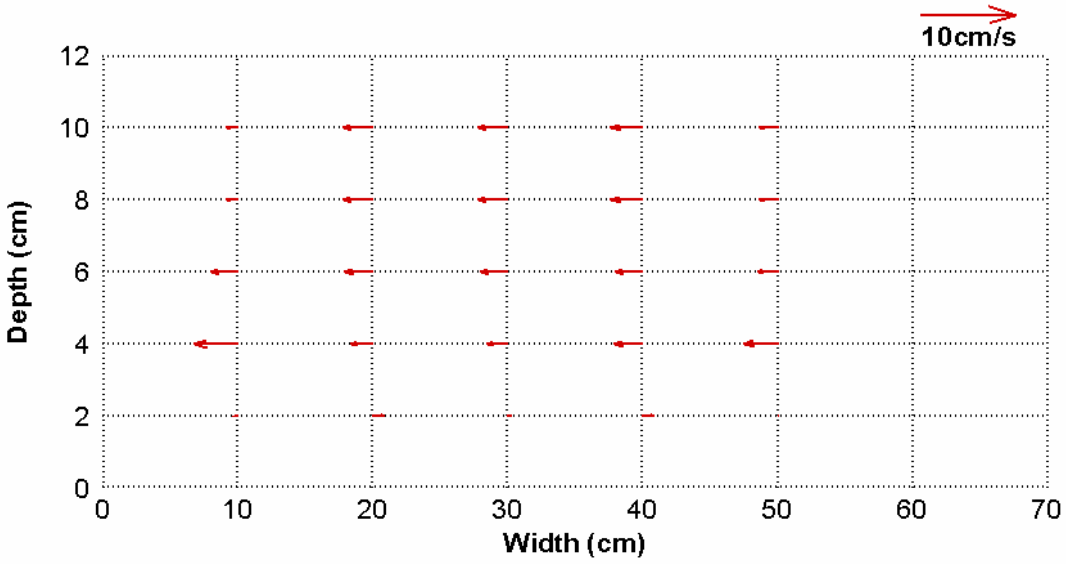

(b) Transversal Velocities

Figure C.40 Initial Velocity Profiles at ST5 (Clay Test Case 08)

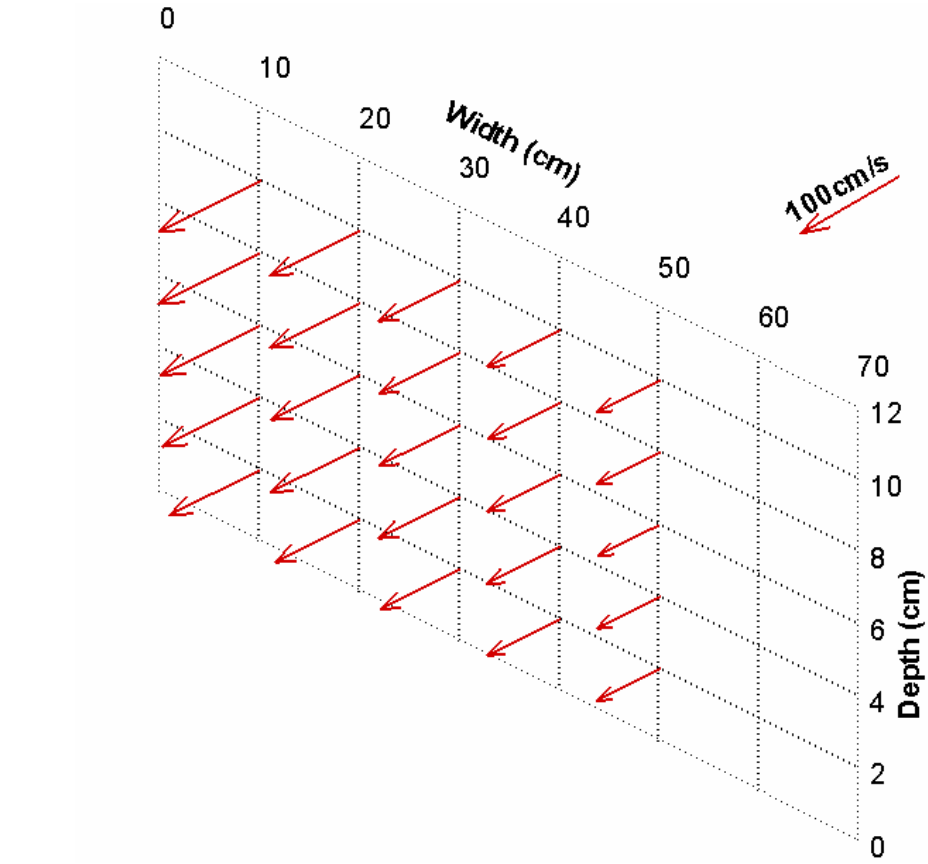

(a) Longitudinal Velocities

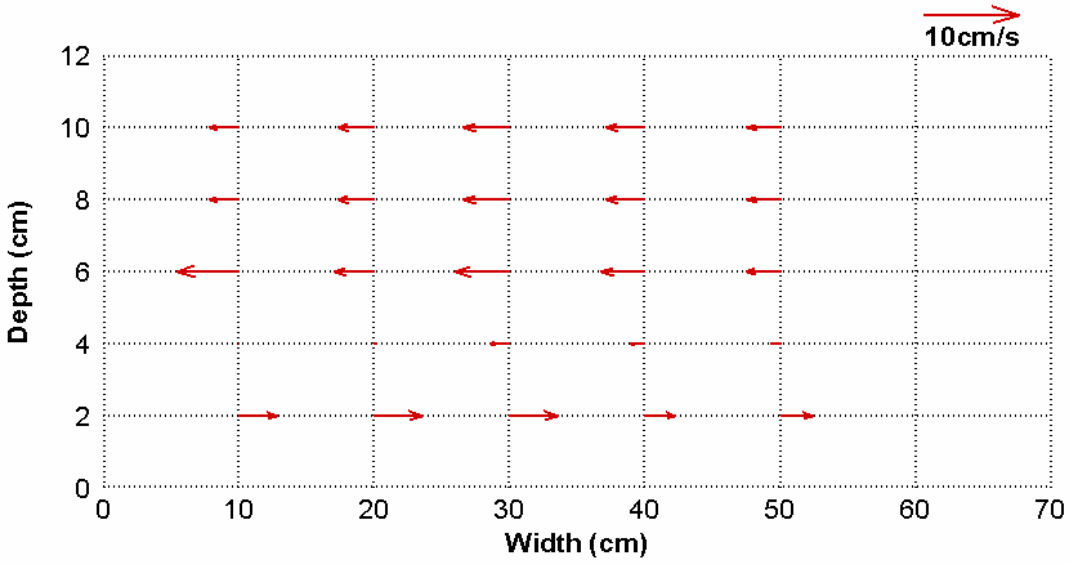

(b) Transversal Velocities

Figure C.41 Initial Velocity Profiles at ST6 (Clay Test Case 08)

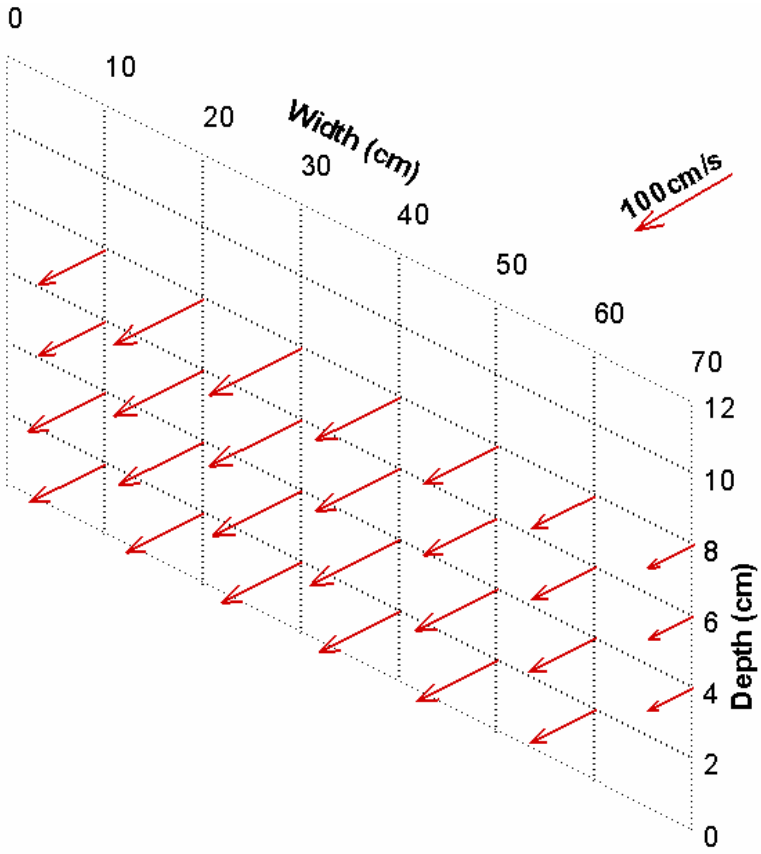

(a) Longitudinal Velocities

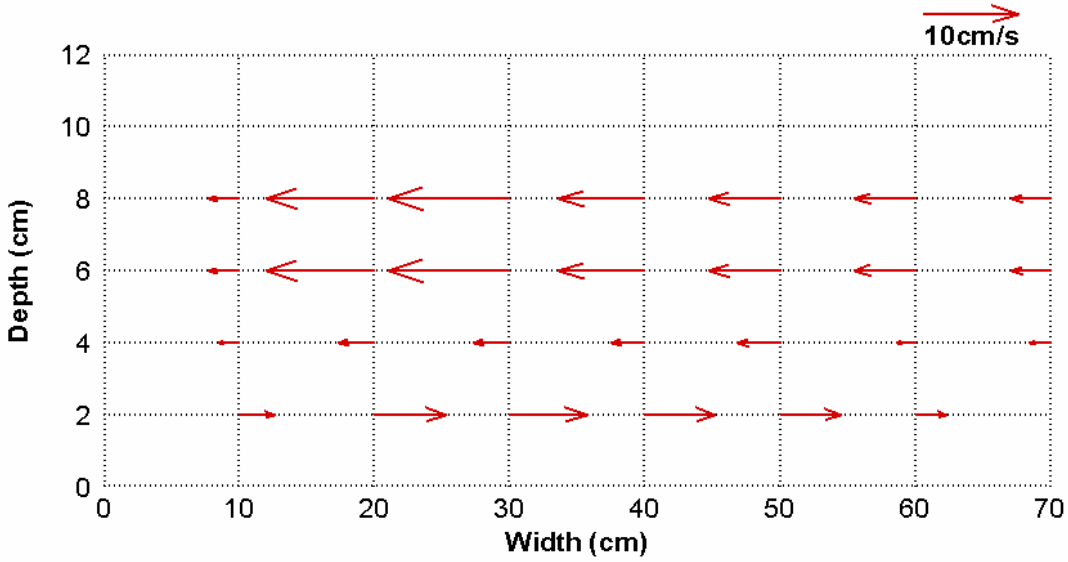

(b) Transversal Velocities

Figure C.42 Velocity Profiles at ST4 after 240 Hours (Clay Test Case 08)

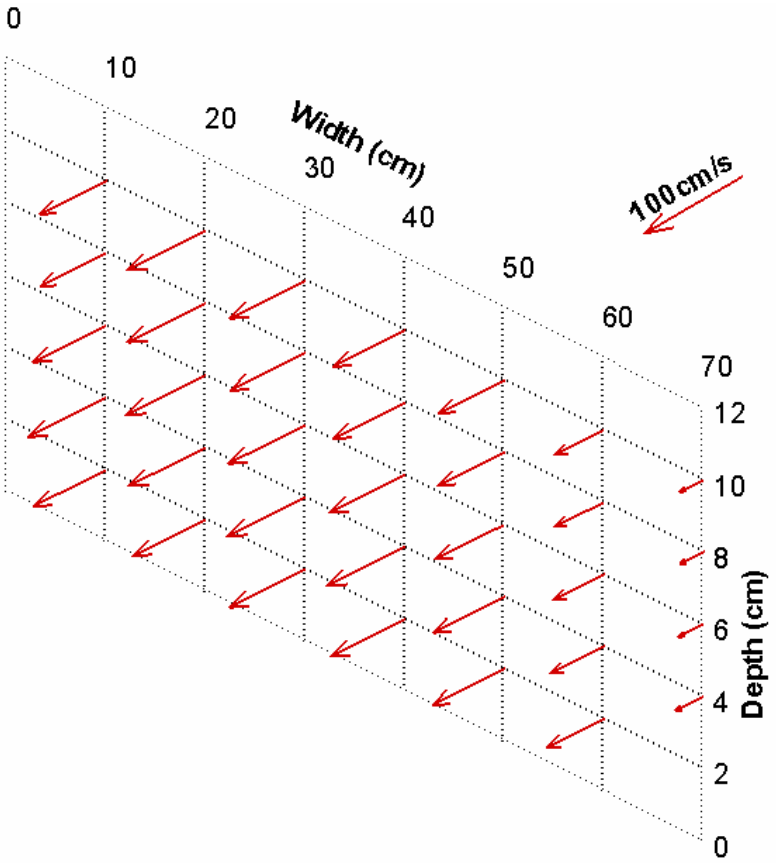

(a) Longitudinal Velocities

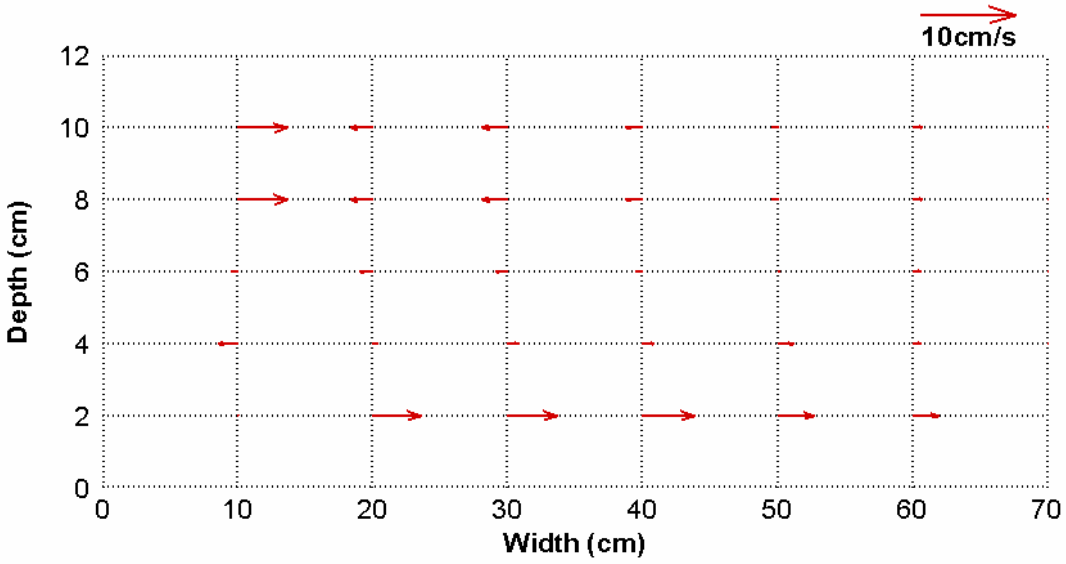

(b) Transversal Velocities

Figure C.43 Velocity Profiles at ST5 after 240 Hours (Clay Test Case 08)

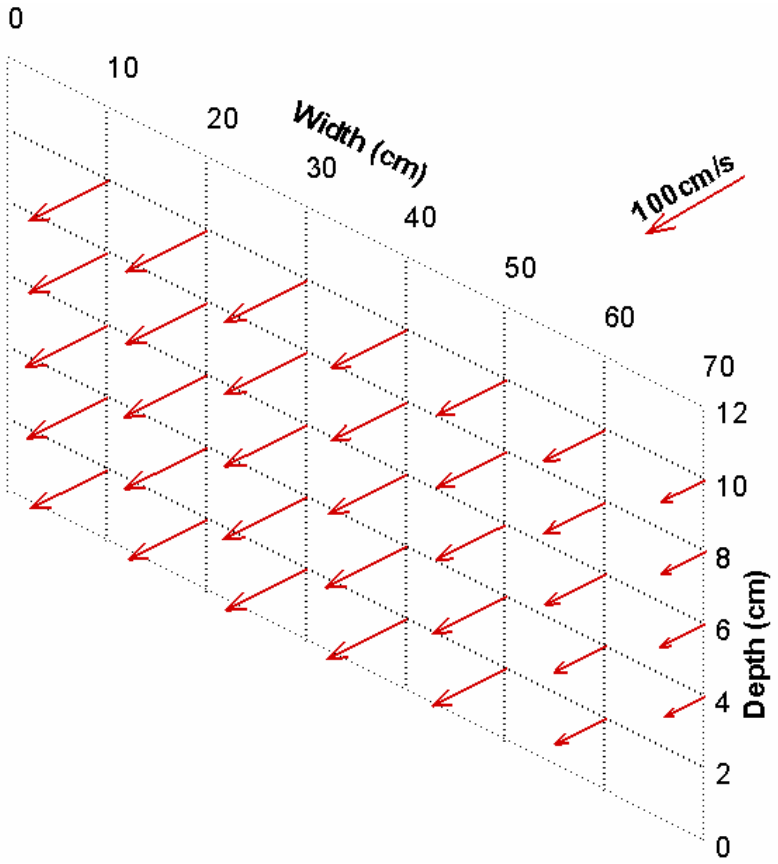

(a) Longitudinal Velocities

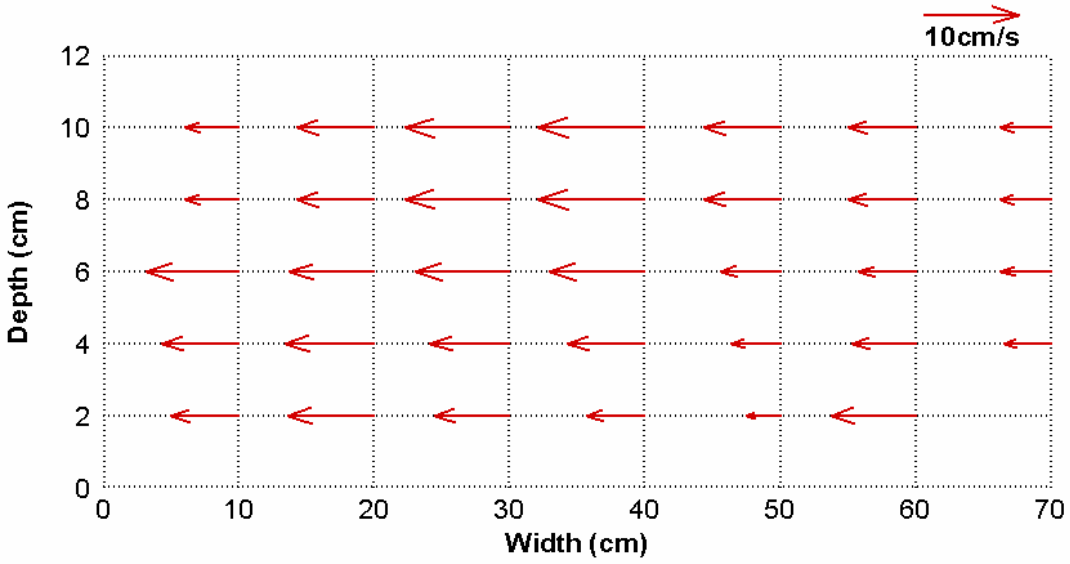

(b) Transversal Velocities

Figure C.44 Velocity Profiles at ST6 after 240 Hours (Clay Test Case 08)

APPENDIX D

PHOTOGRAPHS OF THE BRAZOS RIVER AT SH 105

APPENDIX E

BORING LOGS OF THE BRAZOS RIVER AT SH 105

LOG OF BORING NO. B-1

Van and Sons Drilling Service, INC.
319 John Alber Road
Houston, TX 77076

JOB NO. : 510102
PROJECT : Brazos river at SH105
DATE : 1-9-07

LOCATION :
LATITUDE : N 30° 22' 0.66"
LONGITUDE : W 96° 8' 57.48"

DEPTH (FEET)	SAMPLE SYMBOL	SHELBY(S) / SPT(B)	HAND PENETROMETER	BLOW COUNTS (X / X / X)	CONSISTENCY	COLOR	MINOR MATERIAL	MAJOR MATERIAL	CHARACTERISTICS	WATER CONTENT (%)	UNIT WEIGHT (kN/m3)	UNDRAINED SHEAR STRENGTH(kPa) by Vane	LIQUID LIMIT (%)	PLASTICITY INDEX (%)	SOIL CLASSIFICATION	ERODIBILITY CAT.
0		S	1.5		Stiff	Gray		Sand	Silty Sand/Organics							
		B	12/14/17		Very Dense	Tan		Sand	Silty Sand							
5		B	13/16/15		Very Dense	Light Tan		Sand	Fine Sand							
		S	4.5		Very Stiff/ Hard	Brown		Clay	Fe Stains							
		S	4.5		Very Stiff/ Hard	Brown		Clay	Fe Stains							
10		S	4.5		Very Stiff/ Hard				Shelby Tube							
		S	4.0		Very Stiff	Brown	Sand	Clay	Fe Stains							
15																
		S	2.5		Stiff	Brown	Sand	Clay	Fe Stains							
20		S	2.5		Stiff				Shelby Tube							
		S	2.5		Stiff	Gray		Clay	Fe Stains							
25																
		S	3.5		Very Stiff	Dark Gray		Clay	Fe Stains							
30 ▽		S	3.0		Stiff				Shelby Tube	28.2	20.5	83.0	65.7	45.5	CH	IV
		S	1.75		Stiff	Gray/ Brown		Clay	Fe Stains							
35																
		S	2.75		Stiff	Light Tan		Silt Clay	Fe Stains							
40		S	1.0		Stiff				Shelby Tube	30.0	20.3	34.0	32.3	19.0	CL	II
		S	0.25		Very Soft	Gray	Clay	Silt	Fe Stains							
45																
50		S	2.75		Stiff				Shelby Tube	24.4	20.9	20.0	17.0	3.0	SM	II

DRY AUGER : 0 TO 50 ft
WET ROTARY : _____ TO _____ ft

COMPLETION DEPTH : 50 ft
TECHNICIAN : Leonardo

LOG OF BORING NO. B-2

Van and Sons Drilling Service, INC.
319 John Alber Road
Houston, TX 77076

JOB NO. : 510102
PROJECT : Brazos river at SH105
DATE : 1-9-07

LOCATION :
LATITUDE : N 30° 21' 51.78"
LONGITUDE : W 96° 9' 4.5"

DEPTH (FEET)	SAMPLE SYMBOL	SHELBY(S) / SPT(B)	HAND PENETROMETER / BLOW COUNTS (X / X / X)	CONSISTENCY	COLOR	MINOR MATERIAL	MAJOR MATERIAL	CHARACTERISTICS	WATER CONTENT (%)	UNIT WEIGHT (kN/m3)	UNDRAINED SHEAR STRENGTH(kPa) by Vane	LIQUID LIMIT (%)	PLASTICITY INDEX (%)	SOIL CLASSIFICATION	ERODIBILITY CAT.
0		S	2.5	Stiff	Brown	Sand	Clay	Organics							
		S	4.5	Very Stiff/ Hard	Brown		Clay	Fe Stains							
5		S	4.5	Very Stiff/ Hard	Brown		Clay	Fe Stains							
		S	4.5	Very Stiff/ Hard	Brown		Clay	Fe Stains							
		S	4.5	Very Stiff/ Hard	Brown		Clay	Fe Stains							
10		S	4.5	Very Stiff/ Hard				Shelby Tube							
		S	4.0	Very Stiff	Brown		Clay	Fe Stains							
15															
		S	3.5	Very Stiff	Brown		Clay	Fe Stains							
20		S	4.5	Very Stiff/ Hard				Shelby Tube							
		S	2.0	Stiff	Brown	Sand	Silt Clay	Fe Stains							
25								Sand at 26'							
		B	6/4/10	Medium Dense	Brown	Sand	Silt Clay								
30 ▽		S	2.3	Stiff				Shelby Tube	21.7	20.8	43.0	38.5	23.4	CL	III
		B	16/24/36	Very Dense	Brown	Sand	Silt Clay								
35															
		B	23/36/45	Very Dense	Brown	Sand	Silt	Silty Sand	20.8	18.7	N/A	N/A	N/A	SM	II
40															
		B	16/37/50	Very Dense	Tan		Sand	Fine Sand							
45															
		B	21/31/34	Very Dense	Gray		Sand	Fine Sand	19.6	20.6	N/A	N/A	N/A	SP	II
50															

DRY AUGER : 0 TO 25 ft
WET ROTARY : 25 TO 50 ft

COMPLETION DEPTH : 50 ft
TECHNICIAN : Leonardo

LOG OF BORING NO. B-3

Van and Sons Drilling Service, INC.
319 John Alber Road
Houston, TX 77076

JOB NO. : 510102
PROJECT : Brazos river at SH105
DATE : 1-9-07

LOCATION :
LATITUDE : N 30° 21' 40.92"
LONGITUDE : W 96° 9' 23.34"

DEPTH (FEET)	SAMPLE SYMBOL	SHELBY(S) / SPT(B)	HAND PENETROMETER	BLOW COUNTS (X / X / X)	CONSISTENCY	COLOR	MINOR MATERIAL	MAJOR MATERIAL	CHARACTERISTICS	WATER CONTENT (%)	UNIT WEIGHT (kN/m3)	UNDRAINED SHEAR STRENGTH(kPa) by Vane	LIQUID LIMIT (%)	PLASTICITY INDEX (%)	SOIL CLASSIFICATION	ERODIBILITY CAT.
0		S	2.5		Stiff	Gray		Clay	Organics							
		S	2.5		Stiff	Brown/ Gray		Clay	Fe Stains							
5		S	4.5		Very Stiff/ Hard	Dark Gray		Clay	Fe Stains							
		S	4.5		Very Stiff/ Hard	Gray		Clay	Fe Stains							
		S	4.5		Very Stiff/ Hard	Brown/ Gray		Clay	Fe Stains							
10		S	4.5		Very Stiff/ Hard				Shelby Tube	12.1	23.3	26.0	12.0	14.0	SC	II
		S	4.25		Very Stiff	Olive Green		Clay	Calkurius							
15																
		S	3.75		Very Stiff	Olive Green / Tan		Clay	Calkurius							
20		S	3.0		Stiff				Shelby Tube	23.3	20.4	92.0	47.0	34.0	CL	III
		S	3.75		Very Stiff	Olive Green / Tan		Clay	Calkurius							
25																
		S	4.5		Very Stiff/ Hard	Olive Green		Clay	Calkurius							
30		S	4.5		Very Stiff/ Hard				Shelby Tube	25.5	21.2	140.0	64.2	40.0	CH	II
		S	4.25		Very Stiff	Gray		Clay	Fe Stains							
35		S	4.5		Very Stiff/ Hard	Gray		Clay	Fe Stains							
		S	4.5		Very Stiff/ Hard				Shelby Tube	29.9	19.3	140	81.9	55.9	CH	III
40																
		S	4.0		Very Stiff	Gray/ Brown		Clay	Fe Stains							
45																
		S	4.25		Very Stiff				Shelby Tube	31.6	20.1	140.0	85.0	56.0	CH	II
50																

DRY AUGER : 0 TO 35 ft
WET ROTARY : 35 TO 50 ft

COMPLETION DEPTH : 50 ft
TECHNICIAN : Leonardo

VITA

Namgyu Park was born in Busan, Korea. He attended Sunkyunkwan University in Korea, from March 1990 to February 1996. He graduated with a Bachelor of Science degree in civil engineering. He performed his military service in the Korean army from January 1992 to July 1993. From February 1996 to October 1999, he worked as a structural engineer for the Korea Power Engineering Company in Korea, designing steel structures for large bore pipe supports in nuclear power plants. Then, he came to the University of Michigan in August 2000 to study geotechnical engineering where he obtained a Master of Science under the guidance of Dr. Radoslaw L. Michalowski in December 2001. After he got his M.S., he transferred to Texas A&M University for his PhD study in geotechnical engineering. He worked with Dr. Briaud on the meander migration research sponsored by TxDOT.

Mr. Park can be reached at: Department of Civil Engineering, Texas A&M University, 3136 TAMU, College Station, Texas 77843-3136. His email is ngpark71@tamu.edu.